BEHAVIOUR OF UNPLUGGED PIPE PILES IN GRANULAR SOIL

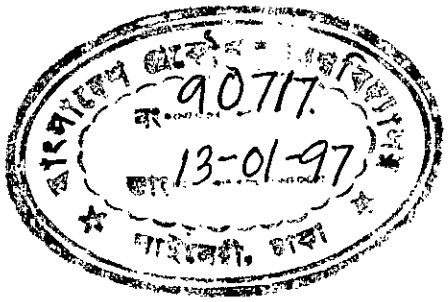

A THESIS BY

ASHUTOSH SUTRA DHAR

Submitted in partial fulfilment of the requirements for the degree of

MASTER OF SCIENCE IN CIVIL ENGINEERING

DEPARTMENT OF CIVIL ENGINEERING
BANGLADESH UNIVERSITY OF ENGINEERING
AND TECHNOLOGY

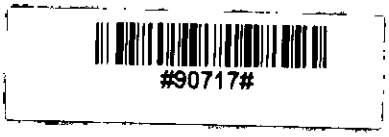

OCTOBER, 1996

BEHAVIOUR OF UNPLUGGED PIPE PILE IN GRANULAR SOIL

A THESIS BY

ASHUTOSH SUTRA DHAR

Approved as to the style and content for the degree of M.Sc Engg.(civil):

A.M.M. Safiullah

Dr. A.M.M. Safiullah
Professor
Department of Civil Engineering
BUET, Dhaka.

Chairman
(Supervisor)

Dr. Md. Saiful Alam Siddiquee
Assistant Professor
Department of Civil Engineering
BUET, Dhaka.

Member
(Co-supervisor)

Dr. M. Azadur Rahman
Professor and Head
Department of Civil Engineering
BUET, Dhaka.

Member

Dr. M. Zoynul Abedin
Professor
Department of Civil Engineering
BUET, Dhaka.

Member

Dr. Ahsanul Jalil Khan
Managing Director
Construction and Development Co.
44, Dhanmondi, Road No. 4A, Dhaka.

Member
(External)

DECLARATION

Declared that, except where specified references are made to other investigators, the work embodied in this thesis is the result of investigation carried out by the author under the supervision of Dr. A.M.M. Safiullah, Professor of Civil Engineering, BUET and co-supervision of Dr. Md. Saiful Alam Siddiquee, Assistant Professor of Civil Engineering, BUET.

Neither the thesis nor any part thereof has been submitted or is being concurrently submitted in candidature for any degree at any other institution.

_____

Author

ACKNOWLEDGEMENT

The author wishes to express his indebtedness to Dr. A.M.M. Safiullah, Professor of Civil Engineering, BUET for his continuous guidance, invaluable suggestions and affectionate encouragement at every stage of this study.

The author expresses his profound gratitude to Dr. Md. Saiful Alam Siddiquee, Assistant Professor of Civil Engineering, BUET for his constant guidance, suggestions and encouragement at all phases of this work.

Heartiest thanks are expressed to Dr. M. Azadur Rahman, Professor and Head, Department of Civil Engineering, BUET for his co-operation.

Acknowledgement is also made to Dr. A.B.M. Bodruzzaman, Assistant Professor and Lab-in-charge of the Computer Laboratory, Department of Civil Engineering, BUET for his co-operation in using the computer facility.

The author also express his thanks to Mr. M.A. Malek for his help in typing the scripts.

ABSTRACT

Open-ended pipe piles are commonly used for offshore foundations. Capacity of an open-ended pipe pile is controlled by depth and property of the soil within the pile. Under static loading in compression, open-ended piles may fail in a plugged mode or in an unplugged mode depending upon the stress conditions of the internal soil. Due to the development of arching in the internal soil, stresses in the soil increase exponentially. When the stresses at the base of the internal soil is greater than the end bearing capacity of pile, the pile may be assumed to fail as a closed ended pile, in plugged mode. In this study attempts have been made to determine the behaviour of the soil inside the pile under axial loading. Finite element analysis is performed by using critical state program- CRISP to investigate the effect of soil depth and pile diameter on pile capacity. Distribution of stresses in pile and internal soil is also studied to understand the mechanism of plug development.

Experiments were carried out with varying diameter of piles (three types) having different depths of internal soil. Density of the internal soil of pipe piles were measured before and after the experiment. Electronic strain gauges were attached on the pipe pile outer surface to study the load transfer mechanism.

It was found that depth ratio (L/D) and the displacement of pile played the most important roles in the development of arching in the soil within the pipe pile. Capacity of soil plug was found to increase linearly with the increase of soil depth within the pile before the developement of arching. But when arching started to develop, the pile capacity increased exponentially up to a depth required for the development of full plugging. It was observed that depth ratio required to develop arching was about 9 to 15. After the development of full plugging, further increase of soil depth did not result in significant increase of pile capacity. Attempts was made to explain the results obtained from experiments by numerical simulation. Finite element analysis was performed with varying soil properties to simulate the experimental results. Soil properties were assumed to change in a zone near the pile tip as suggested by Terzaghi (1936).

An empirical formula has been proposed after extensive study of the experimental results. The formula is capable of calculating plug capacity for any allowable settlement. A formula is also proposed to calculate the ultimate plug capacity assuming allowable settlement of 10% of the pile diameter.

CONTENTS

LIST OF FIGURES

LIST OF TABLES

NOTATION

b	Least foundation dimension
b_i	Length of interface element
C	Cohesion of the soil
C_a	Adhesion
C_{ijki}	Response function of only the stress tensor
d	Internal diameter of pipe pile
D	Diameter of pile
D_{10}	Effective grain size
D_c	Critical depth for limiting value of q_p
D_r	Relative density
D_{rf}	Relative density after loading
D_{ri}	Relative density before loading
E	Young's modulus
E_o	Modulus at depth Y_o of soil
E_p	Modulus of elasticity of pile material
E_s	Modulus of elasticity for sand
f	Friction coefficient
f	Unit skin friction
F.M.	Fineness modulus
f_{ij}	Response functions
G	Shear modulus
$g(\sigma ,h)$	Plastic potential function
G_{res}	Residual shear modulus
G_s	Shear modulus of interface elements
h	Overall length of soil plug
J_1,J_2,J_3	First, Second and third invariant of the deviatoric stress tensor
K	Coefficient of lateral earth pressure
k	Yield strength of material determined from pure shear
K_n	Modulus in the normal direction of the interface element
L	Length of internal soil
M	Effective stress ratio at critical state
N_c,N_q,N_γ	Bearing capacity factors

N_i	Shape functions
p	Effective surcharge
P	Applied load on pipe pile
P_p	Total load carried by the pile
P_u	Ultimate load at 0.1D settlement
q	Effective overburden pressure
q_e	Limiting end bearing capacity
q_{en}	Effective normal pressure
q_{max}	Limiting point bearing
q_p	End bearing capacity
Q_{pl}	Ultimate axial capacity in plugged mode
Q_{up}	Ultimate axial capacity in unplugged mode
S	Settlement of pile
S_c, S_q, S_γ	Shape factors
t	Thickness of the pile
t_i	Thickness of interface element
W_i	Weighted function
z	Depth
z_c	Critical depth
φ	Internal angle of friction
δ	Interface friction angle between soil and pile
ε	Strain
κ	Bulk modulus
σ	The normal effective stress on the failure surface
η	Stress ratio
α , κ	Drucker-Prager parameters
σ_1	Major principle stress
σ_2	Intermediate principle stress
σ_3	Minor principle stress
φ_a	Angle of friction between structure and soil
γ_{bulk}	Bulk unit weight of sand
τ_i	Shear stress in the pile-soil interface
τ_L	Limiting shear stress
ε_p	Strain of pile at any level
σ_p	Stress of pile at any level
φ_{res}	Residual friction angle of sand

γ_s	Effective unit weight of the soil
ν_s	Poisson's ratio for sand
σ_s	Stress in the soil
σ_v	Vertical stress in the soil
σ_{vo}	Effective overburden pressure at pile point
σ_y	Yield stress under uniaxial tension
[B]	Strain-displacement transformation matrix
$[C]_i$	Constitutive matrix
$[D]_i$	Inverse of $[C]_i$
$[D_{ep}]$	Modulus matrix
[F]	Vector equivalent nodal loads
[k]	Stiffness matrix of interface element
{q}	Nodal displacement matrix
{Q}	Vector of nodal forces

CHAPTER 1

INTRODUCTION

1.1 General

Large diameter pipe piles are commonly used for offshore foundation. Traditionally, a part of the soil inside the pile is replaced with a concrete plug to ensure sufficient capacity of internal soil (soil inside the pile). Use of concrete plug in the pipe piles has a number of disadvantages. Concrete grout shrinks with time and degrades. This causes the plug capacity to be reduced gradually. On the other hand, the concrete in pipe causes extra cost of foundation. To avoid the situation, more recently, use of tubular steel pile without concrete fill was proposed for Jamuna multi-purpose bridge in Bangladesh. It was assumed that the pile may be plugged during driving with soil arching near the pile tip. But due to uncertainty in its behaviour now concrete filled tube piles are used.

During installation of pile, a plug of soil will move up inside the pile, with the top of the soil maintaining approximately its original levels. Entrance of soil into the pile continues until the inner soil cylinder develops sufficient resistance to prevent further soil intrusion. If the stresses in the inner soil is sufficient to resist further soil intrusion, the pile will act as a closed ended pile. Thus if the shear resistance along the length of the soil plug exceeds the end bearing capacity at the base of the plug, the pile will fail in plugged mode. On the other hand pipe pile will fail in unplugged mode when shear failure occur between the soil plug and the pile shaft. Open ended pipe pile, therefore, might be used without any concrete plugging to achieve sufficient pile capacity if it can be ensured that the pile is acting in the plugged mode.

Kishida and Isemoto (1977) have demonstrated experimentally that arching action of soil within pipe piles lead to a high value of internal friction. If axial stress is increased at the base of the soil plug, due to arching, the increased axial stress will lead to a corresponding increase in the lateral stress and hence the skin friction. As a result shear capacity of the soil plug is increased considerably. If this shear capacity exceeds the end-bearing capacity of pile, the pile will fail in a plugged mode.

Development of arching in the internal soil plug depend on a number of factors such as depth of soil, relative movement of pile and soil, soil density, pile diameter etc. Thus the plugging in soil is a complex phenomenon. For this reason use of pipe pile without concrete grout requires extensive investigations and research. The present research includes the study of behaviour of open-ended pipe pile both numerically and experimentally. In the subsequent articles the scope and the main area of this research are briefly outlined.

1.2 Present State of The Art of Research Topic

Open-ended pipe piles are widely used for foundations in construction on both land and offshore. Most open-ended piles will fill up with soil during driving, but fail as closed ended piles during static loading (Paikowshy et al. 1990). This frequent occurrence of soil plugging increase the pile capacity sharply. In spite of this important effect, only limited attention has so far given to the subject.

Some attempts have been made to visualise the behaviour of plug in pipe piles. Kishida & Isemoto (1947) first demonstrated based on their experiments that arching of the soil within the pipe pile increases the internal friction to very high values. Matsumoto and Takei (1991) used wave theory to the offshore open-ended pipe pile to clarify the effects of the soil plug on the behaviour of the pile during driving. Comparisons with full scale measurements are necessary to examine the validity of their conclusions.

One dimensional analysis of the soil plug under partially drained condition in calcareous soil was performed by Randolph, Leong and Houlsby (1990). They used finite difference operators to estimate derivatives and either explicit or implicit integration in time. Solution procedure is implemented in computer program SPA (Soil Plug Analysis). An axisymmetric finite element analysis, based on the modified Cam Clay soil model was also performed and the experimental results have been simulated. These analytical and numerical model do not carry out the full description of real situation. Application of the analysis has concentrated on carbonate soils and the assumptions comparable internal and external friction during static loading is highly conservative and inconsistent with the recent experimental evidence.

Effects of plugging on pile performance and design are examined by Paikowsky et al (1990) in reference to the aspects: ultimate static capacity, time dependent pile capacity and dynamic behaviour. The investigation does not attempt to provide solutions to the associated engineering problems and the results presented can not be applied to all pile diameters. Besides, results of static and dynamic pile testing with open-ended steel piles driven into soft rock are presented by Matsumoto, Michi and Hirano (1995). Thus all of the results provide reliable data for further research in understanding the behaviour of unplugged pipe pile.

1.3 Objectives of The Research

This research is aimed at studying the behaviour and the load transfer mechanism of open ended steel pipe piles. The principal objectives of the present research are

a) to observe the load settlement responses of open-ended pipe piles for pipes of different diameters with different depths of penetrations;

b) to observe the load transfer phenomenon and the distribution of stress in the pile, and internal and external soil;

c) to determine the parameters affecting the development of plugging in the internal soil and recommend on the values required to develop plugging;

d) to verify Randolph (et al. 1990)'s one dimensional formula of calculating plug capacity;

e) to observe experimentally the frictional resistance of soil within a pipe pile for different depths.

f) to simulate the experimental results numerically and explain the soil behaviour based on analysis.

1.4 Scope of The Research

Ultimate goal of the research was to determine the principal parameters affecting bearing capacity of pipe piles. It is evident that depth of soil and the diameter of the pile play an important role on the bearing capacity of pile. Since the friction of the outer soil can be determined in the same way as that of solid pile, emphasis were given on the behaviour of the soil within the pile.

In order to study the effect of internal soil depth and diameter of pile on plugging and on bearing capacity of pile numerically, finite element analysis was performed with varying diameter of piles with different depth of pile penetration. Three diameter (102 mm, 152 mm and 203 mm) were used in this analysis. Depth of penetration of piles were taken as 5, 10, and 15 times the pile diameter in all cases.

Effect of the depth of soil on the development of soil plug is determined from the above analysis. Depth of soil required for the development of plugging is then recommended.

Experiments were performed to investigate the response of the internal soil only. Effects of depth on plug capacity are studied extensively for 102 mm diameter pile. Depth of soil used in the tests were 5, 7, 9 and 11 times the pile diameter. Properties of the soil and pile material were determined from the laboratory experiments.

Plugged and unplugged behaviour of the piles are interpreted from experimental results reviewed through numerical analysis under various boundary conditions.

CHAPTER 2

LITERATURE REVIEW

2.1 Introduction

Bearing capacity of a pipe pile largely depends on the skin friction of the soil within and outside the pile. Internal skin friction depends on the arching of the internal soil. Arching phenomena is the outcome of loading in a hollow pile under a particular geometric configuration with a certain material properties. This field of study attracted many researchers due to its application in the construction industry. Load transfer mechanism of open-ended pipe piles has also been an area of interest.

Interest in the mechanical behaviour of soils arose historically from the needs of construction on soils. Simulation of geomechanical behaviour are hampered partly by the heterogeneity of the soil and partly by the complicated mechanical material behaviour. Understanding of the behaviour of soil can be achieved if intelligent simplifications of real soil are made and analysis are performed using simplified models of the real soil. A review of the constitutive models used in Geomechanics and load transfer mechanism of pipe piles are presented in this chapter from the available literature.

2.2 Bearing Capacity of Pipe Piles

According to the static approach of calculation, ultimate load capacity of an open-ended pipe pile can be estimated by using one of the following equations as appropriate:

$$Q_{up} = \sum f_{so} A_o + \sum f_{si} A_i + q_p A_t \qquad 2.1$$

$$Q_{pl} = \sum f_{so} A_0 + q_p A_p \qquad 2.2$$

where,

Q_{up} = ultimate axial load capacity (Unplugged mode)

Q_{pl} = ultimate axial load capacity (plugged mode)

f_{so} = ultimate unit shaft friction outside the pile

f_{si} = ultimate unit shaft friction inside the pile

A_o = shaft area of the pile outside

A_i = inside shaft area of the pile

A_p = cross sectional area of the pile base

A_t = cross sectional area of the steel tip

q_p = unit end bearing capacity. It is assumed same for both the steel area and total cross section

Under static loading in compression open-ended pipe pile shows tendency to fail in unplugged mode with shear failure occurring between the soil plug and the pile shaft until the shear capacity along the length of the internal soil exceeds the end bearing capacity at the base of the pile. In unplugged mode pile fails through entering of soil into the pile. In that case the ultimate capacity of the pile can be determined by the equation (2.1).

Kishida and Isemotto (1977) have demonstrated experimentally that arching action occurs within pipe piles, leading to very high values of internal friction. Consequently, as load is applied to the base of the soil plug, the increased axial stress will lead to a corresponding increase of lateral stress and hence the skin friction at the pile-soil interface. At a stage inner-soil cylinder develop sufficient resistance to prevent further soil intrusion. Thus the pile is plugged and it acts as a closed ended pile. Capacity of closed ended pile can be obtained by using equation (2.2).

To evaluate the stress components in a working pile, the load transfer mechanism of the pile should be properly understood. Following sections discuss the load transfer mechanism of plugged and unplugged pipe pile.

2.2.1 Skin friction of the internal soil

Fig.2.1 shows idealized stress conditions in an open ended pipe pile under (a) unplugged and (b) plugged condition. Skin friction of the internal soil plays an important key role in determining whether the soil will fail in unplugged mode or plugged mode. The term $\sum f_{si} A_i$ in equation (2.1) express the contribution of skin friction of the internal soil. In granular soil the value of f_{si} depends on various factors, such as soil density, surface roughness. Even with these factors, an identical shaft friction depend on the arching phenomenon and the normal stress along the interface (Paikowsky 1989). For a pipe pile of internal diameter

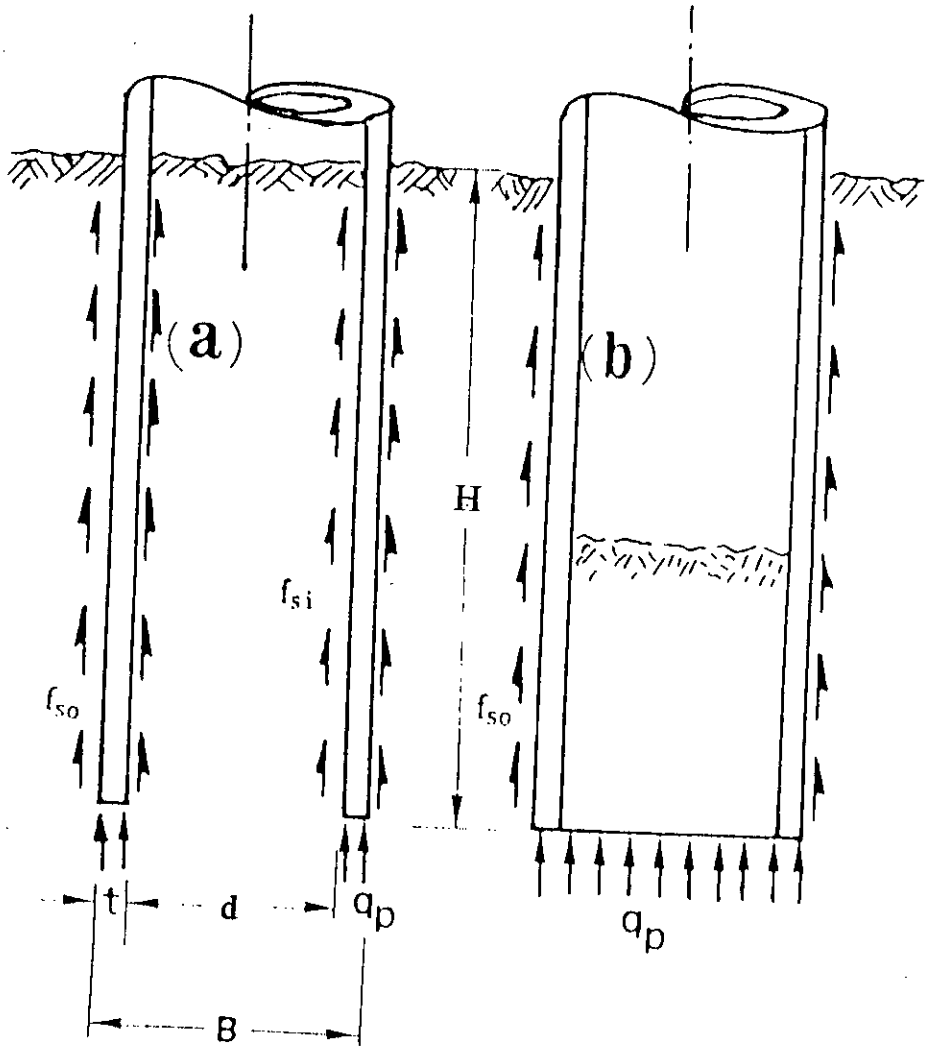

Figure 2.1 Stresses acting on open pipe pile under (a) Unplugged and (b) plugged conditions

d, containing a soil plug of overall length h, if the average internal skin friction is assumed to be f_{si}, the accumulated inside skin friction will be given by

$$Q_i = \pi d h f_{si} \qquad 2.3$$

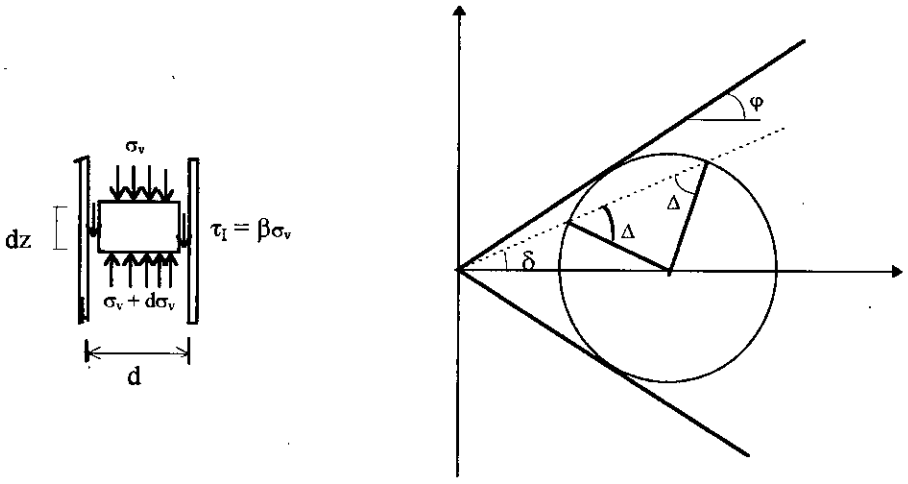

Figure 2.2 Stress condition within soil plug.

A simple analytical treatment of the soil plug response under drained condition has been presented by Randolph (1988). As an one dimensional idealisation, the soil plug is treated as a series of horizontal disc (Fig. 2.2), with each disc acted upon by vertical stress, σ_v at the top and $\sigma_v + d\sigma_v$ at the bottom and shear stress, f_{si} at the pile wall. The internal shear stress between the soil and the pile wall was related to the local vertical stress as

$$f_{si} = \beta\sigma_v$$

The value of β will depend on the ratio of horizontal to vertical effective stress in the plug, which is difficult to estimate. However, for design purposes a minimum value of β may be obtained by assuming that the soil near the edge of the plug is of active failure, with internal angle of friction φ and interface friction angle between soil and pile, δ. From the limiting Mohr's circle (Fig. 2.2) it may be shown that

$$\beta = \frac{\mathrm{Sin}\varphi\mathrm{Sin}(\Delta - \delta)}{1 + \mathrm{Sin}\varphi\mathrm{Cos}(\Delta - \delta)} \qquad 2.4$$

Where $\Delta = \mathrm{Sin}^{-1}\left(\frac{\mathrm{Sin}\delta}{\mathrm{Sin}\varphi}\right)$

Consideration of the vertical equilibrium of each horizontal slice of soil leads to an expression for the effective stress at any depth z,

$$\sigma_v' = p + \left(e^{4\beta z/d} - 1\right)\left(p + \frac{p\gamma'}{4\beta}\right) \qquad 2.5$$

where p is an initial effective surcharge acting at $z = 0$ and γ' is the effective unit weight of the soil.

At the base of a soil plug of height h, where the initial effective stress is $p + \gamma' h$, the limiting end bearing capacity in excess of the initial effective stress is:

$$q_l = \left(e^{\alpha} - 1\right)\left(p + \frac{\gamma' h}{\alpha}\right) - \gamma' h \qquad 2.6$$

This bearing capacity is equivalent to that given by equation (2.3). For the case of zero surcharge, the plug capacity is

$$q_i = \left(\frac{e^{\alpha} - 1}{\alpha}\right)\gamma' h \qquad 2.7$$

If this end bearing capacity of soil plug exceeds the ultimate static bearing capacity of the soil below the toe of the pile, then the pile behaves as though it is closed ended pile, otherwise it behaves as a unplugged pile.

When a pile is loaded under static condition, axial stress at the base of the pile increases. The effects of stress increase at the base of the soil plug will gradually propagate up the plug. To mobilise the internal skin friction local relative displacement between the central part of the plug and the pile wall is necessary. The displacement to mobilise internal skin friction is proposed to be of the order of 0.2-0.5% of the pile diameter (Randolph, 1987). The length of plug over which internal skin friction is mobilised is active length of plug (Fg.2.3). Weight of the soil above that depth may be treated as surcharge. For analyses it is

convenient to take the datum for z at the depth where skin friction mobilisation start.

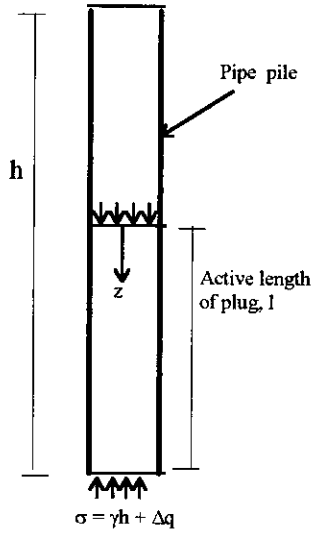

Figure 2.3 Concept of active length of soil plug.

2.2.2 Skin friction of the outer soil

The interaction between the soil and the pile is very complex and poorly understood. A little attention has been given so far in the theoretical determination of side friction in sand. Meyerhof (1959) and Nordlund (1963) considered this portion of bearing capacity of piles with adequate attention. The determination of the ultimate unit side resistance f_{so}, is based on the laws of mechanics, considering friction between two different surfaces. The magnitude of f_{so} is commonly determined using

$$f_{so} = Kp \tan\delta \qquad 2.8$$

in which K is the coefficient of lateral earth pressure, p is the average effective overburden pressure along the segment of pile being considered and tanδ is the coefficient of friction between pile and the soil.

Meyerhof and Nordlund dealt theoretically with the problem of the determination of the lateral earth pressure coefficient, K. Potyondy (1961) determined the coefficient of friction between various construction materials and

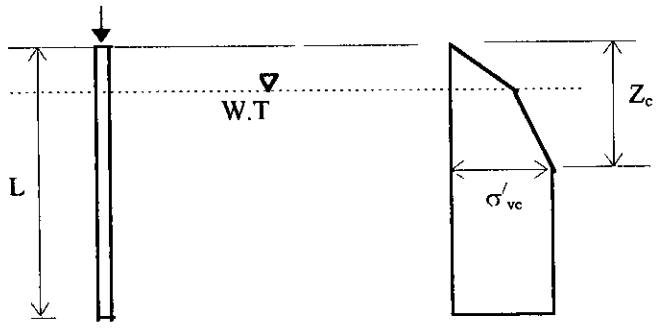

Figure 2.4 Simplified distribution of vertical stress adjacent to pile in sand

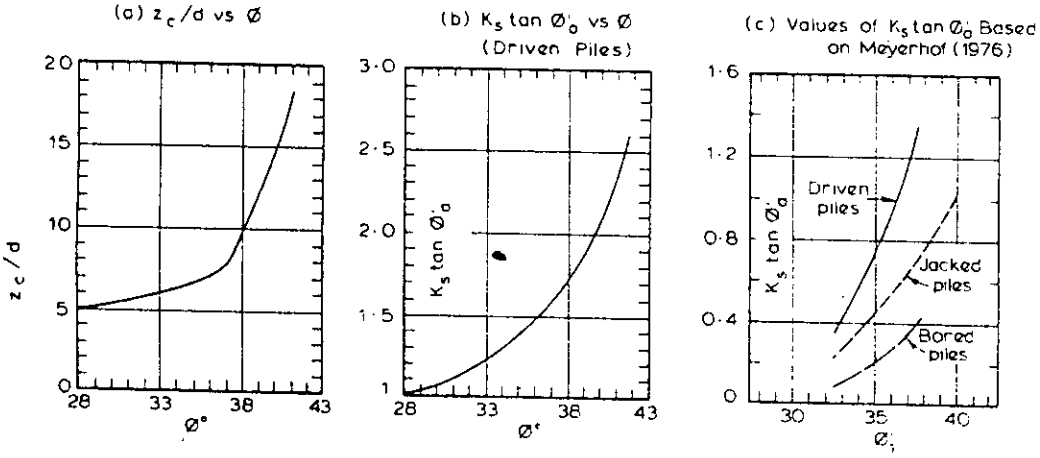

Figure 2.5 Values of z_c/d and $K_s \tan\varphi_a'$ for piles in sand

cohesionless soils using direct shear tests in the laboratory. In addition to the determination of the coefficient of friction, tanδ between the soil and the pile materials, the angle of internal friction of the sand, φ was also determined.

Vesic (1977) proposed a different approach for the determination of tanδ. The sand located at the interface between the soil and the pile is considered to be at a state of ultimate failure for determination of side resistance. Consequently the angle of friction between the pile and the soil, δ is independent of the soil density and pile material. It is considered equal to the residual friction angle of the sand, φ_{res} .

Some design approaches have effectively incorporated Vesic's findings by specifying an upper limit to the shaft resistance. An idealised distribution of effective vertical stress, σ_v' with depth adjacent to a pile in shown in Fig.2.4. σ_v' is assumed to be equal to the overburden pressure up to some critical depth z_c , beyond which σ_v' remains constant. Then the frictional contribution of the outer soil is given by

$$Q_s = \int f_{so} dA_s = \int_0^L c\sigma_v' k \tan\delta dz \qquad 2.9$$

c is a factor provided to calculate skin friction area.

On the basis of the test results of Vesic (1967), values of Ktanδ and the dimensionless critical depth Z_c/d have been evaluated. Meyerhof (1956) also suggested more appropriate values of these parameter. Relationship between K tanδ and φ and Z_c/d and φ are shown in Fig. 2.5.

2.2.3 Skin friction by β method

Three procedures are currently used for computing the skin resistance of piles in cohesive soils. These will be called α, λ and β methods. The β method is also used for pile in cohesionless soils and hence discussed here. In all the methods the skin resistance capacity part of the bearing capacity equation is computed as

$$p_s = \sum A_s f_s$$

where f_s = skin resistance to be computed

A_s = effective pile surface area on which f_s acts.

The β method was suggested by Burland (1973) and makes the following assumption:

1. Soil remoulding adjacent to the pile during driving reduces the effective stress cohesion intercept on a Mohr's circle to zero.

2. The effective stress acting on the pile surface after dissipation of excess pore pressures generated by volume displacement is at least equal to the horizontal effective stress (K_o) prior to pile installation.

3. The major shear distortion during pile loading is confined to a relatively thin zone around the pile shaft and drainage of this thin zone occurs rapidly during loading - or has already occurred in the delay between driving and loading.

With these assumptions Burland (1973) developed a simple design equation written as

$$f_s = K\bar{q}\tan\delta \qquad 2.10a$$

Taking $\beta = K\tan\delta$, the equation for skin resistance can be written as

$$f_s = \beta\bar{q} \qquad 2.10b$$

Since $\bar{q}$ = effective overburden pressure at z_i, modifying for a surcharge q_s to

$$f_s = \beta(q + q_s) \qquad 2.10c$$

As previously used, $\bar{q}$ = average effective vertical stress for the ith element of length L and the friction coefficient, $f = \tan\delta$. So an estimate for the soil-to-pile friction angle must be made.

Most authorities agree that f_s in Eq. (2.10) does not increase indefinitely with depth but rather, beyond some critical depth L/B it increases at an ever decreasing rate. Bhushan (1982) suggests for large displacement piles (closed end pipe, solid concrete, possibly open end pipe with a plug) that a reasonable estimate for K and β be as follows:

$$\beta = K \tan\delta = 0.18 + 0.0065D_r \qquad 2.11$$
$$K = 0.50 + 0.008D_r$$

where D_r is the relative density (as a percent). SPT correlation might be used to obtain D_r with depth.

Zeitlen and Paikowsky (1982) suggest that the "limiting f_s" can be accounted for the decrease in φ with effective normal confining pressure using the following equation:

$$\varphi = \varphi_o - 5.5 \log \frac{\overline{q_{en}}}{q_0} \qquad 2.12$$

where φ is the angle of internal friction at the effective normal pressure $\overline{q_{en}}$ at depth of interest, φ_o is the reference angle obtained at an effective normal pressure q_o.

Some persons suggest a maximum for δ on the order of 0.5 to $0.75\varphi'$, while others routinely use φ'. It has already been pointed out that δ is dependent on the normal pressure at the interface of soil and pile.

Finally, the lateral earth pressure coefficient is questioned. While some use the given equation (2.11) for K in terms of relative density, there are others who use somewhat arbitrary choices based on load tests performed or reported in the literature. For example, Mansur and Hunter (1970) in an extensive pile test program found values as follows

TABLE 2.1 - Recommended value of lateral earth pressure coefficient for different pile

Type of pile	Lateral earth pressure co-efficient
H piles	1.4 to 1.9
Pipe piles	1.2 to 1.3
Precast square concrete piles	1.45 to 1.6
Timber (1 test)	1.25
Tension test (8 all types)	0.4 to 0.9

2.2.4 End bearing

The theoretical determination of the point load has received intensive attention through the years. According to Vesic (1967) the theoretical approach to solve this problem was started by Prandtle (1920) and Reissner (1924). They initiated with the assumptions that soil is elasto-plastic material and the failure is punching failure (Fig.2.6). Main characteristics of a punching failure is that there will be no well defined shear zones at the sides of the footing and no heave will occurs. Terzaghi (1943) extended the classical work on punching failure done by Prandtl and Reissner.

Meyerhof (1953) proposed rigid plastic soil model which means that there are no strains at any point until the failure condition is fulfilled (Fig.2.7a). On the other hand Bishop Collingridge and O'Sullivan (1948) and Vesic (1977) considered the soil to be compressible which was more realistic (Fig.2.7b) Vesic considered soil failure induced by the pile point as a special case of the expansion of a cavity inside a solid mass (Fig. 2.9).

In all the theoretical solution the ultimate unit point resistance, q_o is usually expressed in the form (Coyle and Castello, 1981):

$$q_o = \gamma_s b N_\gamma S_\gamma + C N_c S_c + \sigma'_{vo} N_q S_q \qquad 2.13$$

where, γ_s is the effective unit weight of the soil at the pile points, b is the least foundation dimension, σ'_{vo} is the effective overburden pressure at the pile point level; C is the cohesion of the soil, S_γ, S_c , S_q are the shape factors and N_γ, N_c, N_q are bearing capacity factors, usually depending upon the soil friction angle and the assumed pattern or mechanism of failure.

The first term of the equation (2.13) is very small in comparison to the remaining part and can be neglected. For cohesionless soil the second part of the equation can be neglected. The final simplification concerns thus the form of the remaining term. For pipe pile of circular shape the shape factor is same and so it is reasonable to use the only bearing capacity factor N_q that incorporates this constant shape factor. Therefore, the commonly used form of end bearing capacity,

$$q_p = \sigma'_{vo} N_q \qquad 2.14$$

Vesic observed that ultimate base resistance become constant beyond a certain depth of penetration known as critical depth. That is, the end resistance,

$$q_p = \sigma'_{vo} N_q \leq q_{max}$$

q_{pmax} is the limiting value of q_p at the critical depth D_c.

For loose sand $D_c \cong 7B$
For medium dense sand $D_c \cong 15B$
For dense sand $D_c \cong 18B$

The limiting point bearing in a cohesionless soil is given for $D/B \geq D_c/B$ as

$$q_{max} = A_p(50N_q)\tan\varphi \qquad 2.15$$

All of the bearing capacity theories require the evaluation N_q for the use in Eq.(2.14), should be considered. A summary of the ranges of values of N_q according to the different theories is presented in Table 2.2. It is evident that there are major deviation from one theory to another, leading to the conclusion that the true failure mechanism is not, generally well understood. Zeitlen and Paikowsky (1982) proposed relation of N_q which may be used for pipe pile.

2.3 Constitutive Models

Soil shows inelastic or plastic behaviour when loaded. For this, recent finite element analysis incorporates a elastic-plastic strain hardening-softening soil models. Study and analyses of the behaviour of materials that experience plastic deformation constitutes the theory of plasticity. Thus the reviews in this section are mainly based on information of the theory of plasticity.

The modelling of materials is primarily governed by their stiffness and strength of the materials. Coulomb (1776) gave a kaleidoscopic views on geotechnical engineering, the formulation of the friction law with cohesion and the calculations related to an earth retaining wall. The first plasticity model involving stresses and concerning the strength was formulated by Tresca in 1868. He included shear criteria for the yielding of materials. In 1882, Mohr

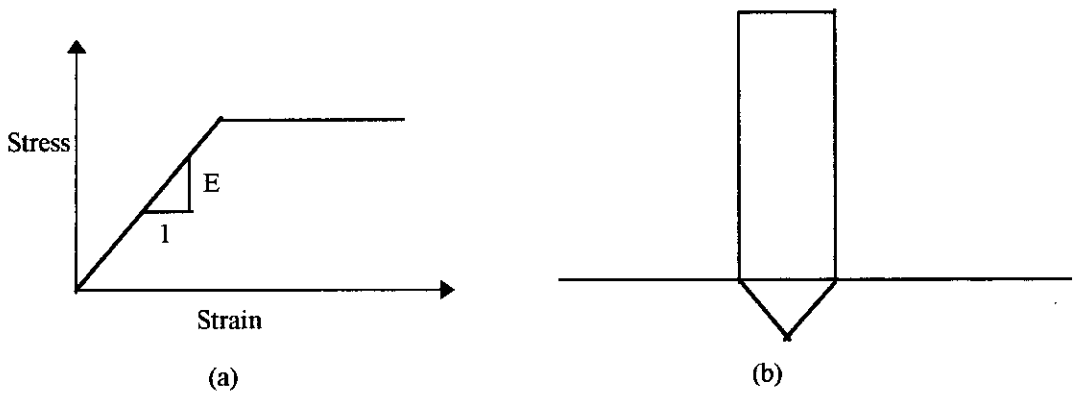

Figure 2.6(a) Stress - Strain diagram for Elasto Plastic Material
(b) Punching Failure Pattern

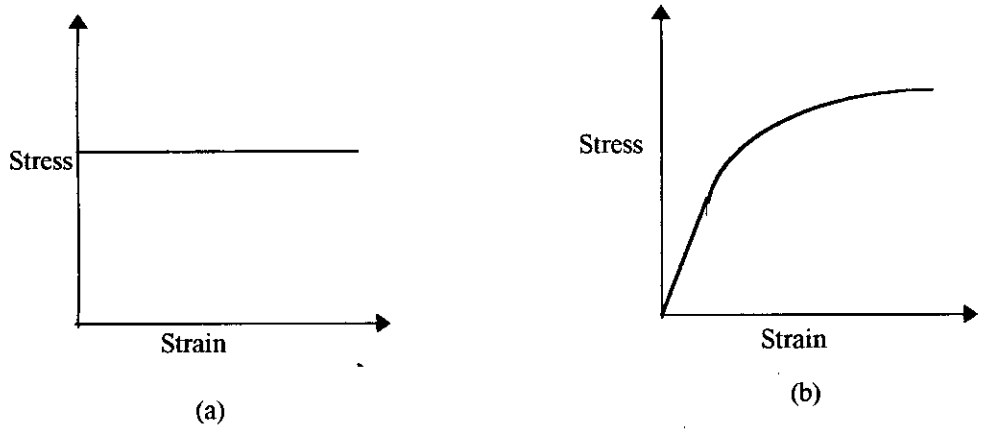

Figure 2.7 (a) Stress - Strain curve for Plastic Material
(b) Stress - Strain Curve for Comprsssive Material

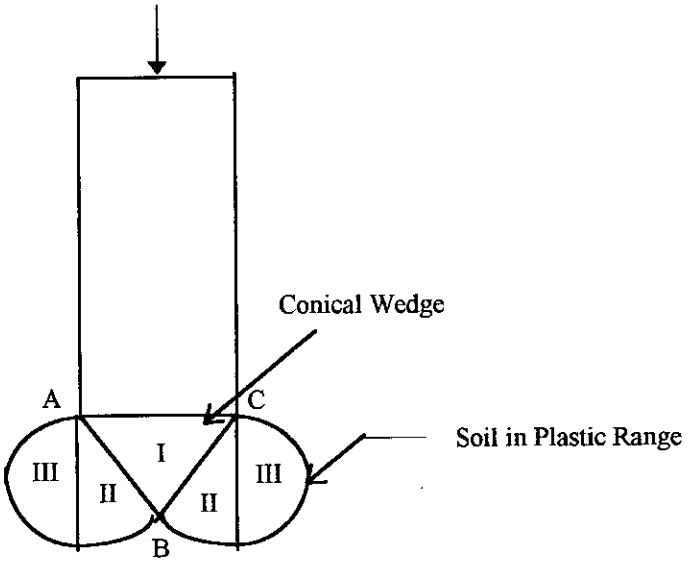

Figure 2.8 Vesic Model of Pile Behaviour

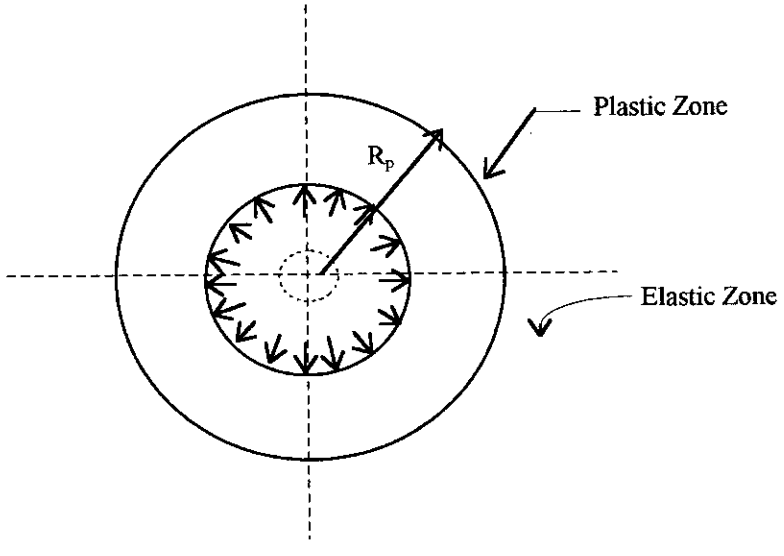

Figure 2.9 Expansion of a Spherical Cavity

represented failure by a line tangential to circles representing the stress conditions at failure. von Mises formulated a yield criterion for metals based on a strain energy per unit of volume in distortion as a criteria for failure. Development of Geomechanical modelling began immediately after an era of huge mathematical impulse from the work of Bernouli, Euler, Leibnitz, Green etc. Here follows a brief description of some constitutive models.

2.3.1 Elasticity model

For an elastic materials, the state of stress is a function of the current state of deformation only. An elastic medium returns to its initial state after a cycle of loading and unloading.

An elastic materials in general can be non-linear (Fig 2-10(a)). A special case is that of linear elastic behaviour (Fig. 2-10(b)). The linear elastic Hooke's law is the simplest example of a constitutive law; for uniaxial loading it can be expressed as:

$$\sigma = E\varepsilon \qquad 2.16$$

where σ is the stress, ε the strain and E the response parameter commonly known as the Young's modulus.

For three dimensional bodies, the generalised Hooke's law can be expressed as:

$$\sigma_{ij} = C_{ijkl}\varepsilon_{kl}$$

or

$$\{\sigma\} = [C]\{\varepsilon\} \qquad 2.17$$

In general, the relation for non-linear elastic law can be expressed as a unique relation stress and strain as:

$$\sigma_{ij} = f_{ij}(\varepsilon_{kl}) \qquad 2.18$$

where the f_{ij} are response functions.

Table 2.2 - Bearing Capacity Factors for Deep Foundation (Vesic, 1972, 1977)

Theories	Approximate N_q Values for Various Friction Angles, φ , in degree				
	25	30	35	40	45
De Beer (1945)	59	155	380	1150	4000
Mayerhof (1953): Driven piles	38	89	255	880	4000
Caquot-Kerisel (1956)	26	55	140	350	50
Brinch Hansen (1961)	23	46	115	350	1650
Skempton-Yassin-Gibson (1953)	46	66	110	220	570
Brinch- Hansen (1951)	32	54	97	190	400
Berezantsev (1961)	16	33	75	186	----
Vesic (1963)	15	28	58	130	315
Vesic (1972): $I_r = 60$	36	46	57	70	84
$I_r = 200$	60	79	103	131	164
Terzaghi (1943): General shear	12.7	22.5	41.4	81.3	173.3
: Local shear	5.6	8.3	12.6	20.5	53.1

I_r = Rigidity Index

Basic laws and equations governing problems in engineering are derived on the basis of the energy stored in a body. There is a definite relationship between the potential of force spent to perform work in deforming a body and the internal strain energy due to deformation. On the basis of this concept Cauchy and Green derived constitutive laws for non-linear elasticity of hyperelastic materials (Desai & Siriwardane, 1984, pp 83). Cauchy's approach is based on the assumption that for elastic material stress is a function of strain. Green's elastic material models are derived, based on the concept that no energy is dissipated during the deformation process.

The behaviour of hypo-elastic material is dependent on the stress path followed. Behaviour of such materials can be simulated from increment to increment rather than for entire load or stress at a time. A simplest form of constitutive law can be expressed as:

$$\sigma_{ij}^{\bullet} = C_{ijkl}\varepsilon_{kl}^{\bullet} \qquad 2.19$$

where σ is the stress, $\sigma^{\bullet}$ the rate of stress, ε the strain and $\varepsilon^{\bullet}$ the rate of strain. C_{ijkl} is the response function of only the stress tensor.

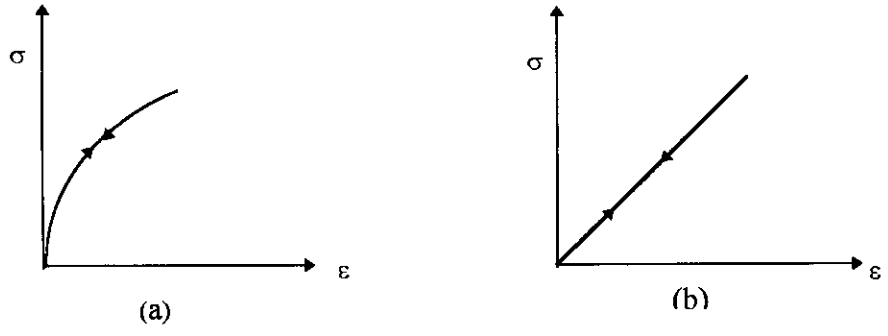

Figure 2.10 Elastic models: (a) nonlinear elastic; (b) linear elastic

2.3.2 Plasticity models

Materials that retain a part of the deformation on unloading is called inelastic or plastic materials. When plastic material is loaded both elastic and plastic deformation will occur.

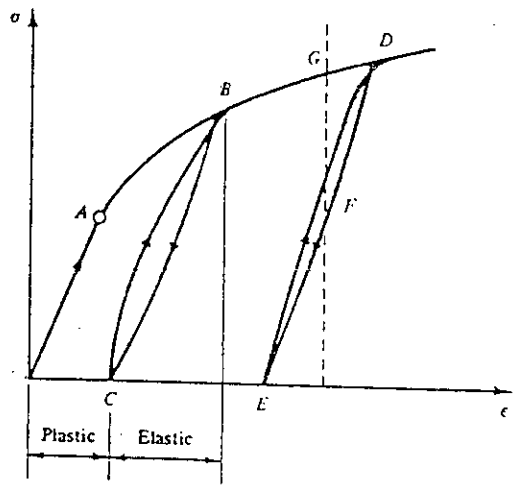

Figure 2.11 Typical stress-strain curve for metal under uniaxial tension

In plasticity models, total incremental strain is decomposed into

$$d\varepsilon_{ij} = d\varepsilon_{ij}^{e} + d\varepsilon_{ij}^{p}$$

where the superscripts e and p denote elastic and plastic components respectively.

The elastic strain increment is assumed to be completely described within the framework of incremental Hooke's law, when bulk modulus κ and shear modulus, G can be a relevant function of stress invariant or other state variables.

Two major aspects that constitute the theory of plasticity are the yield criteria and post yield behaviour. The yield criteria can be defined as the limit of elastic deformations expressed by a combination of states of stress. In case of yielding of materials under three-dimensional states of stress, it is convenient to define a scalar function F as the yield criteria.

$$F=F(\sigma_{11},\sigma_{22},\sigma_{33},\sigma_{12},\sigma_{23},\sigma_{13}) \qquad 2.20$$

This can also be expressed more conveniently in term of the invariant of the stress tensor as follows:

$$F = F(J_1, J_2, J_3) \qquad 2.21$$

where J_1 , J_2 and J_3 are the invariant of the stress tensor.

Experimental evidence shows that the yielding of a metal is not affected significantly by moderate hydrostatic pressure (Desai & Siriwardane, 1984). This leads to the conclusion that the yield criterion depends essentially only on the deviatoric stress. Therefore, the yield function can be expressed in terms of the invariant of the deviatoric stress tensor as

$$F(J_{2D}, J_{3D})=0 \qquad 2.22$$

where J_{2D} and J_{3D} are the second and third invariant of the deviatoric stress tensor.

Different proposed yield criteria are discussed in the following sections.

(a) Tresca model

Tresca (1869) proposed that yield criterion depends only on the invariant of deviatoric stresses S_{ij} . According to this criterion, yielding will initiate when the maximum value of the extreme shear stress is reached. In this theory, yield strength in tension and compression has been assumed to be equal. The Tresca criterion can be expressed in terms of principal stresses as follow:

$$\begin{aligned} \sigma_1 - \sigma_3 &= \pm \sigma_y \\ \sigma_2 - \sigma_3 &= \pm \sigma_y \\ \sigma_3 - \sigma_1 &= \pm \sigma_y \end{aligned} \qquad 2.23$$

where σ_1 , σ_2 and σ_3 are major, intermediate and minor principal stresses respectively and σ_y is yield stress of material under uniaxial condition.

The equation of yield surface can be written as:

$$[(\sigma_1 - \sigma_2)^2 - 4k^2]\,[(\sigma_2 - \sigma_3)^2 - 4k^2]\,[(\sigma_3 - \sigma_1)^2 - 4k^2] = 0 \qquad 2.24$$

where k is the yield strength of material determined from pure shear. According to Tresca yield criterion,

$$k = \frac{1}{2}\sigma_y .$$

The equation represent a hexagonal prism whose generator is parallel to the hydrostatic axis ($\sigma_1 = \sigma_2 = \sigma_3$) in principle stress space [Fig. 2.13(a)]. It is a regular hexagon on π plane (Fig. 2.14) and symmetric hexagon on $\sigma_1 = \sigma_2$ plane (Fig. 2.15).

In case of frictional materials, yielding will depend on first invariant of stress tensor (hydrostatic pressure) in addition to invariant of deviatoric stress. To include the effect of hydrostatic pressure Tresca criterion is modified as:

$$\frac{f(J_2, J_1)}{I_1 + C_1} = C_2 \qquad 2.25$$

(b) von Mises yield criteria

von Mises suggested in 1913 that yielding will initiate when the second invariant of the deviatoric stress tensor reaches a certain value. Actually, this criteria assumes that yielding begins when the distortional energy reaches a value that is equal to the distortional energy at yield in simple tension. According to this criterion, material will yield if

$$J_{2D} = k^2$$

$$\text{i.e. } \frac{1}{6}\left[(\sigma_{11} - \sigma_{22})^2 + (\sigma_{22} - \sigma_{33})^2 + (\sigma_{33} - \sigma_{11})^2\right] + \sigma_{12}^2 + \sigma_{23}^2 + \sigma_{13}^2 = k^2 \qquad 2.26$$

where is a material constant, one can find that , $k = \frac{\sigma_y}{\sqrt{3}}$

von Mises criteria can be represented by a cylinder in the principle stress space [Fig.2.13(b)]. It represent a circle on π plane and an ellipse on $\sigma_1 = \sigma_2$ plane.

To include the effect of hydrostatic pressure von Mises criteria is extended as:

$$\frac{\sqrt{J_2}}{I + C_3} = C_4$$

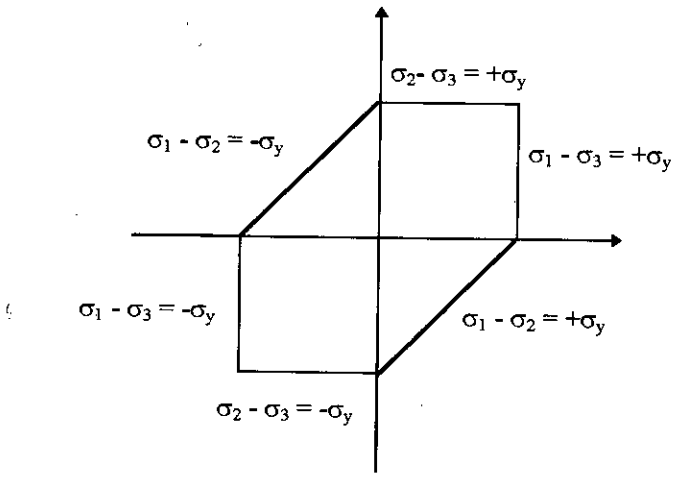

Figure 2.12 Tresca yield criterion under plane stress-state ($\sigma_3 = 0$)

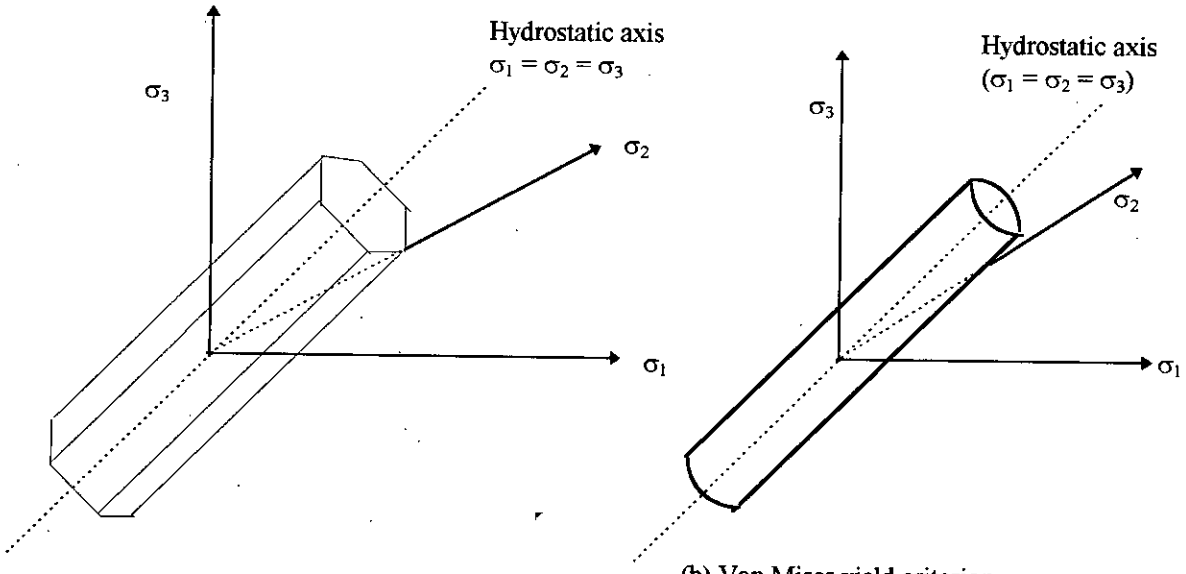

(a) Tresca yield criterion

(b) Von Mises yield criterion

Figure 2.13 Perfectly plastic yield criteria

(c) Mohr- Coulomb model

Above yield criteria are valid for metals which are considered frictionless. Mohr-Coulomb criteria define the yield criterion of frictional materials. According to the Mohr-Coulomb criterion, the shear strength increases with increasing normal stresses on the failure plane.

$$\tau = C + \sigma\tan\varphi \qquad 2.27$$

where τ is the shear stress on the failure plane, C the cohesion of the material, σ the normal effective stress on the failure surface and φ the angle of internal friction.

The Mohr-Coulomb criteria ignores the effects of intermediate principle stress. In the principle stress space this criteria can be described as:

$$\frac{1}{2}(\sigma_1-\sigma_3) = \frac{1}{2}(\sigma_1+\sigma_3)\mathrm{Sin}\varphi + C\cos\varphi \qquad 2.28$$

where σ_1 and σ_3 are the major and minor principle stresses respectively.

This equation represents an irregular hexagonal pyramid in the stress space (Fig.2.16); the projection of this surface on the π- plane is shown in Figure 2.17.

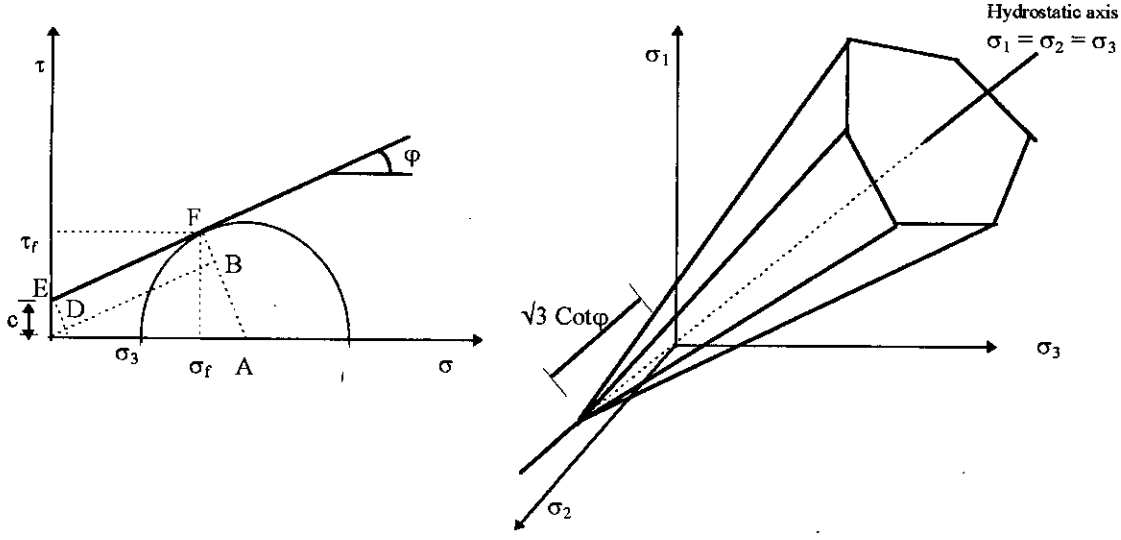

Figure 2.16 Mohr-Coulomb criteria

Its representations can be changed to a more convenient form in term of J_1, J_{2D} and θ (Lode angle) in a three dimensional space as:

$$f = J_1 \mathrm{Sin}\varphi + \sqrt{J_{2D}}\mathrm{Cos}\theta - \frac{\sqrt{J_{2D}}}{3}\mathrm{Sin}\varphi\mathrm{Sin}\theta - c\mathrm{Cos}\varphi = 0 \qquad 2.29$$

$$\text{where } \theta = -\frac{1}{3}\mathrm{Sin}^{-1}\left(-\frac{3\sqrt{3}}{2}\cdot\frac{J_{3D}}{J_{2D}}\right) \quad \text{and} \quad -\frac{\pi}{6} \le \theta \le \frac{\pi}{6}$$

Mohr-Coulomb model can represent the strength characteristics of most of the geotechnical materials quite reasonably.

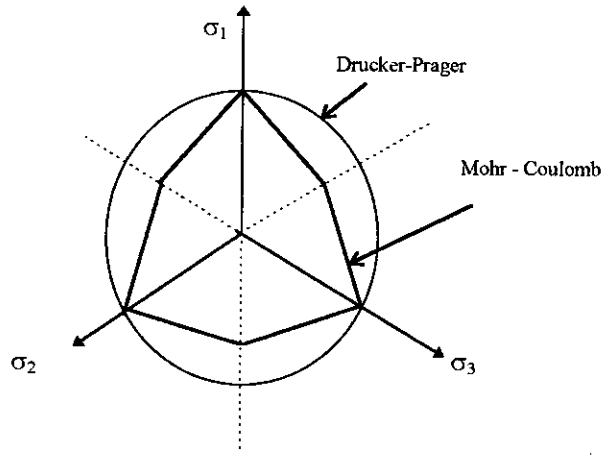

Figure 2.17 Mohr - Coulomb and Drucker - Prager criteria on the π - plane

(d) Drucker-Prager model

Drucker and Prager (1952) suggested a yield surface using the invariant of the stress tensor. The generalised criteria can be written as ;

$$f = \sqrt{J_{2D}} - \alpha J_1 - \kappa \qquad 2.30$$

where α and κ are positive material parameters, J_1 is the first invariant of the stress tensor and J_{2D} is the second invariant of the deviatoric stress tensor.

The equation represent a straight line on a J_1 versus J_{2D} plot (Fig. 2.18). In the three dimensional stress space, the criterion plots as a right circular cone and the

projection on the π - plane is a circle (Fig. 2.19). When the state of stress reaches the failure surface (Eq.2.30), the material undergoes plastic deformations. According to the criterion, a state of stress outside the surface is not stable.

The value of α and κ of Drucker-Prager model can be expressed in terms of angle of internal friction φ and cohesion C .

For conventional triaxial compression

$$\alpha = \frac{2\mathrm{Sin}\varphi}{\sqrt{3}(3-\mathrm{Sin}\varphi)}$$
$$\kappa = \frac{6c\mathrm{Cos}\varphi}{\sqrt{3}(3-\mathrm{Sin}\varphi)} \qquad 2.31$$

For plane strain condition

$$\alpha = \frac{\tan\varphi}{\left(9+12\tan^2\varphi\right)^{1/2}}$$
$$\kappa = \frac{3c}{\left(9+12\tan^2\varphi\right)^{1/2}} \qquad 2.32$$

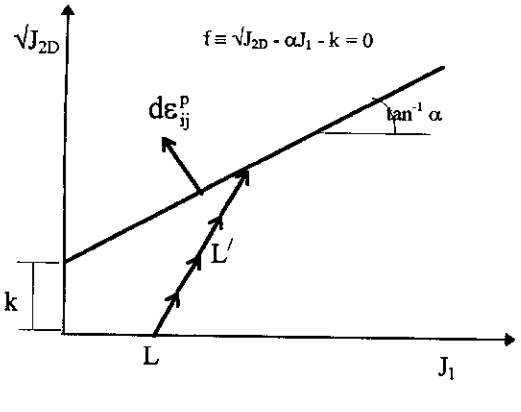

Figure 2.18 Drucker - Prager criterion

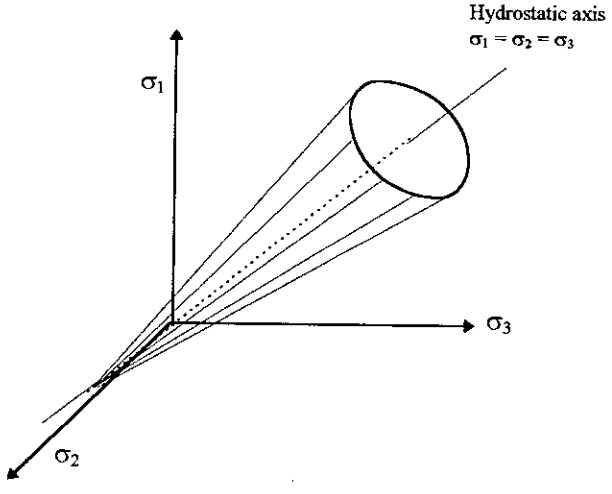

Figure 2.19 Drucker - Prager criteria on 3 - D space

2.4 Yielding of Soils Based on Theory of Plasticity

Many geologic materials experience plastic deformations almost from the very start of loading. During any loading path LL^1 (Fig. 2.18), the material undergoes a process of continuous yielding until it finally reaches the conventional failure or ultimate state defined by yield function, which may be considered as the final yield surface. At this state plastic shearing continue indefinitely without changes on volume or effective stresses. This condition of perfect plasticity is known as critical state. The attainment of critical state can be expressed by

$$\frac{\partial p'}{\partial \varepsilon_q} = \frac{\partial q}{\partial \varepsilon_q} = \frac{\partial v}{\partial \varepsilon_q} = 0 \qquad 2.33$$

These critical states were reached with an effective stress ratio,

$$\frac{q_{cs}}{p'_{cs}} = \eta_{cs} = M$$

In normally compressed soil, yielding first occurs with stress ratio $\eta<M$. Continued loading, whether drained or undrained, is associated with plastic hardening, expansion of yield loci, and increase of stress ratio until ultimately the perfectly plastic critical state is reached with $\eta=M$.

It is possible to define the foregoing behaviour by defining a series of yield surfaces prior to reaching the failure or the final yield surfaces. During the successive yielding, the material generally hardened and exhibits strain or work hardening behaviour. For such a hardening materials, when stress point moves beyond the current yield surface, a new yield surface is established. The yield surfaces that define the hardening behaviour are often called hardening caps. Here in the following sections two models are discussed that allow for the continuous yielding and hardening behaviour.

2.4.1 Cap models

The cap models are expressed in terms of three-dimensional state of stress and it is formulated on the basis of consistent mechanics. The model is composed of

moving caps that play the main role in defining yielding and the fixed yield surface used essentially to define the critical state. The fixed yield surface , which can be considered to be an ultimate yield surface, is expressed as:

$$f_1\left(J_1, \sqrt{J_{2D}}\right) = 0 \qquad 2.34\ a$$

and the yield caps are expressed as:

$$f_2\left(J_1, \sqrt{J_{2D}}, \kappa_1\right) = 0 \qquad 2.34\ b$$

Where κ_1 defines the deformation history and usually is taken as the volumetric plastic strain.

The fixed and moving yield surfaces are assumed to intersect such that the tangents to the yield surfaces at the intersection are parallel to the J_1 axis, implying no volume change once the fixed surface is reached. The yield surfaces intersect the J_1 axis at right angles, implying that under isotropic compression there are no shear deformations.

Fixed yield surface

In the cap model, the fixed surface was assumed to be composed of an initial portion of the Drucker-Prager envelope joined smoothly to the subsequent von-Mises surface (Fig.2.20). The expression for f_1 adopted by DiMaggio and Sandler (1971) is given by :

$$f_1 = \sqrt{J_{2D}} + \gamma e^{-\beta J_1} - \alpha = 0 \qquad 2.35$$

where α, β and γ are material parameter

Within the range of stress levels for the artificial soil, the failure surface was found to be somewhat different from Eq.2.35. It was assumed to be composed of an initial Drucker-Prager surface which is connected by a smooth curve to another Drucker- Prager surface at higher stress (Fig. 2.21).

A modified form of 'Drucker-Prager I' surface is

$$f_1' = \sqrt{J_{2D}} + \gamma e^{-\beta J_1} - \theta J_1 - \alpha = 0 \qquad 2.36$$

and the equation of 'Drucker-Prager II' surface is

$$f_1' = \sqrt{J_{2D}} - \theta J_1 - \alpha = 0 \qquad 2.37$$

where θ is an additional material parameter.

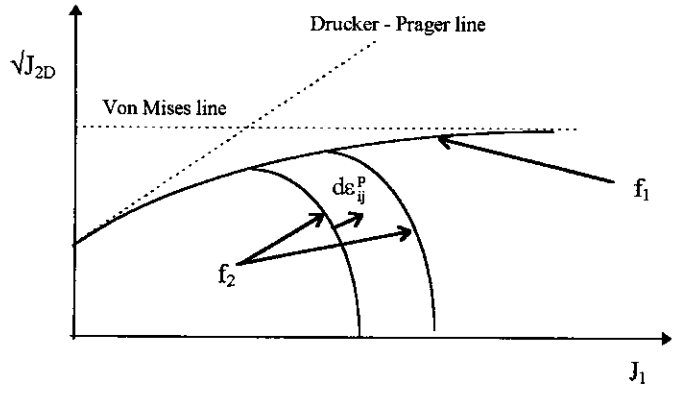

Figure 2.20 Cap model

Yield Caps

DiMaggio and Sandler adopted an elliptic cap for representing yield surfaces for the cohesionless materials. The expression for yield caps used was

$$f_2 = R^2 J_{2d} + (J_1 - C)^2 = R^2 v^2 \qquad 2.38$$

where Rb=(X-C)

R is the ratio of the major to minor axis of ellipse, X is the value of J_1 at the intersection of the cap with the J_1-axis, C is the value of J_1 at the centre of ellipse, and b is the value of $\sqrt{J_{2D}}$ when $J_1 = C$.

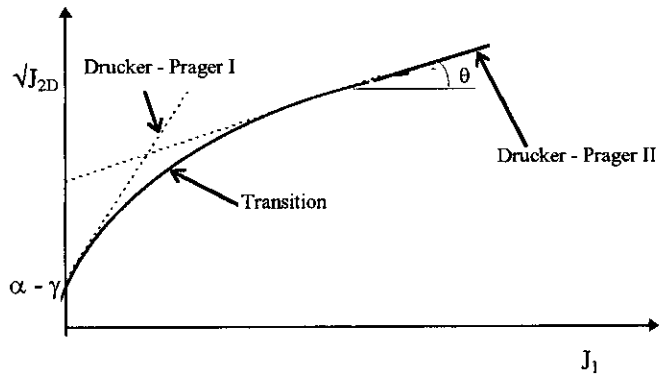

Figure 2.21 Interpretation of parameters of modified Drucker - Prager model

2.4.2 Cam Clay model

Cam-Clay is the name given to an elasto-plastic model of soil behaviour expressed on p-q plane. In this model, the critical state surface is treated as an open fixed yield surface, and additional yielding surfaces are introduced to account for the continuous yielding of soil.

Ultimate states or failure points lie on the same critical void ratio line. The slope of this line on the p-q plot is denoted by 'M', which is a material parameter (Fig.2.22).

$$M = \frac{q}{p'} \quad \text{where} \quad p' = \frac{p'_o}{2}$$

Along the critical state line, unlimited plastic shear strain develop with no plastic volumetric strain. This represent the fixed failure surface.

When cam-clay is yielding, the plastic work done is given by $Mp' \partial\varepsilon$. Therefore

$$p'\partial v^p + q\partial\varepsilon^p = Mp'\partial\varepsilon^p \qquad 2.39$$

Applying the condition of normality, the Cam-Clay yield locus can be derived as:

$$q = Mp' \ln\left(p'_c / p_1\right) \qquad 2.40$$

Modified Cam-Clay change the assumption for dissipated work in Cam-clay yielding to $p'\sqrt{\left\{\left(\partial v^p\right)^2+\left(M\partial\varepsilon^p\right)^2\right\}}$ and therefore

$$p'\partial v^p+q\partial\varepsilon^p=p'\sqrt{\left\{\left(\partial v^p\right)^2+\left(M\partial\varepsilon^p\right)^2\right\}}$$

The flow rule can be applied to find the modified yield locus as:

$$q^2+M^2p'^2=M^2p'p'_c$$

This equation describes a set of ellipses, all having the same shape, all passing through the origin and having sizes controlled by p'_c.

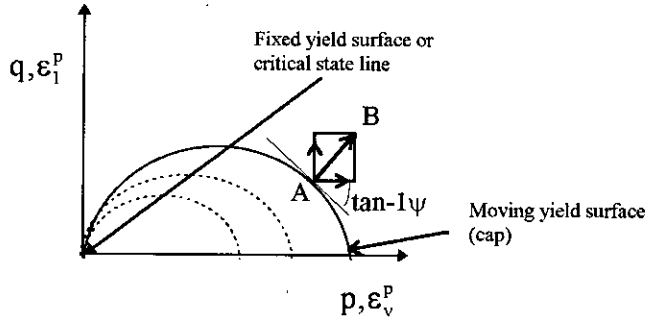

Figure 2.22 Yield locus in q-p space

2.5 Flow Rule

The flow rule for a plastic material gives the ratios of the plastic strain increments when the material is yielding in a particular stress state. The flow rule can be explained by defining a function known as plastic potential.

The function, g defining the ratios of the components of the plastic strain increments is known as the plastic potential. The ratios of the components of the plastic strain increment depend on the current stress and not on the stress increment. It follows that the equation of the potential surface:

$$g\left(\sigma_a,\sigma_b,\sigma_c\right)=\text{constant}$$

The plastic potential defines a surface in principle stress space. If vectors representing plastic strain increments are plotted in stress space, then the strain increment vectors are normal to the potential surface (Fig. 2.23).

With the help of plastic potential, the mathematical expression of the flow rule can be written as:

$$\partial\varepsilon_{ij}^{p} = \lambda\frac{\partial g}{\partial\sigma} \qquad 2.41$$

λ is known as the plastic multiplier which is positive scalar factors of proportionality.

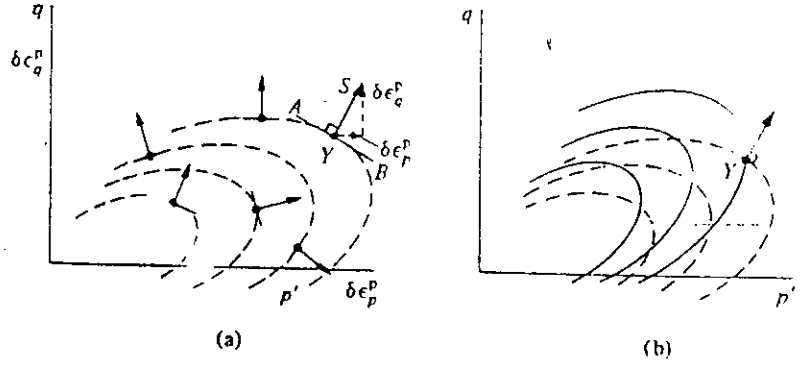

Figure 2.23 Plastic strain increment vector

The plastic potential of materials can be determined by performing careful experiments. In case of metal plasticity the plastic potentials and yield loci coincide and two sets of curves are identical (g=f). Such materials are said to obey the postulate of normality: the plastic strain increment vector is in the direction of the outward normal to the yield surface. Alternatively, the materials can be said to follow a law of associated flow: the nature of the plastic deformations, or flow, is associated with the yield surface of the material. However, for many frictional materials like soil, plastic potentials and yield

surfaces are not identical. These materials are considered to follow non-associative flow rules of plasticity.

2.6 Zone of Interest for Ultimate Pile Capacity

Settlement of a pile significantly depend on the bulb of pressure or the isobars. A isobar of practical significance is the one which enclose the soil mass which is responsible for the settlement of pile. The depth in this stressed zone may be termed as significant depth.

Based on this observation Terzaghi recommended that direct stresses are considered of negligible magnitude when they are smaller than 20 percent of the intensity of the applied stress and that most of the settlement, approximately 80 percent of the total, takes place at a depth less than D_s. The depth D_s is approximately equal to 1.5 times the width of square or circular footing (Fig.2.24). If several loaded footings are spaced closely enough, the individual isobars of each footing in question would combine and merge into one large isobar of the intensity as shown in Fig. 2.24(b). Pressure isobars for piles are shown in Fig.2.25. It appears that open ended pipe piles behave similarly to closed end piles due to the plug of soil inside the pipe.

In case of general theory for ultimate bearing capacity different types of failure surfaces are assumed by different investigations. On the basis of the failure surface, qualitative zone of interest for ultimate point capacity can be assumed as shown in Fig. 2.26 (Bowles, 1988).

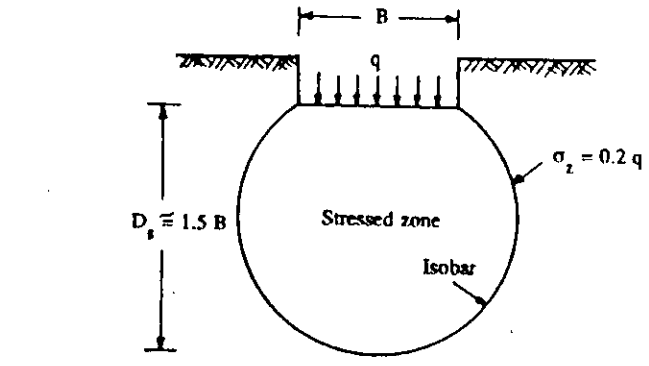

(a) Significant depth of stressed zone

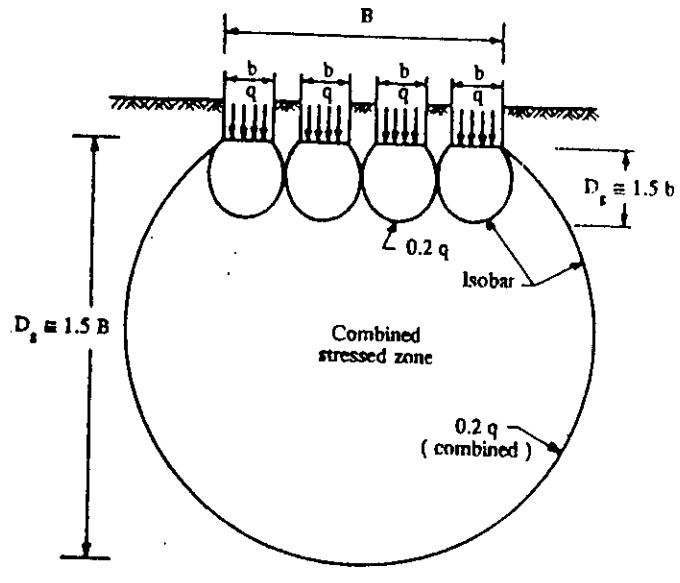

(b) Effect of closely placed footings

Figure 2.24 Significant depth of stresses zone

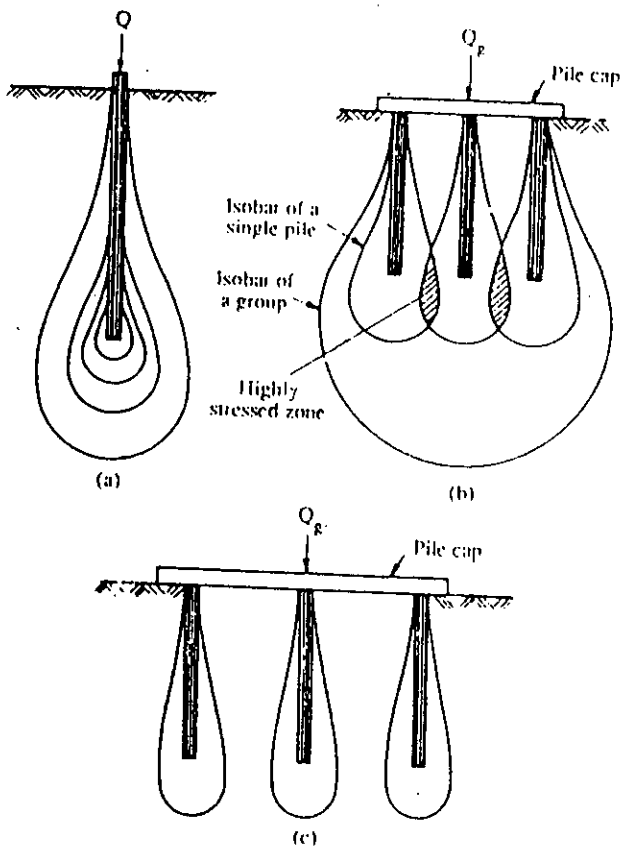

Figure 2.25 Pressure isobars of (a) single pile (b) group of piles, closely spaced, and (c) group of piles with piles for apart

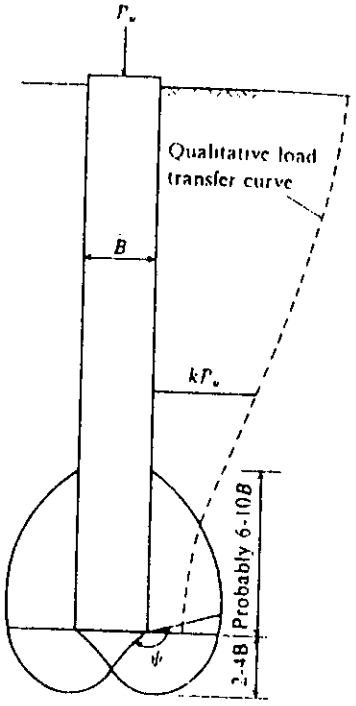

Figure 2.26 Qualitative zone of interest for ultimate capacity

CHAPTER 3

LABORATORY INVESTIGATION AND MODEL EXPERIMENTS

3.1 Introduction

Load carrying capacity of a pipe pile develops due to the skin frictional resistance of the soil within and outside the pile and the end bearing resistance. Skin friction from external soil for a pipe pile is same as that of a solid pile. Various empirical formula are available from literature survey to determine the skin friction from external soil. Conventional methods of calculating ultimate skin friction of external soil are proposed by Broms, Vesic and others (Poulos & Davis, 1980). But very little research has been carried out to determine the skin frictional resistance due to internal soil.

This investigation is aimed at determining the load resisting capacity of a pipe pile due to internal soil reaction and to determine stress distribution along the length when the pile is subjected to axial load. Steel pipes of different diameters (102 mm, 152 mm and 203 mm) were used here for this purpose. Pipes are axially loaded with soil filled to different depths within the pile. Due to the limitation of the loading device, it was not possible to vary depths of soil within 152 mm and 203 mm diameter pipe piles. Only 102 mm diameter pipe pile was tested with different internal soil depths to observe the variation of pile capacity with depth. Sylhet sand is used in all the tests in the current research. The details of test arrangement and test procedures are discussed in the following sections.

3.2 Evaluation of Material Properties

Soil used in the pipe piles were tested for grain size analysis in accordance with ASTM D422-63 (1972) to establish the gradation, fineness modulus and uniformity coefficient. Figure 3.1 represent the grain size distribution curve of the sand used. Maximum and minimum densities were also determined to estimate the relative density of the soil during test. Direct shear test (ASTM D3080-72) was carried out to find the angle of internal friction ϕ at maximum and minimum densities. Figures 3.2 and 3.3 represent the stress-displacement curves and shear

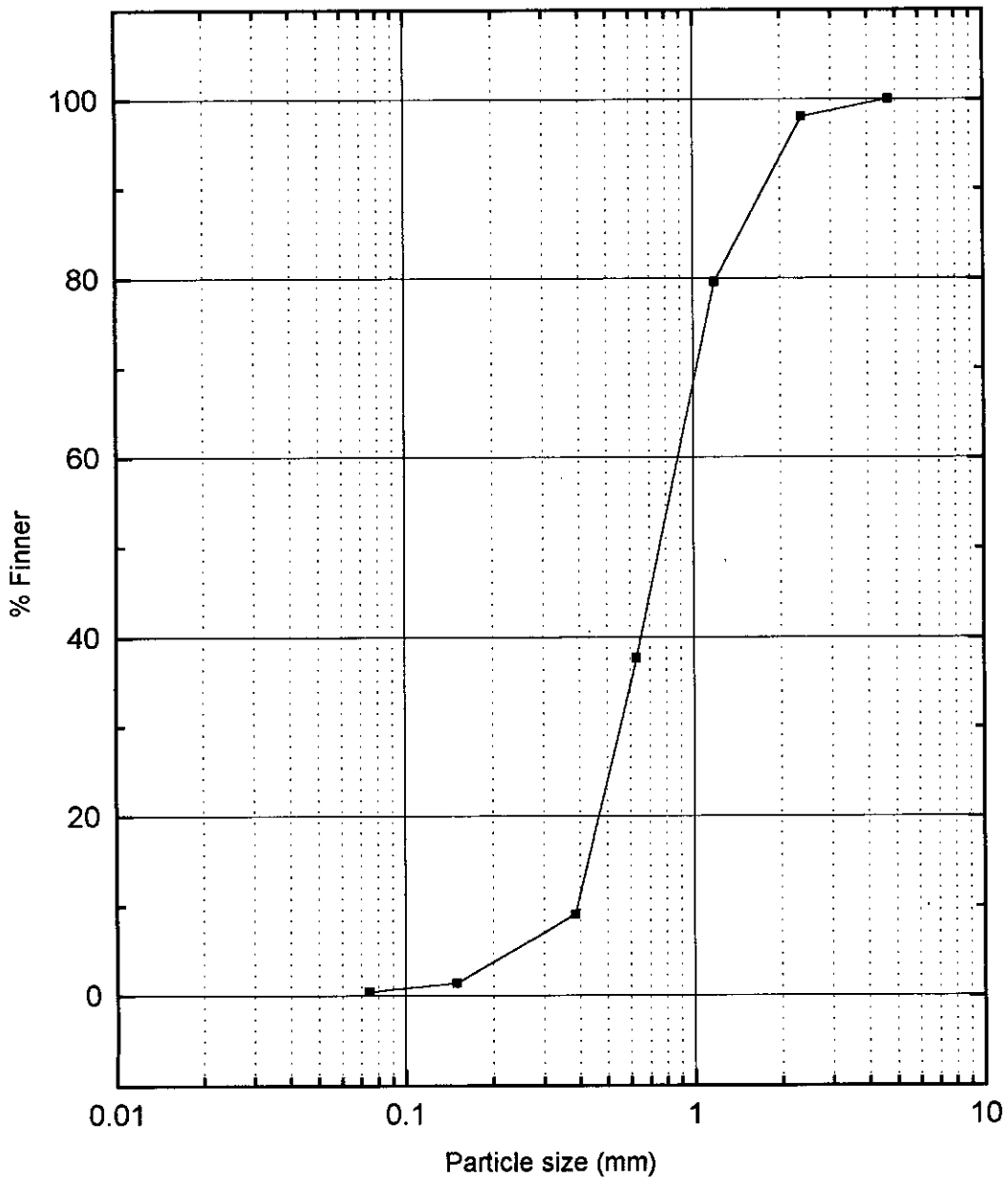

Figure 3.1 Grain size distribution curve

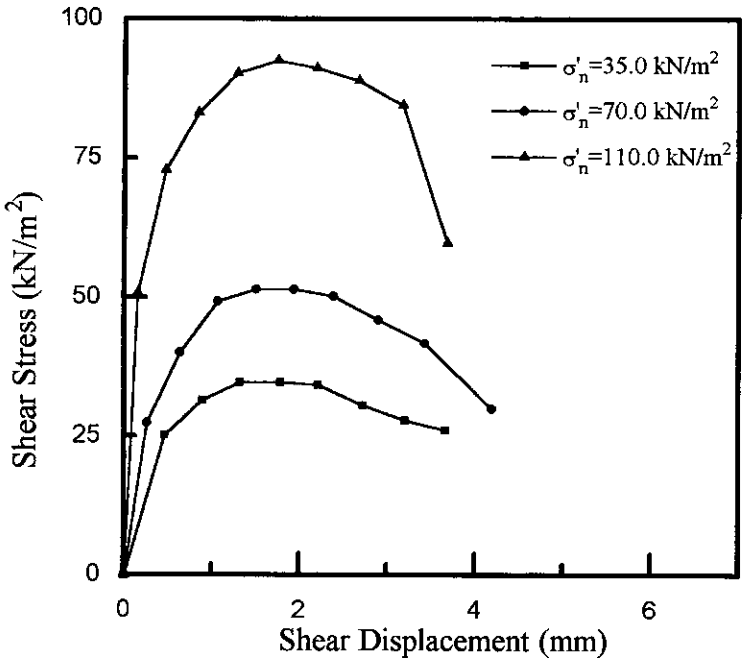

(a) Densest condition (γ_d = 16.3 kN/m^3).

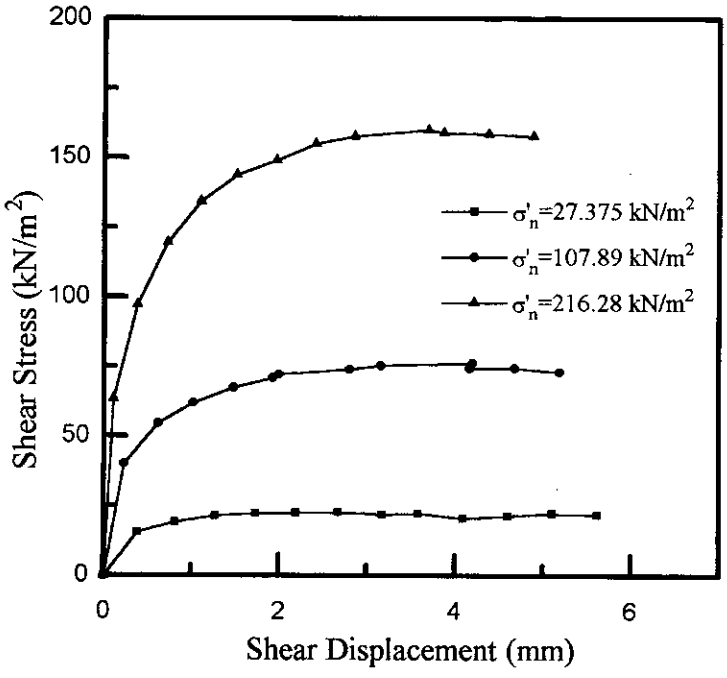

(a) Loosest condition (γ_d = 14.0 kN/m^3).

Figure 3.2. Shear stress vs. shear displacement curves of direct shear test.

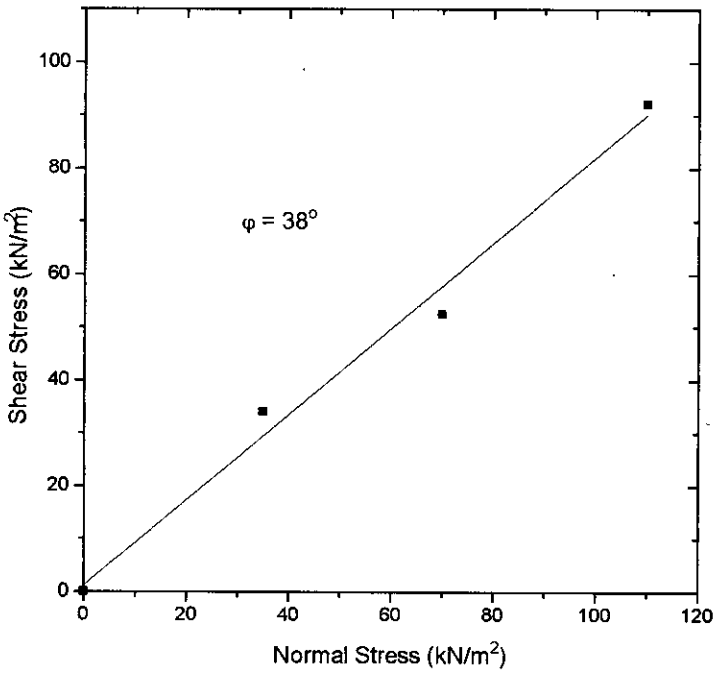

(a) Densest state.

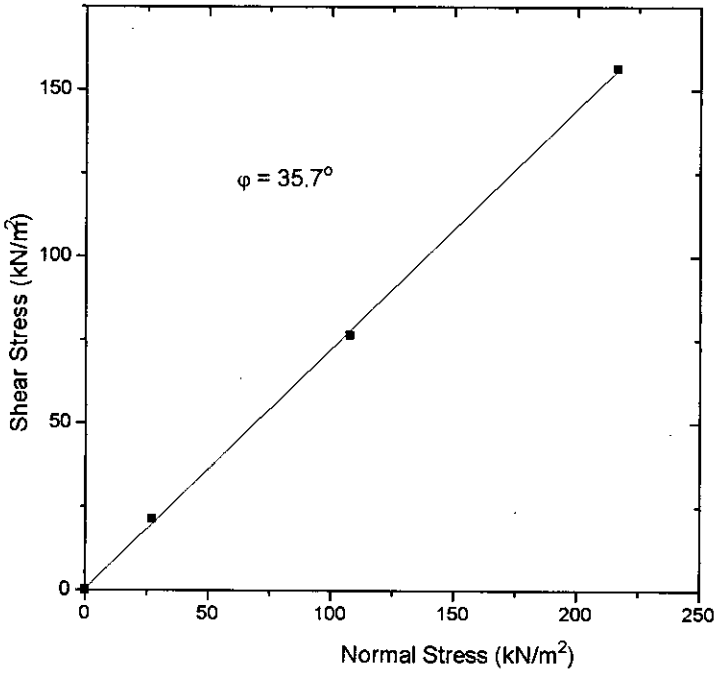

(b) Loosest state.

Figure 3.3. Angle of internal friction in densest and loosest conditions.

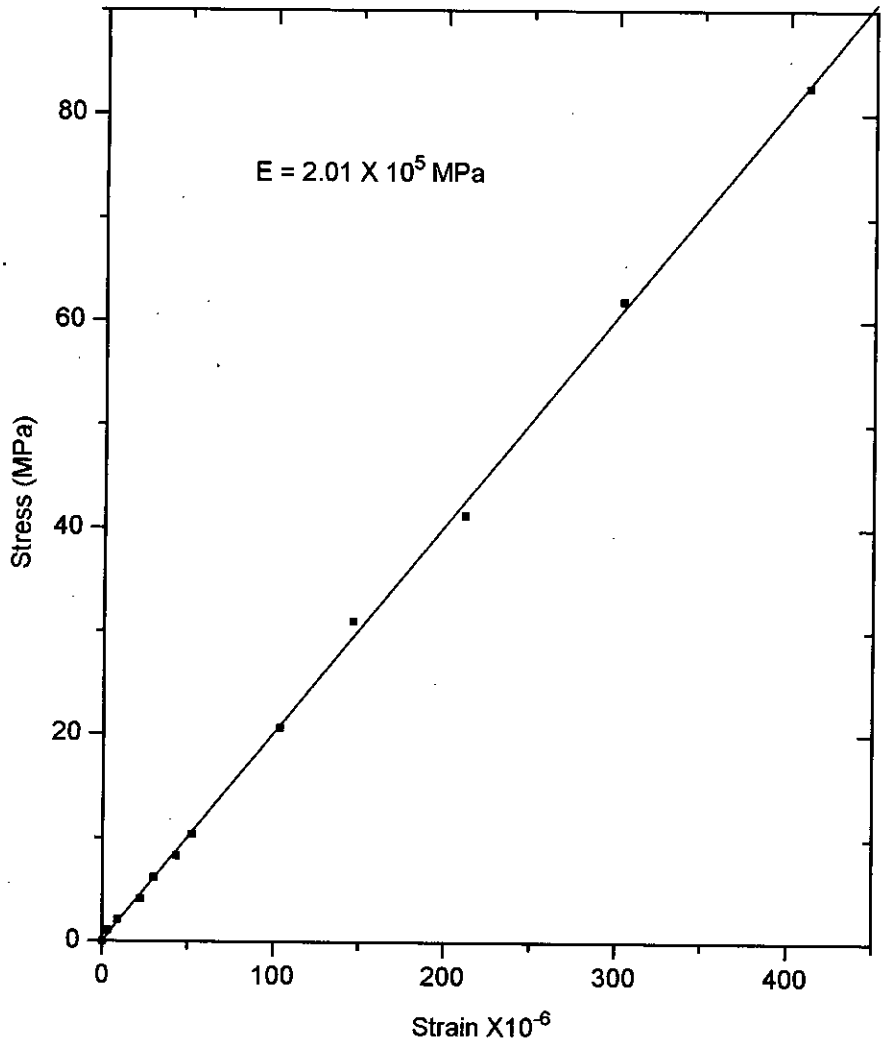

Figure 3.4 Stress - strain curve of steel pipe.

stress versus normal stress curves respectively from direct shear test results for both loosest and densest conditions. Modulus of elasticity of pipe material was determined from stress-strain curve in compression loading (Fig. 3.4). Properties thus obtained from standard tests are shown in Table 3.1.

Table 3.1. Material properties

Material	Property Assessed	Test Results
Soil	Fineness modulus (F.M)	2.74
	Effective particle size, D_{10}	0.386 mm
	Uniformity coefficient	2.41
	Coefficient of curvature	0.89
	Maximum density	16.3 kN/m^3
	Minimum density	14.0 kN/m^3
	Angle of internal friction at densest state	38°
	Angle of internal friction at loosest state	35°
Steel Pile	Modulus of elasticity of pile	2.01x10^5 MPa

3.3 Pipe Pile Test Arrangement

A universal testing machine is used as the loading device for the pipe piles. The machine consists of a loading cap and a base assembly. The model steel pipe pile was set on the base assembly as shown in Fig.3.5. The bottom of the pipe was seated over a piston like wooden block (Fig.3.6). The wooden block consist of a top plate, a vertical stand and a base plate. Diameter of the top plate of the wooden block was made slightly less than the inside diameter of the pile to avoid friction of the block with pipe. A rubber o-ring is fitted on the top edge of the top plate to prevent soil particles from moving downward and reduce friction.

Sand of known physical properties (Table 3.1) are poured in the pipe in different layers and compacted by gentle tapping with a mallet. Attempt is made to achieve sand in the densest condition, although density could not be controlled very

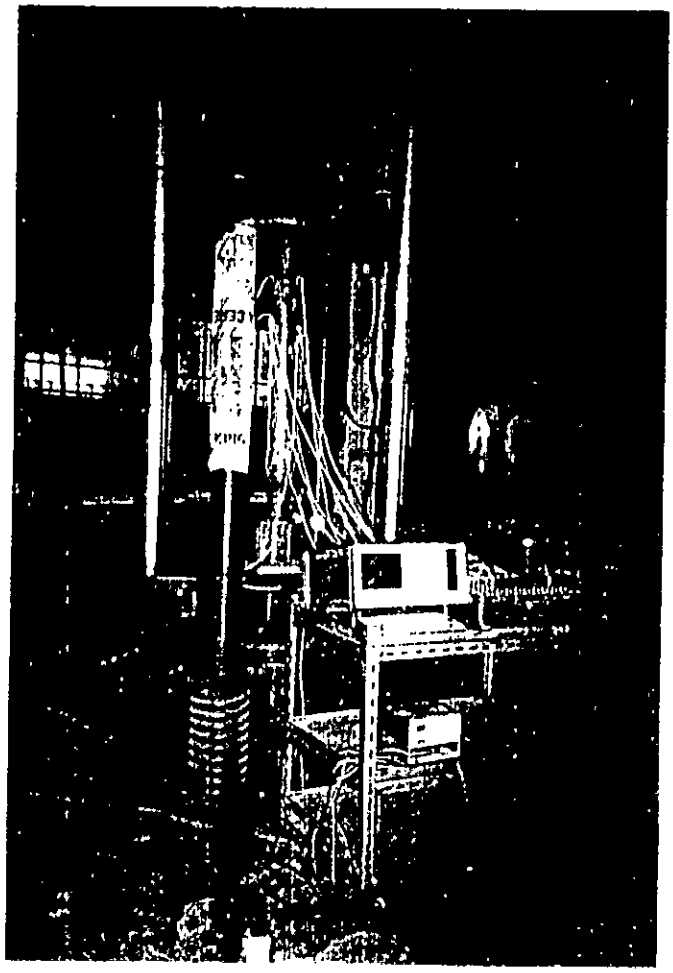

Figure 3.5 Load arrangement

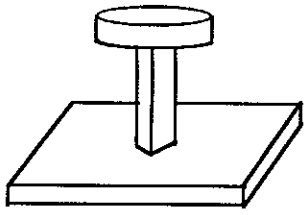

(a) Wooden Block

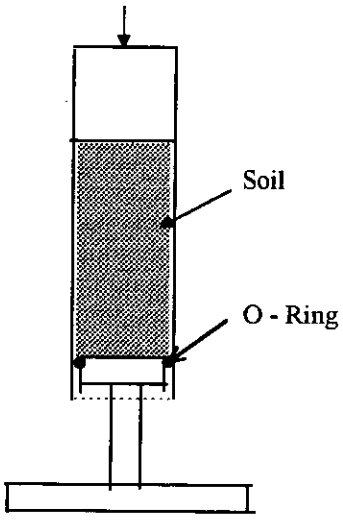

(b) Test Arrangement

Figure 3.6 Wooden block and arrangement of Test

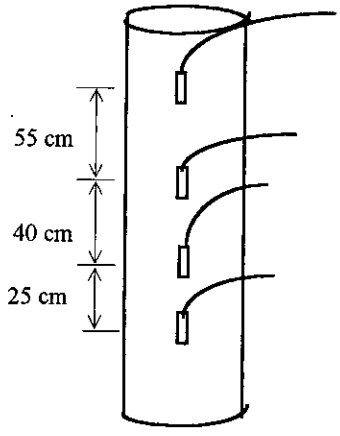

Figure 3.7 Strain gauge setup in piles

precisely due to lack of space inside the loading frame. Next the load is applied through the loading block of the machine on to pile top.

3.4 Measurement of Load Response

Electronic strain gauges were used to measure the strain at five locations along the outer surface of the pipe piles. Gauge length and resistance of the strain gauge were 10 mm and 120 ± 0.3 ohms respectively. Thus the gauges were capable of measuring very small strain of the model piles. Fig. 3.7 shows the arrangement of strain gauges along the length of the pile. Spacing of the strain gauges were kept closer along the lower portion of the pipe. Spacing is increased throughout the upper portion. A displacement transducer and a dial gauge were used in measuring pile tip displacement. A datalogger was used to record the strain from the strain gauge and the displacement of the pile from displacement transducer at various stages of loading.

As the loads were applied, pile movement caused densification of the soil in pile. Density of the internal soil was measured before and after loading. In order to measure the initial density, soil of known weight was poured in the pile. Length of soil column in the pile was then measured. Thus volume of the soil inside was calculated from the known cross section of pile and hence average density was obtained.

Displacement of the bottom and top face of the soil column inside the pile was measured to determine the density of the soil after loading. From the relative movement of the two faces, the actual length of the soil column, inside, was calculated to obtain the final density.

3.5 Interpretation of Experimental Results

Limited number of experiments were conducted to examine the settlement of the pipe pile with vertical load and to check the stress distribution along the pile length and inside soil. Soil depths were varied to demonstrate the effect of soil depth on pile capacity. Piles were loaded axially. Results of the experiments are presented in graphical form and discussed in the following sub-sections.

3.5.1 Load-settlement response

Fig. 3.8 represent load settlement response of 102 mm diameter pipe. Depths of the internal soil used in the experiment of 102 mm diameter pipe were 5, 7, 9 and 11 times the diameter of the pile. Load was applied in each case increasing from 0 at an increment of 900 N up to such an amount that caused a pile movement of 25 mm or more. Ultimate load of pile is defined as the load that causes a settlement of 10% of the pile diameter to the pile (Tomlinson, 1980). The 152 mm diameter and 203 mm diameter pipes are tested with soil depth of 5 times the diameter. Fig. 3.9 shows the effect of diameter on the internal soil capacity from the plotting of load-settlement curves for 102 mm, 152 mm and 203 mm diameter pipes with inside soil depth of 5 times the pile diameter .

In Fig. 3.10 and Fig. 3.11 load displacement curves are plotted in non-dimensional form by dividing the axial load at any stage by ultimate load and plotting it in y-axis. The settlement is divided by 1/10th of the pile diameter and plotted in X-axis.

Pile movement is large for shorter depth of internal soil. Due to large pile movement soil is densified and gradually stiffened. As a result the load-displacement curve moves upward with an increasing slope. After a certain value of settlement the curve shows decreasing tendency of slope. The decreasing tendency in the load-displacement curves signifies the end of densification process and start of continuous plastic deformation inside the pile soil. Attempt was taken to explain the phenomena numerically in the subsequent sections.

The research is oriented to determine the depth of internal soil required to attain sufficient pile capacity due to soil plug. In order to observe the variation of soil plug capacity with the soil depth, pile capacity is plotted against soil depth in Fig.3.12 for 102 mm diameter pile. Soil depth is expressed as a multiple of pile diameter. Several curves are plotted here at different level of pile settlement. Thus equilibrium load at different soil depths and settlement are demonstrated.

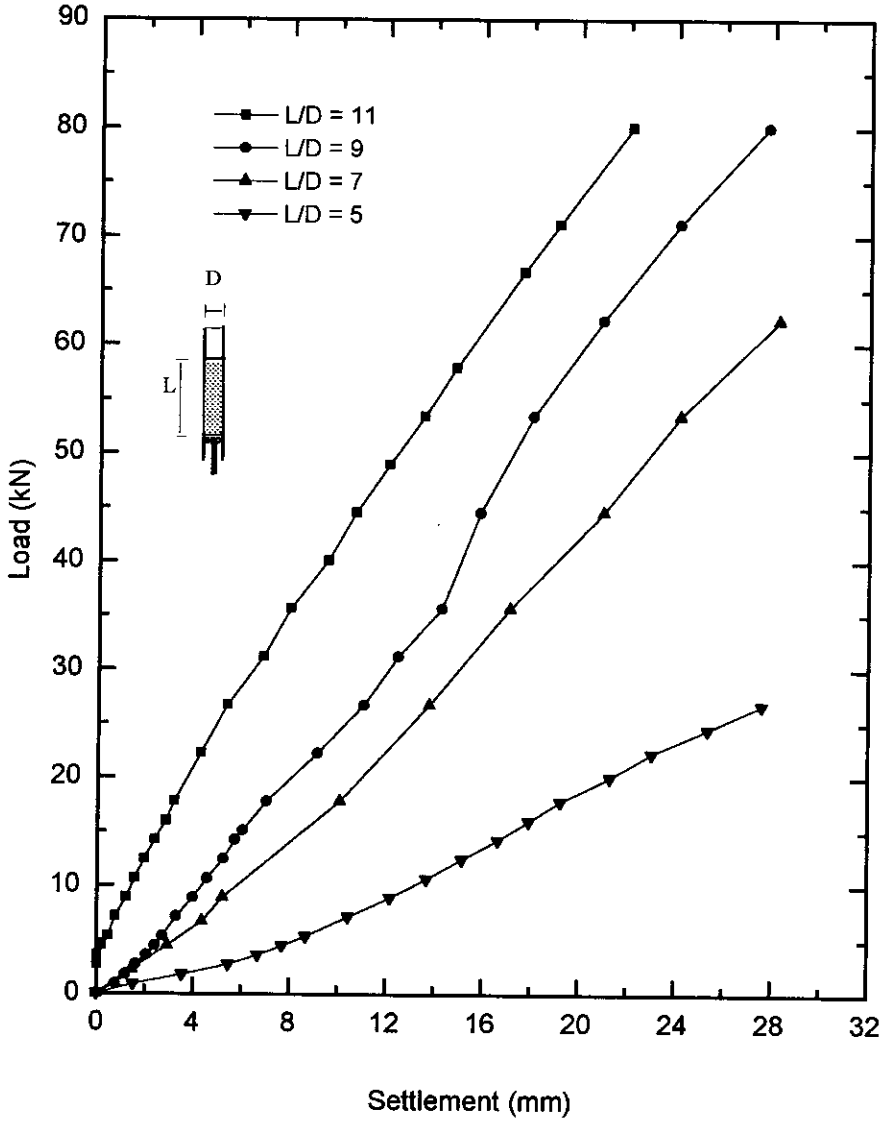

Figure 3.8. Load - settlement curves of 102 mm diameter pile.

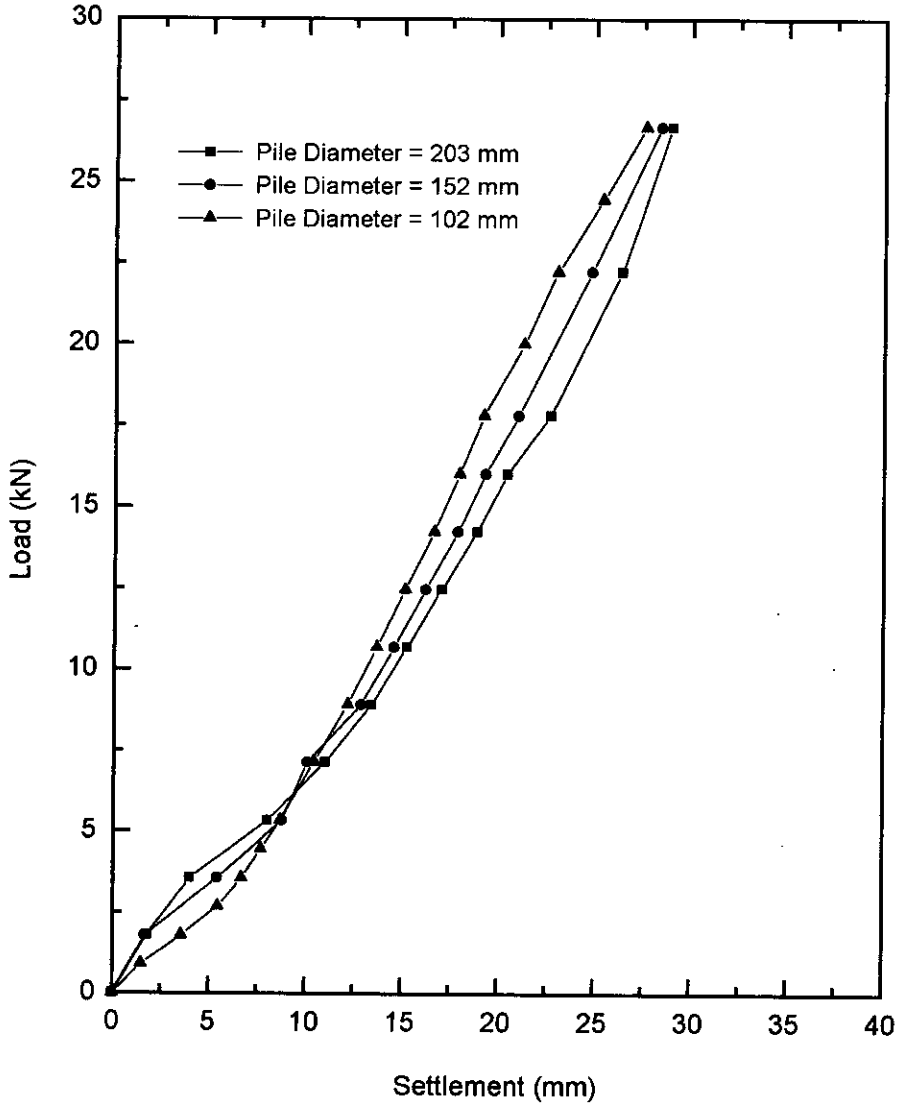

Figure 3.9. Load- settlement curves for L/D = 5 with various pile sizes

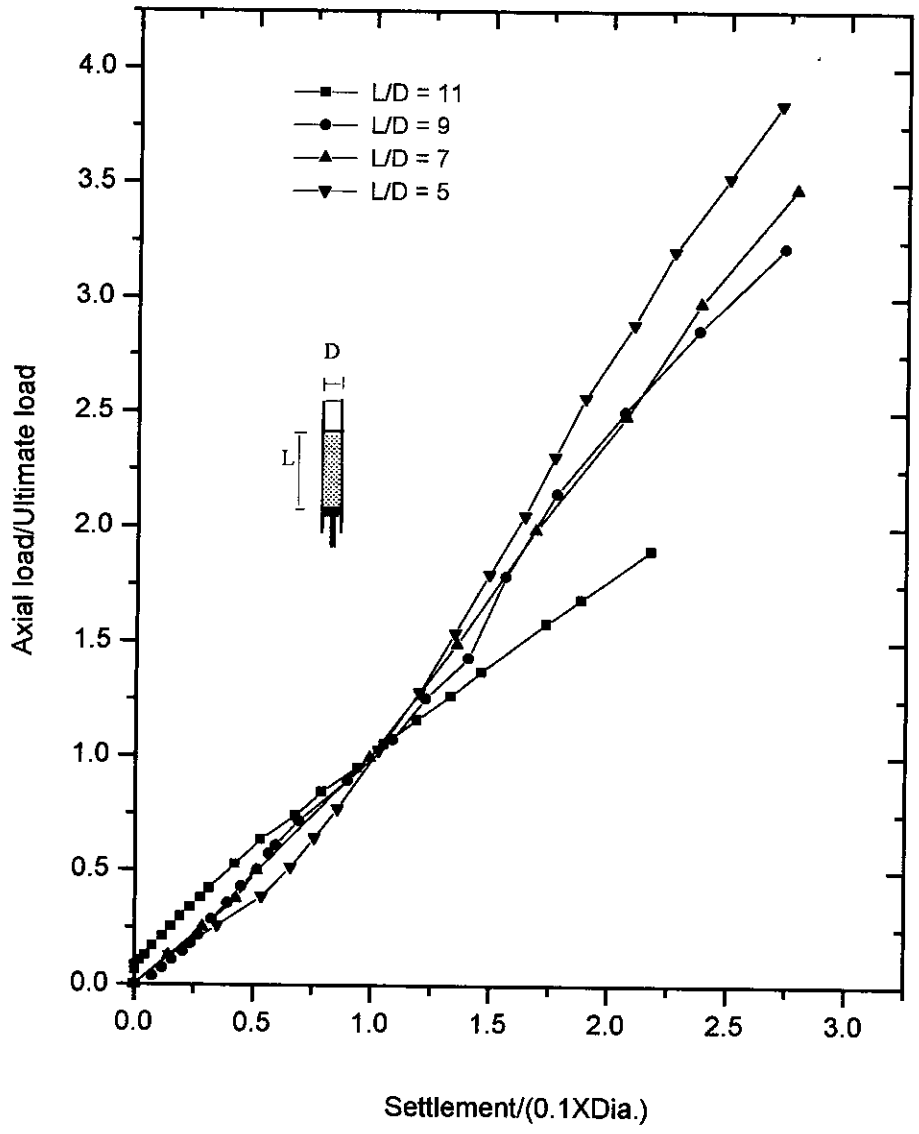

Figure 3.10. Nomalized load- settlement curves for102 mm diameter pile.

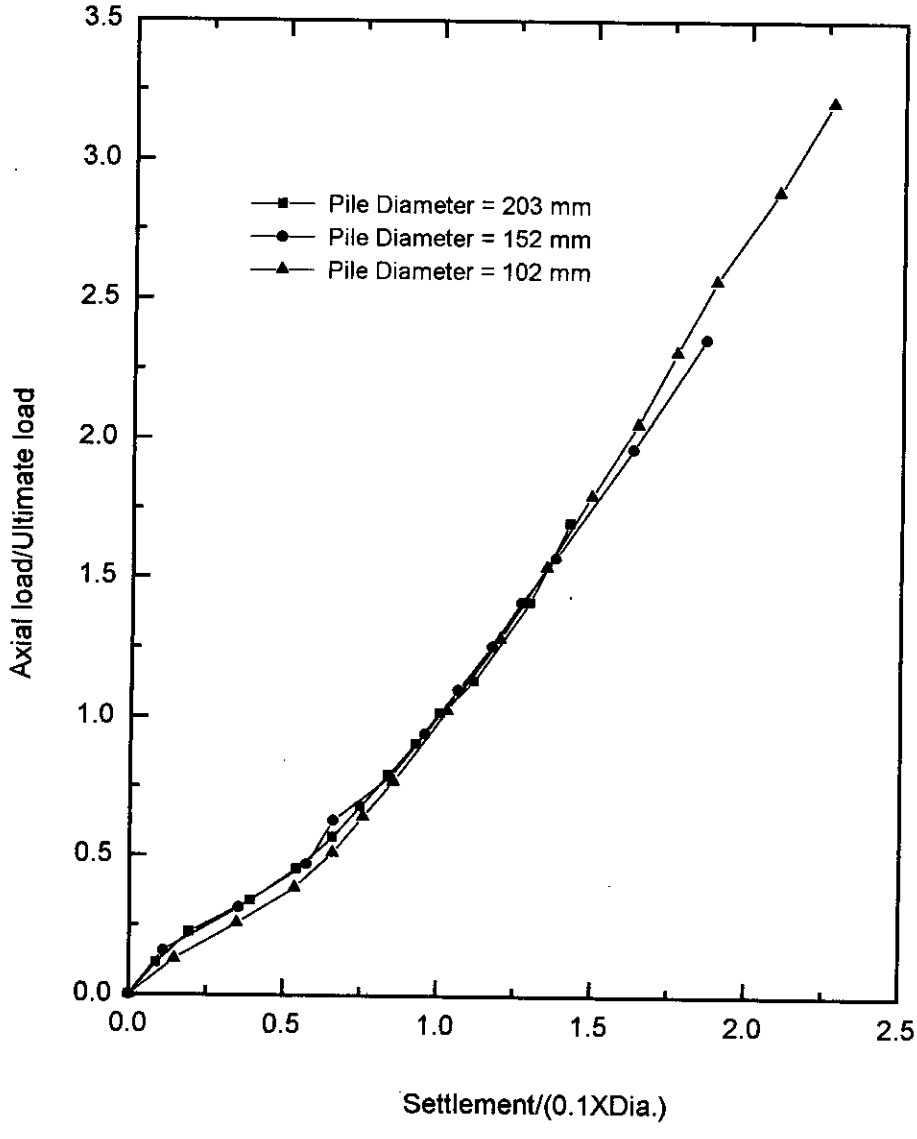

Figure 3.11.Normalized load - settlement curves (L/D = 5).

3.5.2 Load transfer

Axial load is transferred first from the pile to the soil through skin friction and then to the base wooden block. Due to the transfer of load through skin friction, vertical stress along the pile length will be different at different elevations. To measure the pile stress an indirect technique is used. At any level pile strain is measured by electric strain gauge. Then pile stress is calculated as:

$$\sigma_p = E_p \varepsilon_p \qquad 3.1$$

where

ε_p = strain of pile at any level
σ_p = stress of pile at that level
E_p = Modulus of elasticity of pile material

Total load carried by the pile is calculated by multiplying pile stress by pile area.

$$P_p = \sigma_s A_p$$

$$= \sigma_p \pi (D + t) t \qquad 3.2$$

where

D = diameter of the pile
t = thickness of the pile

Load transferred to the internal soil can be calculated by deducting pile load from the total load applied. It may be assumed that stress in soil is uniform at any depth over a horizontal slice. The average stress along the pile can be obtained by dividing the load by cross sectional area of the soil plug. To observe the transfer of load from soil to pile with the increase of load, curves are plotted at different level of load. Fig.3.13 shows variations of strain in pile material at different soil depths at various loading states (Depth measured from bottom of pile). Fig.3.14 shows the distribution of pile stress at different stress level and Fig.3.15 depicts load taken by soil within pile at different depths.

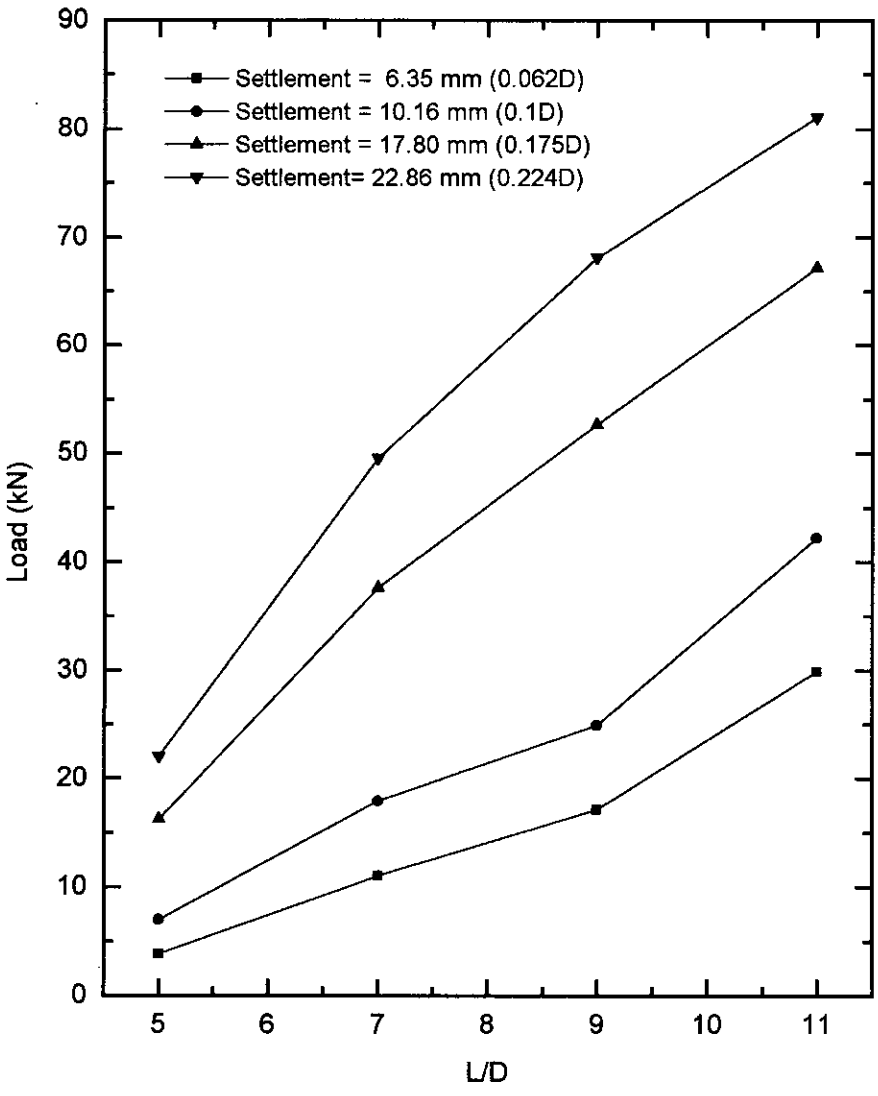

Figure 3.12. Variation of pile capacity with depth/diameter ratio at different level of settlement (D = 102 mm).

From the Fig.3.14 it can be observed that with the increase of the distance from pile top vertical stress in pile decreases. This is due to the transfer of load to the soil through skin friction. Decrease in pile vertical stress with depth follow an exponential form. This indicates that the vertical stress on the internal soil increases exponentially with depth. Figure 3.16 shows the distribution of vertical stress on internal soil with depth. The relation justify the increase of pile capacity due to the development of arching of the soil inside the pile. From Fig. 3.13 to 3.16 it is observed that at lower level of applied load, variation of pile vertical stress with depth is not significant. This is due to absences of arching in the soil. At higher level of load, and hence settlement, arching of internal soil develops. As a result vertical stress of internal soil is increased with depth in an exponential rate. If the vertical stress of soil at the bottom is greater than the end bearing capacity of pile, the pipe pile will act as a closed ended pile i.e. in plugged mode. Thus it is observed here that a certain level of settlement of the pile is necessary to develop arching in the soil that increase the pile capacity. This settlement can be taken as 10% of the pile diameter.

3.5.3. Effect of diameter on frictional resistance

Load-displacement curves of different diameter piles with soil depth to diameter ratio of 5 is plotted in Fig.3.9. Due to the physical limitation of the experiment performed, it was not possible to test all the pile with different soil depth.

Fig.3.9 explains the variation of frictional resistance with diameter. It is observed that initially, capacity of larger diameter pile is greater than that of smaller diameter pile. But after a certain limit frictional resistance of smaller diameter pipe is greater. This is because after a certain displacement arching of the internal soil of smaller diameter pile develop and for this reason the frictional resistance of that pile is higher. On the other hand a larger displacement is required to develop soil arching in large diameter pipe pile. Hence the capacity of larger diameter pile is smaller than that of smaller diameter pipe pile. Fig.3.9 shows that after certain displacement the frictional resistance of larger diameter pile is greater than that of smaller diameter pile.

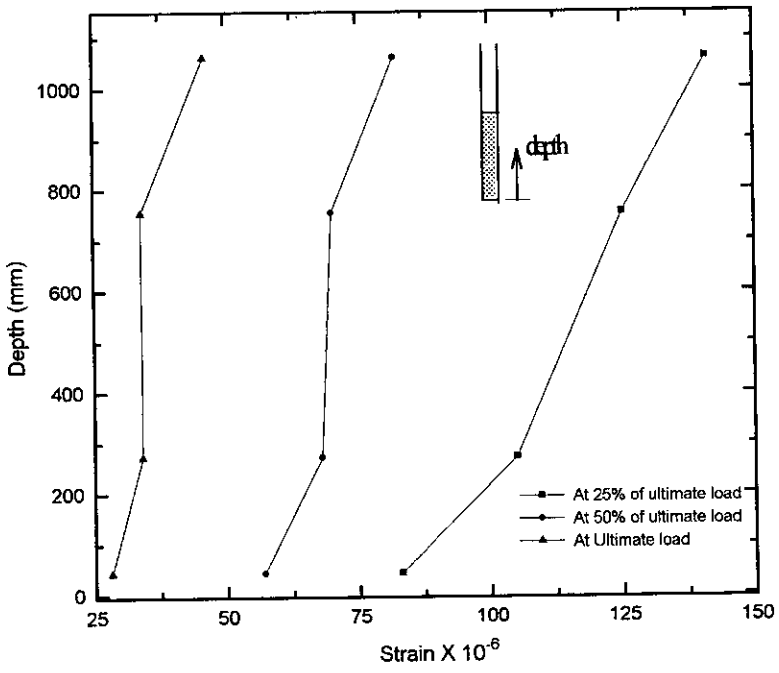

Figure 3.13. Variation of strain in pile material with depth.
(D = 102 mm, L/D = 11)

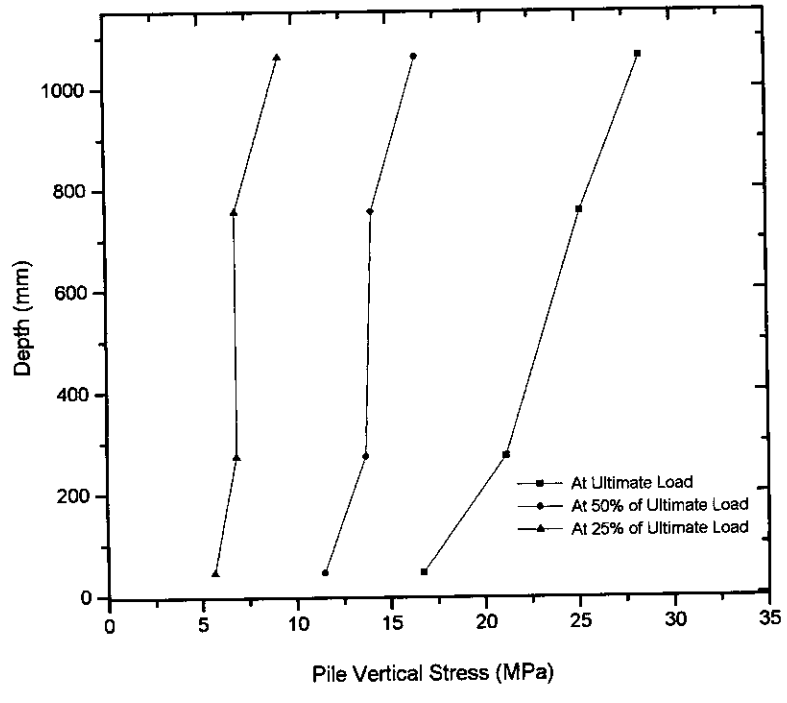

Figure 3.14. Variation of pile vertical stress with depth in 102 mm diameter pile (L/D =11).

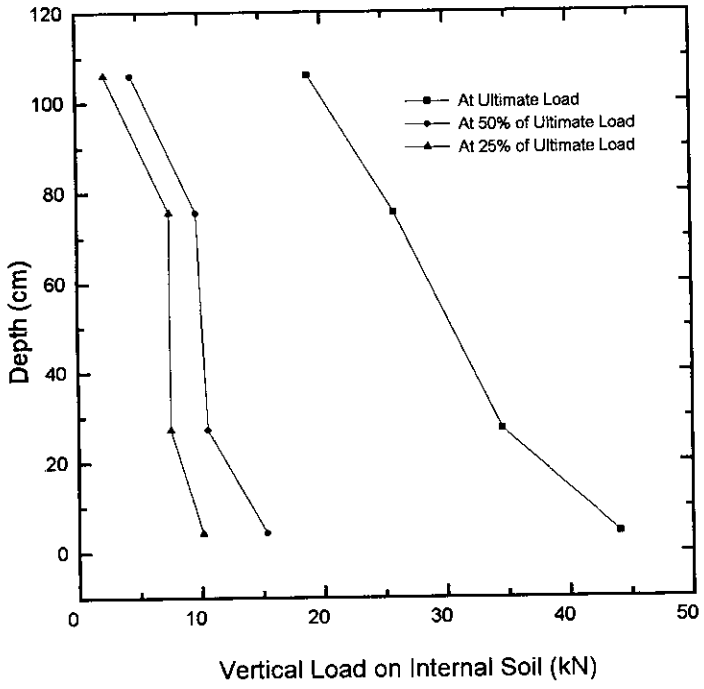

Figure 3.15. Variation of vertical load of in soil with depth (D = 102 mm , L/D = 11).

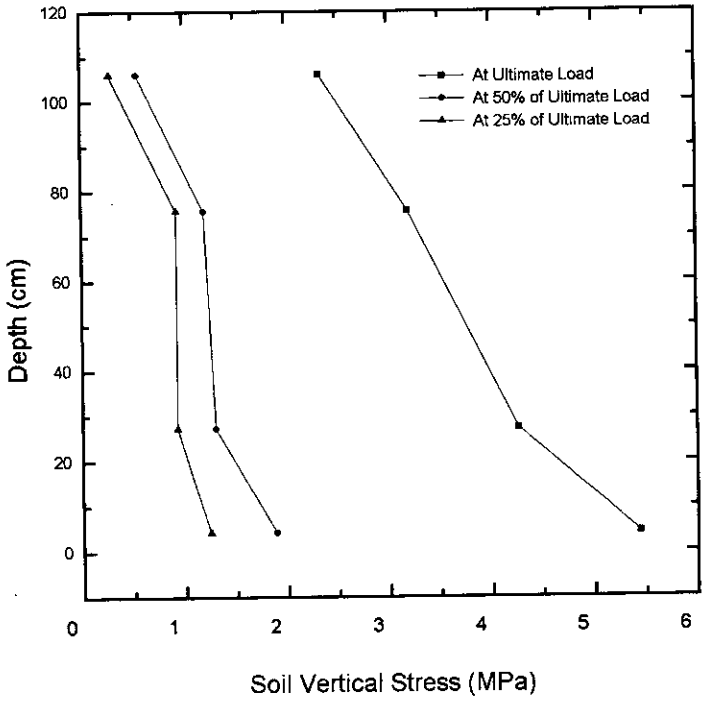

Figure 3.16. Variation of vertical stresses in soil with depth (D = 102 mm, L/D = 11).

Before the development of arching, skin friction of internal soil is determined in the same way as that of outer soil as proposed by Terzaghi (1943). According to Terzaghi (1943) skin friction mobilised in a pile at a given depth z is given by

$$f = \gamma_s z k \tan\delta \qquad 3.3$$

Where,

f = Unit skin friction

γ_s = Unit weight of soil

k = Coefficient of earth pressure

δ = Angle of friction between soil and pile

Frictional area of larger diameter pipe pile is greater than that of smaller diameter pipe pile . Besides, coefficient of earth pressure has a general tendency to increase with diameter (Siddiquee et al. 1988). For this reason up to a certain level of settlement, frictional resistance of larger diameter pile is observed to be higher than that of smaller diameter pile (Fig.3.9). After a certain level of displacement skin friction of soil in smaller diameter pile is fully mobilised and arching is developed in the internal soil. When arching is developed normal force to pile wall and hence the frictional resistance increases exponentially with depth. As a result total frictional resistance of smaller diameter pile may be greater than that of larger diameter pile in which no arching is developed. Settlement required to develop arching for different diameter pile is not the same. It may be observed that settlement required to develop arching is higher for larger diameter pile. When arching is developed in both larger and smaller diameter pile capacity of larger diameter pile will definitely be higher.

3.5.4 Variation of pile capacity with soil depth

Pile capacity can be expressed as a resistance to the pile movement due to the friction of the internal soil. Skin friction of the internal soil depends on the normal stress on the pile wall. For this reason as depth of the soil increases the resistance due to internal friction also increases.

Arching of the internal soil, if developed, increase the soil stress exponentially. This increases the skin frictional resistance significantly. Sufficient depth of internal soil and certain amount of displacement of pile is required to develop

arching. After arching is developed, further increase of soil depth does not result in increasing pile frictional capacity substantially. Figure 3.12 indicates that at lower value of pile settlement, curves moves upward with increasing slope and after a certain level of settlement, slope of the curve decrease and the increase of pile capacity is insignificant. This is due to the fact that at lower level of settlement, at a certain L/D (=9) slope of the curve increases suddenly indicating the start of arching (plugging). It is observed that a settlement of about 10% of the pile diameter is sufficient to develop arching in the internal soil. From Fig.3.12 it is also observed that for L/D above 14 (extrapolated), the increase of pile capacity with L/D is insignificant. Hence depth of soil required to develop full arching is 14 times the pile diameter. It is reasonable to use 9 to 14 times the pile diameter as required depth of soil to develop arching.

3.6. Numerical Simulation of The Experimental Results

Figure 3.8 and 3.9 represent the load-displacement curves of pipe piles obtained from the experimental investigation. In order to explain the behaviour obtained from experiments theoretically, numerical analysis by finite element method was performed. The problems are idealised as axisymmetric problem during the analysis.

3.6.1. Idealisation of the problem

In the experiment, axial load is applied on a hollow circular pile with symmetric section. So the axisymmetric idealisation of the problem is justified. Finite element mesh and the idealised problem is shown in figure 3.17. Material properties are defined after dividing the problems into four zones: upper portion of soil, lower portion of soil, pile elements and interface elements.

According the arching theory as proposed by Terzaghi (1936), arching is developed in soil mass upto an elevation of about two to three times the width of the opening from the bottom (Terzaghi, 1943). From this consideration it is assumed that soil is densified and the soil modulus is changed in that portion of soil mass. So the soil mass is divided into two zones. Soil modulus is changed in the lower zone at different stress level to simulate the experimental result. Initial soil properties were determined experimentally. Angle of internal friction for

particular relative density was determined by the linear interpolation from the values at maximum and minimum relative density. Initial soil modulus was determined from the available literature relating soil modulus with relative density of soil (Table 3.2, and Table 3.3). Figure 3.18 shows the variation or the load - displacement response with soil modulus. Average value of Poisson's ratio of soil is assumed to be 0.30 (Davis and Poulos, 1980).

Table 3.2 Suggested average values of E_s for piles in sand
(Davis and Poulos, 1980)

Sand Density	Range of Relative Density	Range of E_s	
		(psi)	(MN/mm^2)
Loose	< 0.4	4000 - 8000	27.5 - 55
Medium	0.4 - 0.6	8000 - 10000	55 - 70
Dense	>0.6	10000 - 16000	70 - 110

Interface element (Desai, 1984) was used to define soil - pile interface. Width of the interface element was so selected that the aspect ratio is 0.05. It satisfies the criteria of t_i/b_i ratio within 0.01 to 0.1 as suggested by Desai. Normal behaviour of interface element is obtained from soils normal behaviour as suggested by Desai. The value of G_s has been assumed very low using a very high value of ν as recommended by Jayatheran (1996). Trial curves are plotted to fit the experimental result (Figure 3.19) and to select the value of G_s.

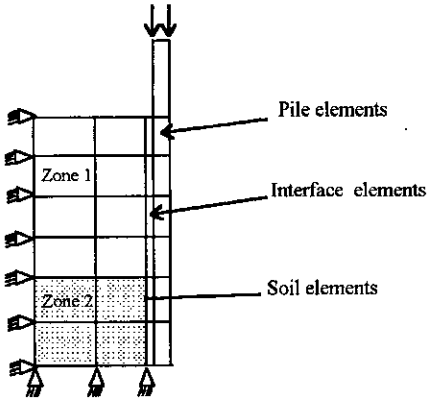

Figure 3.17 Finite element idealisation of the Problem

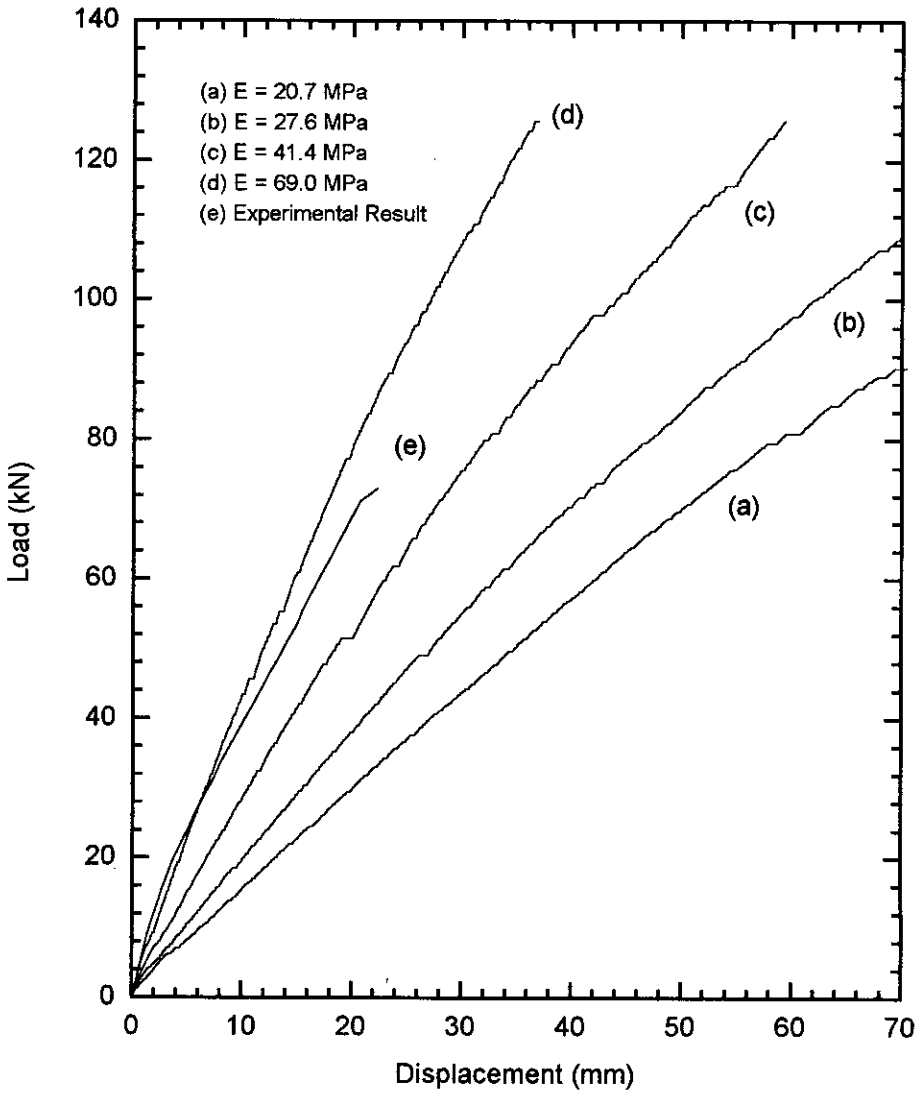

Figure 3.18 Effect of soil modulus on load - displacement curves

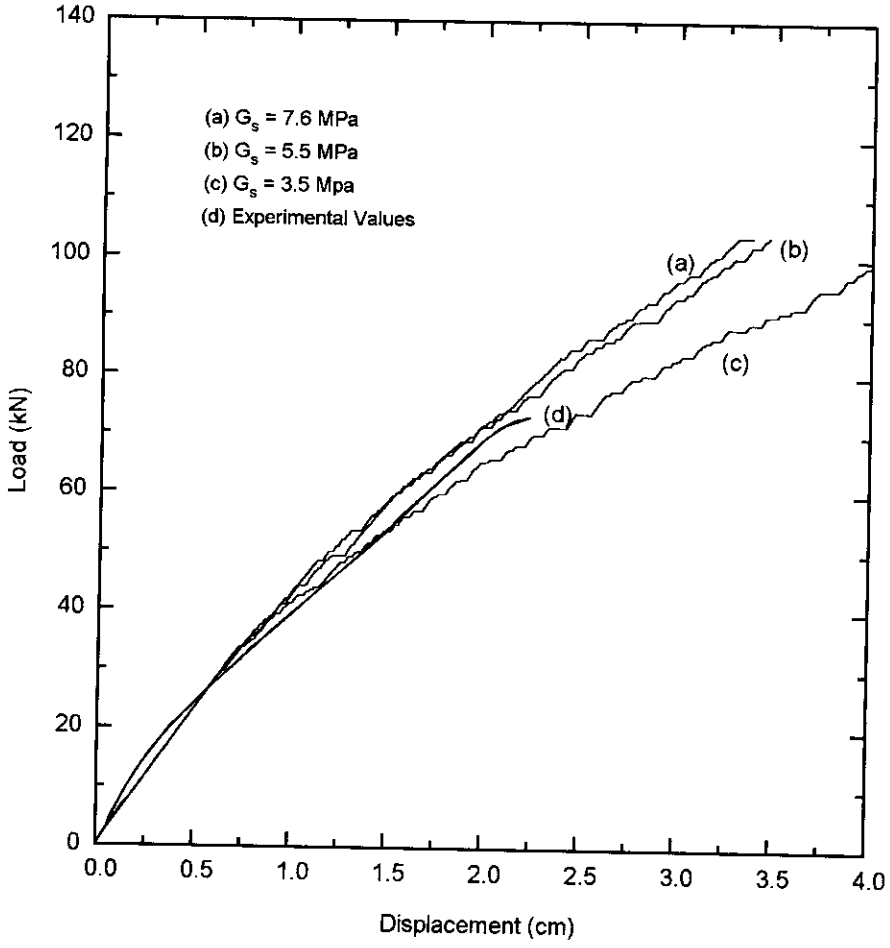

Figure 3.19 Effect G_s on load - displacement curves (E=69MPa).

Table 3.3 Typical range of values for the static stress - strain modulus E_s for selected soils

(Bowles, 1988)

Soil	E_s	
	ksf	**MPa**
Clay		
Very soft	50 - 250	2 - 15
Soft	100 - 500	5 - 25
Medium	300 - 1000	15 - 50
Hard	1000 - 2000	50 - 100
Sandy	500 - 5000	25 - 250
Glacial till		
Loose	200 - 3200	10 - 150
Dense	3000 - 15000	150 - 720
Very dense	10000 - 30000	500 - 1440
Loess	300 - 1200	15 - 60
Sand		
Silty	150 - 450	5 -20
Loose	200 - 500	10 - 25
Dense	1000 - 1700	50 - 81
Sand and gravel		
Loose	1000 - 3000	50 - 150
Dense	2000 - 4000	100 - 200
Silt	40 - 400	2 - 20

3.6.2. Results from numerical analysis

Here, purpose of the finite element analysis is to explain the experimental results. Behaviour of the soil in the model pipe pile is changed due to pile and soil movement when subjected to load. It is assumed that soil properties are changed in Zone 2 (Fig.3.17). Suitable properties of the soil are adjusted to simulate the results from the experiments. Figure 3.20 to 3.23 represent the numerical simulation of the experimental results.

The most significant parameter whose influence on the load-displacement response is very high, is the soil modulus. Change of the value of soil modulus and the rate of change depends on various parameters as initial soil density, relative density, depth of soil, rate of loading etc. The concave upward nature of load-displacement curves can only be explained by continuous densification near the pile tip within a zone, suggested by Terzaghi (1936). So finite element analysis were carried out with different Young's modulus as suggested from the experimental density change. Variation of the soil modulus with different level of load and settlement for pipes with different soil depth is observed. Figure 3.24 represent the variation of soil modulus with the level of applied load, required to simulate the experimental result.

3.7 Model for The Prediction of Plug Capacity

A series of tests were performed to interpret the mechanism of plugging in pipe pile. The diameter of the pile was kept constant (102 mm) and the load displacement responses for different L/D ratio were determined. Fig.3.8 shows the load-displacement curves from the tests. In the experiment, densification played a major role in determining the shape of the load-displacement curves. The densification phenomena in a pipe pile is further explained by FE analysis in section 3.6. The load-displacement curves are normalised by a consistent ultimate load and settlement (section 3.5.1) to reduce the influencing factors. Trend of the curves of normalised load displacement responses is then observed. The nature of the normalised load-displacement curves shows two apparent factors affecting its shape. First factor is the (L/D) ratio and second factor is the change in density during the loading.

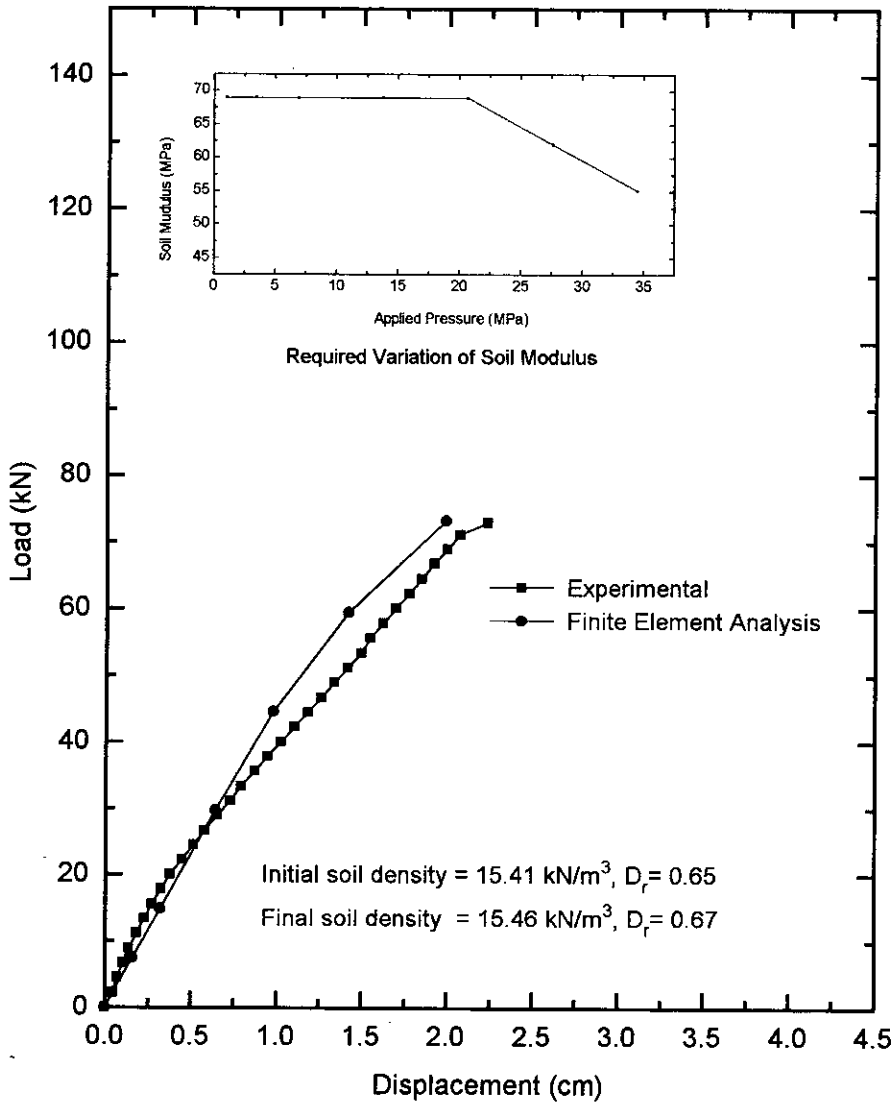

Figure 3.20 Numerical simulation of experimental result
For pile with L/D = 11 (D = 102 mm).

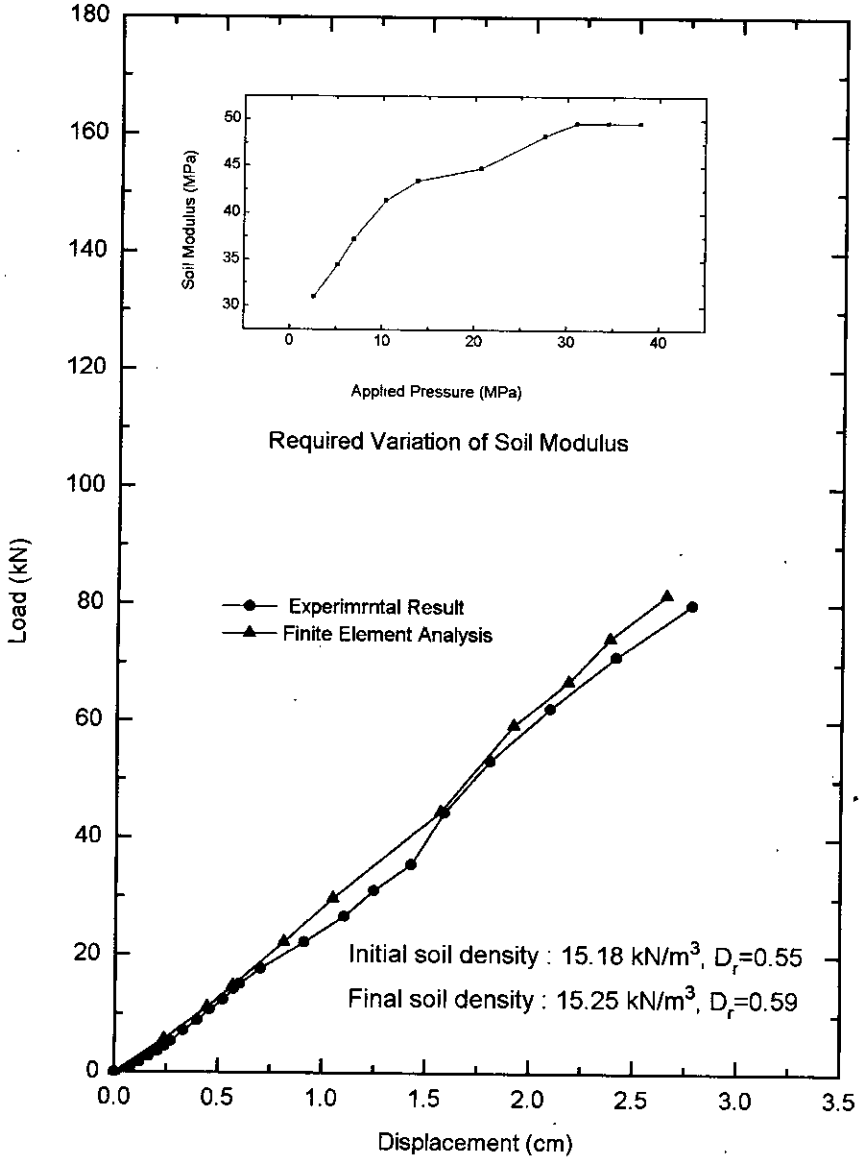

Figure 3.21 Numerical simulation of experimental result for pile with L/D = 9 (D = 102 mm).

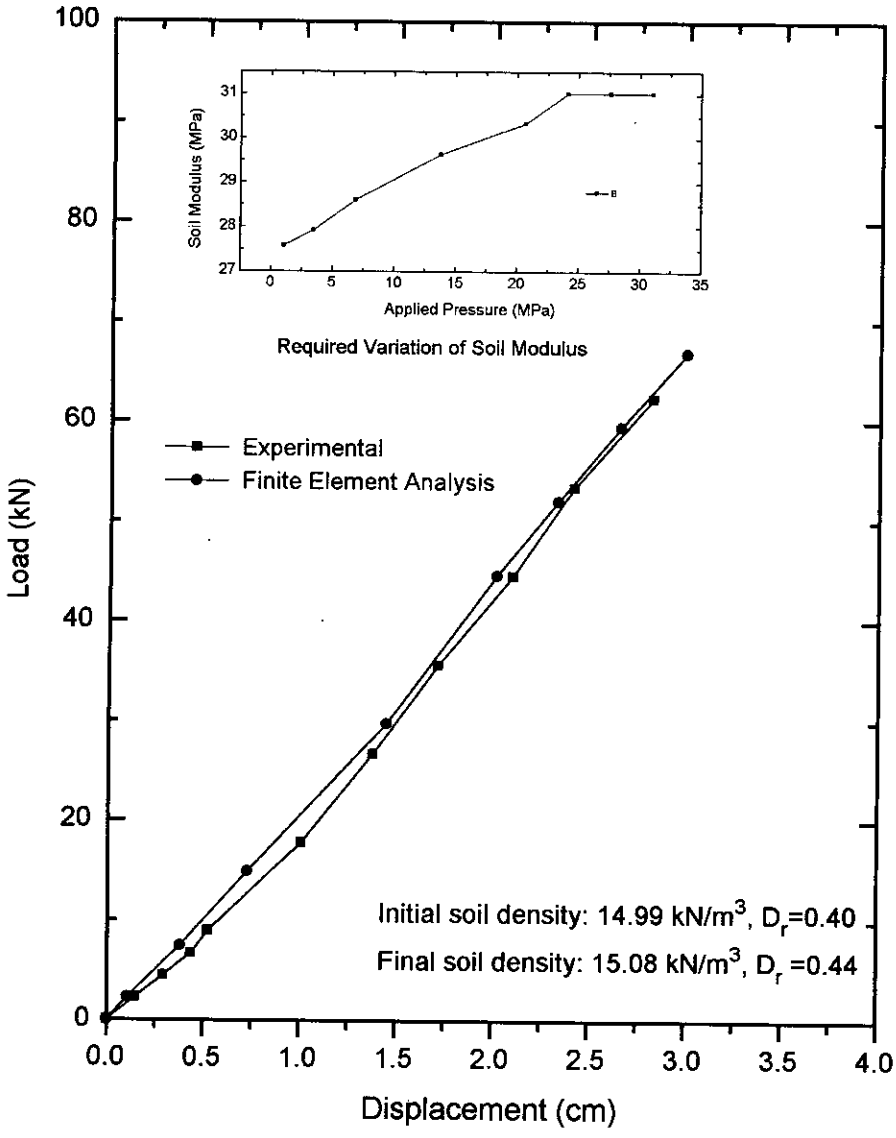

Figure 3.22 Numerical simulation of experimental result for pile with L/D = 7 (D = 102 mm).

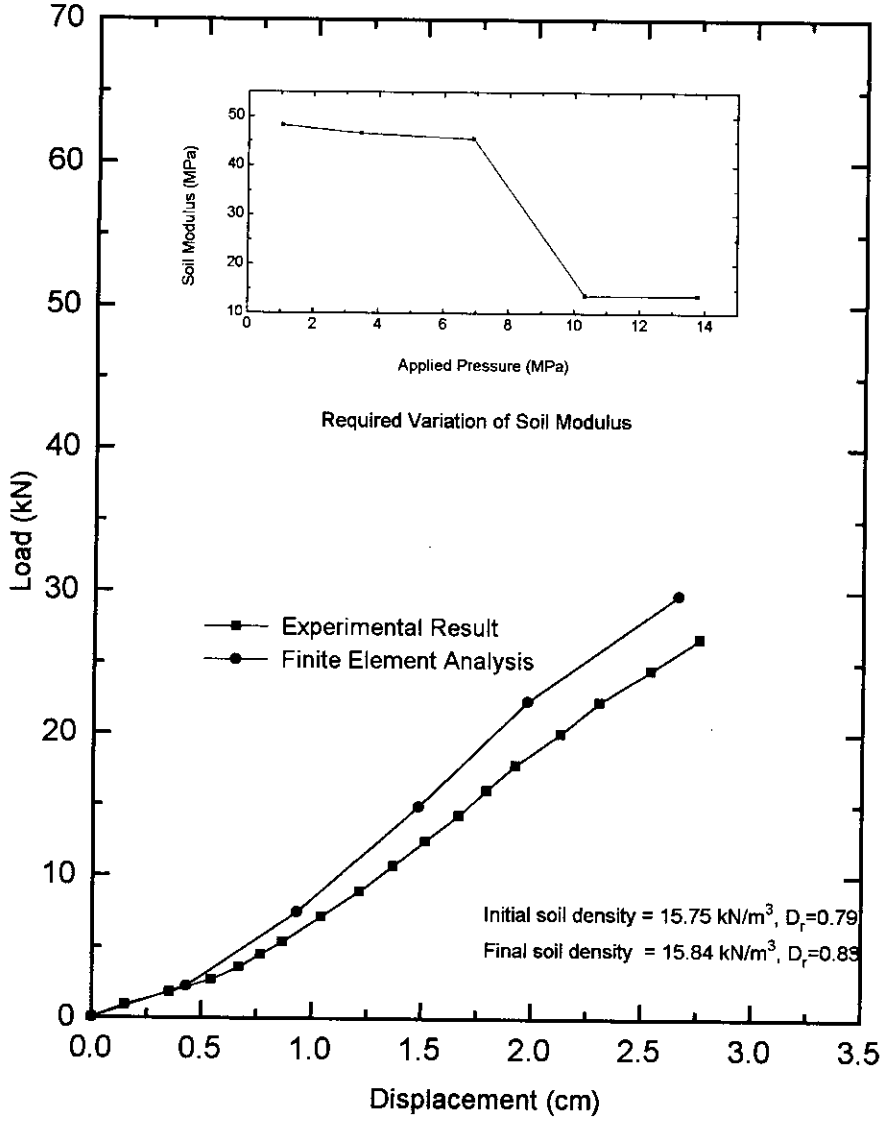

Figure 3.23 Numerical simulation of the experimental result for pile With L/D =5 (D = 102 mm).

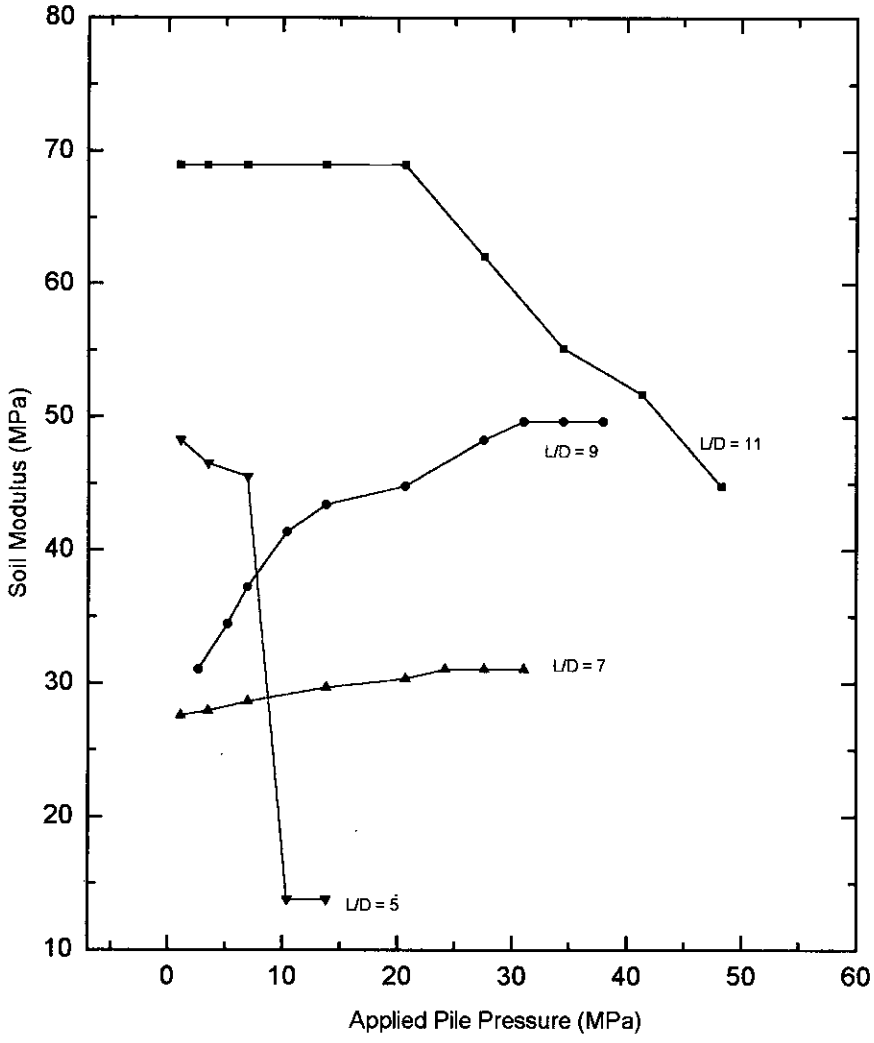

Figure 3.24 Variation of soil modulus with applied load

An empirical equation is proposed to formulate the general trend of these normalised load displacement curves. In doing so, an exponential function in the form of Eq. 3.4 has been selected. The rationale of choosing an exponential function to represent the model for determining plugged pile capacity is lying in the exponential nature of normal stress distribution during arching and subsequent plugging. The proposed empirical equation is,

$$\frac{P}{P_u} = a\left(\frac{S}{0.1 \times D}\right)^n \qquad 3.4$$

where, P = Applied load on pipe pile

P_u = Ultimate load at 0.1D settlement

S = Settlement of pile

a and n are parameters to be determined.

The proposed equation (Eq.3.4) is regressed by least square method with the normalised load-displacement data (Fig.3.25 to Fig.3.28) to determine the values of the parameters a and n. It is observed here that value of 'a' is almost constant. Average value of 'a' is proposed to be 1.03744. Constant 'n' is correlated with the variation of L/D and change in relative density. An empirical equation for 'n' is proposed as Eq. 3.5. The equation relates n with L/D and change in relative density.

$$n = 0.82326 - 0.03009\frac{L}{D} + 15.6866(D_{ri} - D_{rf}) \qquad 3.5$$

Here, D_{ri} = Initial relative density of soil

D_{rf} = Final relative density of soil

The normalised load displacement behaviours predicted by Eq.3.4 have been compared with the corresponding load displacement behaviours obtained from experiments in Fig.3.29 to Fig.3.32. Value of 'n' has been calculated using Eq.3.5 and value of 'a' has been taken to be 1.03744. It is clear from Fig.3.29 to Fig.3.32 that the load displacement curves obtained from the proposed model and the load displacement responses obtained from experiments are almost same. Thus, it can

be stated that the proposed empirical equation simulates the load displacement responses satisfactorily for pipe of 102 mm diameter.

Table 3.4 Values of 'n' and 'a' From Best Fitted Curves

L/D	Change of relative density	n	a
11	0.02	0.7753	1.0248
9	0.033	1.1537	1.0422
7	0.041	1.1813	1.0510
5	0.042	1.3536	1.0317

Ultimate capacity is defined here as the load required to produce a settlement of 10% of the pile diameter. With this consideration, a formula (Eq.3.6) is proposed for the calculation of ultimate capacity based on the experimental results (Fig.3.12). The nature of the curve (Fig.3.12) shows two distinct phase of frictional capacity of pipe pile. One is before plugging, identifiable by uniform increase in pile load capacity. The other is after plugging which can be determined by sharp change in pile load capacity with (L/D) ratio. As the theoretical variation of plugged pile load capacity is parabolic with (L/D), a second degree parabolic curve is proposed for this part of the empirical equation of P_u.

$$P_u = -14.8063 + 4.4847\frac{L}{D} \quad \text{for} \quad \frac{L}{D} \le 9$$

$$= -119.5644 + 21.9732\frac{L}{D} - 0.6589\left(\frac{L}{D}\right)^2 \quad \text{for} \quad \frac{L}{D} \ge 9 \qquad 3.6$$

Fig.3.33 compares the proposed formula of ultimate capacity with the experimental result.

One limitation of the proposed formula is that it has been formulated for 102 mm diameter pile with (L/D) ratio ranging from 5 to 11 in sand possessing almost uniform properties in the laboratory. Similar empirical relations for piles of other diameter should be obtained. This may lead to the development of a design aid for calculating approximate plug capacity for any allowable settlement. Moreover, this study presents a methodology by which an empirical method can be developed for piles of any diameter with varying soil properties.

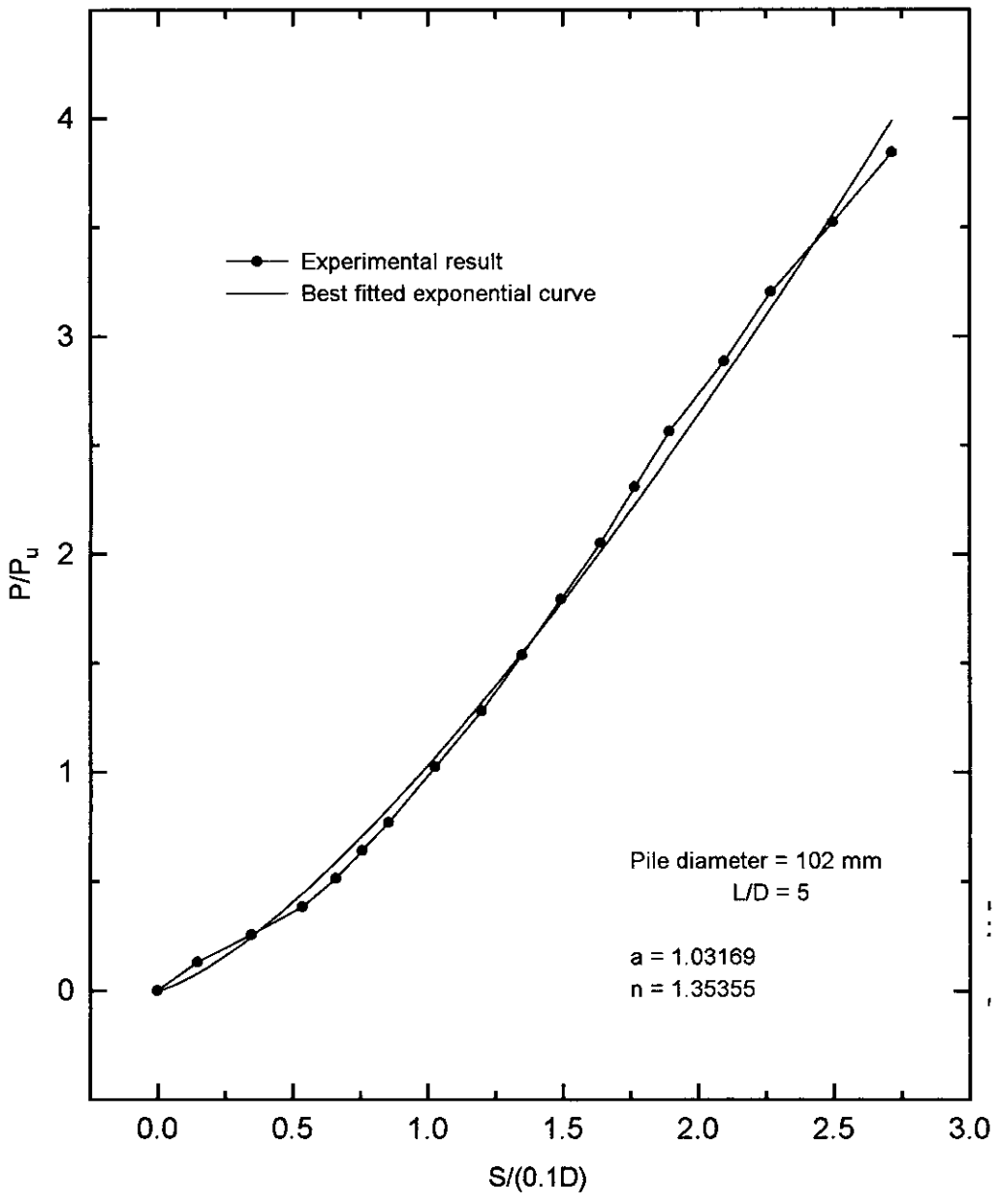

Figure 3.25 Normalized load displacement response along with the best fitted exponential curve

(D = 102 mm, L/D =5)

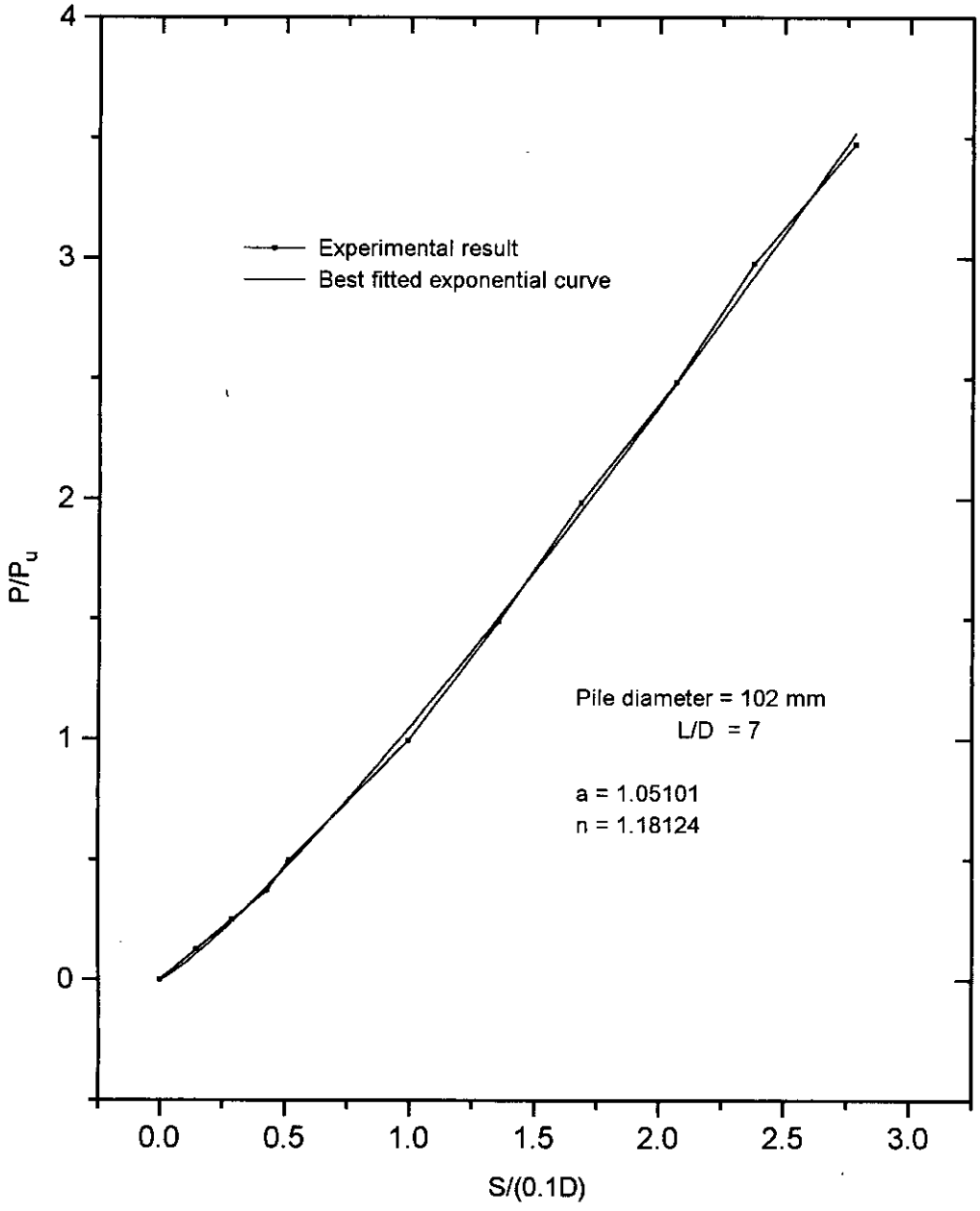

Figure 3.26 Normalized load-displacement response along with the best fitted exponential curve.

(D = 102 mm, L/D = 7)

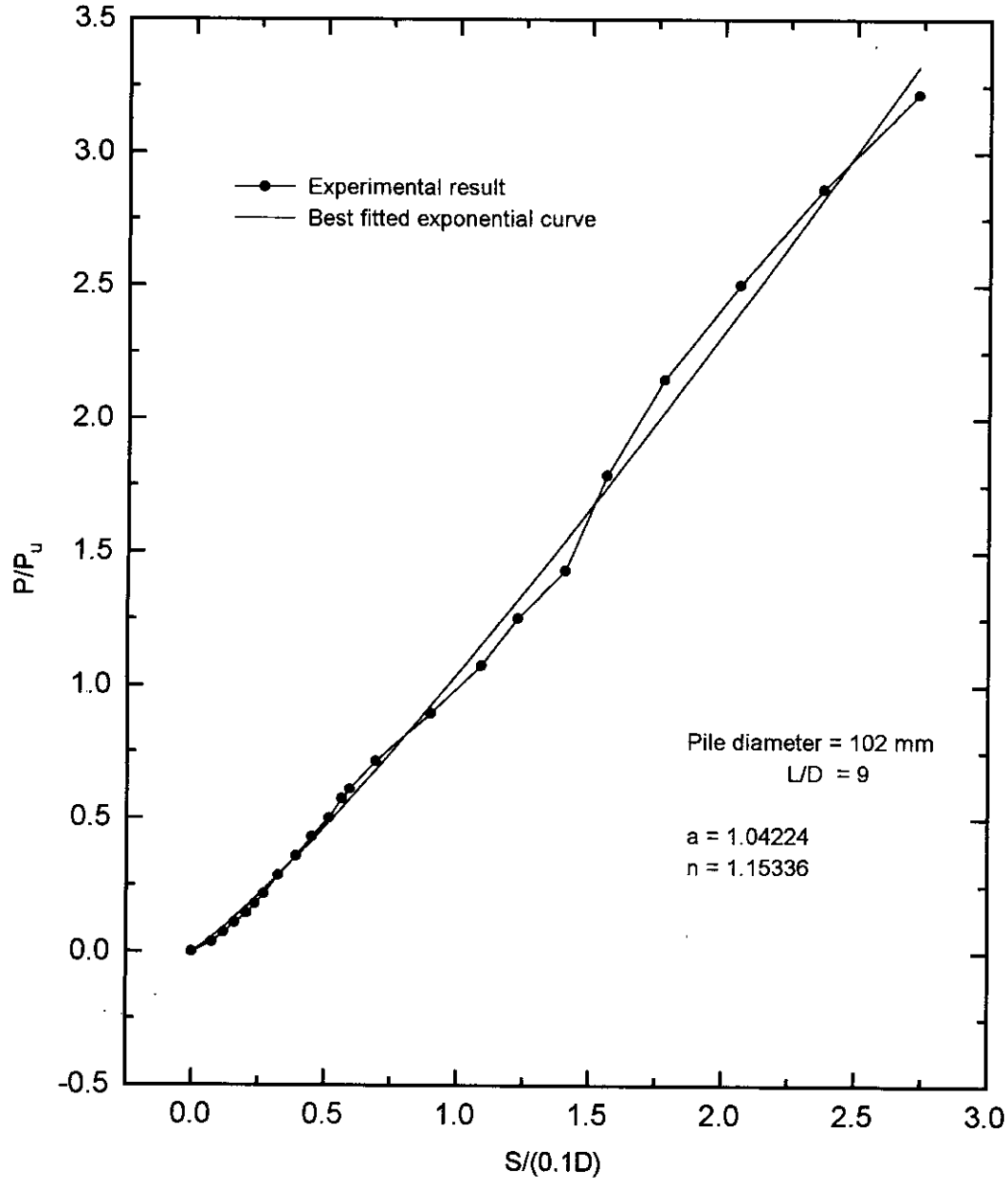

Figure 3.27 Normalized load-displacement response along with the best fitted exponential curve.

(D = 102 mm, L/D = 9)

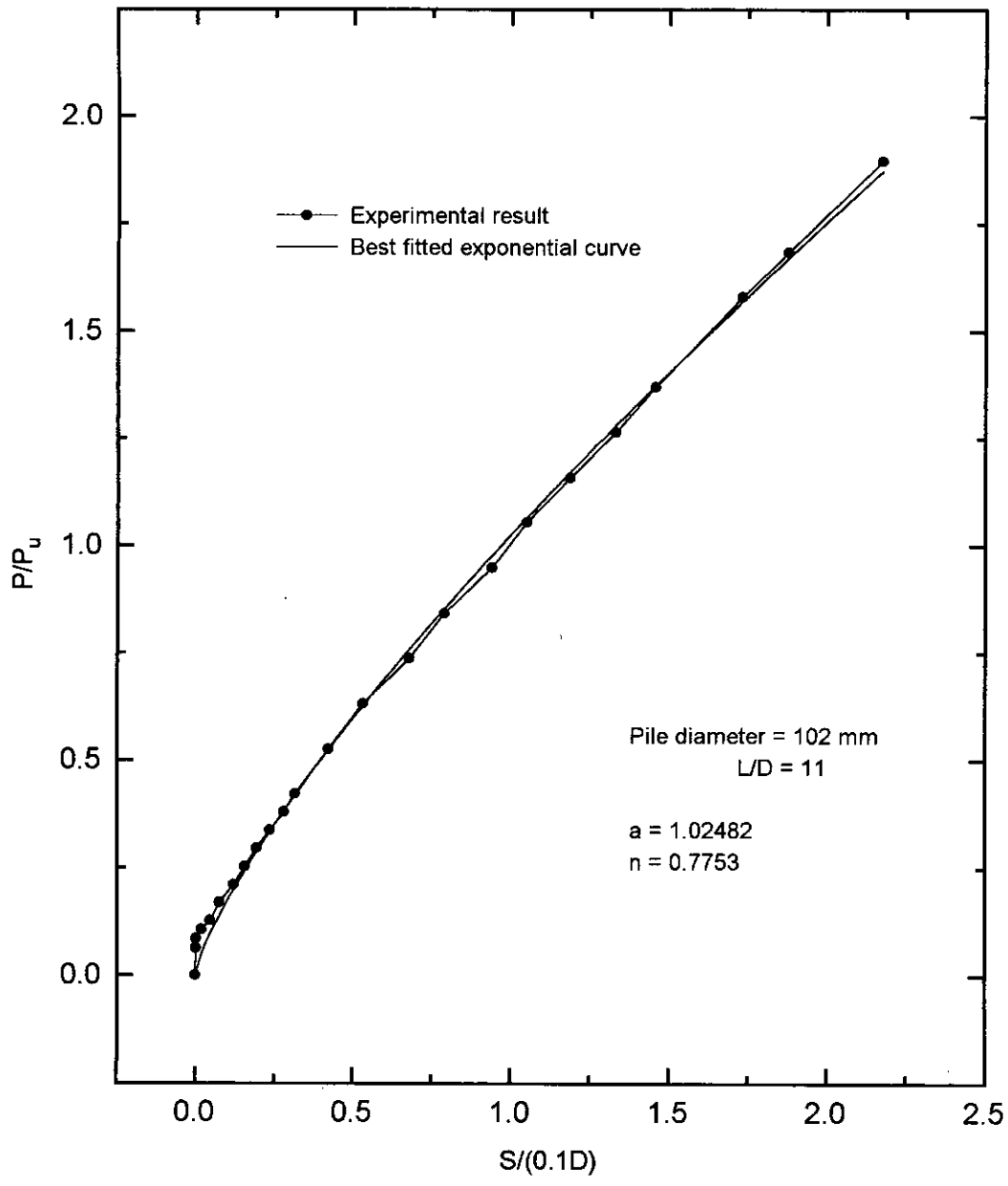

Figure 3.28 Normalized load-displacement response along with the best fitted exponential curve.

(D = 102 mm, L/D = 9)

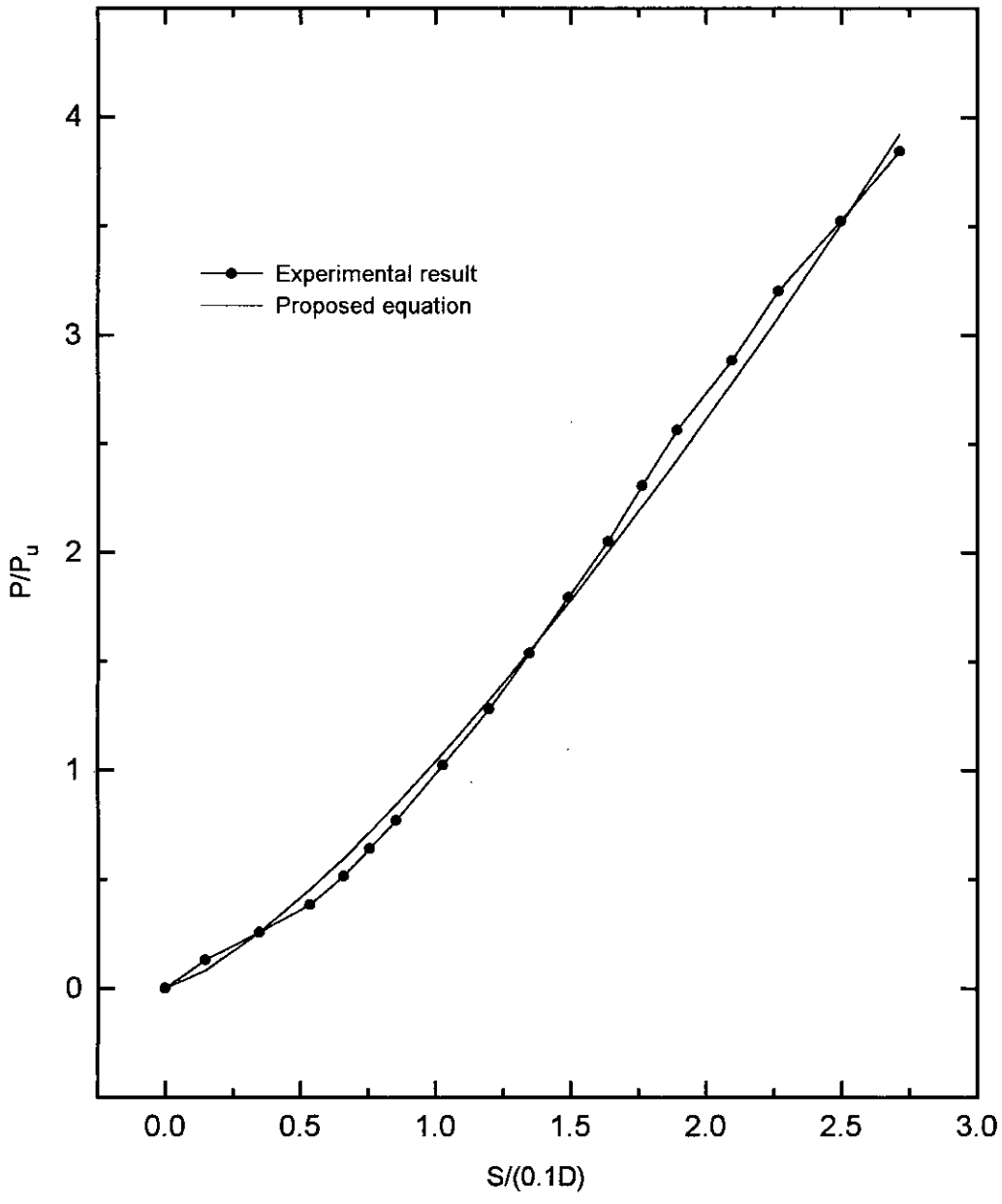

Figure 3.29 Normalized load displacement response from experiment and proposed model (102 mm dia pile, L/D =5)

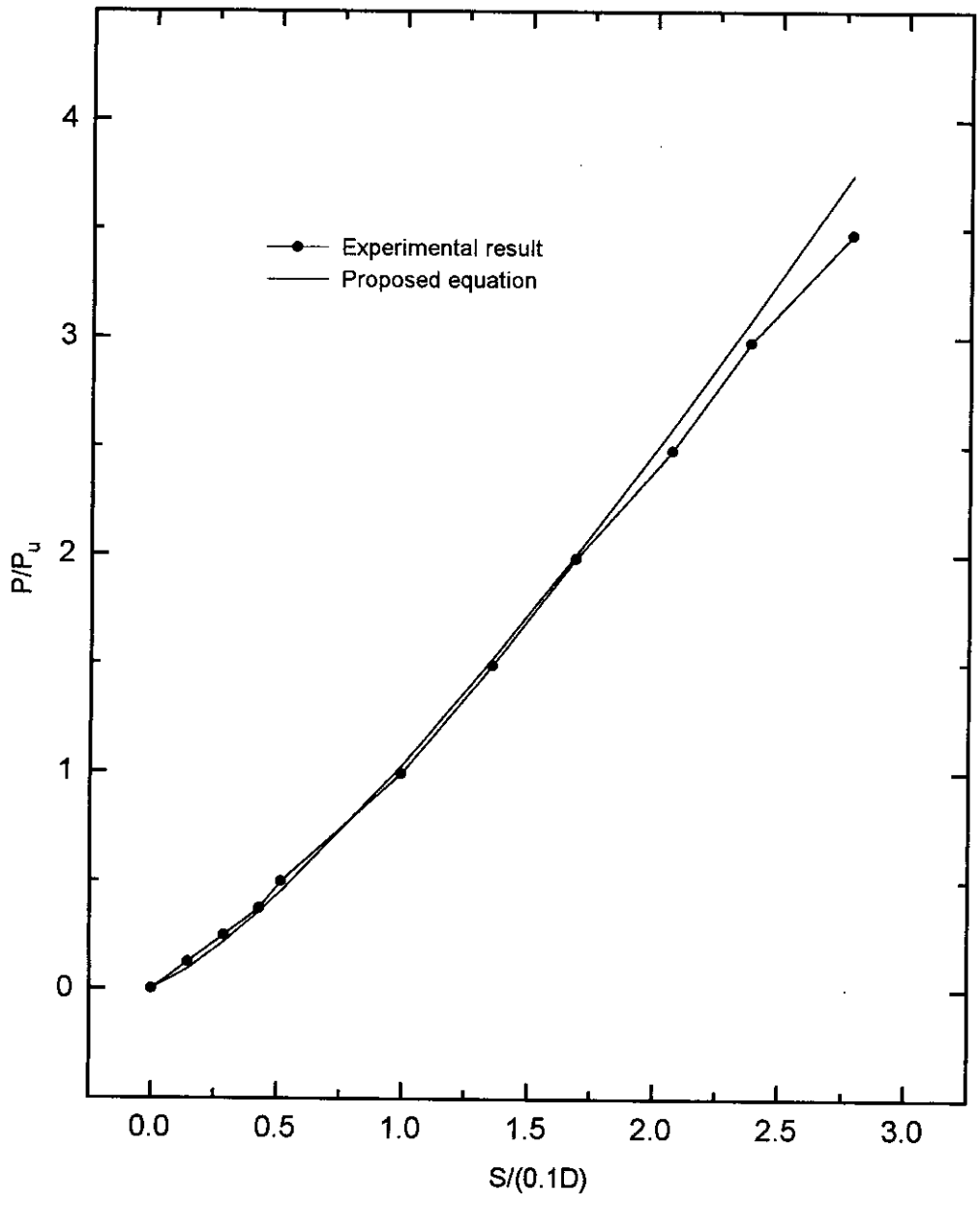

Figure 3.30 Normalized load displacement response from experiment and proposed model (102 mm diameter pile, L/D = 7)

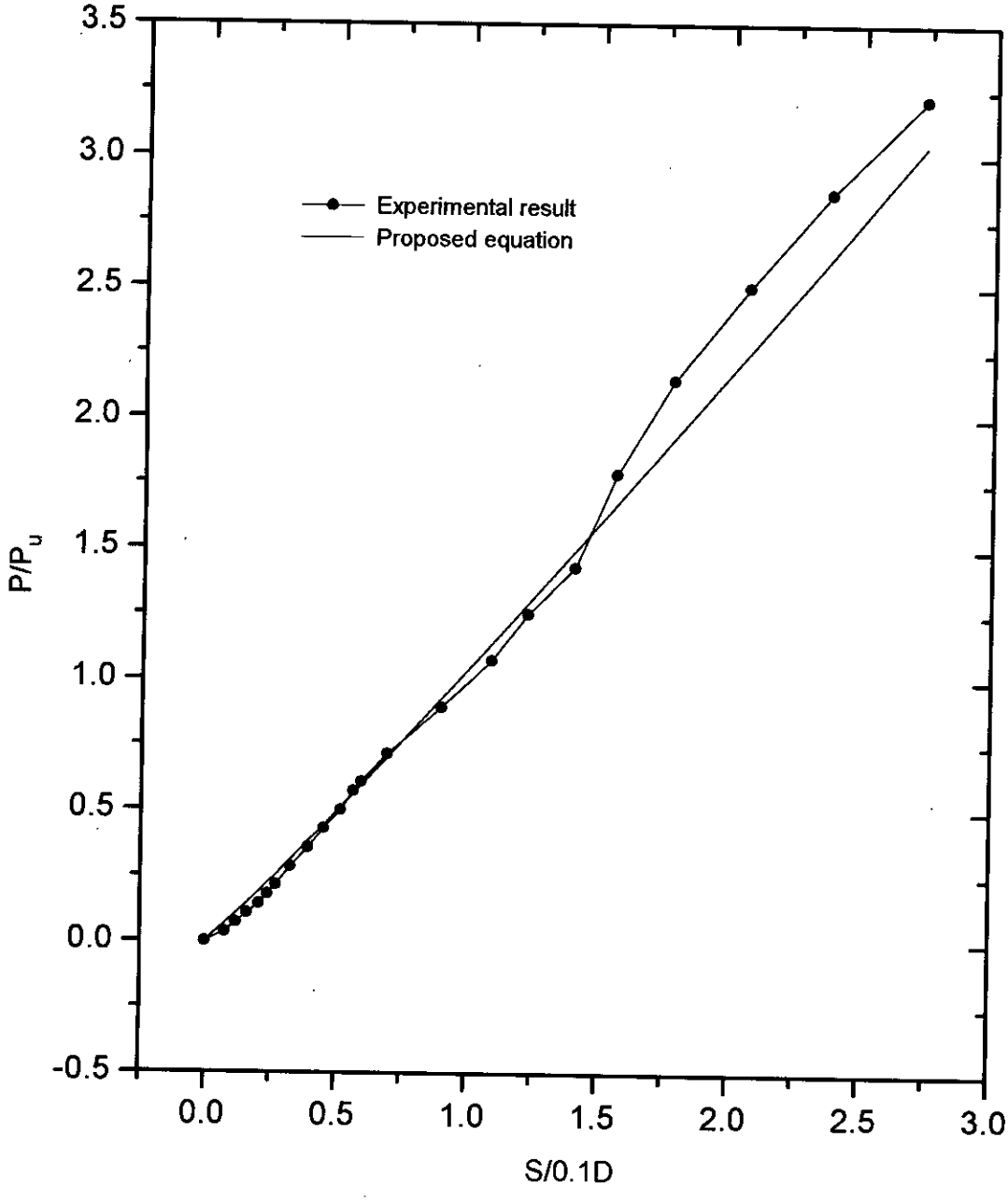

Figure 3.31 Normalized load displacement response from experiment and proposed model (102 mm diameter pile, L/D =9)

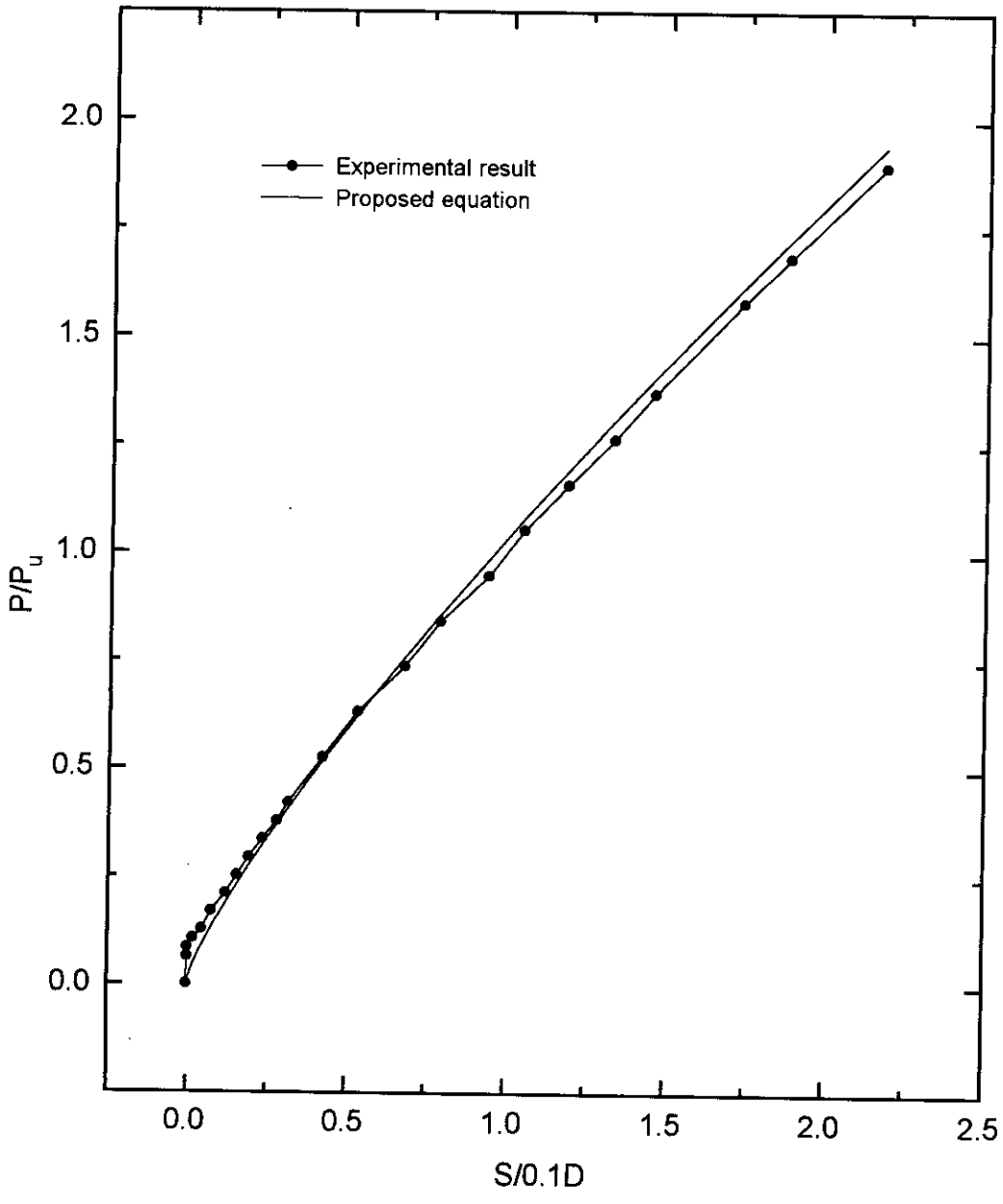

Figure 3.32 Normalized load displacement response from experiment and proposed model (102 mm diameter pile, L/D = 11).

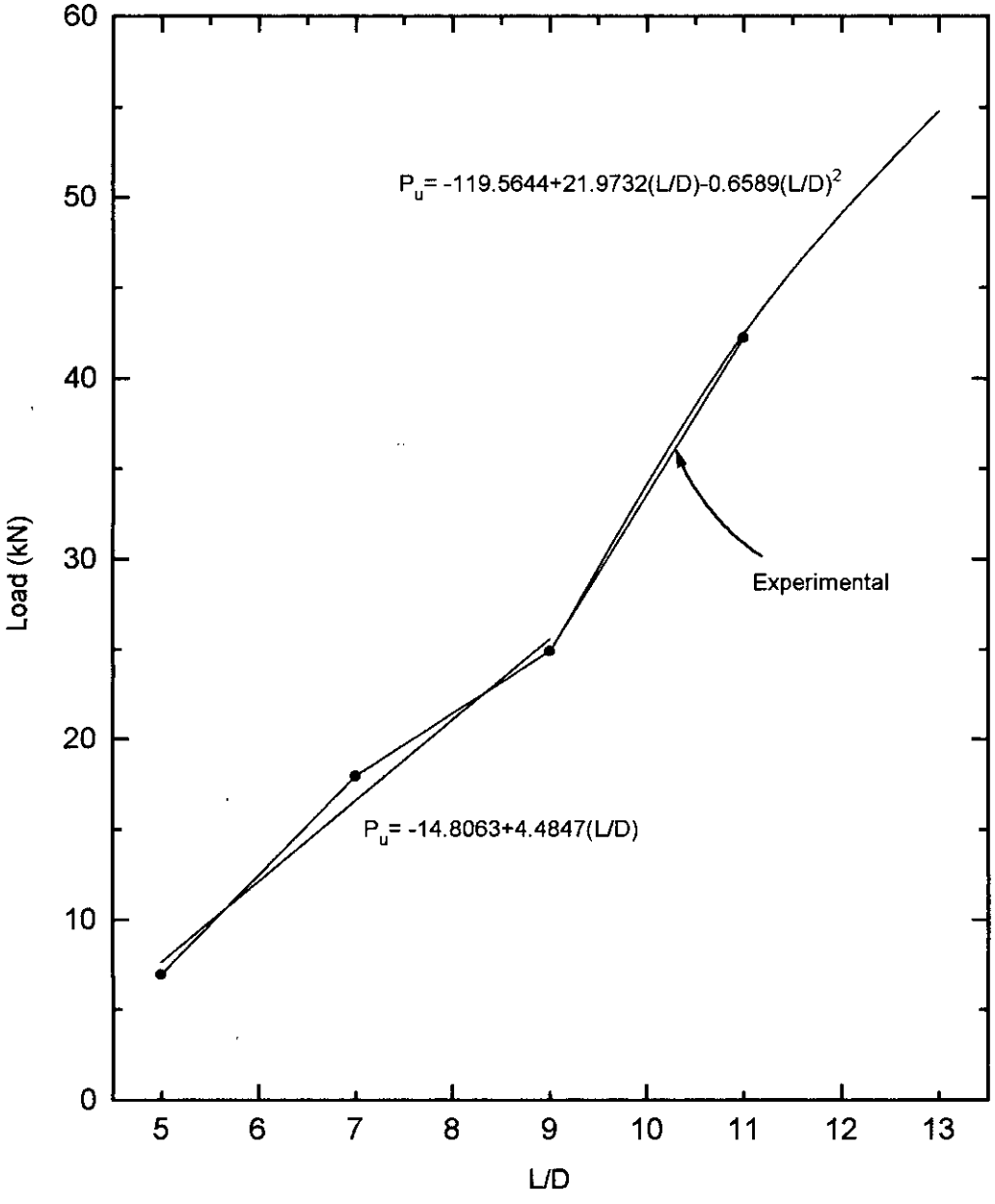

Figure 3.33 Variation of pile capacity with L/D as predicted by proposed equation and the experimental result (D = 102 mm)

CHAPTER 4

DEVELOPMENT OF ANALYSIS SCHEME

4.1 Introduction

Under axial loading sufficient resistance of soil develop inside the pipe pile. It is also observed from the laboratory investigation that the soil density and related properties change with the increase of load on pile. Downward movement of the soil in the experiment was resisted by wooden block. But in the real situation the soil will be resisted by the soil mass at the pile base. So the change in the properties may not be so significant in real situation. To simulate the loading condition numerical analysis by Finite Element Method was performed.

4.2 Analysis Scheme

Analysis of a continuum by finite element method comprises idealisation of continuum into descretized elements, evaluation of element characteristics by a suitable constitutive law and analysis of element assemblage by an efficient non-linear solution techniques.

The finite element programme, CRISP (CRItical State Programme) (Britto & Gunn ,1987) is used in the analysis of pipe pile. Features of the CRISP are discussed in Appendix E. An axisymmetric finite element analysis is performed for axially loaded pile soil system. Load-displacement behaviour, stress distribution in the soil, pile and pile-soil interface are observed from the analysis. Then the effect of the depth of inside soil on pipe pile capacity is viewed.

4.3 Description of Finite Element Model

Idealisation of the problem and selection of suitable element type is very important in finite element method. For axially loaded pile it is quite reasonable to idealise the problem as an axisymmetric case.

There are ten different element types available in CRISP. In this study, linear strain quadrilateral element with displacement unknown has been used for

decretization of both pile and soil. All these elements are basically standard displacement type element (Zienkiewicz, 1971). For interface, the 6 nodded interface element with displacement unknown is used. Fig. 4.1 shows the typical idealised system of the problem. In figure 4.1, zone 1 represent the soil inside the pile, zone 2 represent the interface of pile with the inner soil, zone 3 represent the pile material, zone 4 represent the interface of pile with outer soil, zone 5 represent the pile outer soil and zone 6 represent the soil below the pile. Finite element mesh used in the analysis are shown in Appendix C.

The lateral extent of mesh plays a important role in the analysis of problem. Outer extent of soil for the current research is chosen to be 8 to 10 times the pile diameter. To investigate the effect of pile extent, distribution of the vertical stress over the external soil is observed in the analysis.

It can be observed from pressure bulb for vertical stress that effect of pile stress on soil is insignificant if the depth of soil is larger than 3 to 4 times the pile diameter. For this reason to select the vertical extents of soil for the analysis, depth of soil below the pile tip is taken to be 5 times the pile diameter.

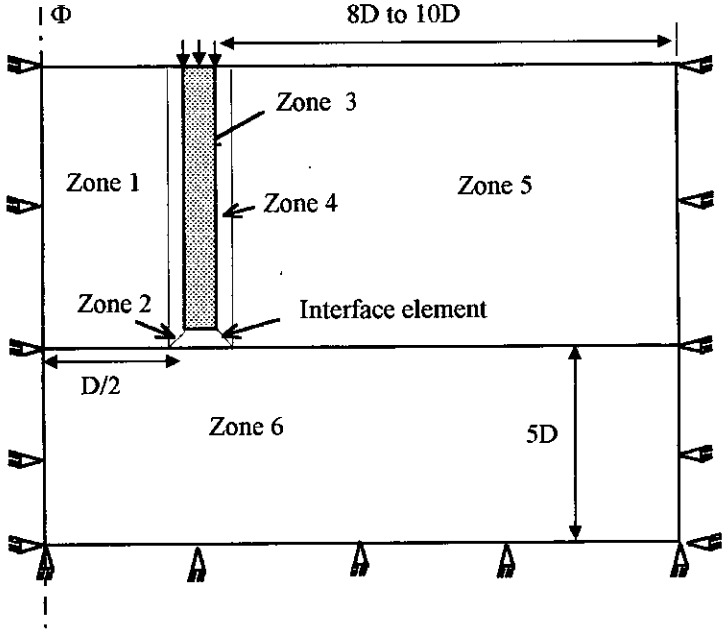

Figure 4.1 Idealisation of pipe pile problem for finite element analysis.

4.4 Material Properties

Any Finite Element Analysis is basically founded on constitutive law of the material being analysed. Constitutive law of the material determines the number and type of material properties to define the material behaviour in its evolution process during loading. In this study, sand is used as internal filler soil of pipe pile. So Mohr-Coulomb type of elasto-plastic constitutive law is used to describe the behaviour of sand. The elasto-plastic J_2 model of sand requires a knowledge of the deformation parameters E_s, ν_s of the soil and the soil shear strength parameters C, φ and the pile soil adhesion. Methods of determining soil shear strength are well-established as described in Chapter 2. However, methods for determining the soil deformation parameters are not so well established. There are three ways to determine these parameter: (1) laboratory triaxial test, (2) pile-loading test, and (3) empirical correlation based on experiences.

In order to determine the value of Young's modulus, E_s for situation in which pile-loading test data are not available, a number of published pile test results have been analysed and values of E_s determined (Table 3.2).

Relatively little information is available in the literature for correlations studied on Poisson's ratio . However, this parameter does not vary greatly. For isotropic elastic materials, the entire range of ν_s is from 0 to 0.5. Values of Poisson's ratio, ν_s , obtained from triaxial tests generally lie between 0.25 and 0.35 at relatively low stress level. An average value of 0.3 is reasonable when no test data are available (Poulos 1980). Typical values of ν_s for several materials are given in Table 4.1 (Bowles, 1988).

Correlations for estimating the effective stress friction angle for cohesionless soils have been presented by numerous authors. Early work on this topic suggested simplified tabulated values for the effective stress friction angle, such as those given in Table 4.2 (Kulhawy & Mayne, 1990). Subsequent approaches have correlated the values of φ with one or more soil index parameters such as soil type, relative density and unit weight or void ratio (Fig. 4.2).

Table 4.1 Values ranges for Poisson's ratio, ν_s
(Bowles, 1988)

Types of Soil	ν_s
Clay, Saturated	0.4 - 0.5
Clay, Unsaturated	0.1 - 0.3
Sandy Clay	0.2 - 0.3
Silt	0.3 - 0.35
Sand, Gravelly Sand	0.3 - 0.4
Rock	0.1 - 0.4
Loess	0.1 - 0.3
Ice	0.36
Concrete	0.15

Table 4.2 Representative value of effective stress friction angle
(Kulhawy & Mayne, 1990)

Soil Material	φ' (degree)	
	Loose	Dense
Sand, round grains, uniform	27.5	34
Sand, angular grains, well-graded	33	45
Sandy gravels	35	50
Silty sand	27 to 33	30 to 34
Inorganic silt	27 to 30	30 to 35

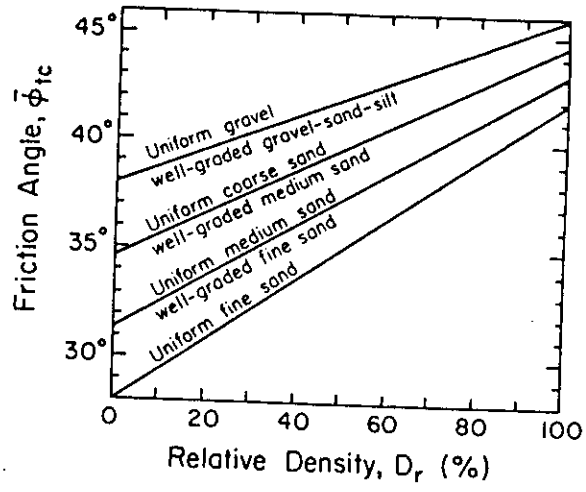

Figure 4.2 Relation of friction angle with relative density.
(Schemertmann, 1978)

Aim of the numerical analysis of the research is to determine the qualitative behaviours of pipe pile in granular soil. In doing so, the average values of different soil parameters have been selected from the readily available literatures based on soil test data. Moreover, this study is mainly concerned with proposing a methodology by which the load response of pipe pile in any soil can be observed. The material properties of different material zones have been presented in Table 4.3, 4.4 and 4.5. A complete input file for both geometry and main part of the program (CRISP) for a typical pipe pile problem has been presented in Appendix A.

Table 4.3 Parameters for sand used in FEM analysis

Zone No.	E_o MN/m^2	ν	C	φ	γ_{bulk} kN/m^3	Rate of Increase of Soil Modulus
1	35	0.3	0	35°	18.9	0
5	35	0.3	0	35°	18.9	0

Table 4.4 Parameters for pile materials used in FEM analysis

Zone No.	E_1 MN/m^2	E_2 MN/m^2	ν	γ kN/m^3
3	200	200	0.25	77

Table 4.5 Parameters for interface elements used in FEM analysis

Zone No.	C	δ	K_n MPa	G_s MPa	G_{res} kPa
2	0	20	41	13.8	7
4	0	20	41	13.8	7

4.5. Data Generation

CRISP requires enormous input data for the both the geometric and main part of the program. It is difficult to write such a large number of data correctly by hand calculation. For this reason a data generation program is developed which requires only a few input data concerning the pile length, depth of soil, pile diameter and lateral extent of soil to be used in the analysis. The program generate the mesh, nodal co-ordinates connectivity of element, element type, total number of elements and nodes, material zone numbers of each element etc. which are necessary to run the geometry part of CRISP, The soil-pile system is first divided into different material zones. For the main part of CRISP, the program generate the boundary conditions for the mesh generated. The program code is presented in Appendix D.

4.6 Load-Displacement Responses

To investigate the effect of the depth of embedment of pile and the variation of pile diameter on the load response of pipe pile, a scheme has been followed in this numerical study. Firstly diameter of the pile has been kept constant and the load

displacement responses for different depth of embedment of pile has been investigated. With the same depth of embedment, analysis is performed for pile of different diameters (102 mm, 152 mm, 203 mm). Fig. 4.3, Fig. 4.5 and Fig. 4.7 represent the load displacement responses of 102 mm, 152 mm and 203 mm diameter piles respectively with different depth of penetration. Normalised load-displacement curves are plotted (Fig. 4.4, Fig. 4.6, Fig. 4.8) by dividing the pile stress by a ultimate stress and the settlements by 0.1 times pile diameter. Ultimate stress is defined as the stress corresponding to settlement of 0.1 times the diameter (Tomlinson, 1980). Depth of penetration is expressed here as a multiple of pile diameter. From figure 4.4, 4.6 and 4.8 it is observed that within the allowable range of settlement, normalised stress-displacement response for any pipe pile with all L/D ratio, is identical. This finding provide a valuable information that in the allowable range of settlement all stress-displacement relation of any pipe pile can be represented by a non-dimensional equation relating stress ratio and settlement ratio.

Now to observe the effect of pile diameter on the load response, load displacement curves are plotted with constant depth of pile penetration for piles of different diameters. Fig. 4.9, Fig. 4.10 and Fig. 4.11 represent the load-settlement curves with different diameters of piles for pile penetration of 5D, 10D and 15D. It is also observed here that for any L/D ratio, normalised stress-settlement curve of pipe pile of any diameter is identical and can be represented by a non-dimensional equation.

Efforts have been made to observe the increase of pile capacity with the increase of depth of pile embedment. Capacity of pile for different pile embedment depend on the allowable level of settlements of the piles. In order to examine the variation of pile capacity with the depth/diameter ratio, investigations were performed at settlements of 5%, 10%, 15% and 20% of pile diameter. Fig. 4.12 to Fig. 4.14 indicates the variation of pile capacity with the pile depth/diameter ratio for different level of settlement for pile of different diameters. It is observed that with the increase of depth/diameter ratio pile capacity increases, but the rate of increase decreases. It is also observed that for depth/diameter ratio greater than 12 to 15 the increase of pile capacity is insignificant. It can be concluded from this observation that penetration of pipe pile to a depth of 12 to 15 times the diameter is sufficient to derive sufficient capacity for a particular pile.

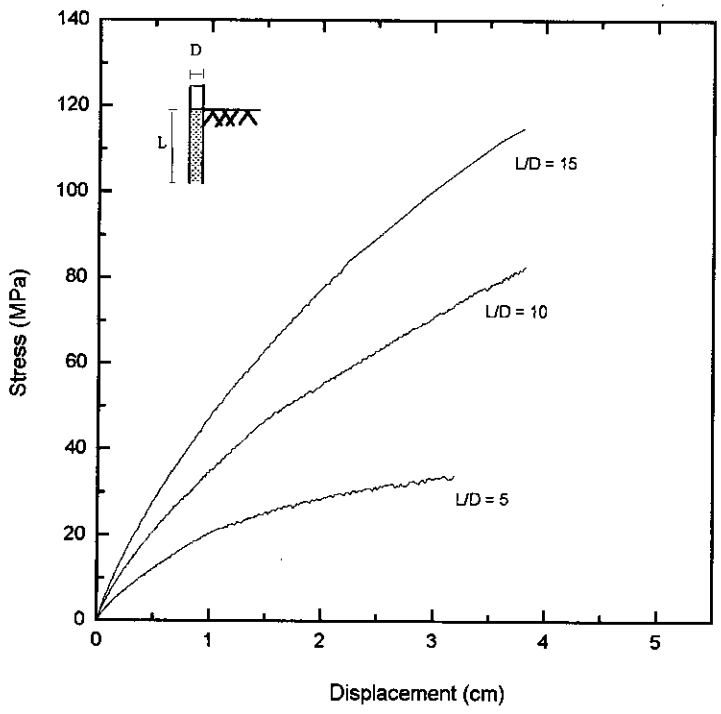

Figure 4.3 Stress-settlement curves of 102 mm diameter pile for different depth of pile penetration.

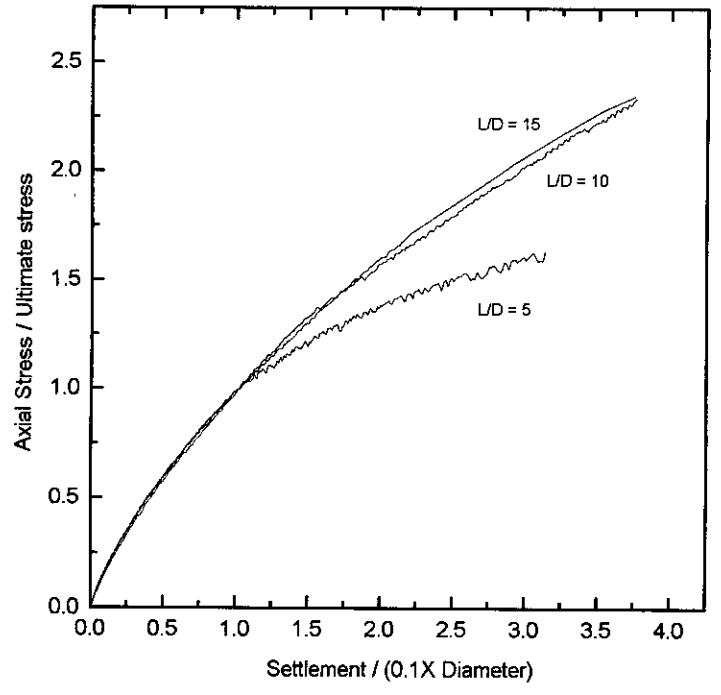

Figure 4.4. Normalized stress-settlement curves of 102 mm diameter pile.

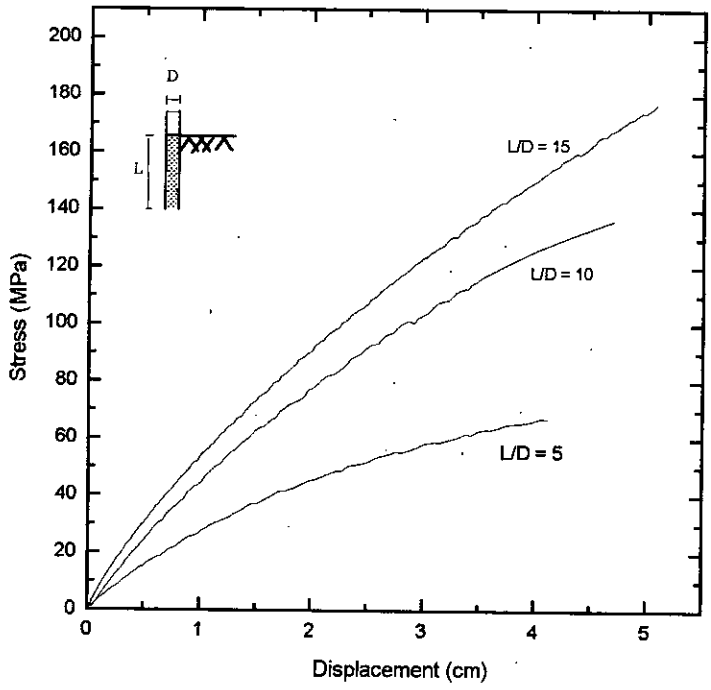

Figure 4.5 Stress - settlement curves for 152 mm diameter pile at different depth of penetration.

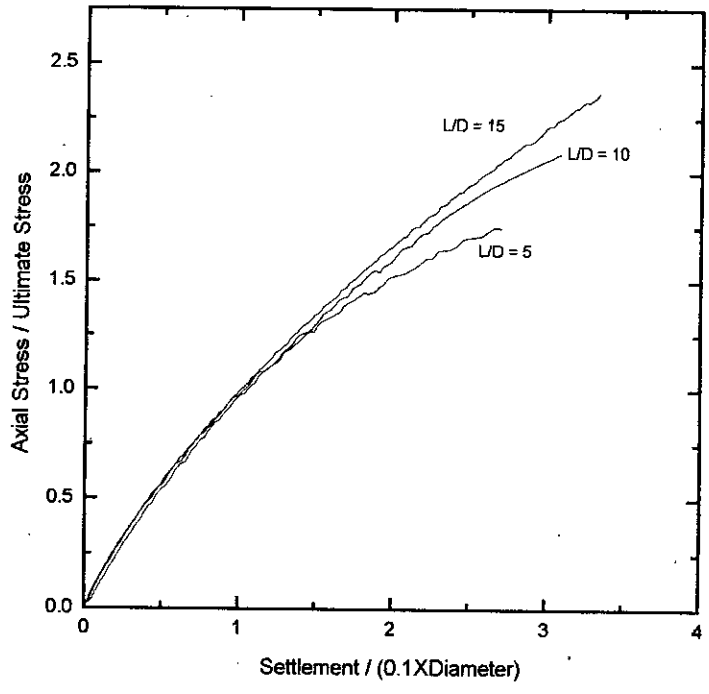

Figure 4.6. Normalized stress - settlement curves of152 mm diameter pile with different depth of penetration.

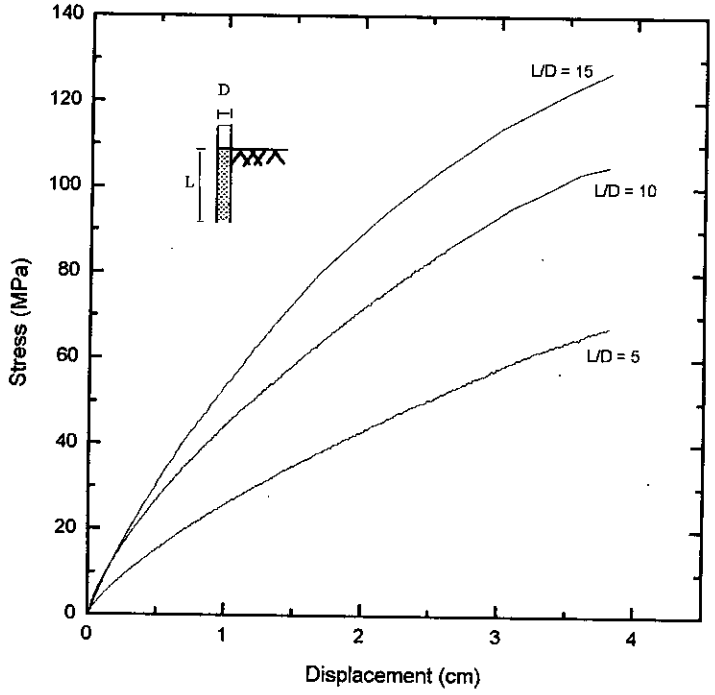

Figure 4.7. Stress -settlement curves of 203 mm diameter pile at different depth of penetration.

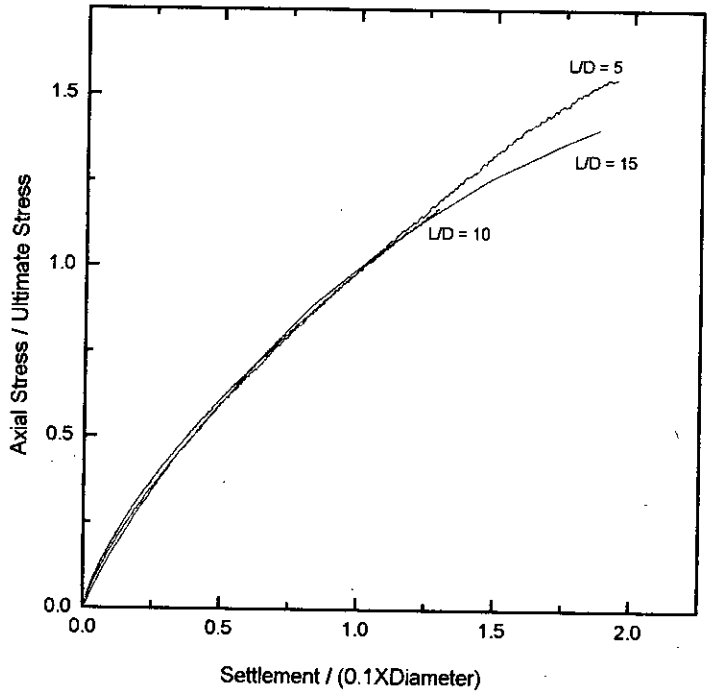

Figure 4.8. Normalized stress - settlement curves of 203 mm diameter pile at different depth of penetration.

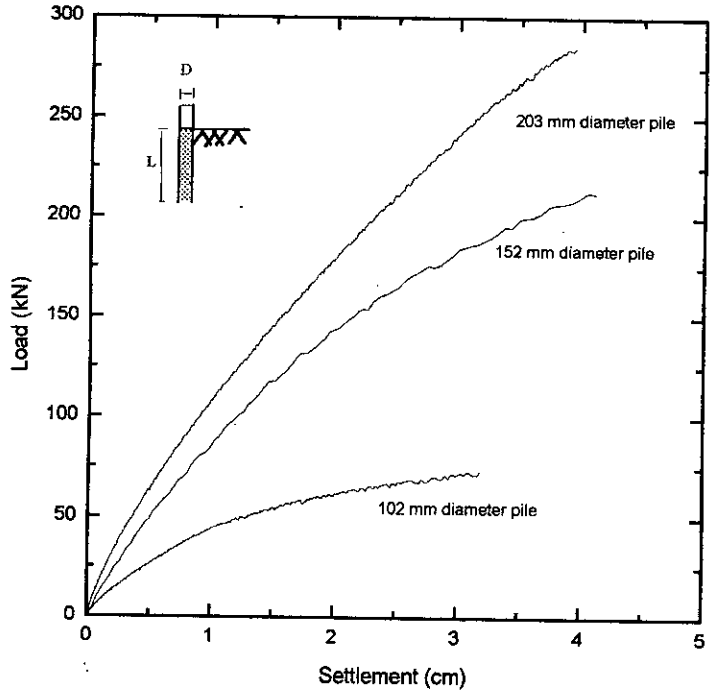

Figure 4.9(a). Load-settlement curves at L/D = 5.

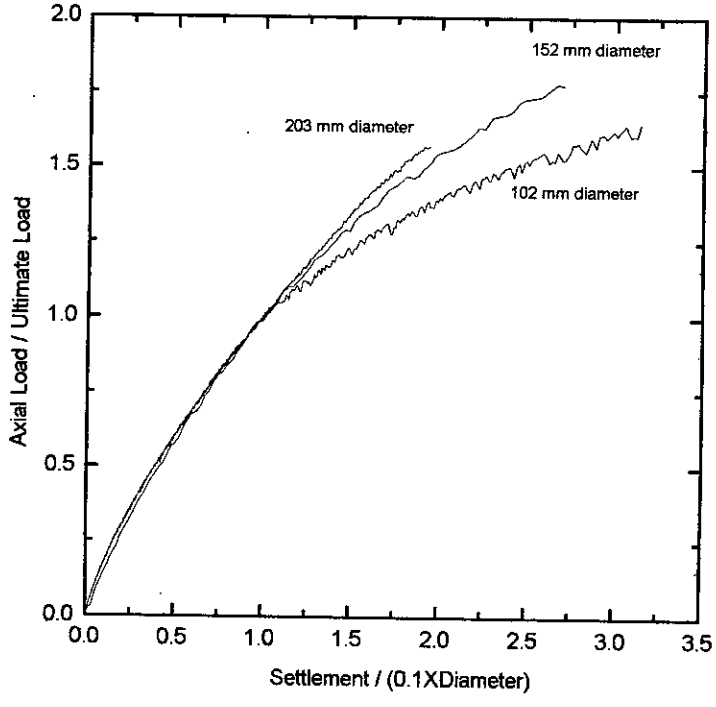

Figure 4.9(b) Normalized load-settlement curves at L/D = 5.

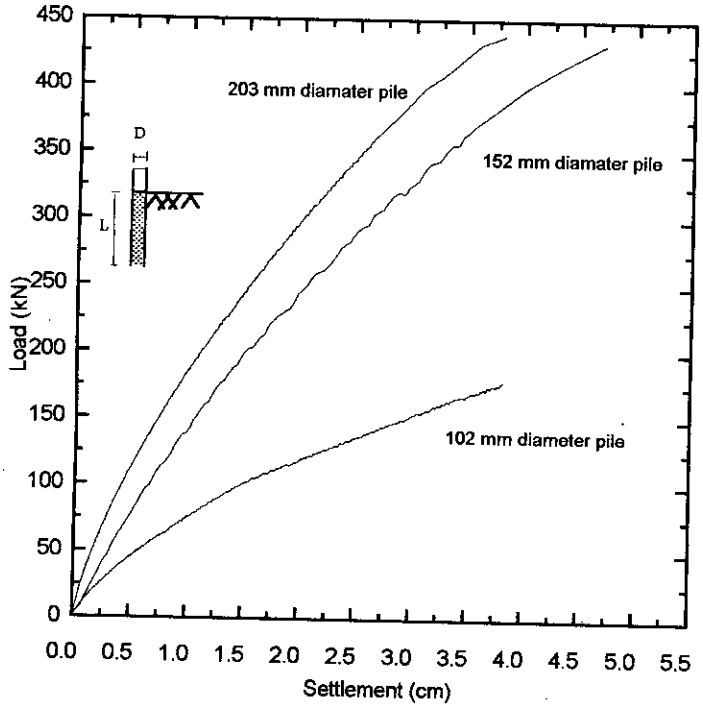

Figure 4.10(a) Load - settlement curves at L/D = 10.

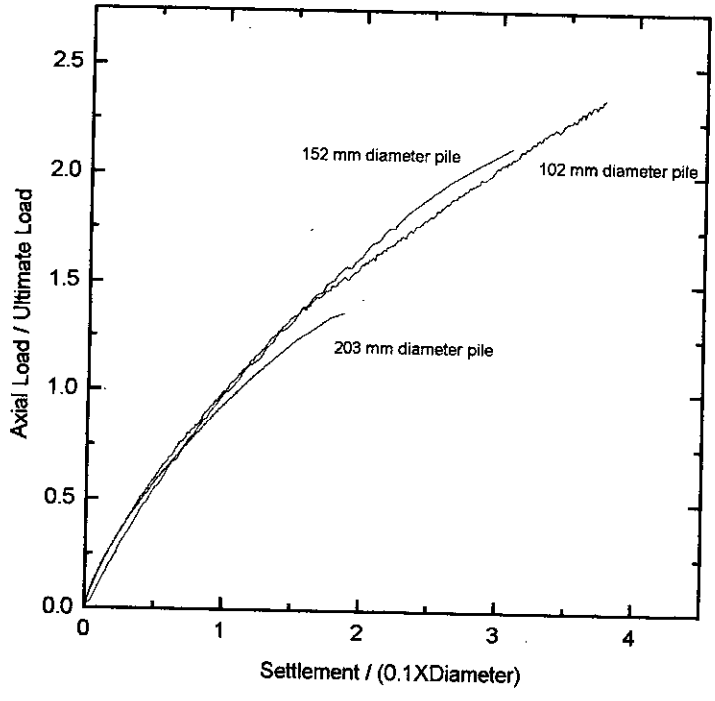

Figure 4.10 (b) Normalized load - settlement curves at L/D =10.

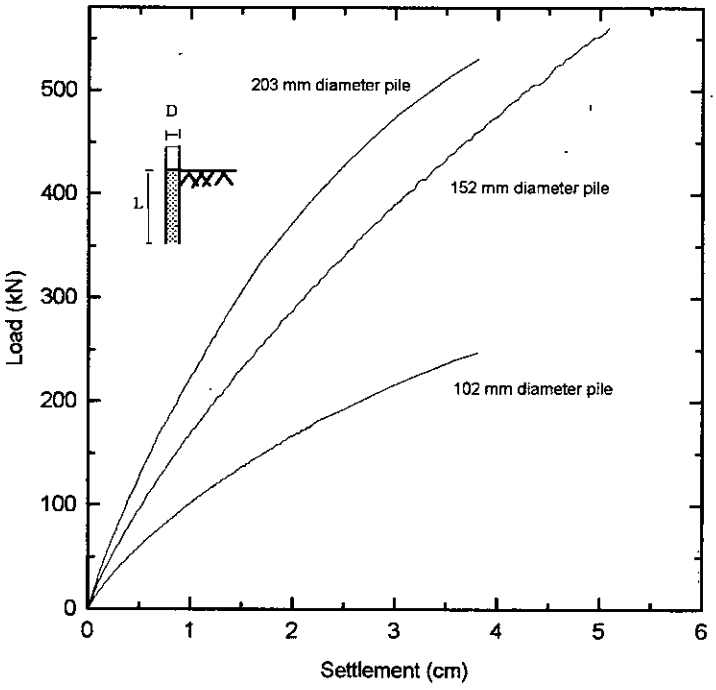

Figure 4.11(a) Load - settlement curves at L/D = 15.

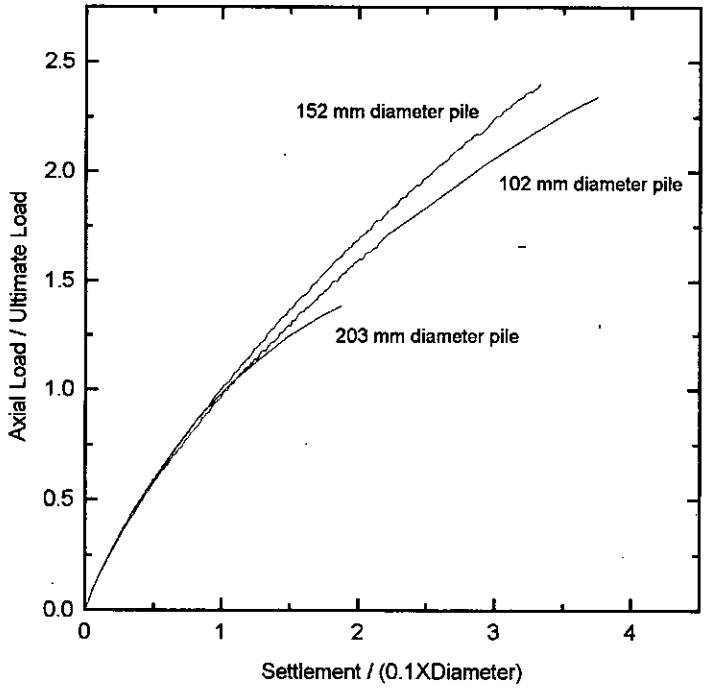

Figure 4.11(b) Normalized load - settlement curves at L/D = 15.

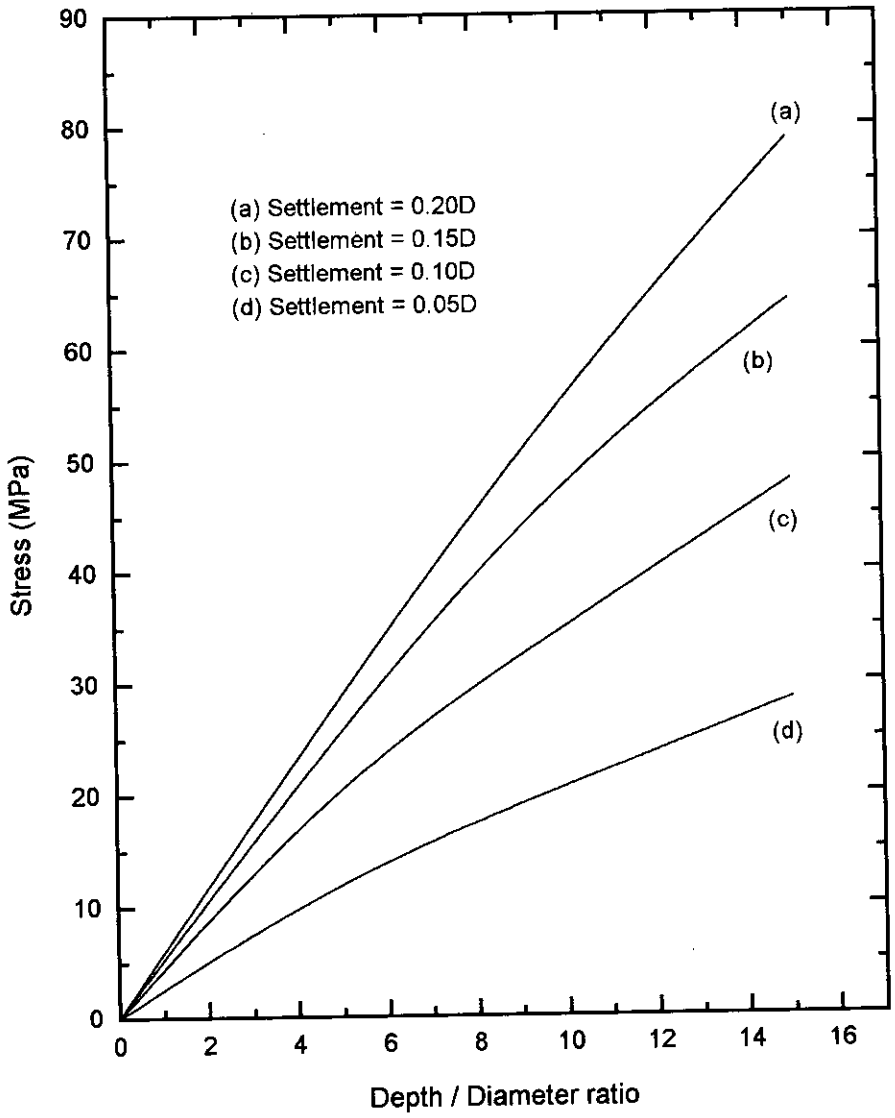

Figure 4.12 Variation of pile capacity with depth/diameter ratio at different level of settlement (D = 102 mm).

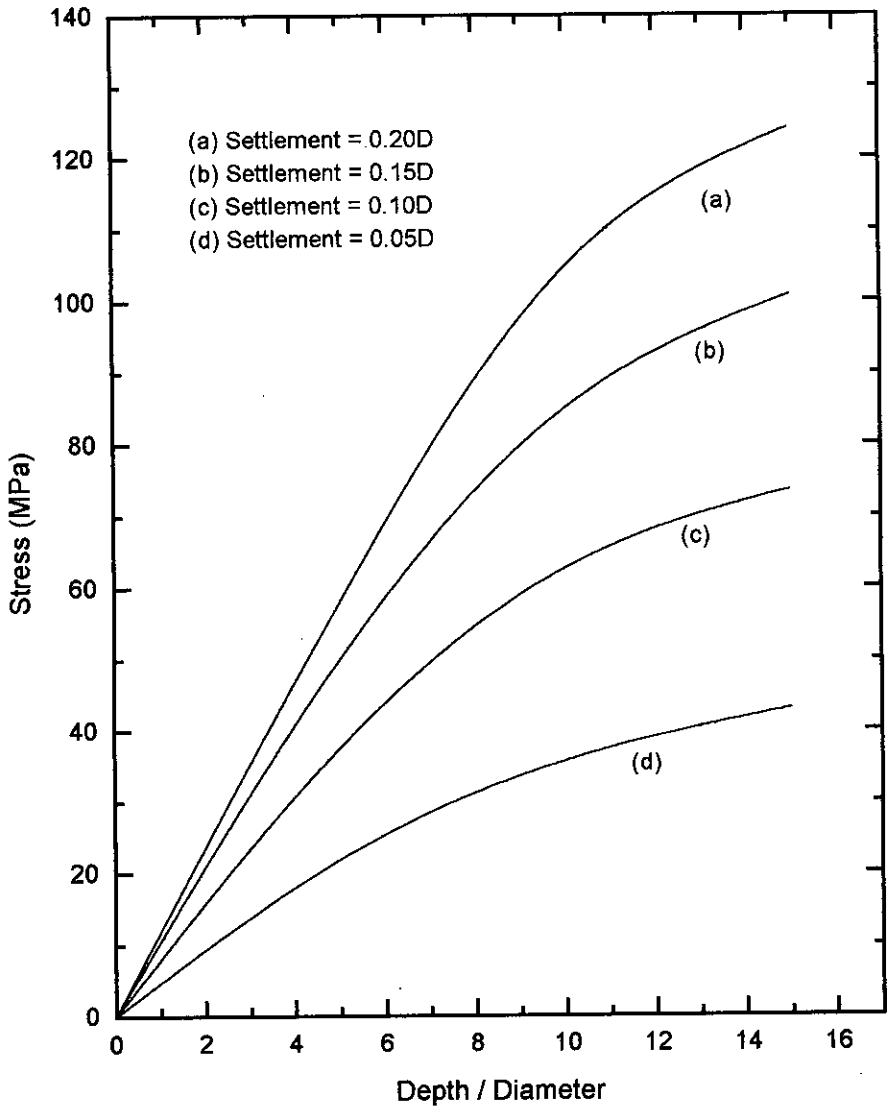

Figure 4.13 Variation of pile capacity with depth/diameter ratio at different level of settlement (D = 152 mm).

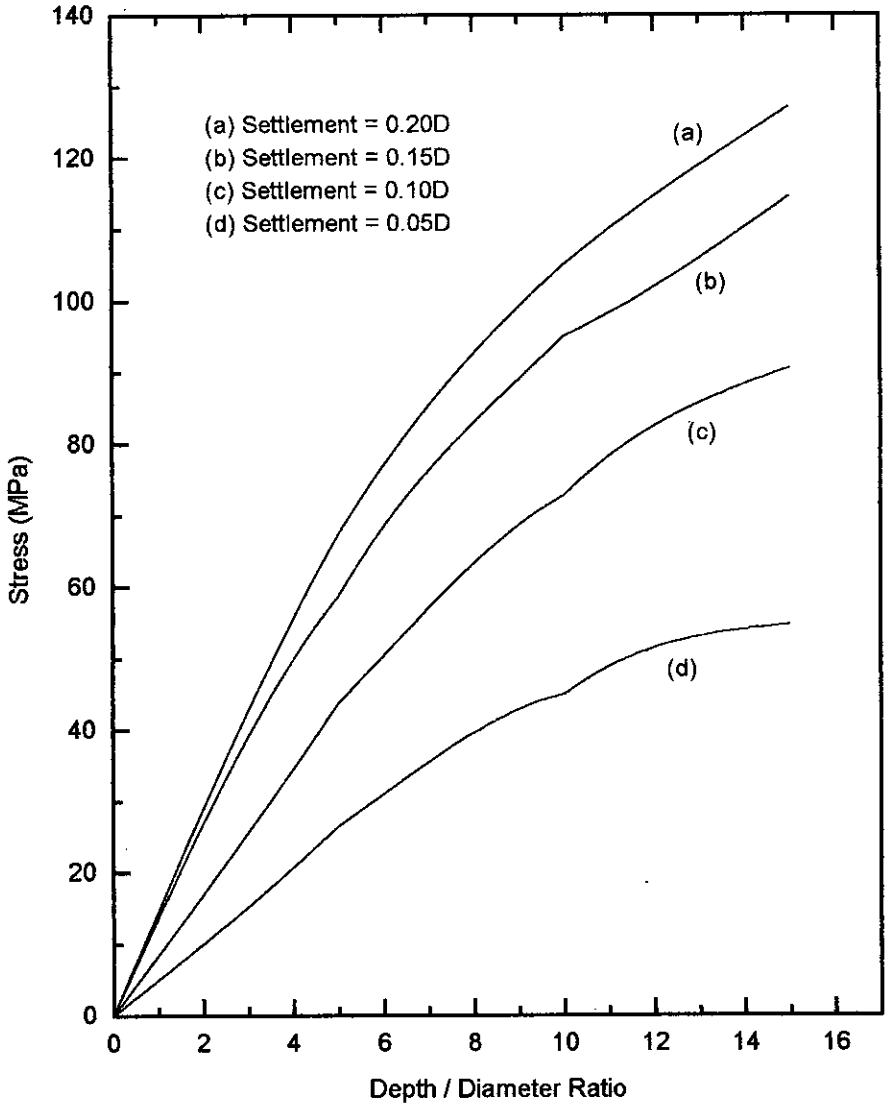

Figure 4.14 Variation of pile capacity with depth/diameter ratio at different level of settlement (D = 203 mm).

Attempts are also made to observe the effect of pile diameter on the variation of pile capacity with depth/diameter ratio (Fig. 4.15). It is observed from Fig. 4.16 that for particular depth of penetration pile capacity increases significantly with the diameter of pile. For piles of diameter larger than 102 mm the rate of increase of pile capacity with diameter is very high. Another important phenomenon observed from Fig. 4.16 is that there is a jumped increase of pile capacity for pile penetration increased from 5D to 10D. But for increase of pile penetration from 10D to 15D, increase of pile capacity is not so high. This observation justifies that for pile penetration of 10D, arching is developed in the soil. After arching is developed, further increase in pile penetration does not increase the pile capacity substantially.

4.7 Pile Load Transfer

The predicted load transfer of 102 mm diameter pipe with pile embedment depth of 10 times pile diameter are shown in Fig. 4.17. A large portion of the pile loads are transferred through the interface shear into the surrounding soil and the rest portion is resisted by the pile. Fig. 4.18 and Fig. 4.19 shows the normal and shear stresses in the internal soil-pile interface for 102 mm diameter pile with L/D = 10. Stress distributions for other piles are shown in Appendix B.

Fig. 4.20 (a,b,c) display the isobars for vertical stress in the soil within the pile. From the stress contour it is observed that at any horizontal level stress is almost same. This justify the Randolph's one dimensional idealisation of the inner soil plug (Randolph et al 1991). Fig. 4.21 shows the vertical stress in the inner soil with depth. The stress is compared with that obtained from the one dimensional analysis. It is clear that the stresses from the one dimensional analysis are less than those at the defined ultimate load, obtained from finite element analysis. Thus the Randolph's theory is somewhat conservative in calculating end bearing capacity of the internal soil mass.

End bearing capacity for 102 mm diameter pile with L/D = 10 is calculated by conventional method and found to be 958 kN/m^2. It is observed from Fig. 4.21 that the calculated end bearing pressure is less than the vertical stress in the inner soil at the base of the pile. That is, the pile is acting as a plugged pile.

In the outer soil of pile-soil system, stress is transferred from the pile through out a interface friction. Stresses are decreased as the distance of soil element from pile increases. The vertical stress contour for different tip settlement of pile are shown in Fig. 4.22(a), (b) and (c). The vertical stress distribution with distance from pile in the outer soil is looked at in Fig. 4.23. All these plots show that the maximum stresses develop near the pile wall with a tendency of stress concentration near the pile tip. For soil elements at a distance more than 5 times the pile diameter from the pile, the effect of pile stresses on soil is negligible.

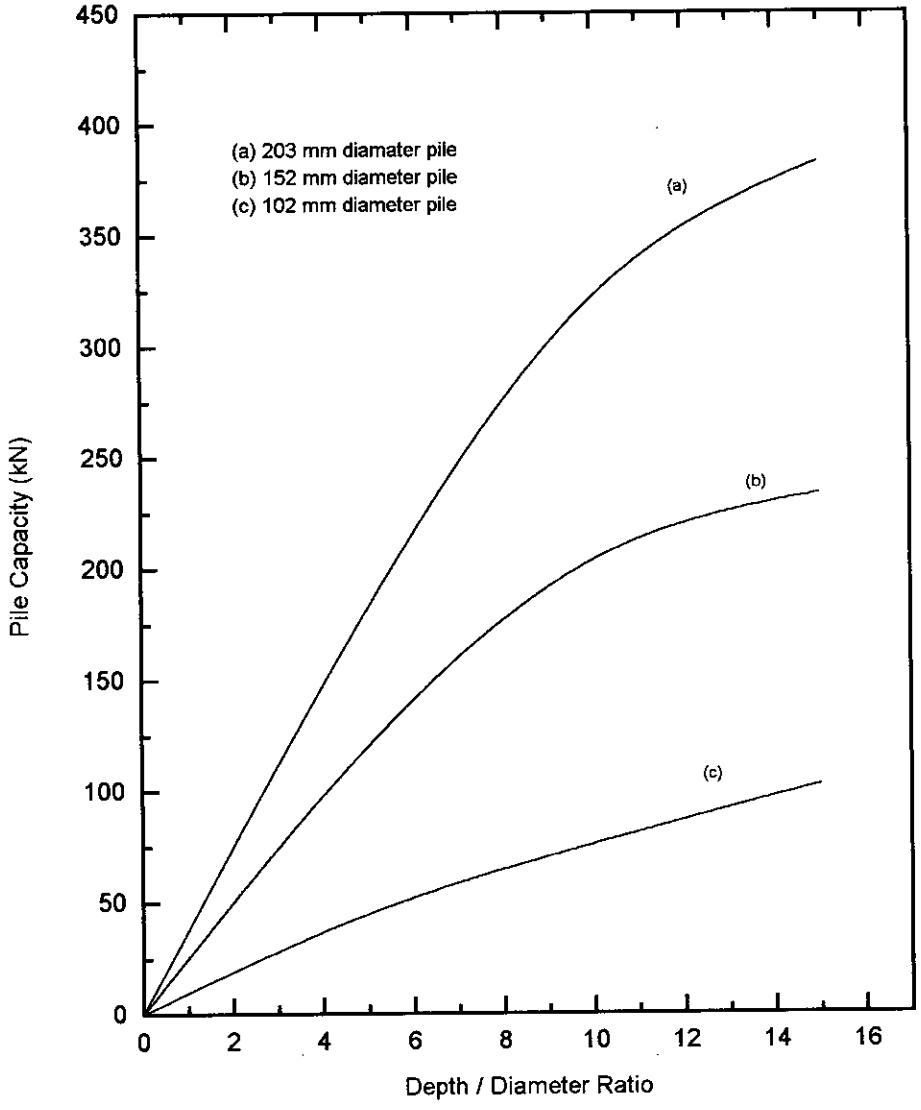

Figure 4.15 Variation of pile capacity with depth/diameter ratio for piles of different diameter.

(Allowable settlement = 0.10D)

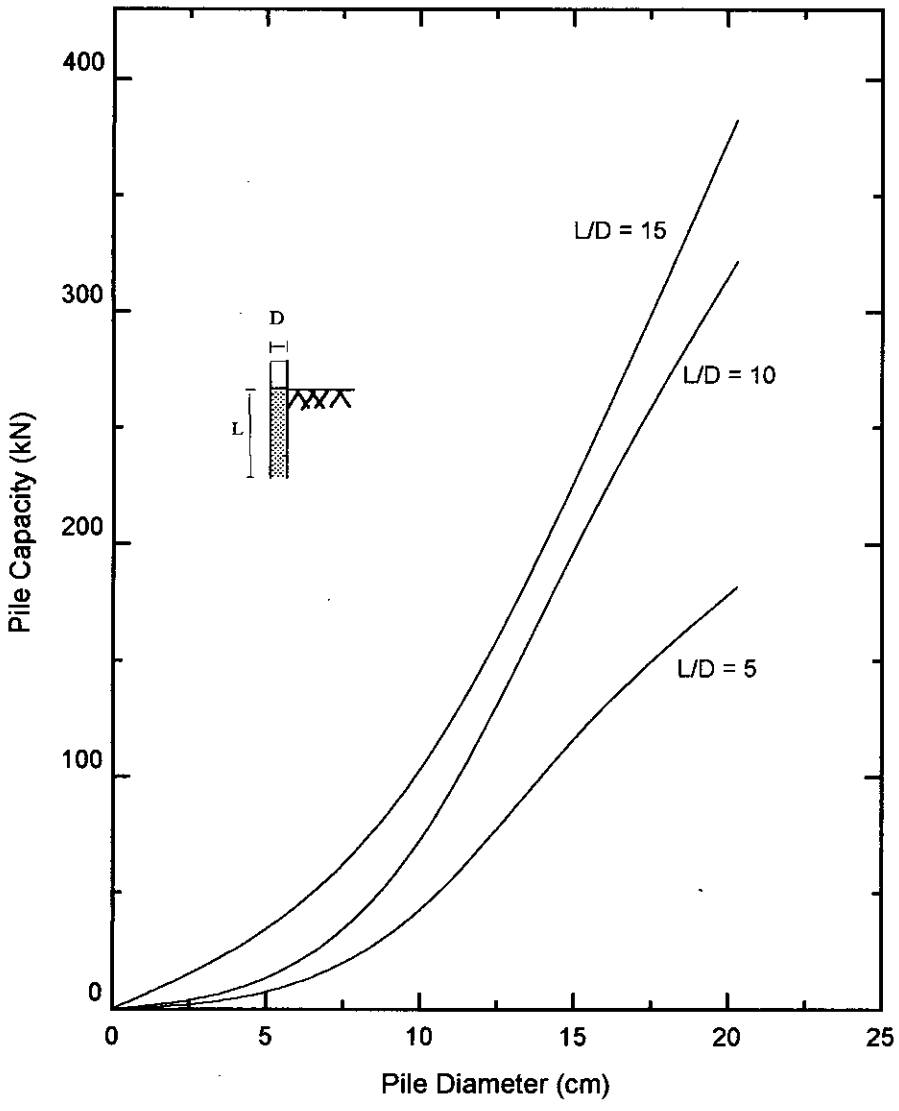

Figure 4.16 Variation of pile capacity with diameter at different depth of penetration.

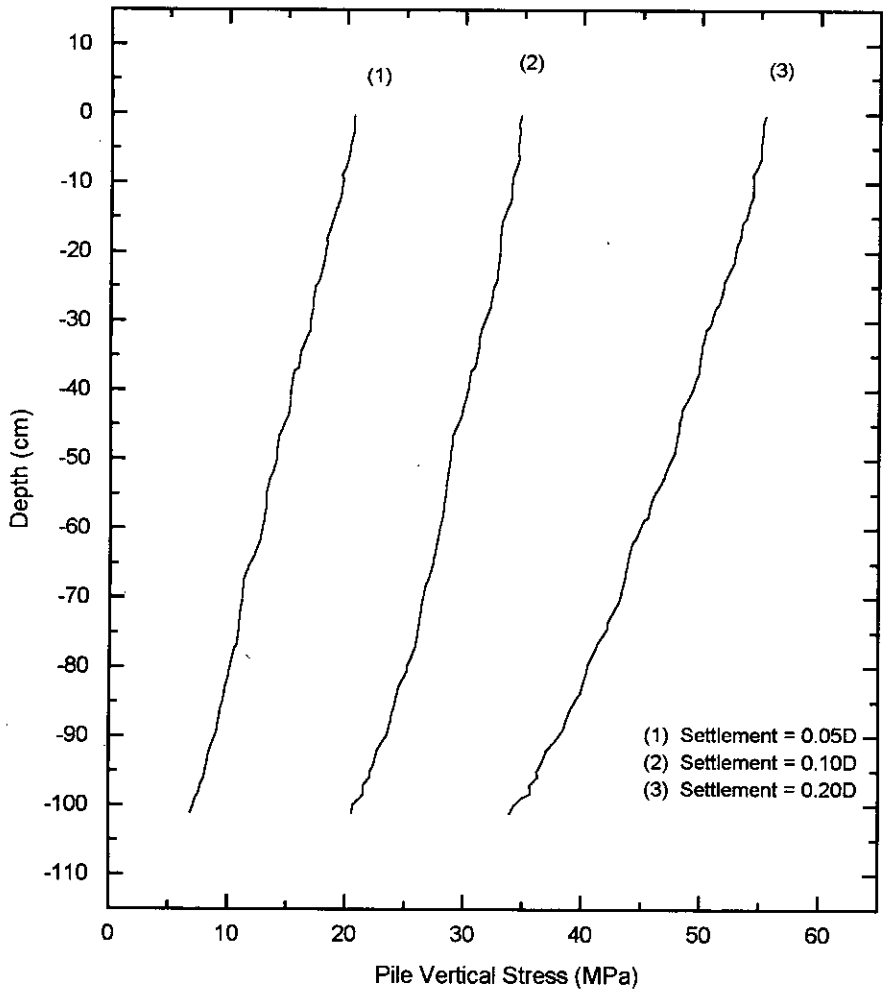

Figure 4.17 Vertical stress along pile depth (D = 102 mm, L/D = 10).

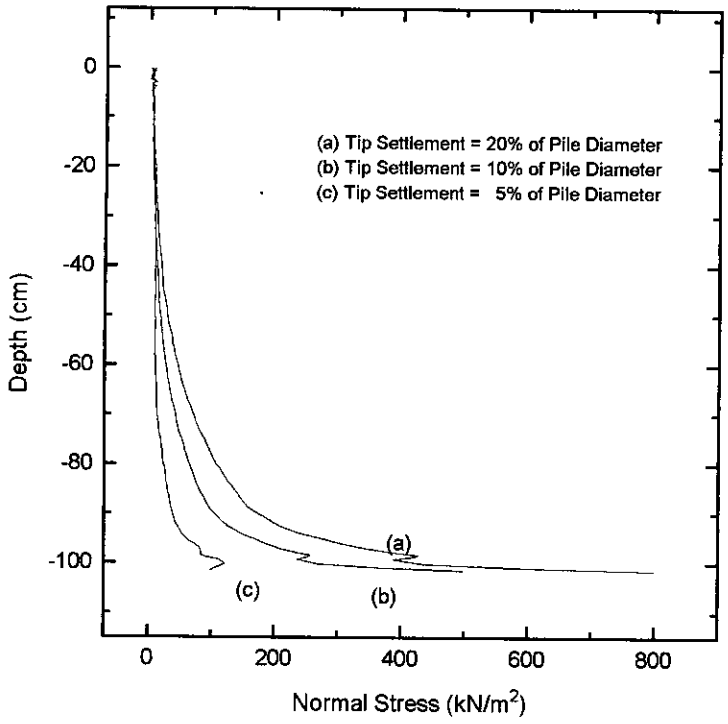

Figure 4.18 Normal stresses along the interface elements.
(D = 102 mm, L/D = 10)

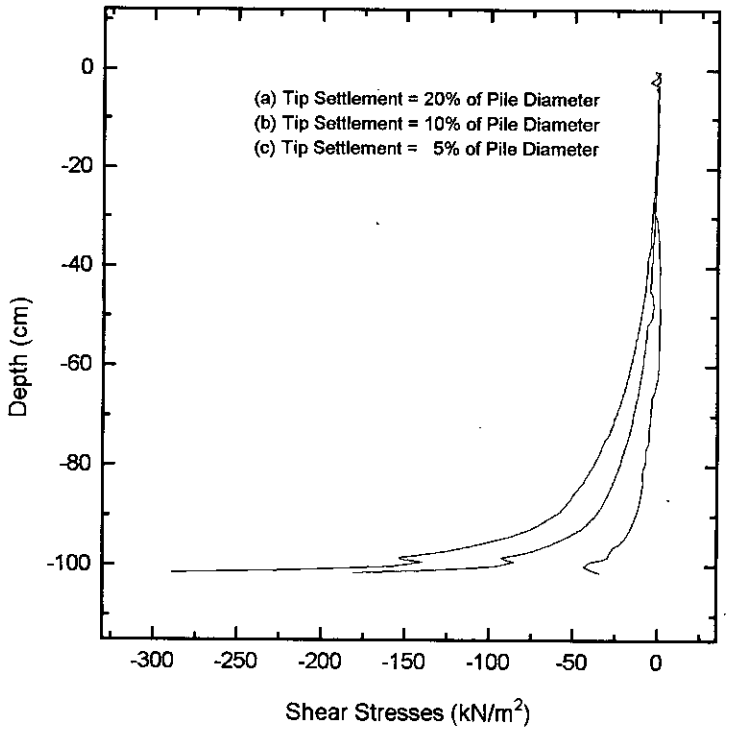

Figure 4.19 Shear stress along the interface elements.

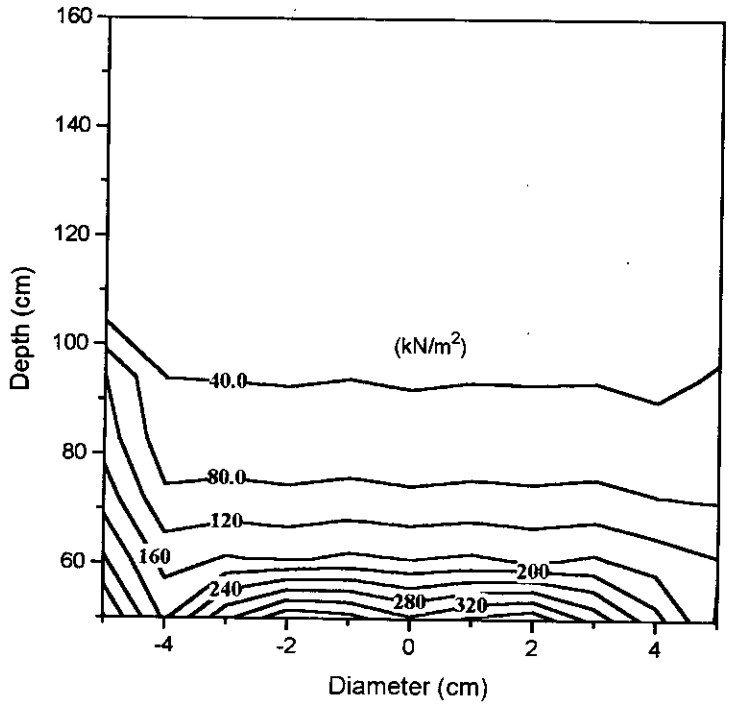

Figure 4.20(a) Vertical stress isobars within soil inside the pile at a settlement of 5% of pile diameter.

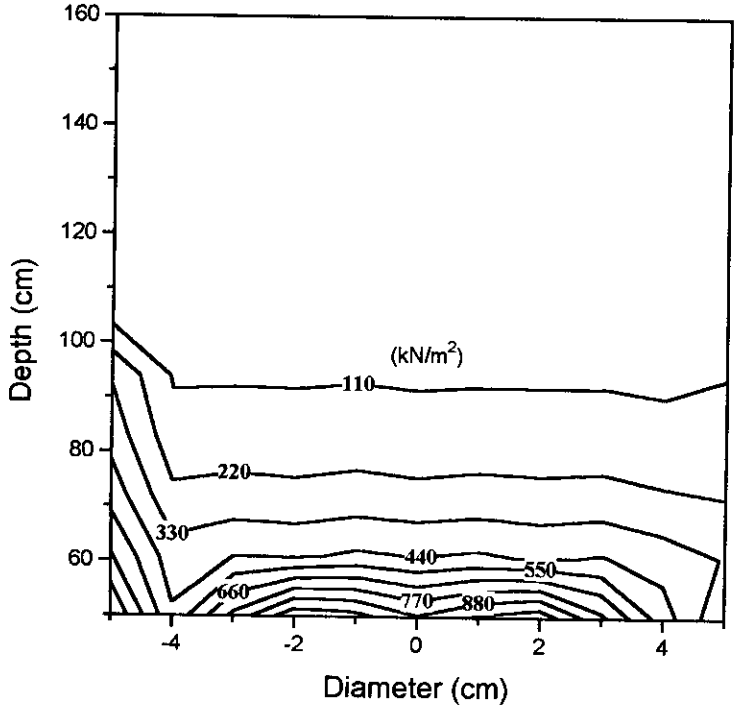

Figure 4.20(b) Vertical stress isobars within soil inside the pile at a settlement of 10% of pile diameter.

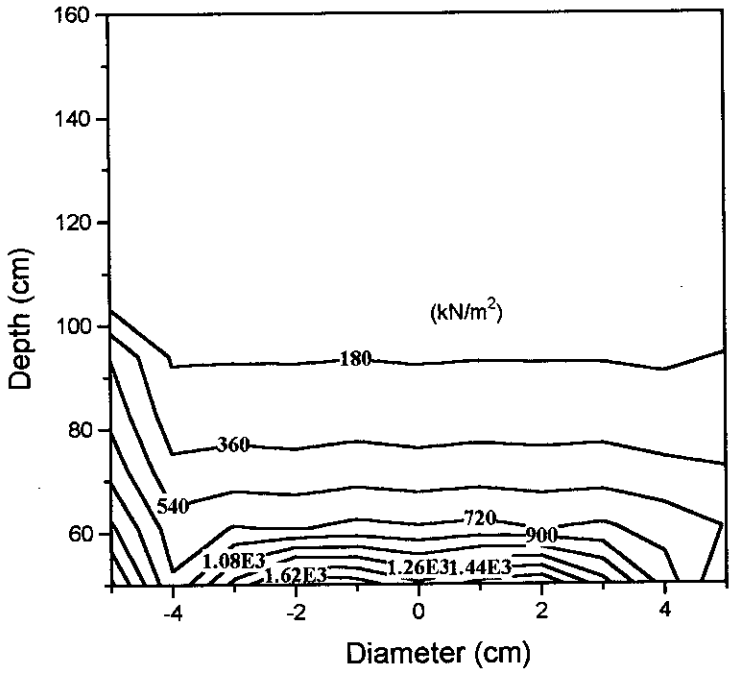

Figure4.20(c) Vertical stress isobars within soil inside the pile at a settlement of 20% of pile diameter.

Figure 4.20 Isobars of vertical stress in the internal soil of pile.
(D = 102 mm, L/D = 10)

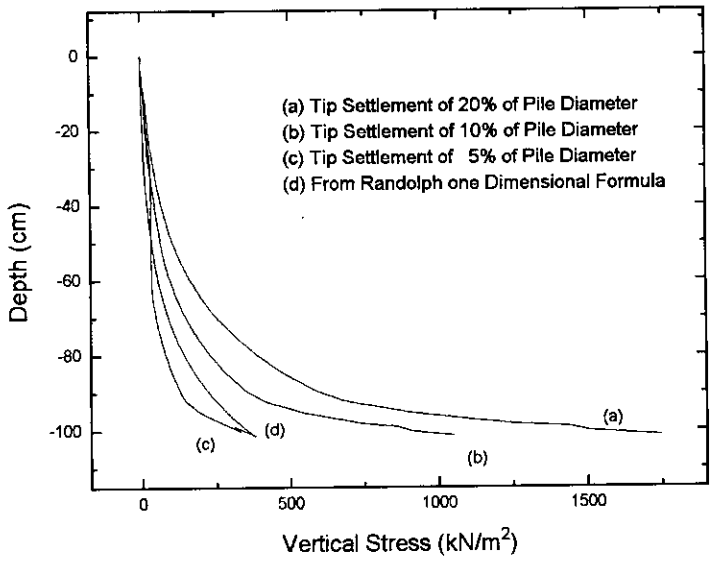

Figure 4.21 Vertical stresses in the internal soil with depth.
(D = 102 mm, L/D = 10)

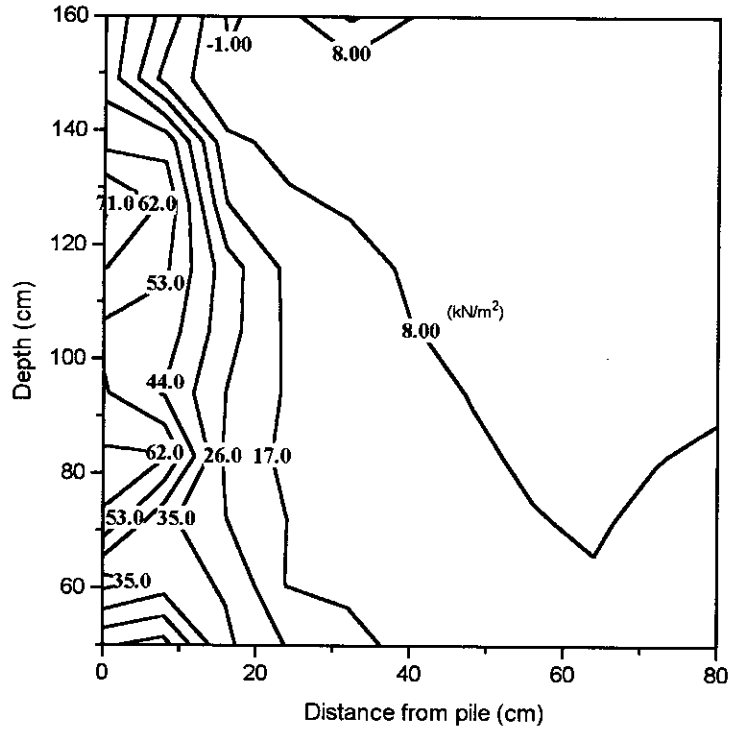

Figure 4.22(a) Vertical stress isobars within soil outside the pile at a settlement of 5% of pile diameter.

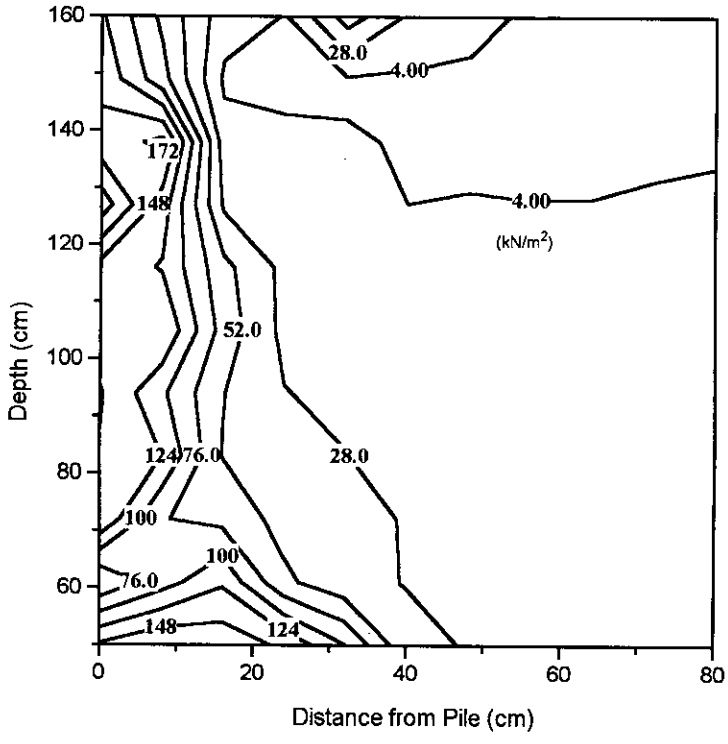

Figure 4.22(b)Vertical stress isobars within soil outside the pile

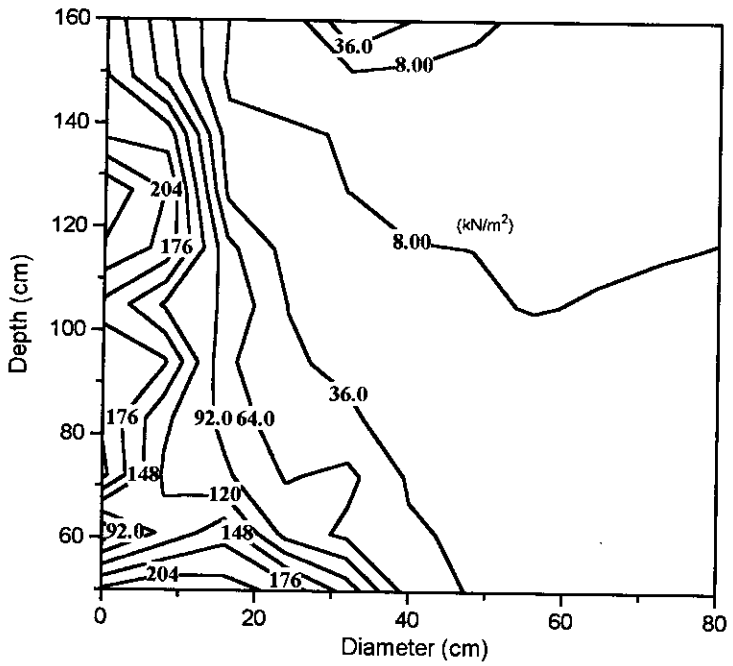

Figure 4.22(c) Vertical stress isobars within soil outside the pile at a settlement of 20% of pile diameter.

Figure 4.22 Isobars of vertical stress in pile outer soil (D = 102 mm, L/D = 10).

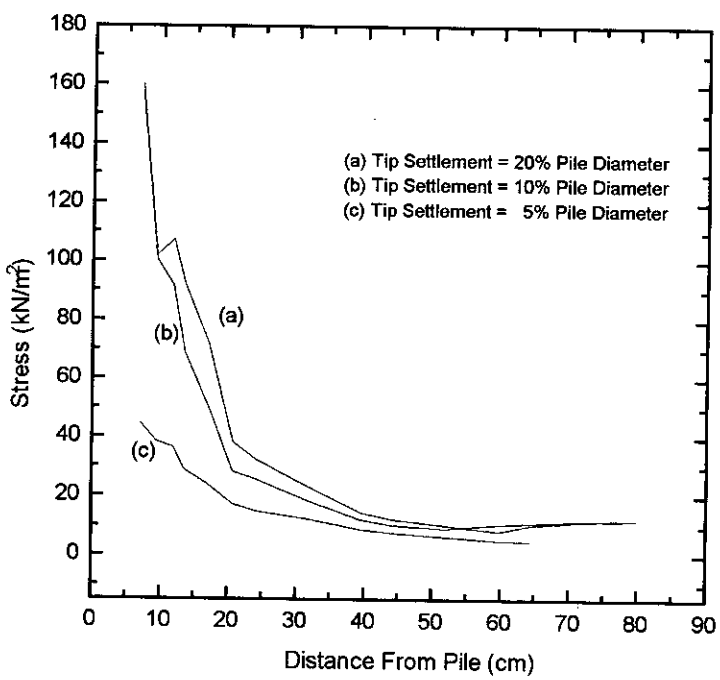

Figure 4.23 Vertical stress along outer soil of pile with distance from pile (D = 102 mm, L/D = 10).

CHAPTER 5

CONCLUSIONS AND RECOMMENDATION

5.1 Conclusion

Behaviour of open-ended steel pipe piles in granular soil is studied in this research. Numerical analysis is performed to perceive the load response and identify the parameters affecting the capacity of pipe piles. From finite element analysis, it is found that plugging is controlled by the behaviour of the soil within the pile. Stress distributions in the pile and soil were calculated by FEM to acquire a basic understanding of the plugging mechanism. Limited experiments were carried out to justify the results obtained from numerical analysis. Effects of the depth of soil and the diameter of the pipe pile on the pile capacity were investigated. Parameters affecting the development of plugging on the internal soil were identified. Experiments were performed to explore the mechanism of soil plug formation within the pipe piles. After an extensive and systematic study, the following conclusions can be drawn from the previous chapters.

(a) Skin frictional resistance of the soil within the pipe pile is significantly higher than common design values for the external soil when arching in the internal soil develop. Plugging happens when the total inner shaft resistance is greater than the end-bearing of the ground below the soil plug at the tip.

(b) Capacity of the pile increases linearly with the increase of internal soil depth, without the formation of plugging. But from the onset of plugging pile capacity increases exponentially and after the full development of plugging, any further increase in the depth of internal soil does not increase the pile capacity significantly.

(c) Required depth ratio (L/D) to develop plug is found to be between 9 and 15.

(d) The pile tip displacement required to develop plugging is about 10% of the internal pile diameter.

(e) For the same L/D ratio, capacity of pipe pile increases significantly with the increase in diameter of the pile. For L/D ratio in the range of 10 to 15, the increase of capacity with diameter is very high.

(f) Stress in the internal soil is almost uniform at any depth. It increases exponentially with increase of depth from the pile top, when plugging occurs.

(g) Randolph's one dimensional formula of calculating stresses in the internal soil for plugged pile is slightly conservative. This is due to the very simplified linear elastic assumptions of material model.

(h) As load is applied on pile, properties of the internal soil is changed continuously. Internal soil stiffness usually increases during loading of pipe pile due to the densification process accompanying with the settlement of pile. This change in basic soil property (stiffness) is attributed to a number of factors, i.e., initial relative density of internal soil, gradation, depth of soil etc.

(i) Maximum stresses develop near the shaft of pile in the outer soil with tendency of stress concentration near the pile tip. As the pile transfers load predominantly as friction along the shaft, this pattern of stress contour is quite expected.

(j) An empirical equation given below is proposed to calculate plugged / non-plugged pile load capacity for a particular type of sand.

$$\frac{P}{P_u} = a\left(\frac{S}{0.1 \times D}\right)^n$$

where, P = Applied load on pipe pile

P_u = Ultimate load at 0.1D settlement

S = Settlement of pile

5.2 Recommendations for Future Research

Current research on the behaviour of pipe pile does not fully cover the field observations. But the results in this study provide reliable information for further investigation of pipe pile behaviour. In order to enhance the findings of this study, the following additional works may be undertaken in a future research:

(a) An extensive experiments can be performed with pipe piles of different diameter and different soil depths to verify the results obtained from this research and comparison can be done with the empirical equations proposed.

(b) Results obtained from the laboratory experiments and numerical analysis may be verified by prototypes in the field. A realistic model for the simulation of field condition may be developed by some modification in the laboratory model.

(c) Plugging behaviour in sand under saturated condition may be observed. Development of pore water pressure and its affect on plugging can be examined.

(d) Investigations can be performed with varying density of soil and the effect of density on plug capacity can observed. Density of the inside soil can be measured continuously with the increase of applied load and the change of density in the inside soil with load may be observed.

(e) Effects of surface roughness of pile shaft on the plug response may be studied by changing the surface condition in model piles and by using piles made of different materials.

(f) The study may be extended to include the effect of lateral load on soil plug response and on the capacity of pipe pile.

(g) Finally a generalised model can be developed for analysis and design of pipe piles that will include all the parameters affecting pile capacity.

REFERENCES

Bari, M.S. (1996) "Development of a Realistic Soil-Structure Interaction System." M.Sc. Engg. Thesis, BUET, Dhaka.

Berezantzev, V.G., Khristoforov, V., & Golubkov, V. (1961), "Load Bearing Capacity and Deformation of Piled Foundations." Proc. 5th Int. Conf. Soil Mech. & Found. Engg., vol.2: 11-15.

Bhushan, K. (1982), "Discussion: New Design Correlations for Piles in Sands", Jnl. of Geotech. Eng. Divn., ASCE, GT 11, 1508-1510.

Bishop, A.W., Collingidge, V.H. and O'Sullivan, T.P. (1948), "Driving and Loading Tests on Six Precast Concrete Piles in Gravel." Geotechnique, London, England, Vol. 1, No. 1, pp. 49-58.

Bowles, J.E., (1988), "Foundation Analysis and Design." Fourth Edition, McGraw-Hill International Editions.

Brinch, Hansan J (1961), A General Formula for Bearing Capacity, Bull. Geotech. Tnst. No. 11.

Britto, A.M. and Gunn, M.J. (1987), "Critical State Soil Mechanics via Finite Elements." John Wiley and Sons.

Burland, J.B. (1973), "Shaft Friction Piles in Clay - A Simple Fundamental Approach", Ground Engineering, vol. 6, No. 3, 30-42.

Caquot, A. and Kerisel, J. (1953), "Sur le terme de surface dans le calcul des fondation en milieu pulverulent." Proc. 3rd Int. Conf. Soil Mechanics & Foundation Engineering, Zurich, Switzerland, pp 336-337.

Carter, J.P., Small, J.C. and Booker, J.R. (1977), "A Theory of Finite Elastic Consolidation.", Int. Jnl. Solid & Structures. 13, 467-478.

Coulomb, C.A. (1776), "Essai Sur Une Application Des Regles Des Maximis et Minimis a Quelques Problems de Statique Relatifs a e' Architecture." Mem. Acad. Roy. Pres. Divers Savants, Vol. 7, Paris.

Coyle, H.M. & Castello, R.R., (1981), "New Design Correlations for Piles in Sand." Jnl. of the Geotech. Eng. Divn., ASCE, vol. 107, No. GT7 : 965 - 983.

Coyle, M. & Sulaiman, H., (1967), "Skin Friction for Steel Piles in Sand." Jnl. of the Soil Mech. and Foundn. Divn., ASCE, Vol. 93, SM6: 261 - 277.

DeBeer E.E., (1970), "Experimental Determination of The Shape Factors and The Bearing Capacity Factors of Sand." Geotechnique 20, No. 4, 387 - 411.

Desai, C.S. (1974), "Numerical Design - Analysis for Piles in Sands." Jnl. Geotech. Eng. Divn., ASCE, vol. 100, No. GT6 : 613-635.

Desai, C.S. and Siriwardane H.J. (1984), "Constitutive laws for Engineering materials." Prentice - Hall International, Inc. London.

Desai, C.S., Zaman M.M., Lightner, J.G. and Siriwardane, H.J. (1984), "Thin-layer Elements for Interfaces and Joints." Int. Jnl. for Numerical and Analytical Methods in Geomechanics, vol. 8L : 19 - 43.

DiMaggio, F.L. & Sandler, I.S. (1971), "Material Model for Granular Soils." Journal of the Engineering Mechanics Division., ASCE, Vol. 97, No. EM3: 935 - 939.

Drucker, D.C. and Prager, W. (1952), "Soil Mechanics and Plastic Analysis or Limit Design.", Quart. Appl. Math. 10, 157-165.

Hanna, T.H., & Tan, R.H.S. (1973), "The Behaviour of Long Piles Under Compressive Loads in Sand." Canadian Geotechnical Jnl., Vol. 10, No. 3: 311 - 340.

Housel, W.S. (1966), "Pile Load Capacity - Estimates and Test Results." Jnl. of Soil Mech. and Found. Divn., ASCE, Vol. 92, SM4: 1 - 29.

Iron, B.M. (1970), "A Frontal Solution Program for Finite Element Analysis.", Int. Jnl. Num. Meth. Eng. 12, 5-32.

Irons, B. & Ahmad, S., (1980), "Techniques of Finite Elements." John Wiley & Sons. New York.

Jeyatheran, K. (1996), "Application of CRISP in Embankments, Excavations and Piles, Presented at a Short Course on Numerical Analysis in Geotechnical Engineering, Held at AIT.

Kishida, H. & Isemoto, N. (1977), "Behaviour of Sand Plugs in Open-Ended Steel Pipe Piles." Proc. 9th Int. Conf. on Soil Mech. and Foundation Eng., Tokyo, Vol. 1, 601 - 604

Kishida, H. (1967), "Ultimate Bearing Capacity of Piles Driven into Loose Sand." Soil and Foundations., Vol. 7, No. 3: 20 - 29.

Kulhawy, F.H. and Mayne, P.W., (1990), "Manual on Estimating Soil Properties for Foundation Design." Final Report, Research Project 1493-6,

Cornell University, New York, USA.

Mansur, C.I. and Hunter, A.H. (1970), "Pile Tests - A Kansas River Project, Jnl. of Soil Mech. and Found. Divn., ASCE, Vol. 96, SM5. pp. 1545-1582.

Matsumoto, T. & Takei, M., (1991), "Effects of Soil Plug on Behaviour of Driven Pipe Piles." Soils and Foundations, Vol. 31, No. 2, 14 - 34.

Matsumoto, T., Michi, Y. & Hirano, T., (1993), "Performance of Axially Loaded Steel Pipe Piles Driven in Soft Rock." Jnl. of Geot. Eng., ASCE, vol. 121, No. 4 : 305 - 315.

Mattes, N.S. and Poulos, H.G. (1969), " Settlement of Single Compression Piles." Jnl. of Soil Mech. and Found. Divn., ASCE, Vol. 95, SM1: 189 - 207.

McClelland, B. (1974), "Design of Deep Penetration Piles for Ocean Structures." Jnl. Geot. Eng. Divn., ASCE, vol. 100, No. GT7 : 705 - 747.

Meyerhof, G.G. (1956). "Penetration Tests and Bearing Capacity of Piles." Jnl. of Soil Mech. and Found. Divn., ASCE, Vol. 82, SM1: 1 - 19.

Meyerhof, G.G. (1976), "Bearing Capacity and Settlement of Foundations." Jnl. Geot. Eng. Divn., ASCE, vol. 102, No. GT3 : 195 - 228.

Meyerhof. G.G. (1959), "Compaction of Sands and Bearing Capacity of Piles." Jnl. of Soil Mech. and Found. Divn., ASCE, Vol. 85, SM6: 1 - 29.

Meyerhof. G.G. (1963), "Some Recent Research on the Bearing Capacity of Foundations." Canadian Geotechnical Jnl., Vol. 1, No. 1:16.

Mohan, D., Jain, G.S., & Kumar, V. (1963), "Load Bearing Capacity of Piles." Geotechnique. Vol. 13, No. 1: 76 - 86.

Morshed, J., (1991), "Prediction of Load Deformation Behaviour of Axially Loaded Piles in Sand", M.Sc. Engg. Thesis, Department of Civil Engineering, Bangladesh University of Engineering and Technology, Dhaka.

Murthy, V.N.S., (1993), "Soil Mechanics and Foundation Engineering." Fourth Edition, Sai Kripa Technical Consultants, Bangalore.

Nordlund, R.L. (1963), "Bearing Capacity of Piles in Cohesionless Soils." Jnl. of Soil Mech. and Found. Divn., ASCE, Vol. 89, SM3: 1 - 35.

Norlund, R.L. (1963), "Bearing Capacity of Piles in Cohesionless Soils." Jnl. of Soil Mech. and Found. Divn., ASCE, Vol. 89, SM3: 1 - 23.

Paikowsky, S.G. & Whitman R.V. (1990), "The Effects of Plugging on Pile Performance and Design." Canadian Geotechnical Jnl., Vol. 27, :429 - 440.

Peck, R.B., Hansen, W.E., & Thornburn, T.H. (1974), Foundation Engineering, 2nd Edn. New York: Wiley.

Potyondy, J.G. (1961), "Skin Friction Between Various Soils and Construction Materials", Geotechnique, vol.2, No. 4, pp. 339-353.

Poulos H.G. & Davis E.H., (1980), "Pile Foundation Analysis and Design." John Wiley & Sons. Singapore.

Poulos, H.G. & Mattes, N.S. (1969), "The Behaviour of Axially - Loaded End - Bearing Piles." Geotechnique, Vol. 19: 285 - 300.

Poulos, H.G. (1979), "Settlement of Single Piles in Non-homogeneous Soil." Jnl. of Geot. Eng. Divn., ASCE, vol. 105, No. GT5 : 627 - 641.

Prandtl, L. (1920), "Uber die Harta Plastischer Korper", Nachr. Kgl. Ges. Wiss. Gottingen, Math. Phys. Klasse.

Randolph, M.F. & Wroth, C.P. (1978), "Analysis of Deformation of Vertically Loaded Piles." Jnl. Geot. Eng. Divn., ASCE, vol. 104, No. GT12 : 1465 - 1488.

Randolph, M.F., Leong, E.C. & Houlsby, G.T. (1991), "One-Dimensional Analysis of Soil Plugs in Pipe Piles." Geotechnique 41, No. 4, 587 - 598.

Randolph, M.F., May, M., Leon, E.C. & Murff, J.D. (1992), "Soil Plug Response in Open-Ended Pipe Piles." Jnl. of Geot. Eng., ASCE, vol. 118, No. 5 : 743 - 758.

Reese, L.C., O'Neill, M.W., & Smith, R.E. (1970), "Generalised Analysis of Pile Foundations." Jnl. of Soil Mech. and Found. Divn., ASCE, Vol. 96, SM1: 235.

Reissner, H. (1924), "Zum Erddruckproblem", Proc. 1st International Congr. Applied Mechanics, Delft (Holland).

Schmertmann, J.H., (1978), "Guidelines For Cone Penetration Test Performance and Design." Report FHWA - TS - 78 - 209. U.S. Department of Transportation, Washington.

Siddiquee, M.S.A., (1988), "Experimental and Numerical Studies of Model Pile Behaviour in Sand." M.Sc Engg. Thesis, BUET, Dhaka.

Siddiquee, M.S.A., (1994), "FEM Simulation of Deformation and Failure of Stiff Geomaterials Based on Element Test Results." Ph.D. Thesis at Institute of Industrial Science at University of Tokyo. Japan.

Terzaghi, K. (1943), Theoretical Soil Mechanics. New York: Wiley.

Teunissen, J.A., (1991), "Analysis of Plasticity and Non-Coaxiality in Geomaterials." Delf Geotechnics.

Tomlinson, M.J. (1977), Pile Design and Construction. 3rd Edn. London: Pitman.

Tomlinson, M.J., (1980), "Foundation Design and Constructions", A Pitman International Text, Fourth edition, pp. 375

Tresca, H. (1869), "Memoire Sur le Poinconnage et la Theorie Mecanique de la Deformation Des Metaux." Comptes Rendus Hebdomadaires Des Seances de L'Academic Des Sciences, Paris 68, 1197-1201.

Van Weele, A. F. (1957), "A method of Separating the Bearing Capacity of a Test Pile into Skin Friction and Point Resistance." Proc. 4th Int. Conf. Soil Mechanics & Foundation Engineering, Vol. 2 : 76.

Vesic, A.S. (1867), "A Study of Bearing Capacity of Deep Foundation.", Final Rep. Proj. B-189, School of Civil Engg., Georgia Inst. Tech., Atlanta.

Vesic, A.S. (1963), "Bearing Capacity of Deep Foundations in Sand." Soil Mechanics Laboratory Report. Georgia Institute of Technology.

Vesic, A.S. (1972), "Expansion of Cavities in Infinite Soil Mass.", Vol. 98, No. SM3, Proc. Paper 8790, March, 1972, pp. 265-290.

Vesic, A.S. (1977), "Design of Pile Foundations.", NCHRP Synthesis of Highway Practice No. 42, Transportation Research Board, 2977.

Wood, D.M. (1990), "Soil Behaviour and Critical State Soil Mechanics." Cambridge University Press.

Zeitlen, J.G., and Paikowsky, S.G. (1982), Discussion on " New Design Correlations For Piles in Sands." Jnl. Geot. Eng. Divn., ASCE, vol. 108, No. GT11 : 1515 - 1518

Zienkiewicz, O.C. (1971), The Finite Element Method in Engineering Science. McGraw-Hill, London.

APPENDIX A

INPUT FILES FOR FINITE ELEMENT ANALYSES

A1. INPUT FILES FOR THE NUMERICAL ANALYSES

A1.1 Geometry program for analysis of 102 mm diameter pile with L/D = 5

"Pipe pile problem"
999
186 160 4 4 2 4
186 160
1 1 1 1 1 1 1 0 0 0
0 0 0 0

1	.00	20.00	40	2.00	29.33
2	.00	21.33	41	2.00	30.67
3	.00	22.67	42	2.00	32.00
4	.00	24.00	43	2.00	33.33
5	.00	25.33	44	2.00	34.67
6	.00	26.67	45	2.00	36.00
7	.00	28.00	46	2.00	37.33
8	.00	29.33	47	2.00	38.67
9	.00	30.67	48	2.00	40.00
10	.00	32.00	49	2.13	20.05
11	.00	33.33	50	2.13	21.33
12	.00	34.67	51	2.13	22.67
13	.00	36.00	52	2.13	24.00
14	.00	37.33	53	2.13	25.33
15	.00	38.67	54	2.13	26.67
16	.00	40.00	55	2.13	28.00
17	1.00	20.00	56	2.13	29.33
18	1.00	21.33	57	2.13	30.67
19	1.00	22.67	58	2.13	32.00
20	1.00	24.00	59	2.13	33.33
21	1.00	25.33	60	2.13	34.67
22	1.00	26.67	61	2.13	36.00
23	1.00	28.00	62	2.13	37.33
24	1.00	29.33	63	2.13	38.67
25	1.00	30.67	64	2.13	40.00
26	1.00	32.00	65	2.38	20.05
27	1.00	33.33	66	2.38	21.33
28	1.00	34.67	67	2.38	22.67
29	1.00	36.00	68	2.38	24.00
30	1.00	37.33	69	2.38	25.33
31	1.00	38.67	70	2.38	26.67
32	1.00	40.00	71	2.38	28.00
33	2.00	20.00	72	2.38	29.33
34	2.00	21.33	73	2.38	30.67
35	2.00	22.67	74	2.38	32.00
36	2.00	24.00	75	2.38	33.33
37	2.00	25.33	76	2.38	34.67
38	2.00	26.67	77	2.38	36.00
39	2.00	28.00	78	2.38	37.33

79	2.38	38.67
80	2.38	40.00
81	2.52	20.00
82	2.52	21.33
83	2.52	22.67
84	2.52	24.00
85	2.52	25.33
86	2.52	26.67
87	2.52	28.00
88	2.52	29.33
89	2.52	30.67
90	2.52	32.00
91	2.52	33.33
92	2.52	34.67
93	2.52	36.00
94	2.52	37.33
95	2.52	38.67
96	2.52	40.00
97	5.18	21.33
98	5.18	22.67
99	5.18	25.33
100	5.18	26.67
101	5.18	29.33
102	5.18	30.67
103	5.18	33.33
104	5.18	34.67
105	5.18	37.33
106	5.18	38.67
107	9.18	20.00
108	9.18	24.00
109	9.18	28.00
110	9.18	32.00
111	9.18	36.00
112	9.18	40.00
113	16.92	20.00
114	16.92	24.00
115	16.92	28.00
116	16.92	32.00
117	16.92	36.00
118	16.92	40.00
119	24.65	20.00
120	24.65	24.00
121	24.65	28.00
122	24.65	32.00
123	24.65	36.00
124	24.65	40.00
125	32.38	20.00
126	32.38	24.00
127	32.38	28.00
128	32.38	32.00
129	32.38	36.00
130	32.38	40.00
131	.00	16.00
132	.00	13.33
133	.00	10.67
134	.00	8.00
135	.00	5.33
136	.00	2.67
137	.00	.00
138	1.00	16.00
139	1.00	13.33
140	1.00	10.67
141	1.00	8.00
142	1.00	5.33
143	1.00	2.67
144	1.00	.00
145	2.00	16.00
146	2.00	13.33
147	2.00	10.67
148	2.00	8.00
149	2.00	5.33
150	2.00	2.67
151	2.00	.00
152	5.18	16.00
153	5.18	13.33
154	5.18	10.67
155	5.18	8.00
156	5.18	5.33
157	5.18	2.67
158	5.18	.00
159	9.18	16.00
160	9.18	13.33
161	9.18	10.67
162	9.18	8.00
163	9.18	5.33
164	9.18	2.67
165	9.18	.00
166	16.92	16.00
167	16.92	13.33
168	16.92	10.67
169	16.92	8.00
170	16.92	5.33
171	16.92	2.67
172	16.92	.00
173	24.65	16.00
174	24.65	13.33
175	24.65	10.67
176	24.65	8.00

177 24.65 5.33
178 24.65 2.67
179 24.65 .00
180 32.38 16.00
181 32.38 13.33
182 32.38 10.67
183 32.38 8.00
184 32.38 5.33
185 32.38 2.67
186 32.38 .00
0
1 4 1 1 17 18 2
2 4 1 2 18 19 3
3 4 1 3 19 20 4
4 4 1 4 20 21 5
5 4 1 5 21 22 6
6 4 1 6 22 23 7
7 4 1 7 23 24 8
8 4 1 8 24 25 9
9 4 1 9 25 26 10
10 4 1 10 26 27 11
11 4 1 11 27 28 12
12 4 1 12 28 29 13
13 4 1 13 29 30 14
14 4 1 14 30 31 15
15 4 1 15 31 32 16
16 4 1 17 33 34 18
17 4 1 18 34 35 19
18 4 1 19 35 36 20
19 4 1 20 36 37 21
20 4 1 21 37 38 22
21 4 1 22 38 39 23
22 4 1 23 39 40 24
23 4 1 24 40 41 25
24 4 1 25 41 42 26
25 4 1 26 42 43 27
26 4 1 27 43 44 28
27 4 1 28 44 45 29
28 4 1 29 45 46 30
29 4 1 30 46 47 31
30 4 1 31 47 48 32
31 13 2 34 33 49 50
32 13 2 35 34 50 51
33 13 2 36 35 51 52
34 13 2 37 36 52 53
35 13 2 38 37 53 54
36 13 2 39 38 54 55
37 13 2 40 39 55 56
38 13 2 41 40 56 57
39 13 2 42 41 57 58
40 13 2 43 42 58 59
41 13 2 44 43 59 60
42 13 2 45 44 60 61
43 13 2 46 45 61 62
44 13 2 47 46 62 63
45 13 2 48 47 63 64
46 13 2 33 81 65 49
47 4 3 49 65 66 50
48 4 3 50 66 67 51
49 4 3 51 67 68 52
50 4 3 52 68 69 53
51 4 3 53 69 70 54
52 4 3 54 70 71 55
53 4 3 55 71 72 56
54 4 3 56 72 73 57
55 4 3 57 73 74 58
56 4 3 58 74 75 59
57 4 3 59 75 76 60
58 4 3 60 76 77 61
59 4 3 61 77 78 62
60 4 3 62 78 79 63
61 4 3 63 79 80 64
62 13 4 66 65 81 82
63 13 4 67 66 82 83
64 13 4 68 67 83 84
65 13 4 69 68 84 85
66 13 4 70 69 85 86
67 13 4 71 70 86 87
68 13 4 72 71 87 88
69 13 4 73 72 88 89
70 13 4 74 73 89 90
71 13 4 75 74 90 91
72 13 4 76 75 91 92
73 13 4 77 76 92 93
74 13 4 78 77 93 94
75 13 4 79 78 94 95
76 13 4 80 79 95 96
77 4 5 81 107 97 82
78 4 5 82 97 98 83
79 4 5 97 107 108 98
80 4 5 83 98 108 84
81 4 5 84 108 99 85
82 4 5 85 99 100 86
83 4 5 99 108 109 100
84 4 5 86 100 109 87
85 4 5 87 109 101 88
86 4 5 88 101 102 89
87 4 5 101 109 110 102

88	4	5	89	102	110	90
89	4	5	90	110	103	91
90	4	5	91	103	104	92
91	4	5	103	110	111	104
92	4	5	92	104	111	93
93	4	5	93	111	105	94
94	4	5	94	105	106	95
95	4	5	105	111	112	106
96	4	5	95	106	112	96
97	4	5	107	113	114	108
98	4	5	108	114	115	109
99	4	5	109	115	116	110
100	4	5	110	116	117	111
101	4	5	111	117	118	112
102	4	5	113	119	120	114
103	4	5	114	120	121	115
104	4	5	115	121	122	116
105	4	5	116	122	123	117
106	4	5	117	123	124	118
107	4	5	119	125	126	120
108	4	5	120	126	127	121
109	4	5	121	127	128	122
110	4	5	122	128	129	123
111	4	5	123	129	130	124
112	4	6	1	131	138	17
113	4	6	17	138	145	33
114	4	6	33	145	152	81
115	4	6	81	152	159	107
116	4	6	107	159	166	113
117	4	6	113	166	173	119
118	4	6	119	173	180	125
119	4	6	131	132	139	138
120	4	6	132	133	140	139
121	4	6	133	134	141	140
122	4	6	134	135	142	141
123	4	6	135	136	143	142
124	4	6	136	137	144	143
125	4	6	138	139	146	145
126	4	6	139	140	147	146
127	4	6	140	141	148	147
128	4	6	141	142	149	148
129	4	6	142	143	150	149
130	4	6	143	144	151	150
131	4	6	145	146	153	152
132	4	6	146	147	154	153
133	4	6	147	148	155	154
134	4	6	148	149	156	155
135	4	6	149	150	157	156
136	4	6	150	151	158	157
137	4	6	152	153	160	159
138	4	6	153	154	161	160
139	4	6	154	155	162	161
140	4	6	155	156	163	162
141	4	6	156	157	164	163
142	4	6	157	158	165	164
143	4	6	159	160	167	166
144	4	6	160	161	168	167
145	4	6	161	162	169	168
146	4	6	162	163	170	169
147	4	6	163	164	171	170
148	4	6	164	165	172	171
149	4	6	166	167	174	173
150	4	6	167	168	175	174
151	4	6	168	169	176	175
152	4	6	169	170	177	176
153	4	6	170	171	178	177
154	4	6	171	172	179	178
155	4	6	173	174	181	180
156	4	6	174	175	182	181
157	4	6	175	176	183	182
158	4	6	176	177	184	183
159	4	6	177	178	185	184
160	4	6	178	179	186	185

A1.2 Main program for analysis of 102 mm diameter pile with L/D = 5

```
PIPE PILE PROBLEM
999
1 6 2 1 1000 0 0 1 0
0 0 0 1 180 0 0 1 160
0
1 5 5000 0.25 0.001 35 0 4 0 0.07 0 0 0 0
2 8 0 20 6000. 2000. 1 0.1 0 0 0 0 0 0
3 1 29E5 29E5 0.3 0.3 11.154E5 0 0 0.283
0 0 0 0
4 8 0 20 6000. 2000. 1 0.1 0 0 0 0 0 0
5 5 5000 0.25 0.001 35 0 4 0 0.07 0 0 0 0
6 5 5000 0.25 0.001 35 0 4 0 0.07 0 0 0 0
1 2
1 40 0 0 0 0 0 0 0 0.0
2 0 0.9 2.8 0.9 0 0 0 0 0.0
0 41 1
   1   1   2  1 1 .0 .0 .0
   2   2   3  1 1 .0 .0 .0
   3   3   4  1 1 .0 .0 .0
   4   4   5  1 1 .0 .0 .0
   5   5   6  1 1 .0 .0 .0
   6   6   7  1 1 .0 .0 .0
   7   7   8  1 1 .0 .0 .0
   8   8   9  1 1 .0 .0 .0
   9   9  10  1 1 .0 .0 .0
  10  10  11  1 1 .0 .0 .0
  11  11  12  1 1 .0 .0 .0
  12  12  13  1 1 .0 .0 .0
  13  13  14  1 1 .0 .0 .0
  14  14  15  1 1 .0 .0 .0
  15  15  16  1 1 .0 .0 .0
 107 125 126  1 1 .0 .0 .0
 108 126 127  1 1 .0 .0 .0
 109 127 128  1 1 .0 .0 .0
 110 128 129  1 1 .0 .0 .0
 111 129 130  1 1 .0 .0 .0
 112   1 131  1 1 .0 .0 .0
 118 180 125  1 1 .0 .0 .0
 119 131 132  1 1 .0 .0 .0
 120 132 133  1 1 .0 .0 .0
 121 133 134  1 1 .0 .0 .0
 122 134 135  1 1 .0 .0 .0
 123 135 136  1 1 .0 .0 .0
 124 136 137  1 1 .0 .0 .0
 124 137 144  2 1 .0 .0 .0
 130 144 151  2 1 .0 .0 .0
 136 151 158  2 1 .0 .0 .0
 142 158 165  2 1 .0 .0 .0
 148 165 172  2 1 .0 .0 .0
 154 172 179  2 1 .0 .0 .0
 155 181 180  1 1 .0 .0 .0
 156 182 181  1 1 .0 .0 .0
 157 183 182  1 1 .0 .0 .0
 158 184 183  1 1 .0 .0 .0
 159 185 184  1 1 .0 .0 .0
 160 186 185  1 1 .0 .0 .0
 160 179 186  2 1 .0 .0 .0
1 1 200 0 -1 0 0 0 00011 0 0 0 0
61 64 80 0. 1000.0 0. 1000.0 0. 1000.0
2 201 1000 0 -1 0 0 0 00011 0 0 0 0
61 64 80 0. 4000.0 0. 4000.0 0. 4000.0

1 1 1 0 -1 0 0 0 00021 0 0 0 0
61 64 80 0. 30.0 0. 30.0 0. 30.0
2 2 800 0 -1 0 0 0 00000 0 0 0 0
61 64 80 0. 23970.0 0. 23970.0 0. 23970.0
3 801 801 0 -1 0 0 0 00121 0 0 0 0
61 64 80 0. 22.5 0. 22.5 0. 22.5
4 802 1500 0 -1 0 0 0 00000 0 0 0 0
61 64 80 0. 16477.5 0. 16477.5 0. 16477.5
5 1501 2200 0 -1 0 0 0 00000 0 0 0 0
61 64 80 0. 15000.0 0. 15000.0 0. 15000.0
6 2201 2201 0 -1 0 0 0 00121 0 0 0 0
61 64 80 0. 22.5 0. 22.5 0. 22.5
7 2202 2400 0 -1 0 0 0 00000 0 0 0 0
61 64 80 0. 4477.5 0. 4477.5 0. 4477.5
```

A2. INPUT FILES FOR THE NUMERICAL SIMULATION OF THE EXPERIMENTAL RESULTS

A2.1 Geometry program for 102 mm diameter pile with L/D = 5

"Pipe pile problem"
999
80 60 4 4 2 4
80 60
1 1 1 1 1 1 1 0 0 0
0 0 0 0

1	.00	20.00	39	2.00	28.00
2	.00	21.33	40	2.00	29.33
3	.00	22.67	41	2.00	30.67
4	.00	24.00	42	2.00	32.00
5	.00	25.33	43	2.00	33.33
6	.00	26.67	44	2.00	34.67
7	.00	28.00	45	2.00	36.00
8	.00	29.33	46	2.00	37.33
9	.00	30.67	47	2.00	38.67
10	.00	32.00	48	2.00	40.00
11	.00	33.33	49	2.06	20.00
12	.00	34.67	50	2.06	21.33
13	.00	36.00	51	2.06	22.67
14	.00	37.33	52	2.06	24.00
15	.00	38.67	53	2.06	25.33
16	.00	40.00	54	2.06	26.67
17	1.00	20.00	55	2.06	28.00
18	1.00	21.33	56	2.06	29.33
19	1.00	22.67	57	2.06	30.67
20	1.00	24.00	58	2.06	32.00
21	1.00	25.33	59	2.06	33.33
22	1.00	26.67	60	2.06	34.67
23	1.00	28.00	61	2.06	36.00
24	1.00	29.33	62	2.06	37.33
25	1.00	30.67	63	2.06	38.67
26	1.00	32.00	64	2.06	40.00
27	1.00	33.33	65	2.31	20.00
28	1.00	34.67	66	2.31	21.33
29	1.00	36.00	67	2.31	22.67
30	1.00	37.33	68	2.31	24.00
31	1.00	38.67	69	2.31	25.33
32	1.00	40.00	70	2.31	26.67
33	2.00	20.00	71	2.31	28.00
34	2.00	21.33	72	2.31	29.33
35	2.00	22.67	73	2.31	30.67
36	2.00	24.00	74	2.31	32.00
37	2.00	25.33	75	2.31	33.33
38	2.00	26.67	76	2.31	34.67

```
 77  2.31  36.00
 78  2.31  37.33
 79  2.31  38.67
 80  2.31  40.00
0
  1  4  4   1  17  18   2
  2  4  4   2  18  19   3
  3  4  4   3  19  20   4
  4  4  4   4  20  21   5
  5  4  4   5  21  22   6
  6  4  4   6  22  23   7
  7  4  1   7  23  24   8
  8  4  1   8  24  25   9
  9  4  1   9  25  26  10
 10  4  1  10  26  27  11
 11  4  1  11  27  28  12
 12  4  1  12  28  29  13
 13  4  1  13  29  30  14
 14  4  1  14  30  31  15
 15  4  1  15  31  32  16
 16  4  4  17  33  34  18
 17  4  4  18  34  35  19
 18  4  4  19  35  36  20
 19  4  4  20  36  37  21
 20  4  4  21  37  38  22
 21  4  4  22  38  39  23
 22  4  1  23  39  40  24
 23  4  1  24  40  41  25
 24  4  1  25  41  42  26
 25  4  1  26  42  43  27
 26  4  1  27  43  44  28
 27  4  1  28  44  45  29
 28  4  1  29  45  46  30
 29  4  1  30  46  47  31
 30  4  1  31  47  48  32
 31 13  5  34  33  49  50
 32 13  5  35  34  50  51
 33 13  5  36  35  51  52
 34 13  5  37  36  52  53
 35 13  5  38  37  53  54
 36 13  5  39  38  54  55
 37 13  2  40  39  55  56
 38 13  2  41  40  56  57
 39 13  2  42  41  57  58
 40 13  2  43  42  58  59
 41 13  2  44  43  59  60
 42 13  2  45  44  60  61
 43 13  2  46  45  61  62
 44 13  2  47  46  62  63
 45 13  2  48  47  63  64
 46  4  3  49  65  66  50
 47  4  3  50  66  67  51
 48  4  3  51  67  68  52
 49  4  3  52  68  69  53
 50  4  3  53  69  70  54
 51  4  3  54  70  71  55
 52  4  3  55  71  72  56
 53  4  3  56  72  73  57
 54  4  3  57  73  74  58
 55  4  3  58  74  75  59
 56  4  3  59  75  76  60
 57  4  3  60  76  77  61
 58  4  3  61  77  78  62
 59  4  3  62  78  79  63
 60  4  3  63  79  80  64
```

A2.2 Main program for 102 mm diameter pile with L/D = 5

```
PIPE PILE PROBLEM
999
1 5 3 1 80 0 0 1 0
0 0 0 60 65 0 0 50 60
0
1 5 1900 0.3 0.001 36 0 4 0 0.056 0 0 0 0
2 8 0 24 2558. 700. 1 0.06 0 0 0 0 0 0
3 1 29E5 29E5 0.3 0.3 11.154E5 0 0 0.283 0 0 0 0
4 5 1900 0.3 0.001 36 0 4 0 0.056 0 0 0 0
5 8 0 24 2558. 700. 1 0.06 0 0 0 0 0 0
1 2
1 40 0 0 0 0 0 0 0.0
2 20 0.37 1.12 0.37 0 0 0 0.0
0 17 1
   1   1   2  1 1 .0 .0 .0
   2   2   3  1 1 .0 .0 .0
   3   3   4  1 1 .0 .0 .0
   4   4   5  1 1 .0 .0 .0
   5   5   6  1 1 .0 .0 .0
   6   6   7  1 1 .0 .0 .0
   7   7   8  1 1 .0 .0 .0
   8   8   9  1 1 .0 .0 .0
   9   9  10  1 1 .0 .0 .0
  10  10  11  1 1 .0 .0 .0
  11  11  12  1 1 .0 .0 .0
  12  12  13  1 1 .0 .0 .0
  13  13  14  1 1 .0 .0 .0
  14  14  15  1 1 .0 .0 .0
  15  15  16  1 1 .0 .0 .0
   1   1  17  2 1 .0 .0 .0
  16  17  33  2 1 .0 .0 .0
1 1 5 0 -1 0 0 0 00000 0 0 0 0
60 64 80 0. 0000.0 0. 0000.0 0. 0000.0
2 6 45 0 -1 0 0 0 00011 0 0 0 0
60 64 80 0. 1500.0 0.  1500.0 0. 1500.0
3 46 80 0 -1 0 0 0 00011 0 0 0 0
60 64 80 0. 0000.0 0. 0000.0 0. 0000.0

1 1 1 0 -1 0 0 0 00021 0 0 0 0
61 64 80 0. 30.0 0. 30.0 0. 30.0
2 2 800 0 -1 0 0 0 00000 0 0 0 0
61 64 80 0. 23970.0 0. 23970.0 0. 23970.0
3 801 801 0 -1 0 0 0 00121 0 0 0 0
61 64 80 0. 22.5 0. 22.5 0. 22.5
4 802 1500 0 -1 0 0 0 00000 0 0 0 0
61 64 80 0. 16477.5 0. 16477.5 0. 16477.5
```

APPENDIX B

DISTRIBUTION OF STRESSES

B1. DISTRIBUTION OF VERTICAL STRESS IN PILE MATERIAL

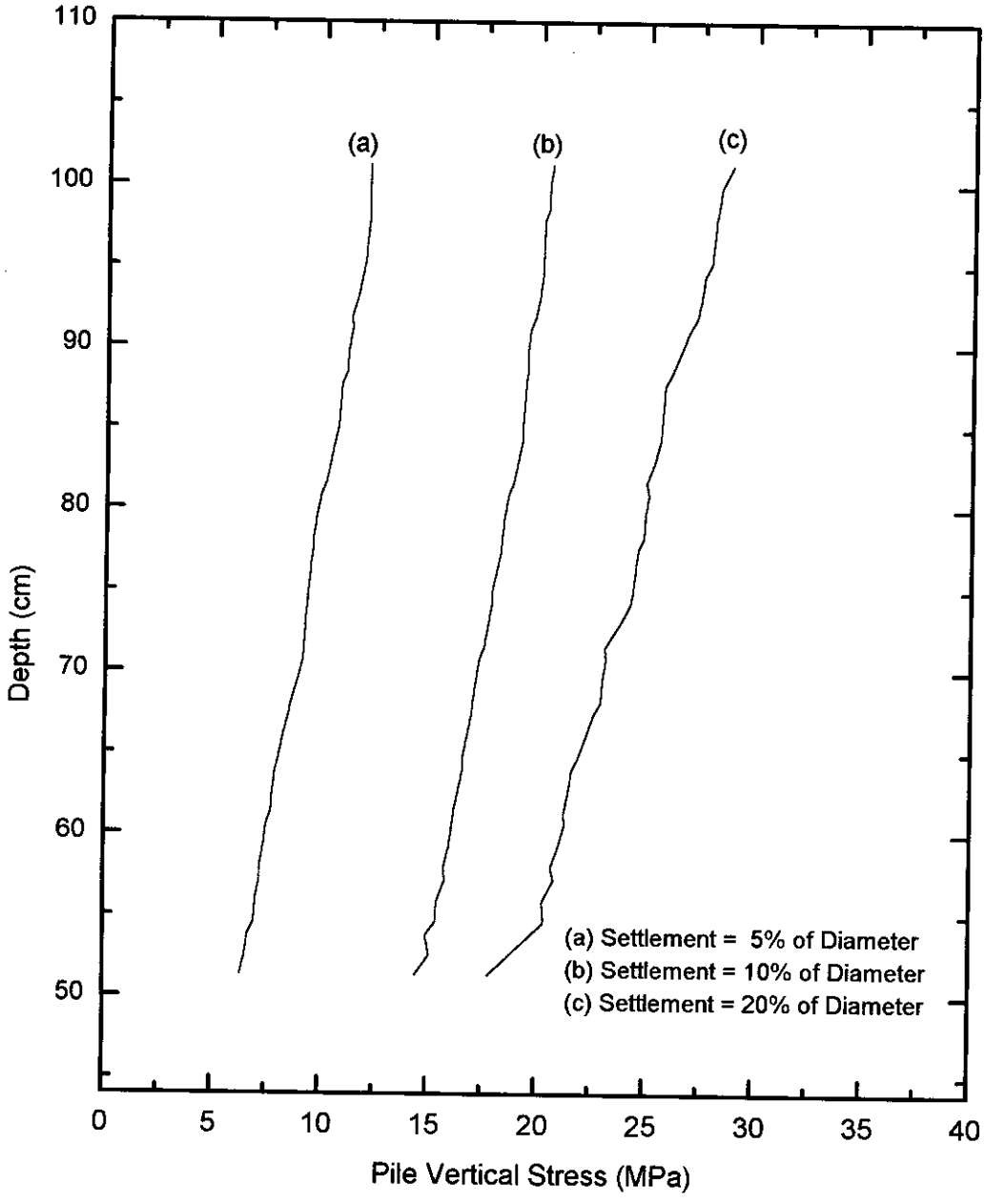

Figure B1.1 Vertical stress along pile depth (D = 102 mm, L/D = 5)

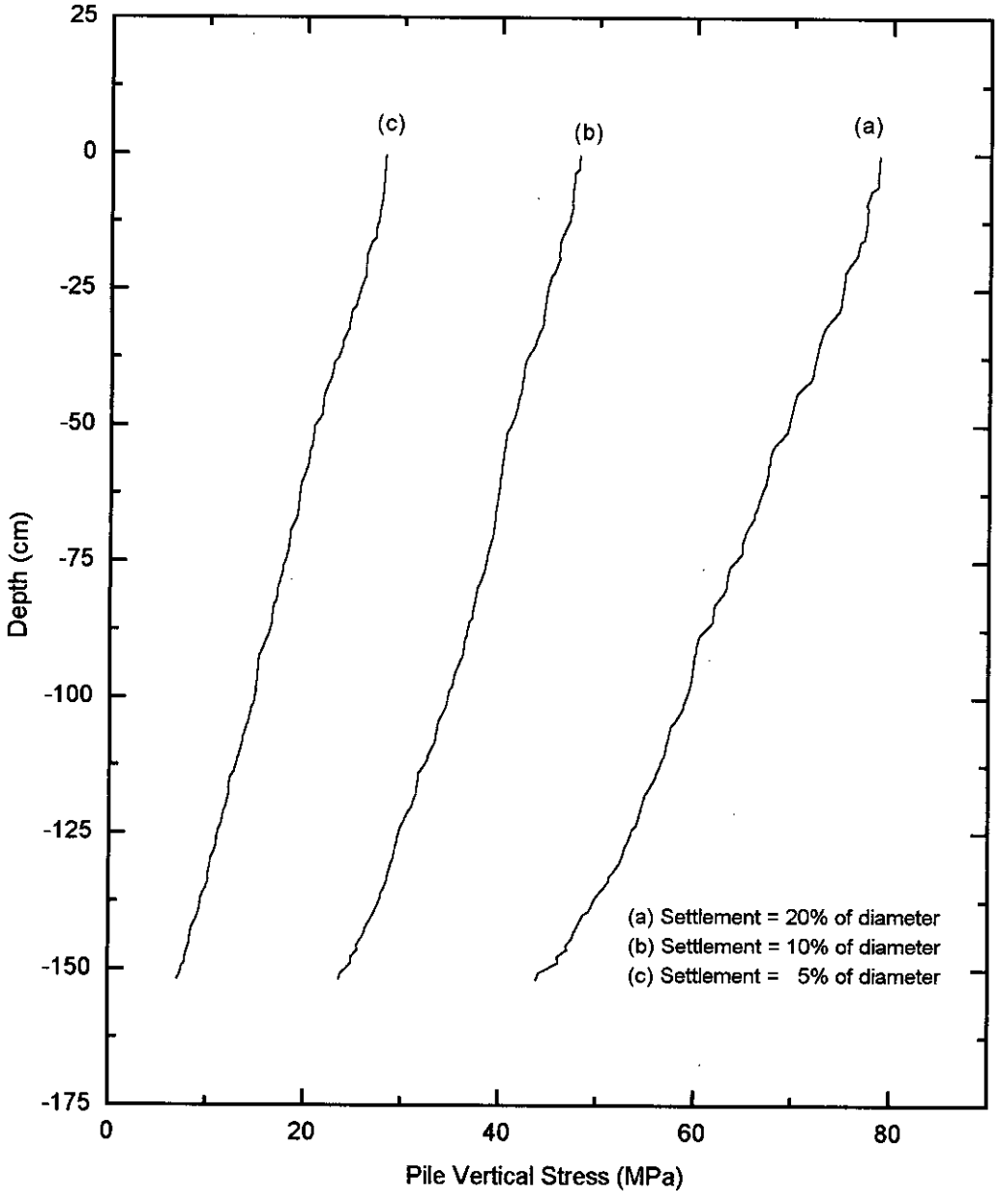

Figure B1.2 Vertical stress along pile depth (D = 102 mm, L/D = 15)

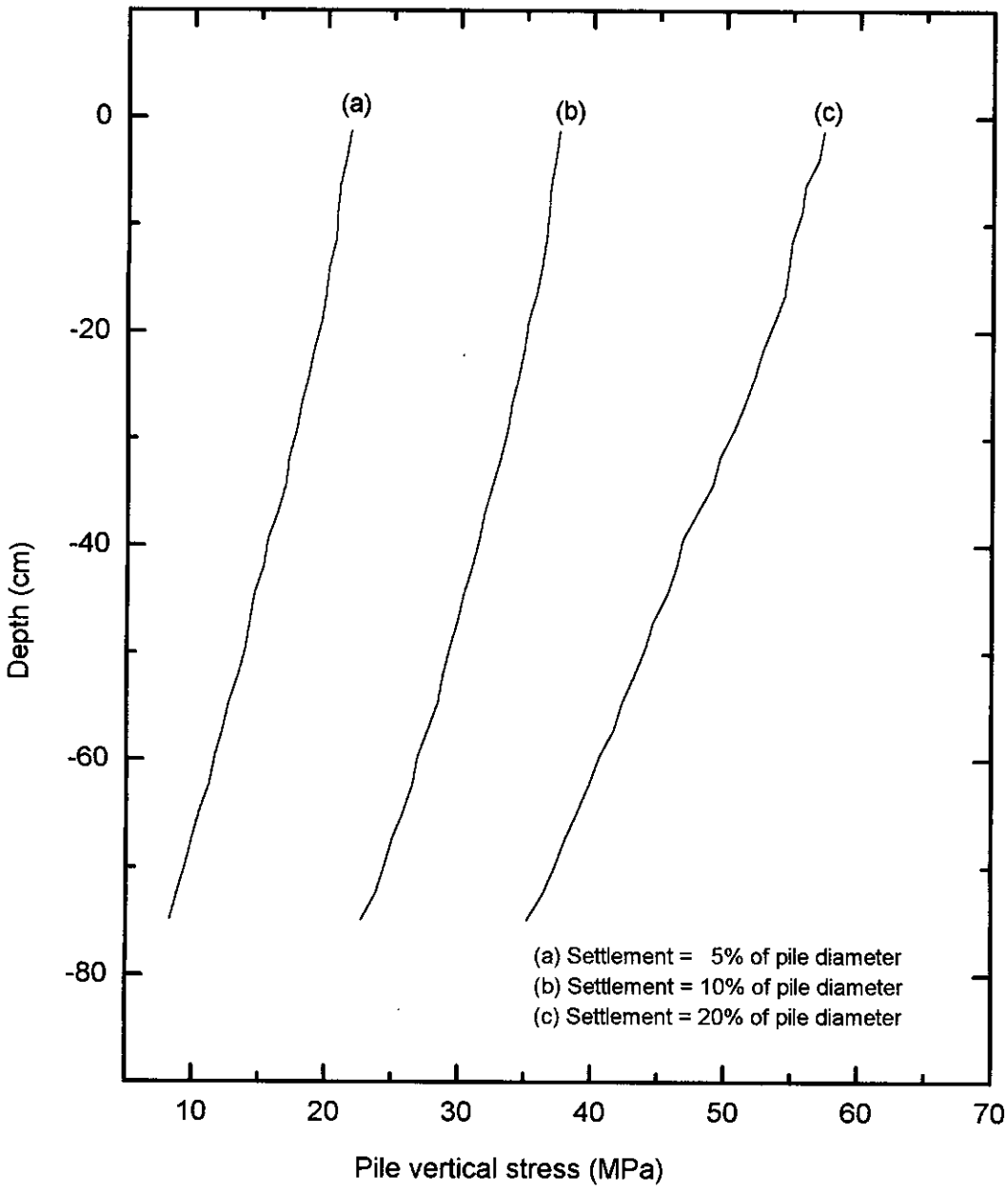

Figure B1.3 Vertical stress along pile depth (D = 152 mm, L/D = 5)

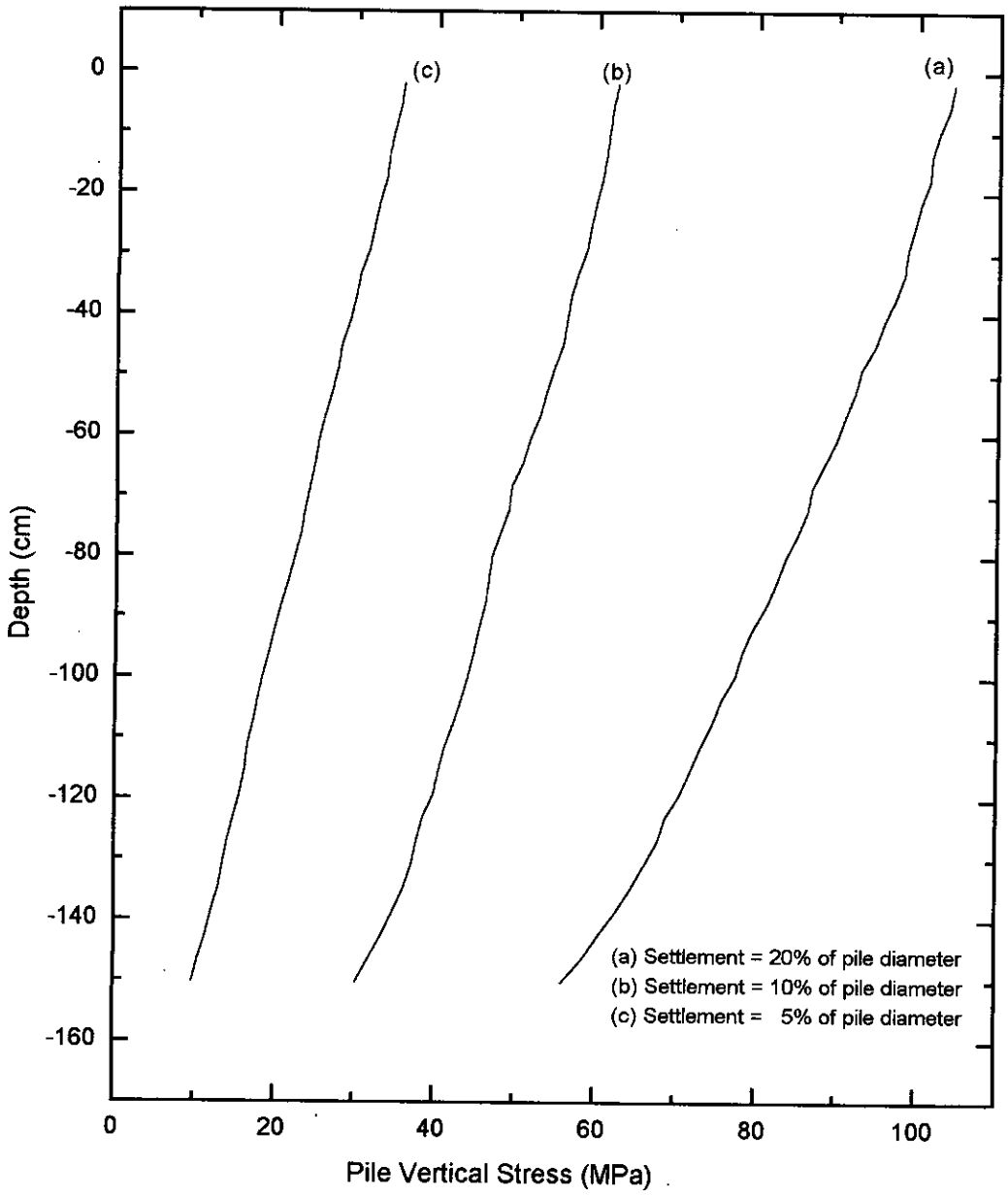

Figure B1.4 Vertical stress along pile depth (D = 152 mm , L/D = 10)

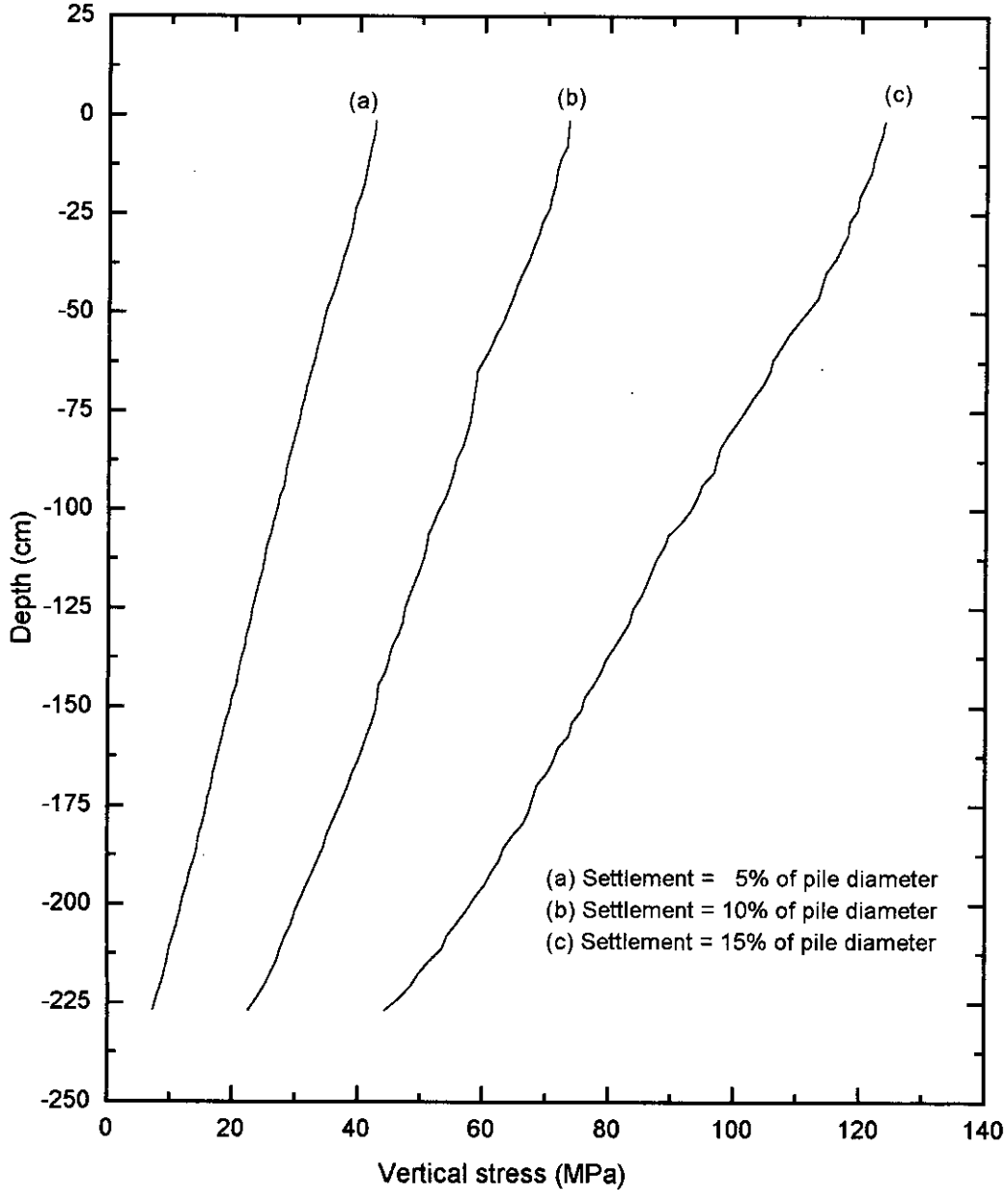

Figure B1.5 Vertical stress along pile depth (D = 152 mm, L/D = 15)

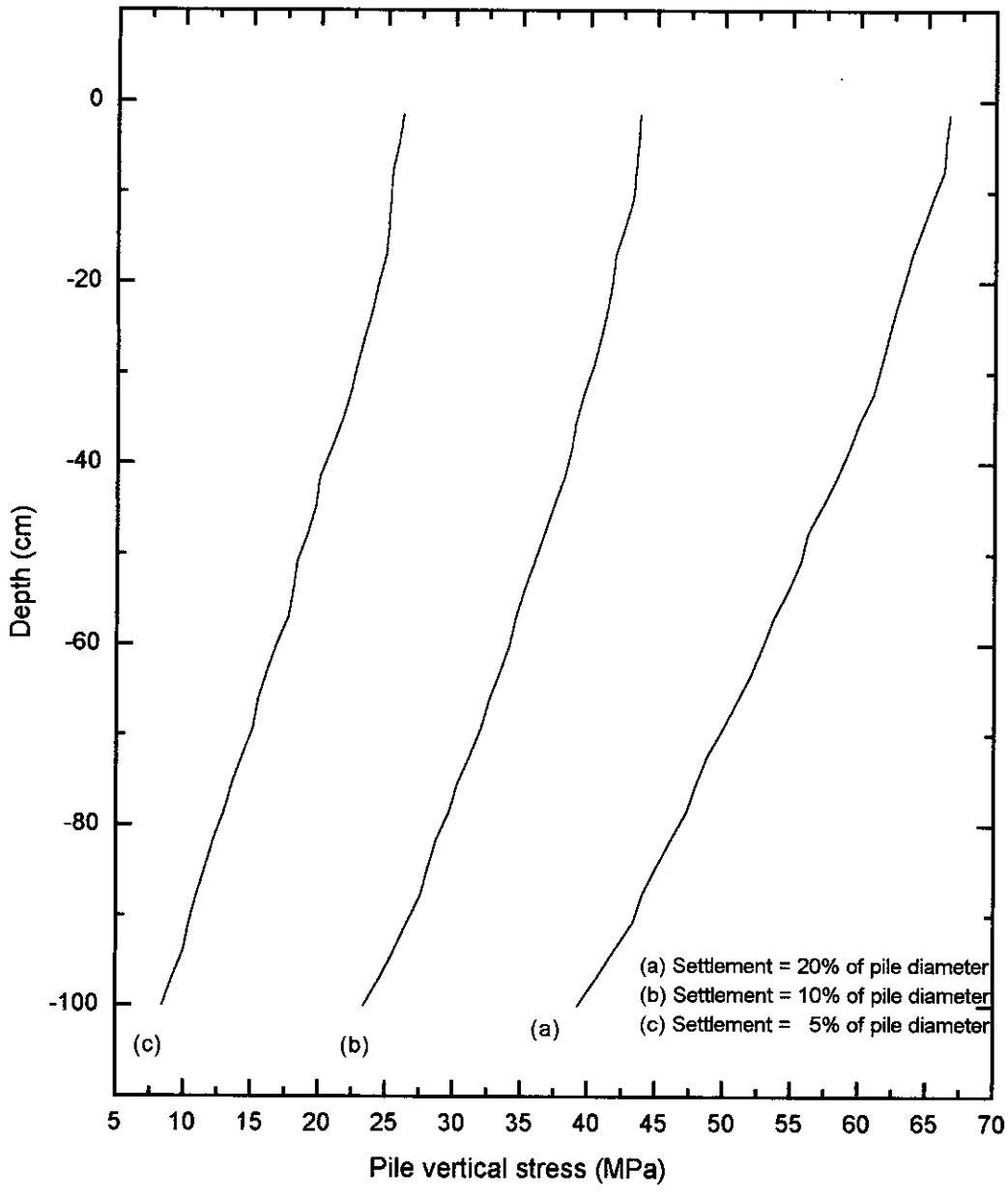

Figure B1.6 Vertical stress along pile depth (D = 203 mm, L/D = 5)

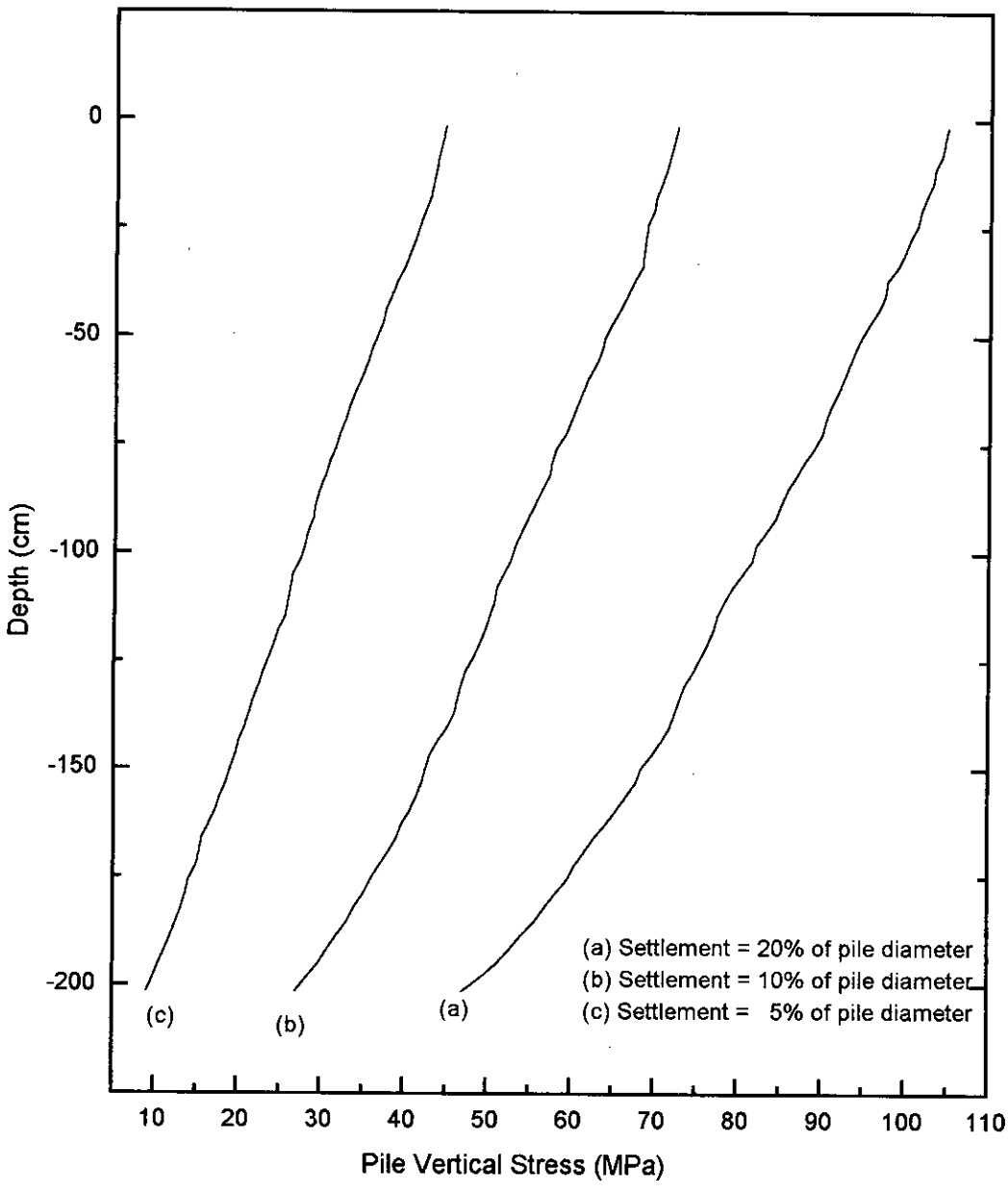

Figure B1.7 Vertical stress along pile depth (D = 203 mm, L/D = 10)

B2. VERTICAL STRESS DISTRIBUTION IN THE INTERNAL SOIL

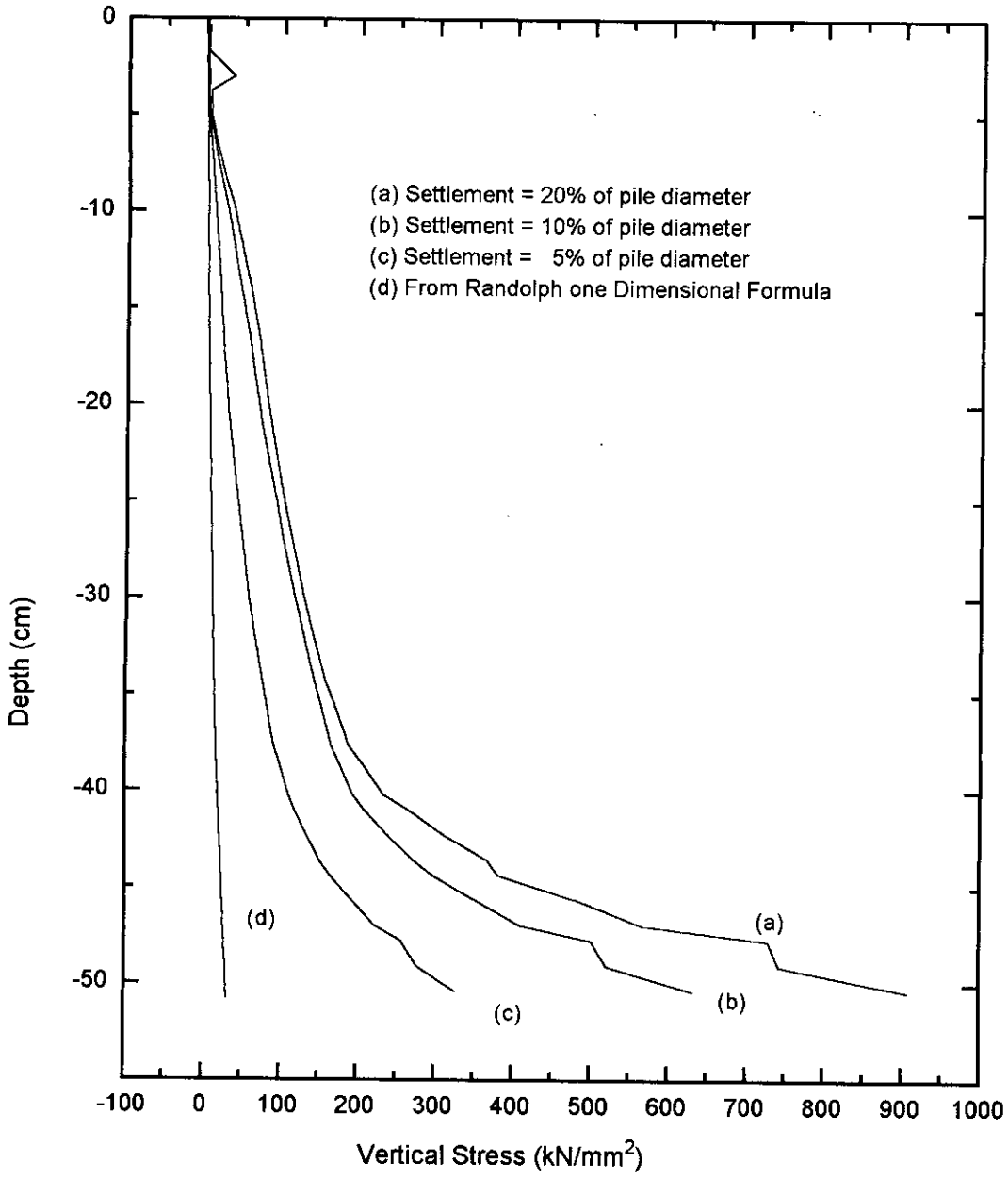

Figure B2.1 Vertical stress in the internal soil with depth

(D = 102 mm, L/D = 5)

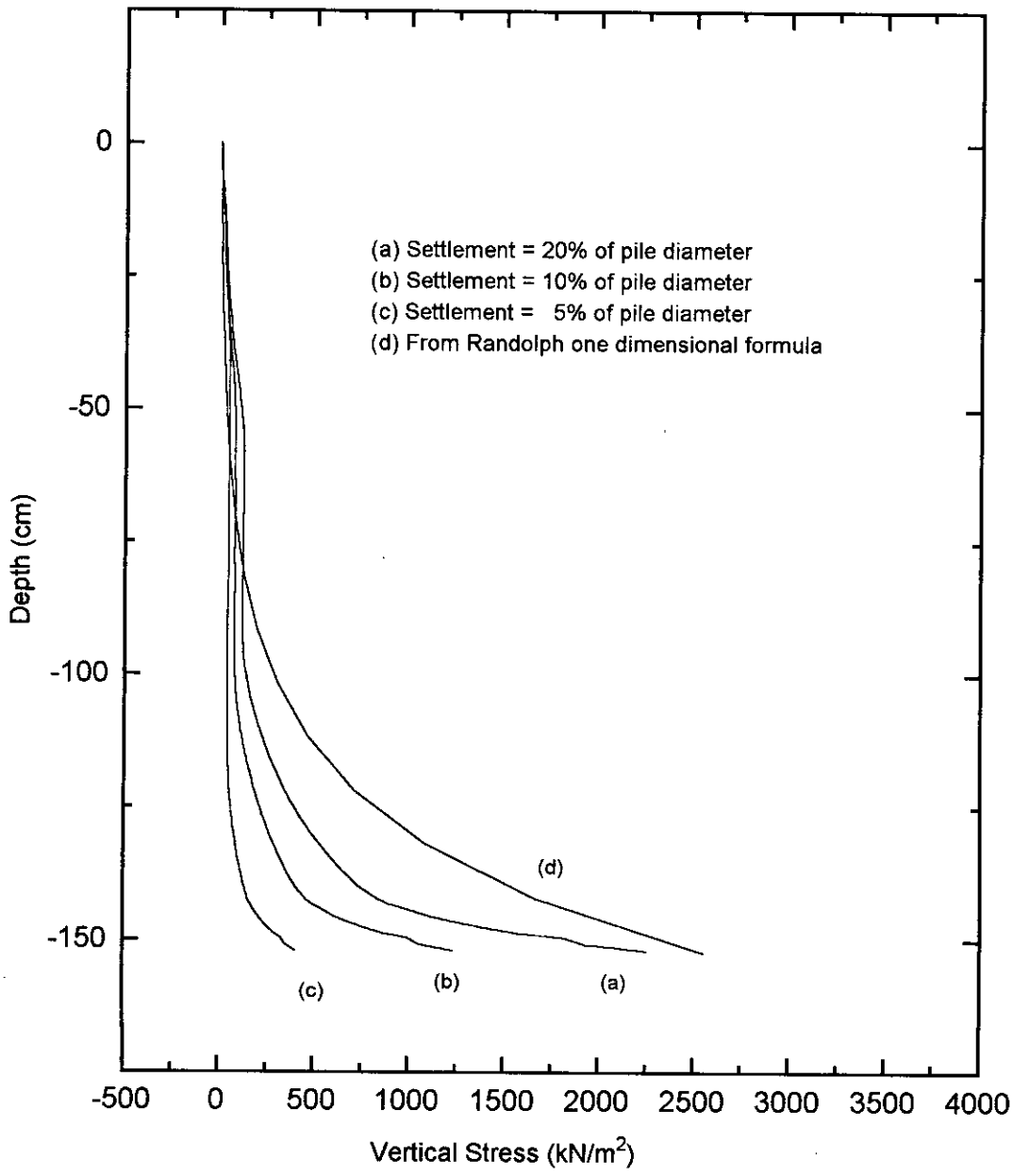

Figure B2.2 Vertical stress in the internal soil with depth

(D = 102 mm, L/D = 15)

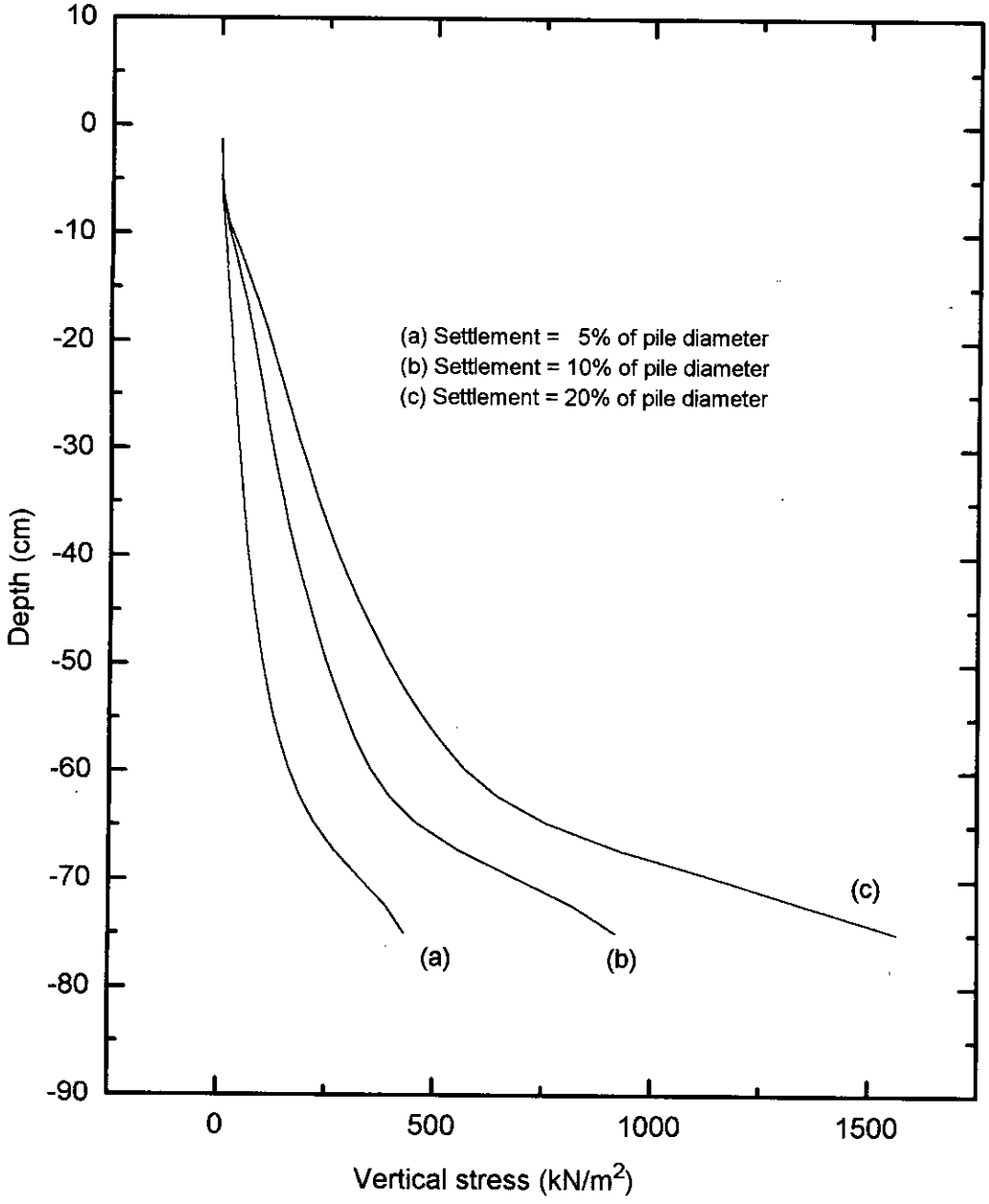

Figure 2.3 Vertical stress in the internal soil with depth

(D = 152 mm, L/D =5)

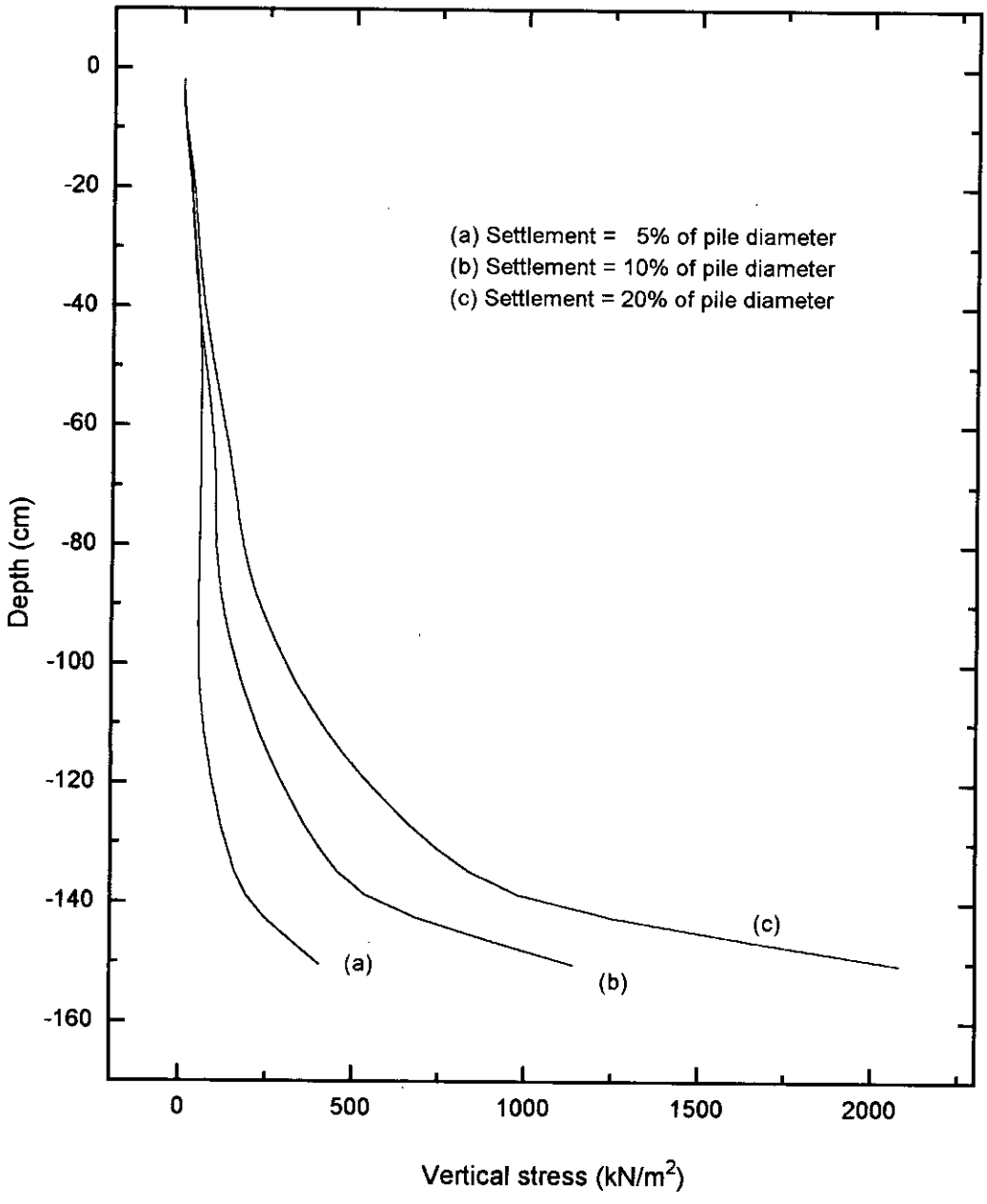

Figure B2.4 Vertical stresses in the internal soil with depth
(D = 152 mm, L/D = 10)

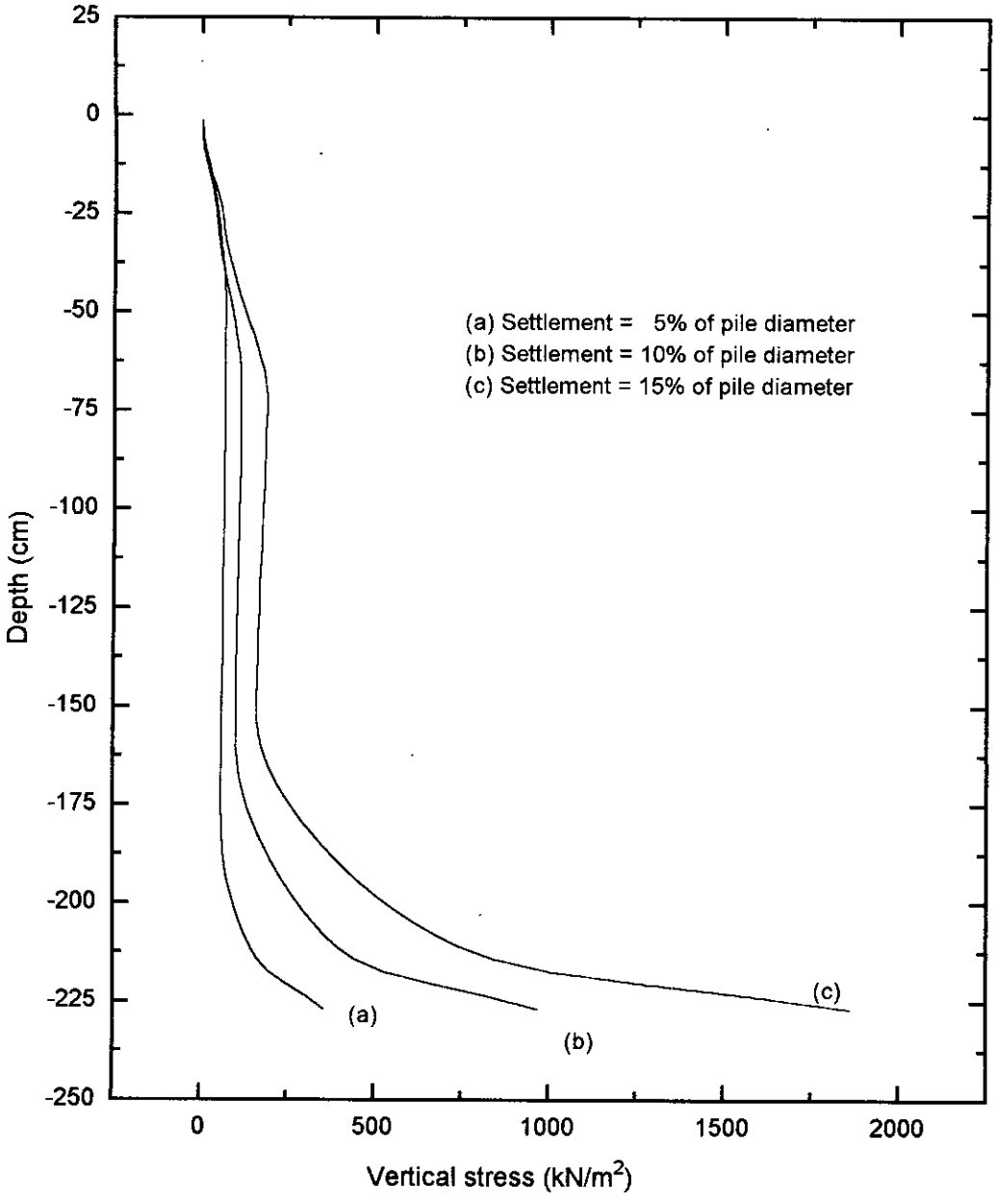

Figure B2.5 Vertical stress in the internal soil with depth
(D = 152 mm, L/D = 15)

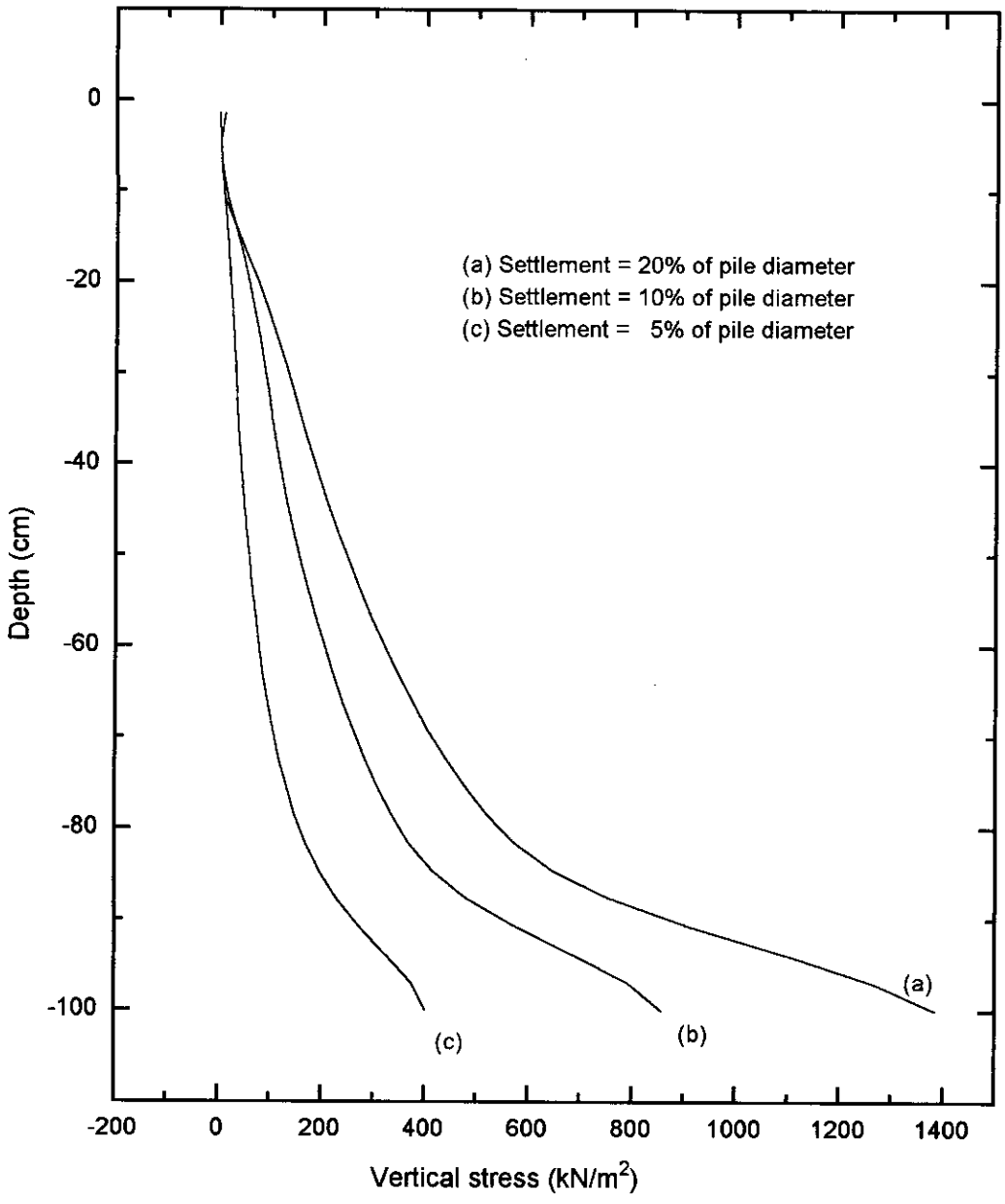

Figure B2.6 Vertical stress in the internal soil with depth
(D = 203 mm, L/D = 5)

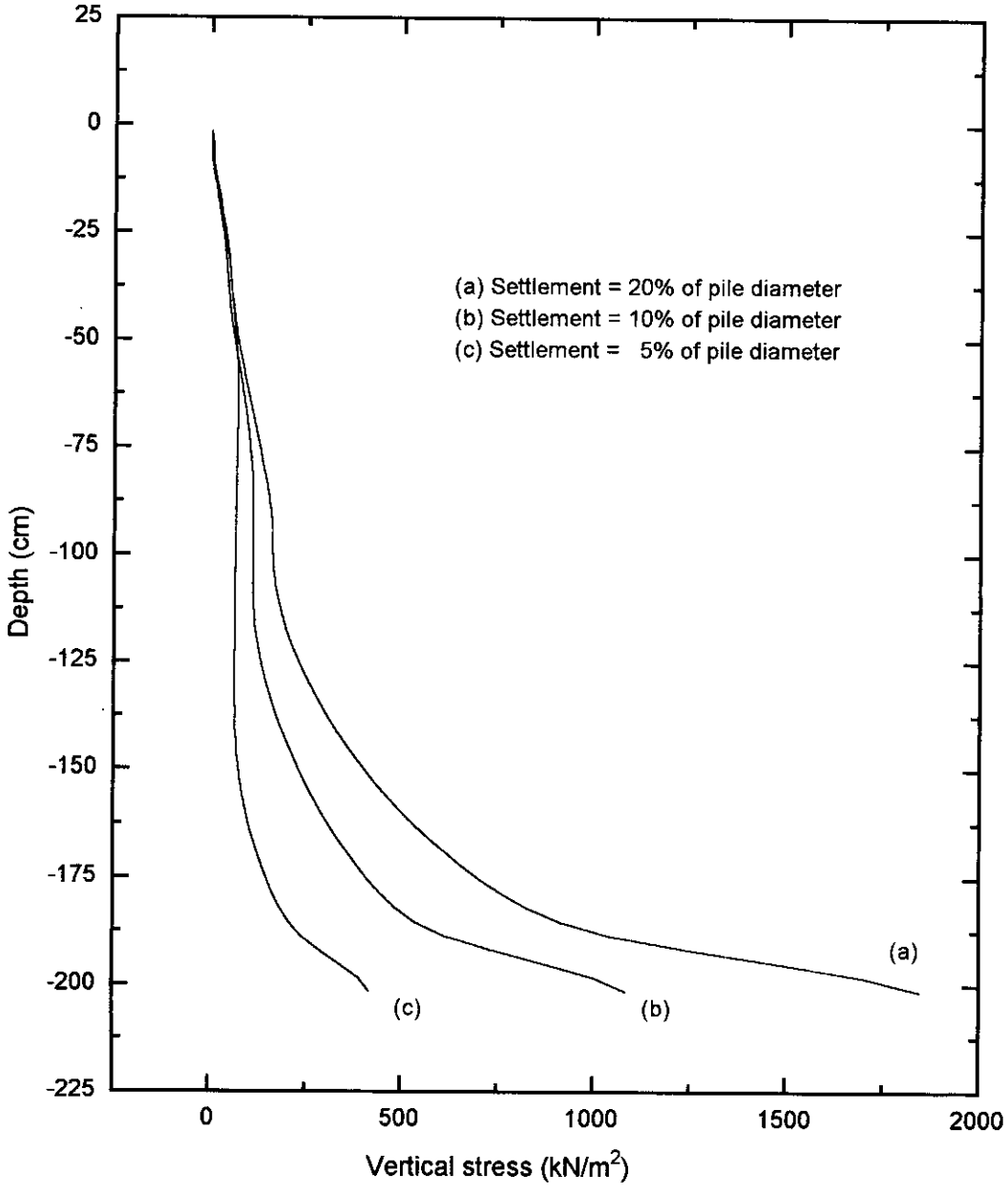

Figure B2.7 Vertical stress in the internal soil with depth
(D = 203 mm, L/D = 10)

B3. NORMAL STRESSES ALONG THE INTERFACE ELEMENTS

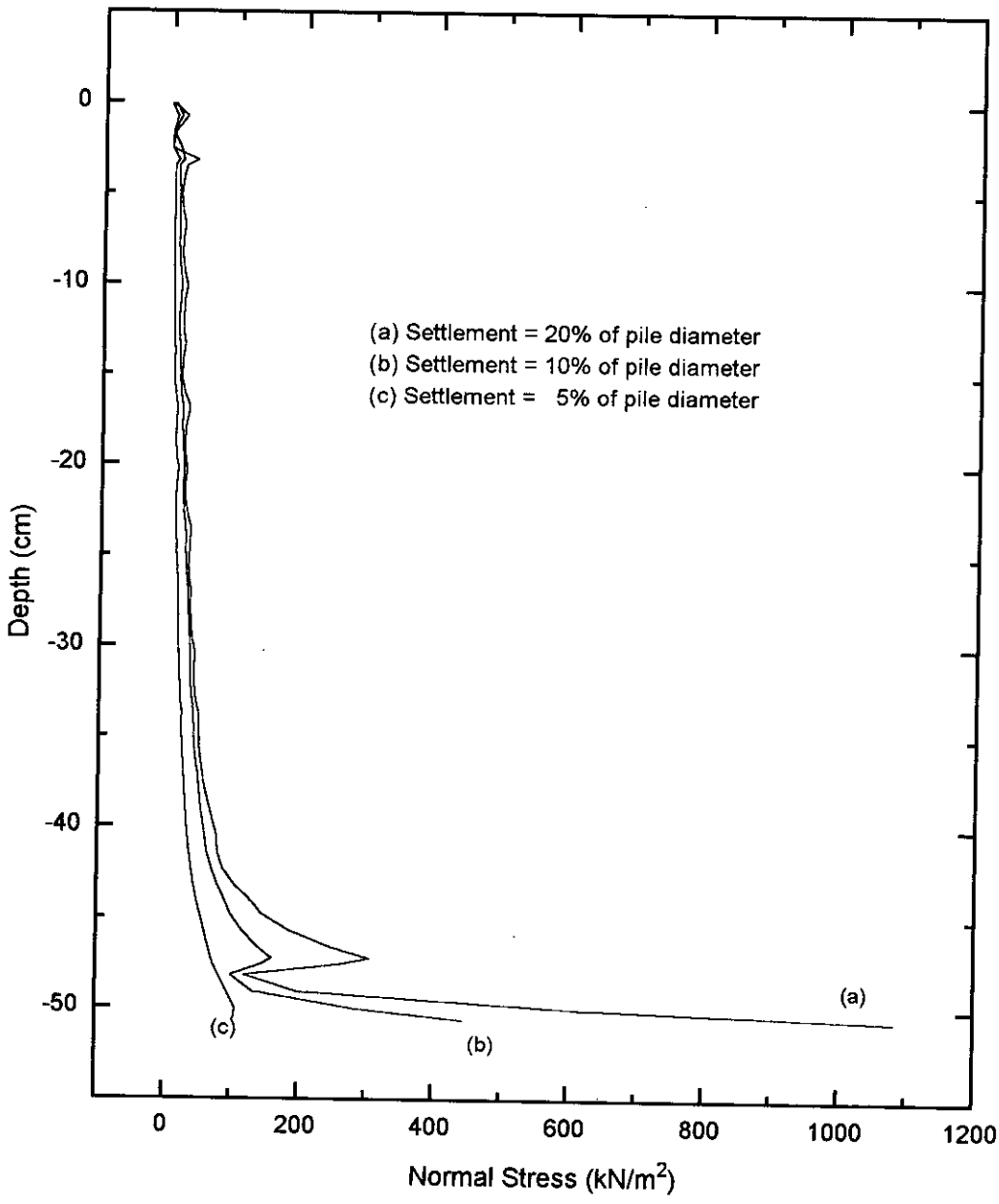

Figure B3.1 Normal stresses along the interface elamants (D = 102 mm, L/D = 5)

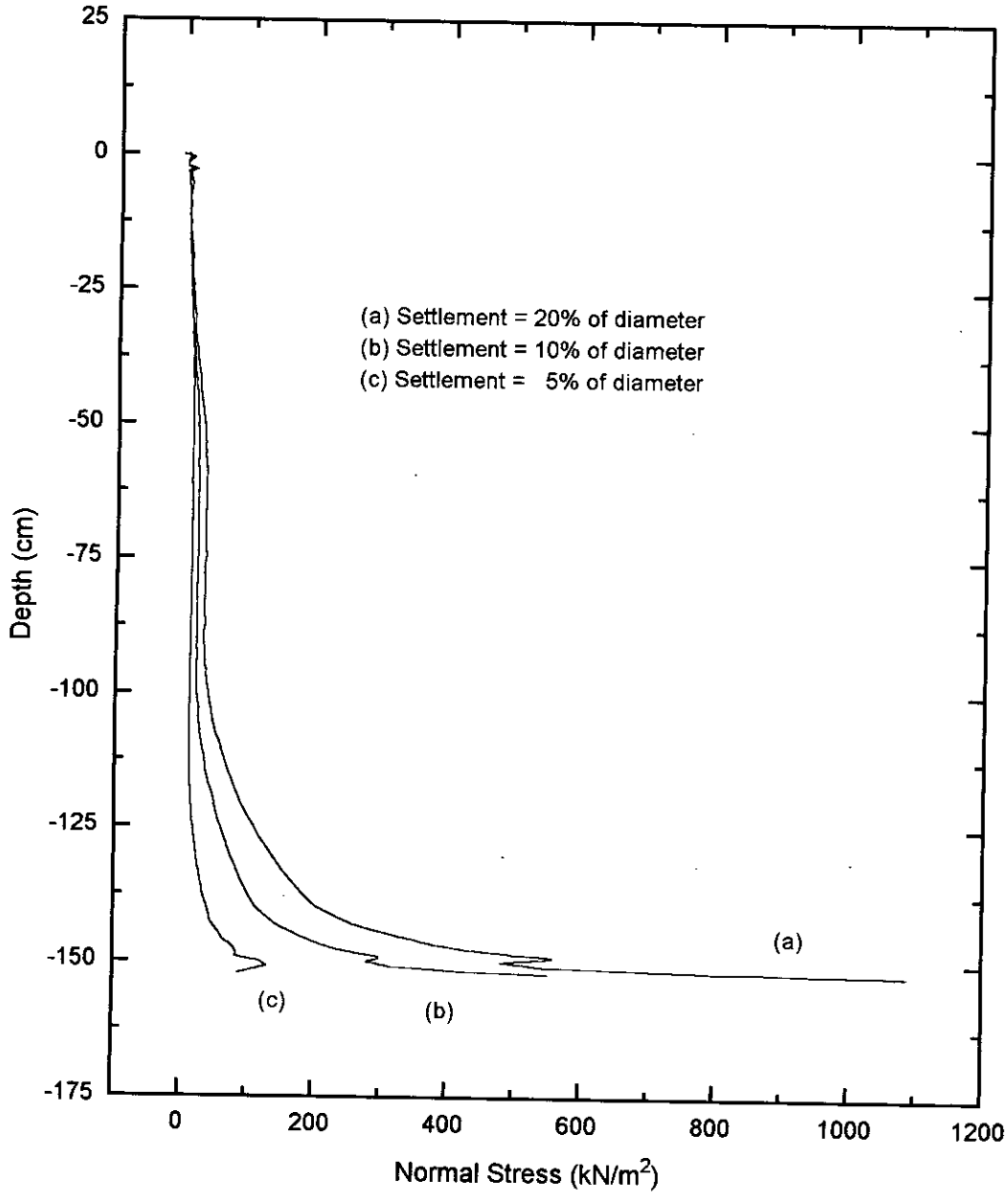

Figure B3.2 Normal stresses along the interface elements

(D = 102 mm, L/D = 15)

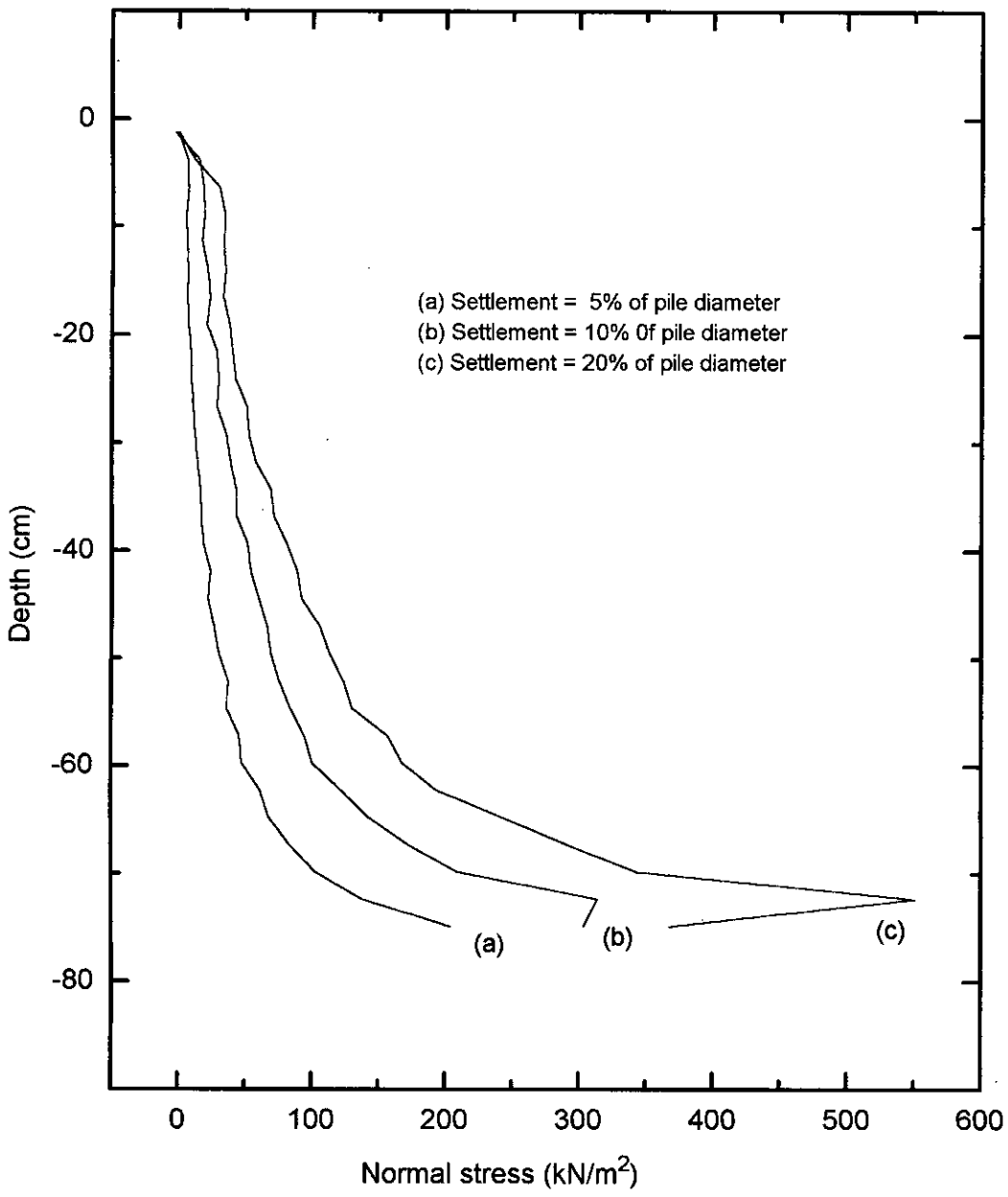

Figure B3.3 Normal stresses along the interface elements
(D = 152 mm, L/D = 5)

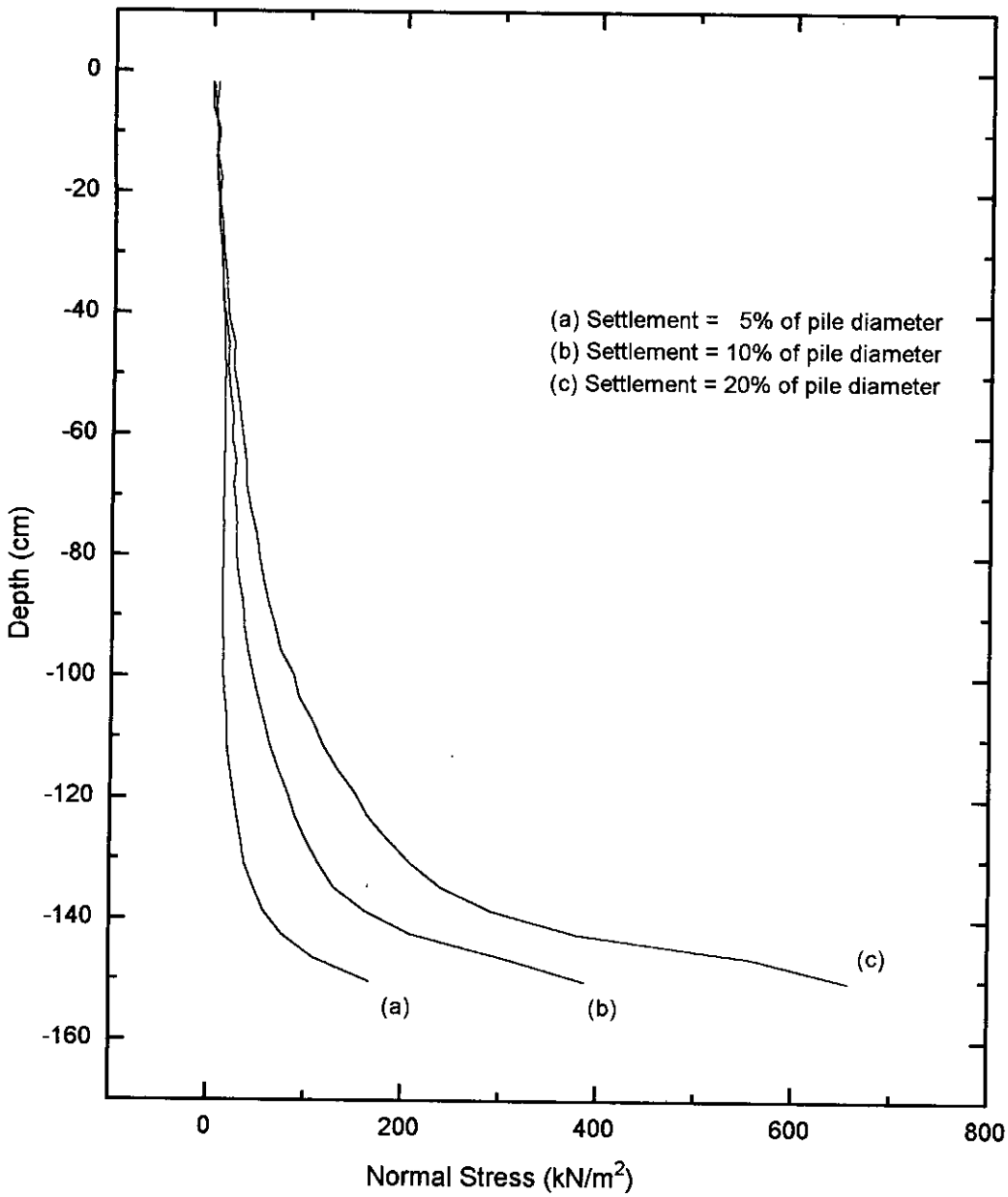

Figure B3.4 Normal stresses along the interface elements
(D = 152 mm, L/D = 10)

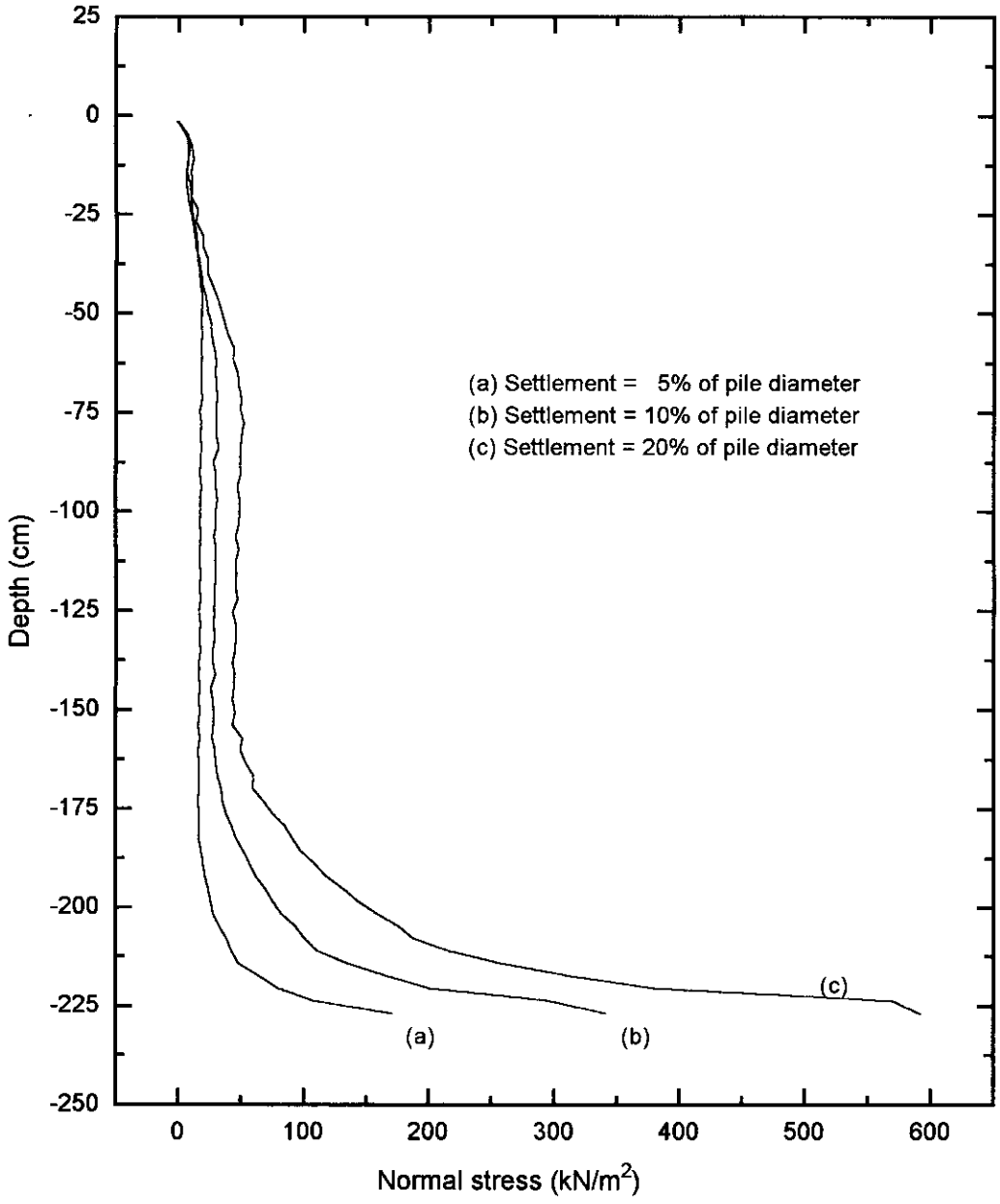

Figure B3.5 Normal stresses along the interface elements
(D = 152 mm, L/D = 15)

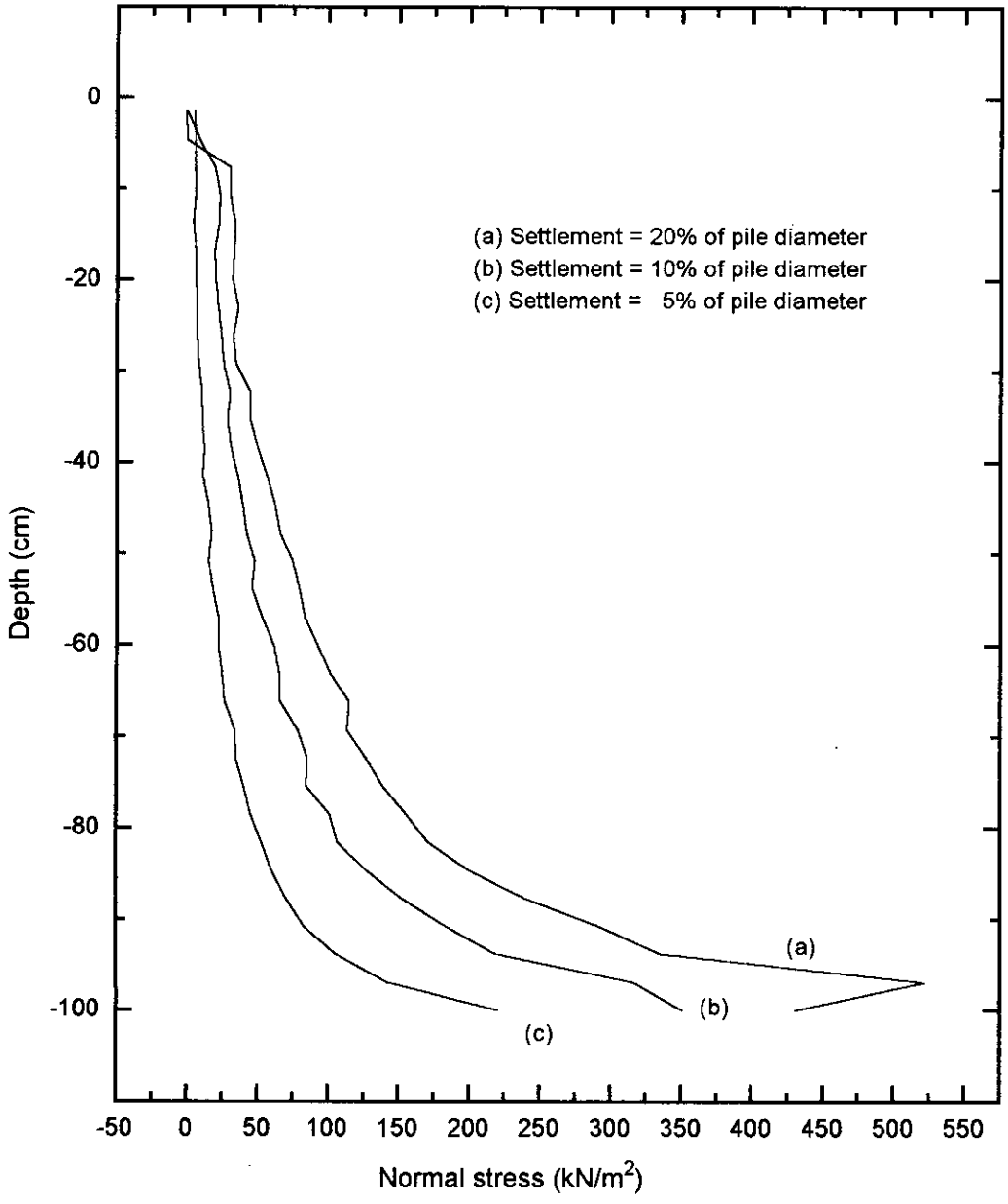

Figure B3.6 Normal stresses along the interface elements

(D = 203 mm, L/D = 5)

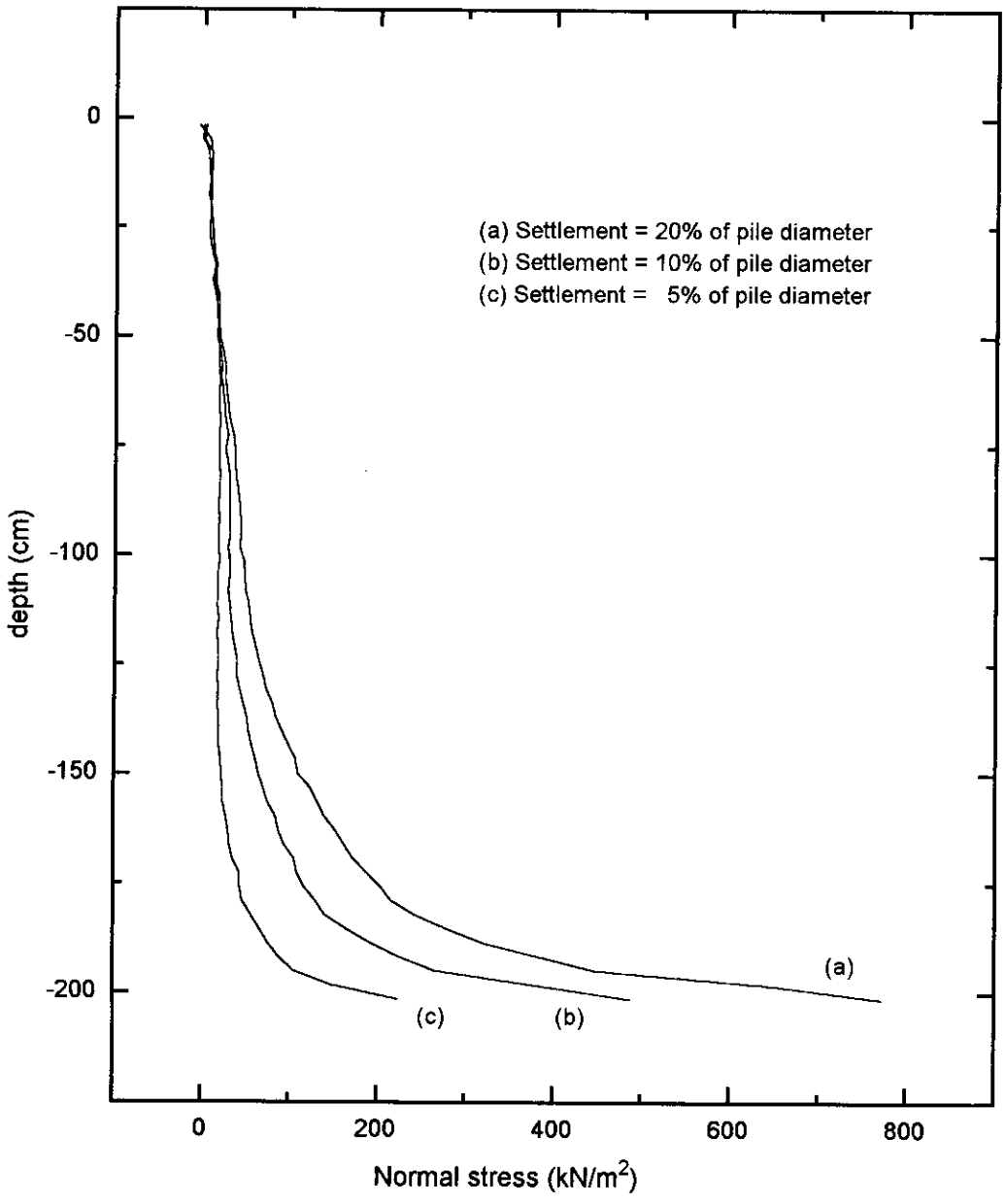

Figure B3.7 Normal stresses along the interface elements
(D = 203 mm, L/D = 10)

B4. SHEAR STRESSES ALONG THE INTERFACE ELEMENTS

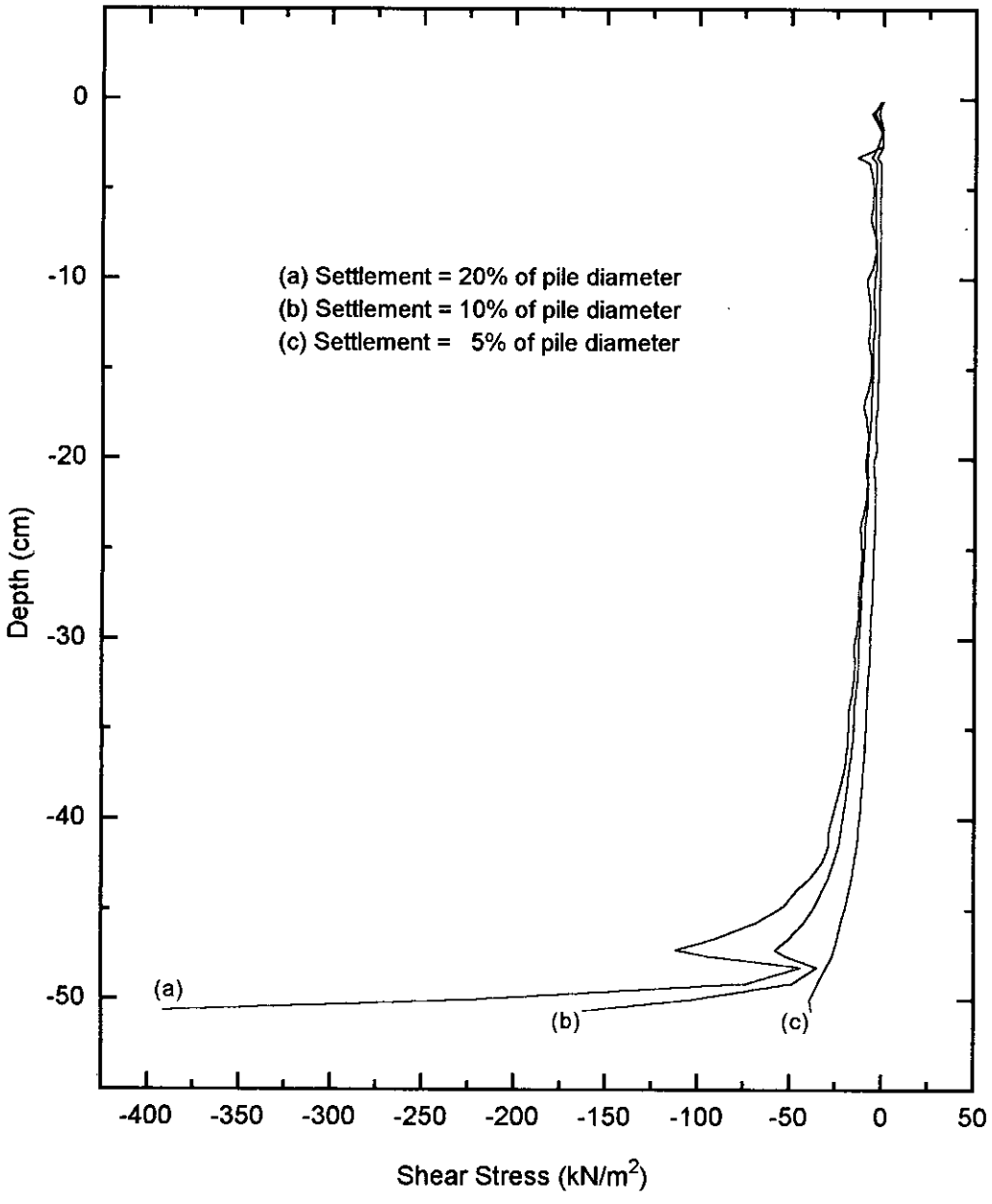

Figure B4.1 Shear stress along interface elements (D = 102 mm, L/D = 5))

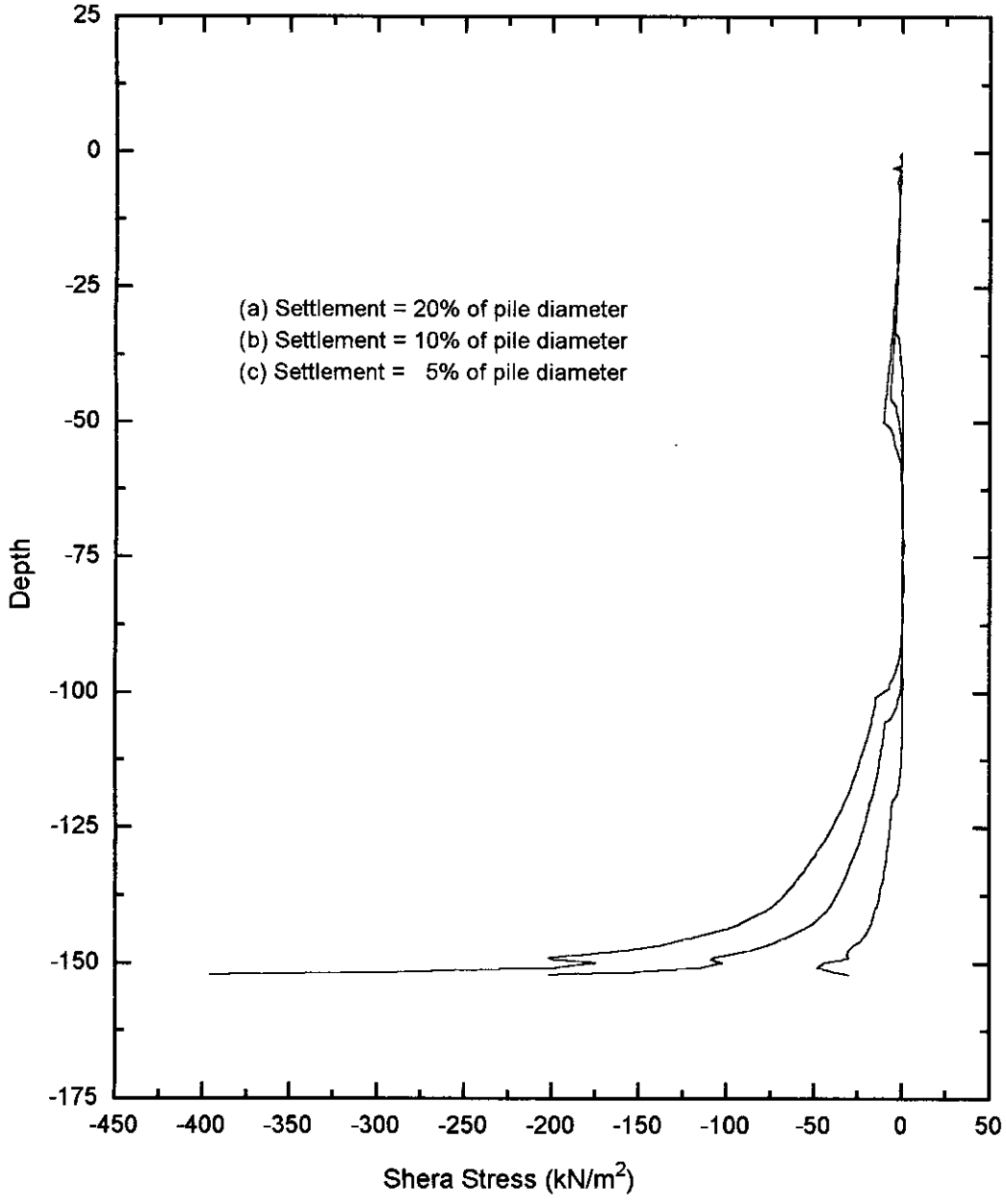

Figure B4.2 Shear stresses along the interface elements
(D = 102 mm, L/D = 15)

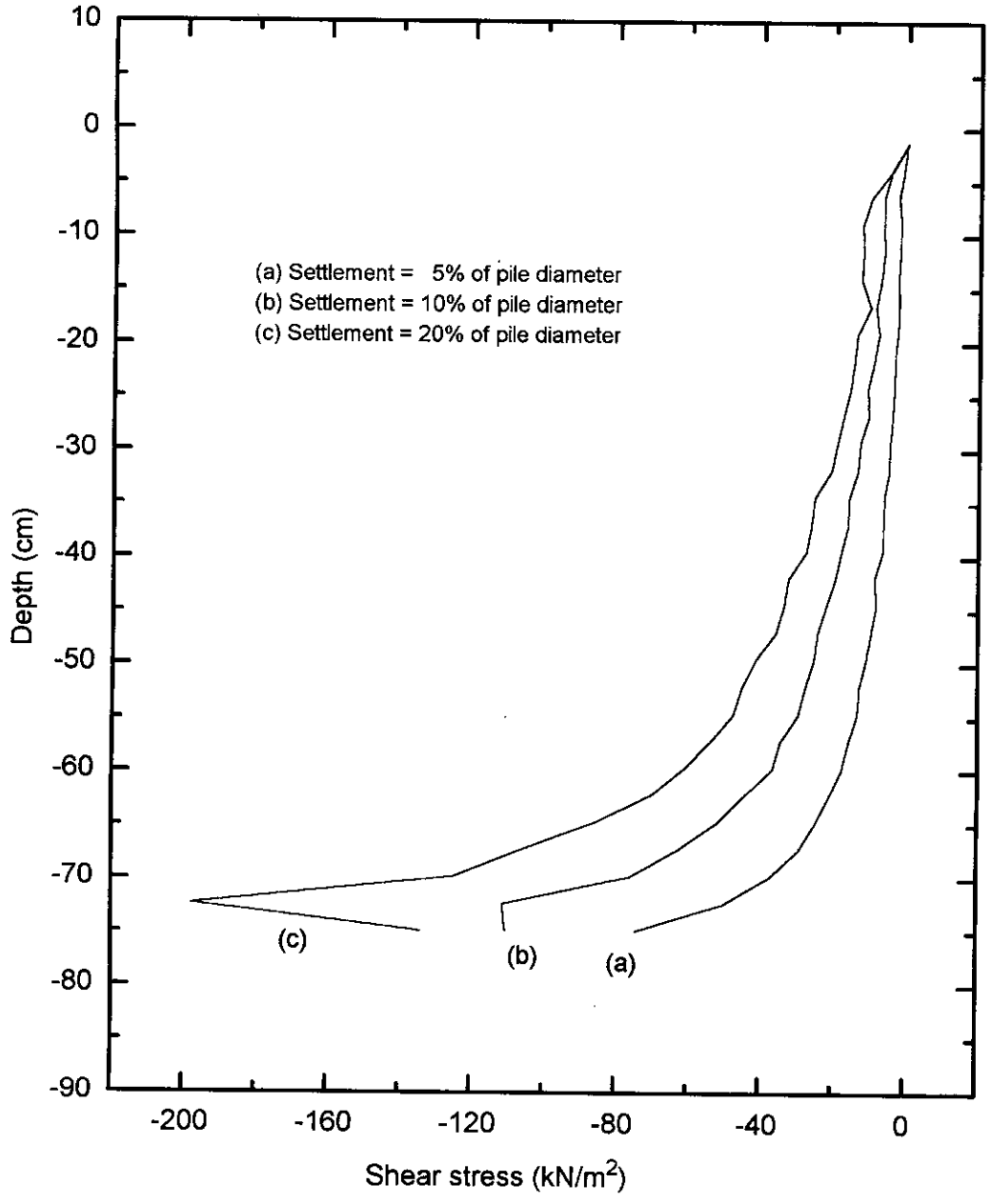

Figure B4.3 Shear stresses along the interface elements
(D = 152 mm, L/D = 5)

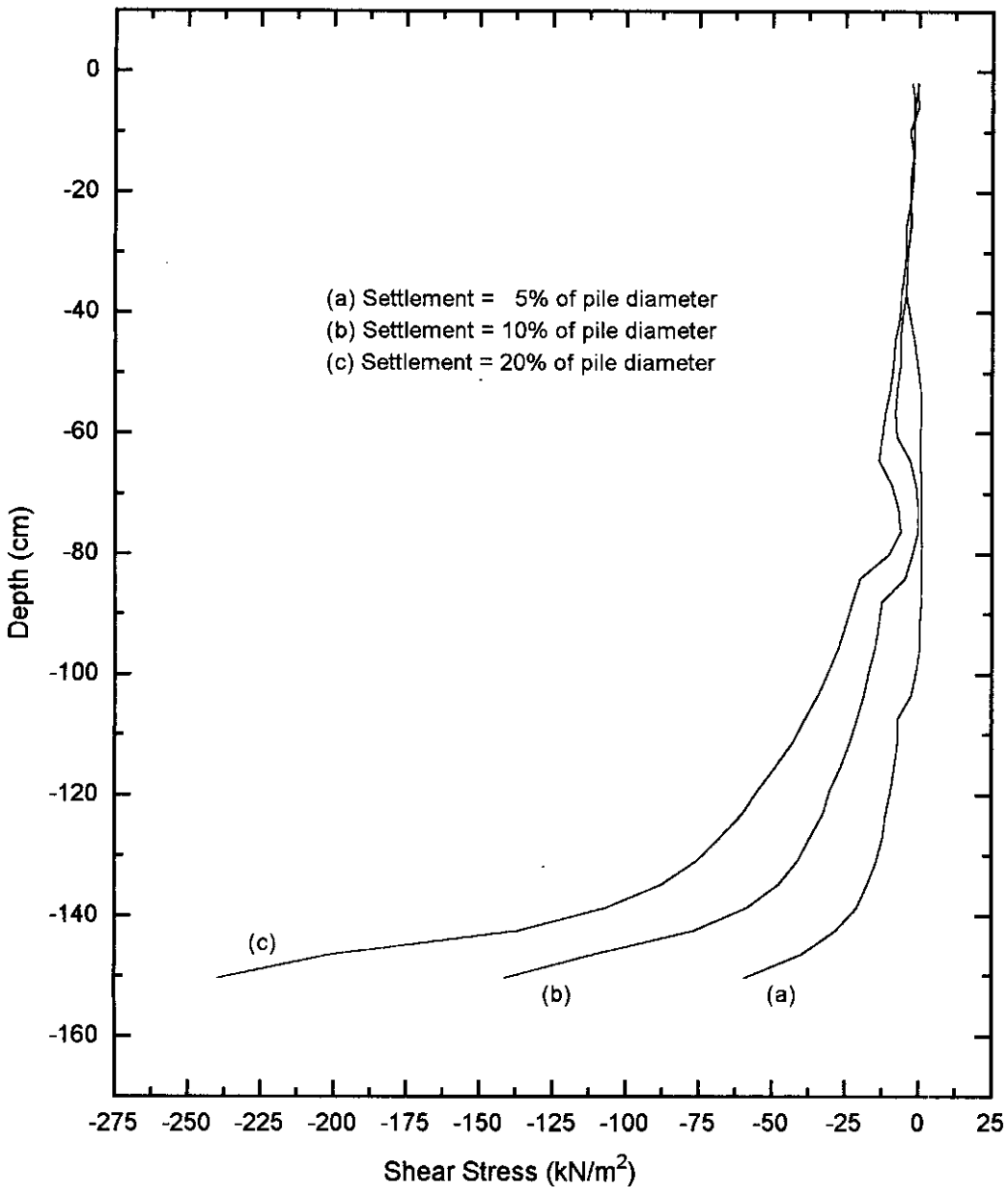

Figure B4.4 Shear stresses along the interface elements
(D = 152 mm, L/D = 10)

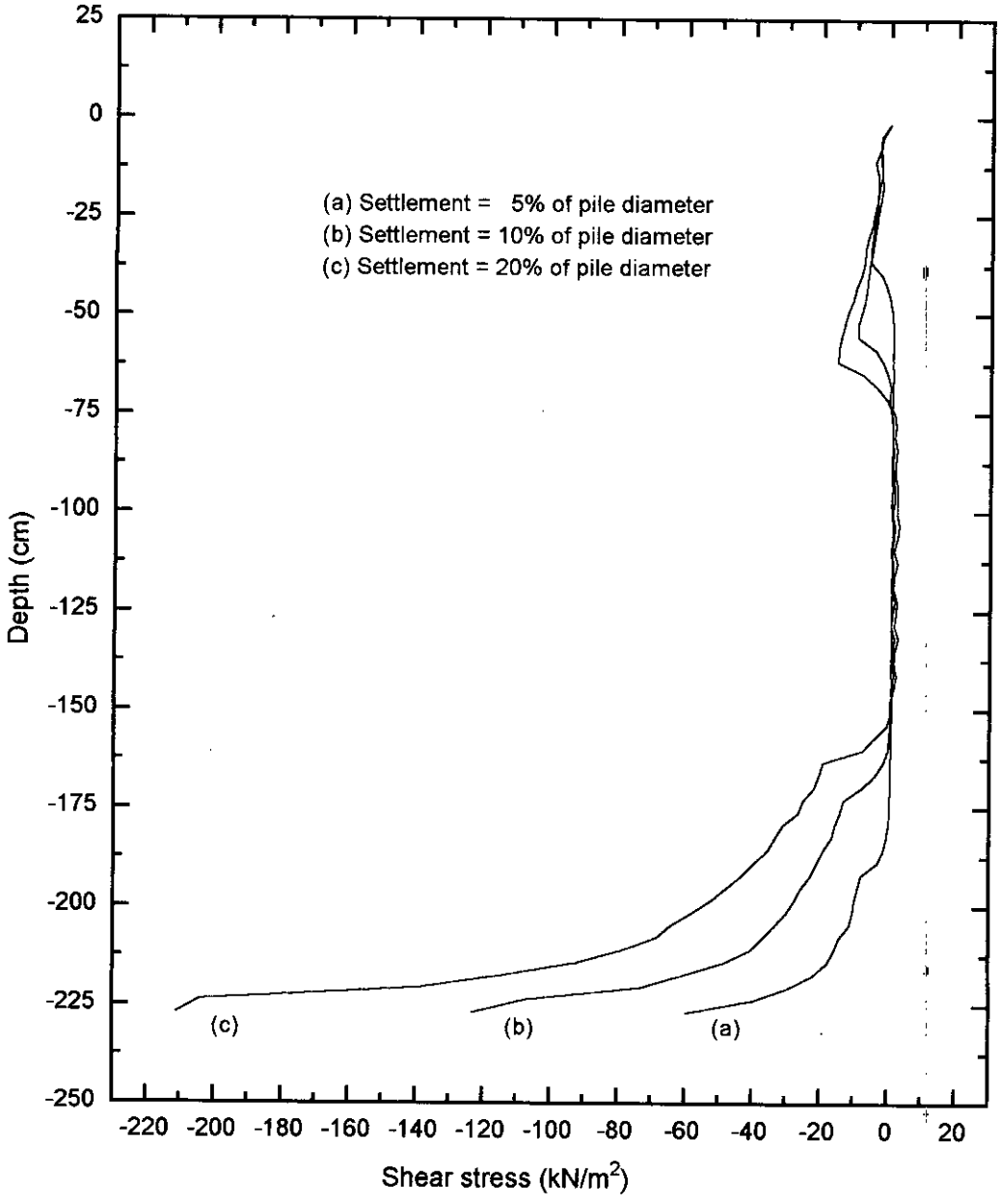

Figure B4.5 Shear stresses along the interface elements
(D = 152 mm, L/D = 15)

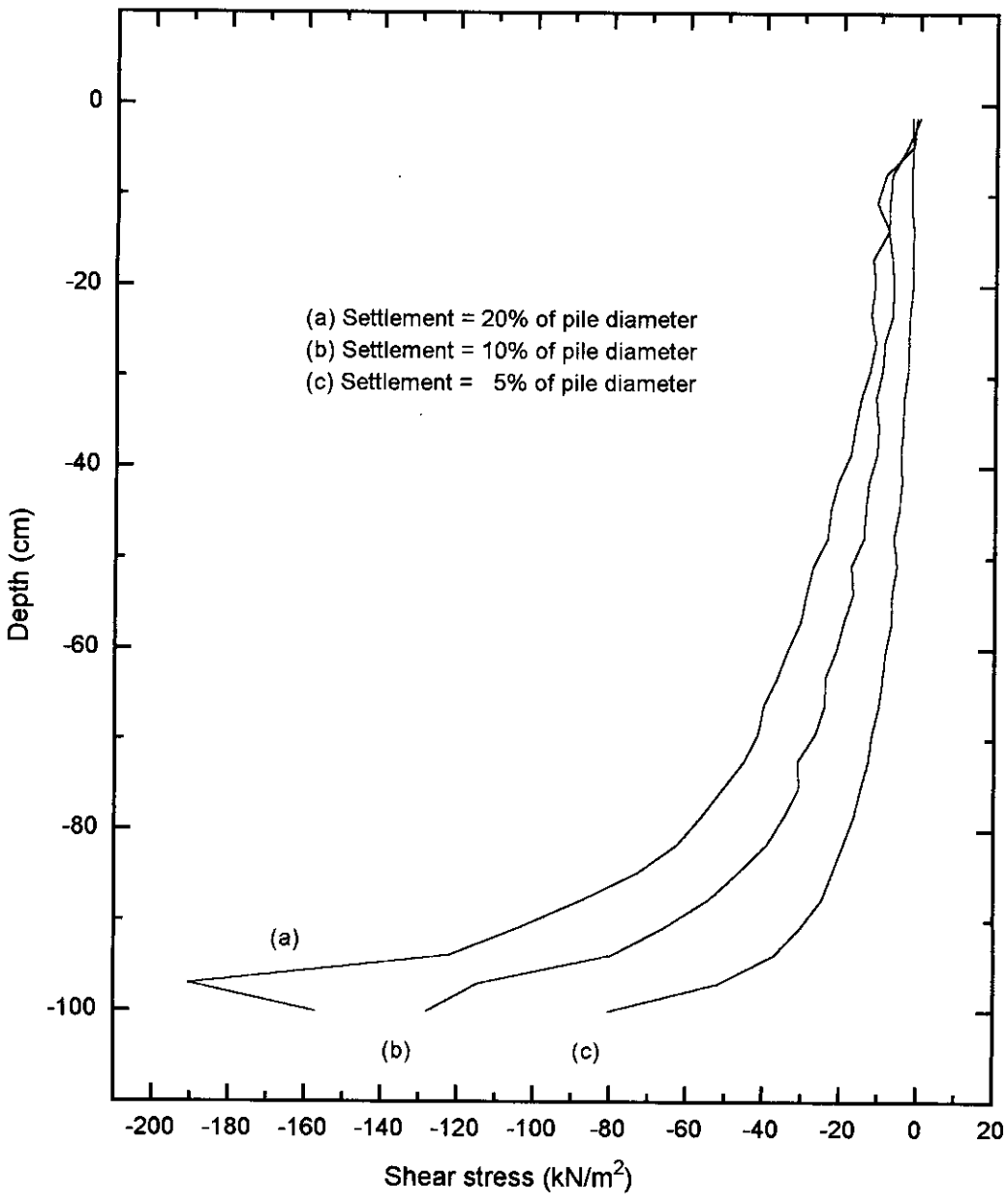

Figure B4.6 Shear stresses along the interface elements
(D = 203 mm, L/D = 5)

B5. VARIATION OF STRESS WITH DISTANCE FROM PILE

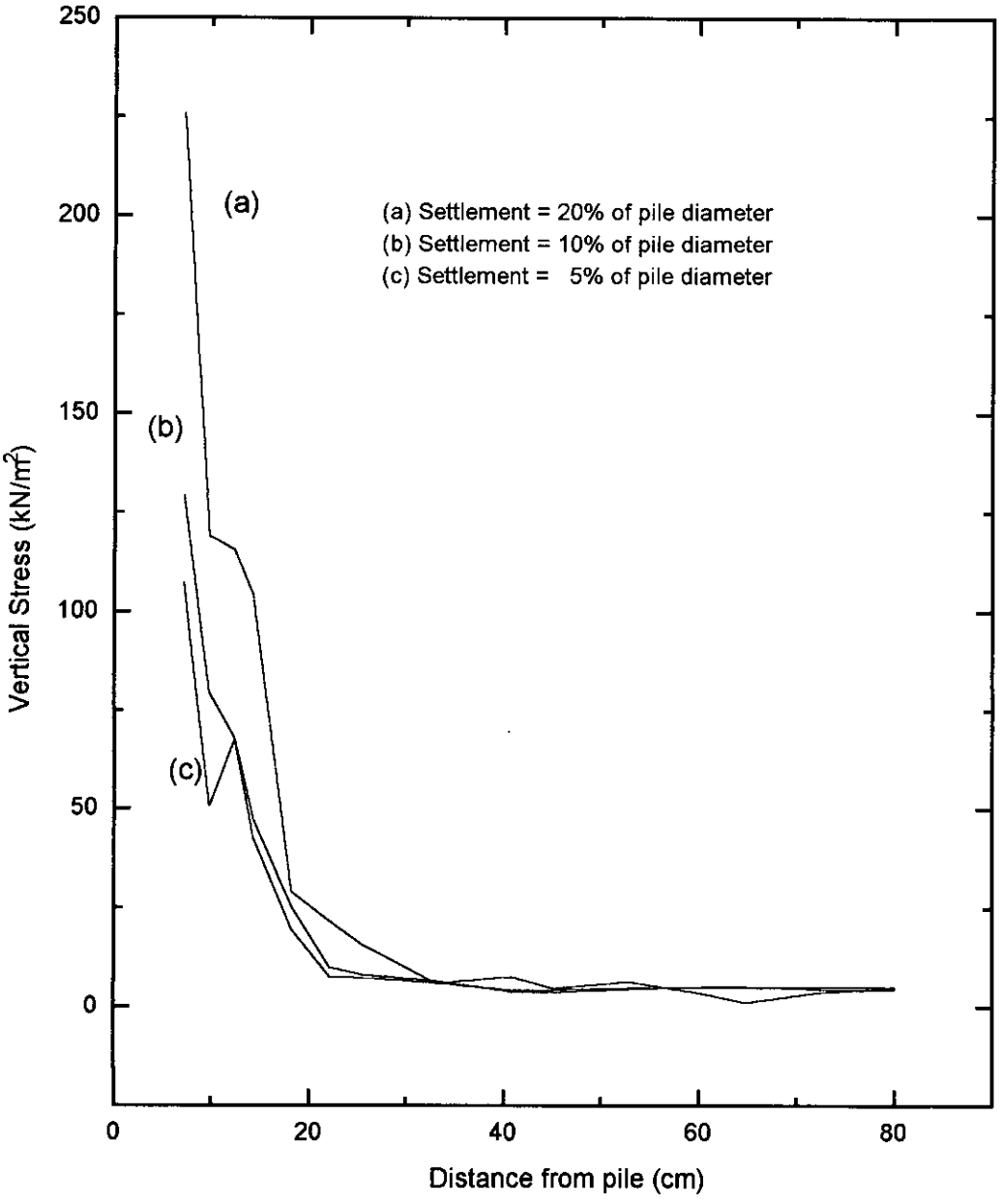

Figure B5.1 Vertical stress along outer soil of pile with distance from pile

(D = 102 mm, L/D = 5)

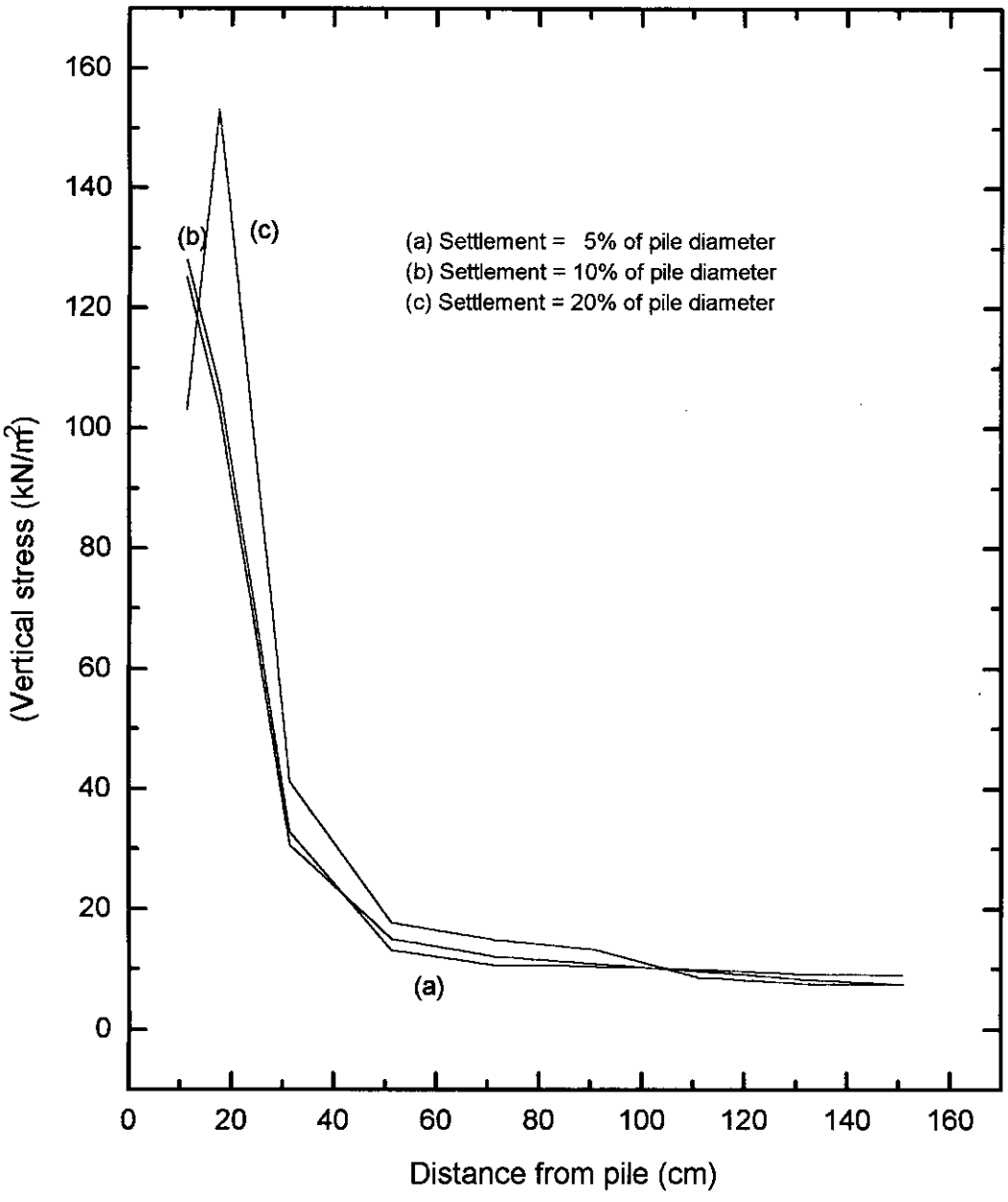

Figure B5.2 Vertical stress along outer soil of pile with distance from pile
(D = 152 mm, L/D = 5)

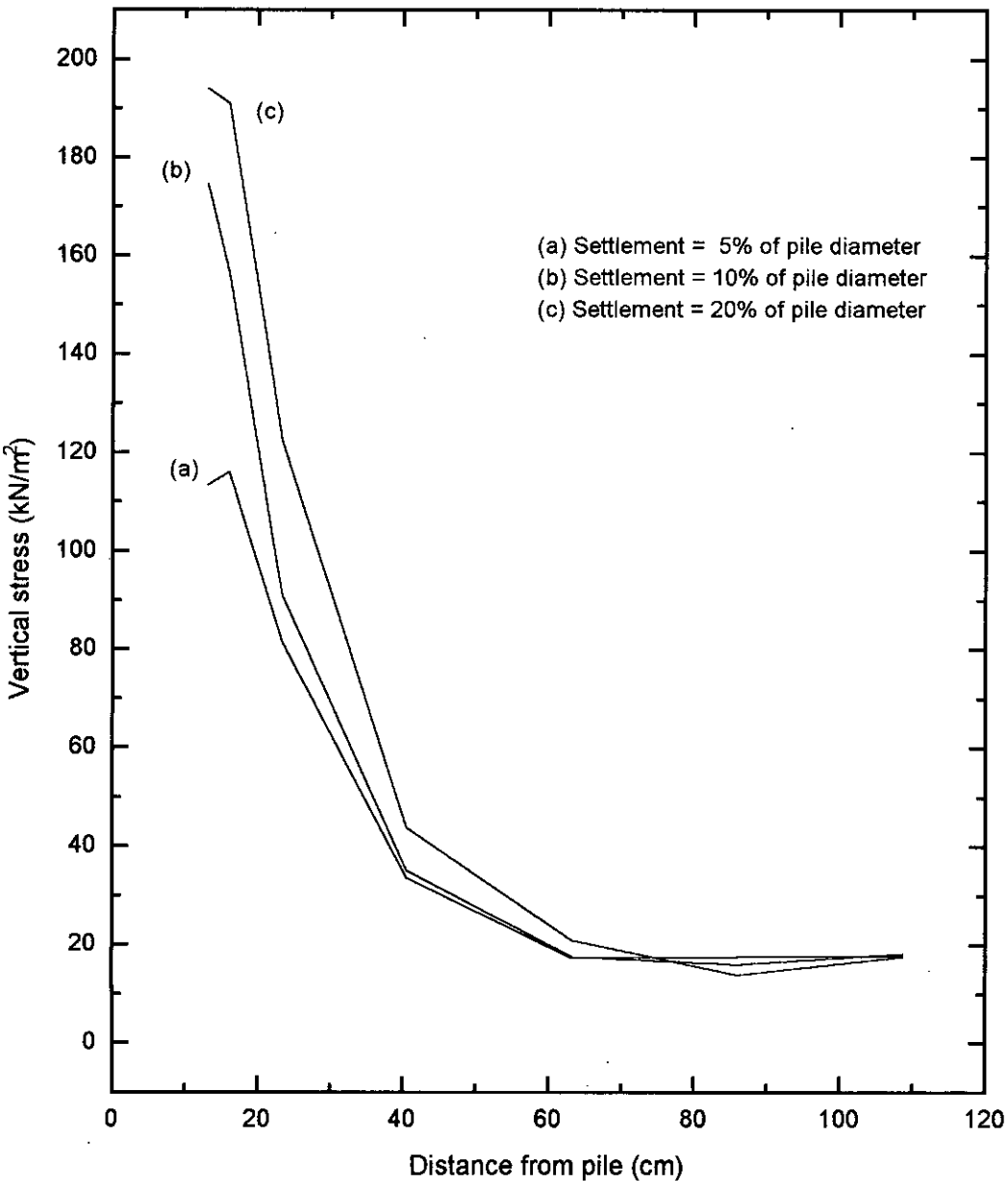

Figure B5.3 Vertical stress along outer soil of pile with distance from pile
(D = 152 mm, L/D = 10)

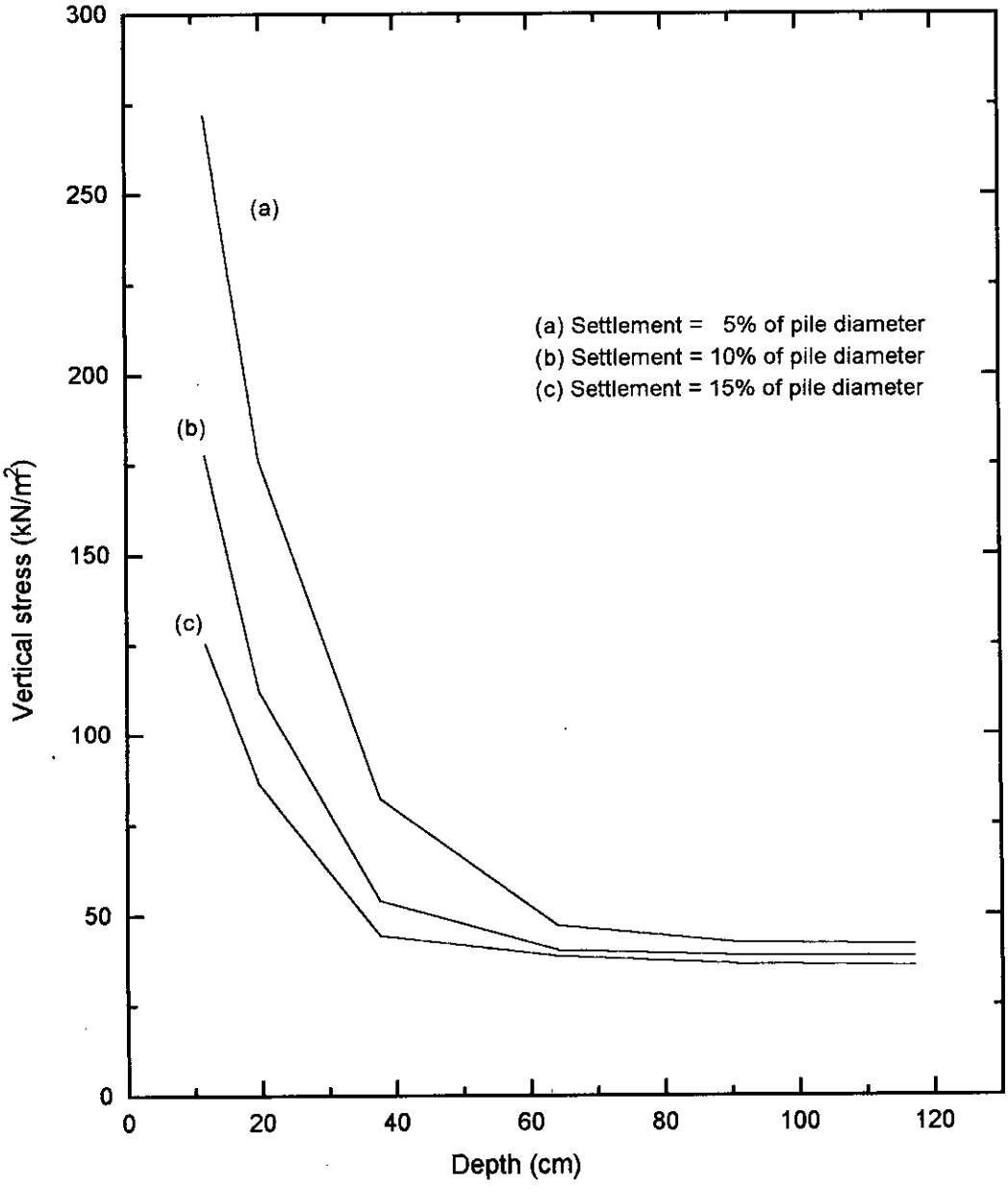

Figure B5.4 Vertical stress along outer soil of pile with distance from pile
(D = 152 mm, L/D = 15)

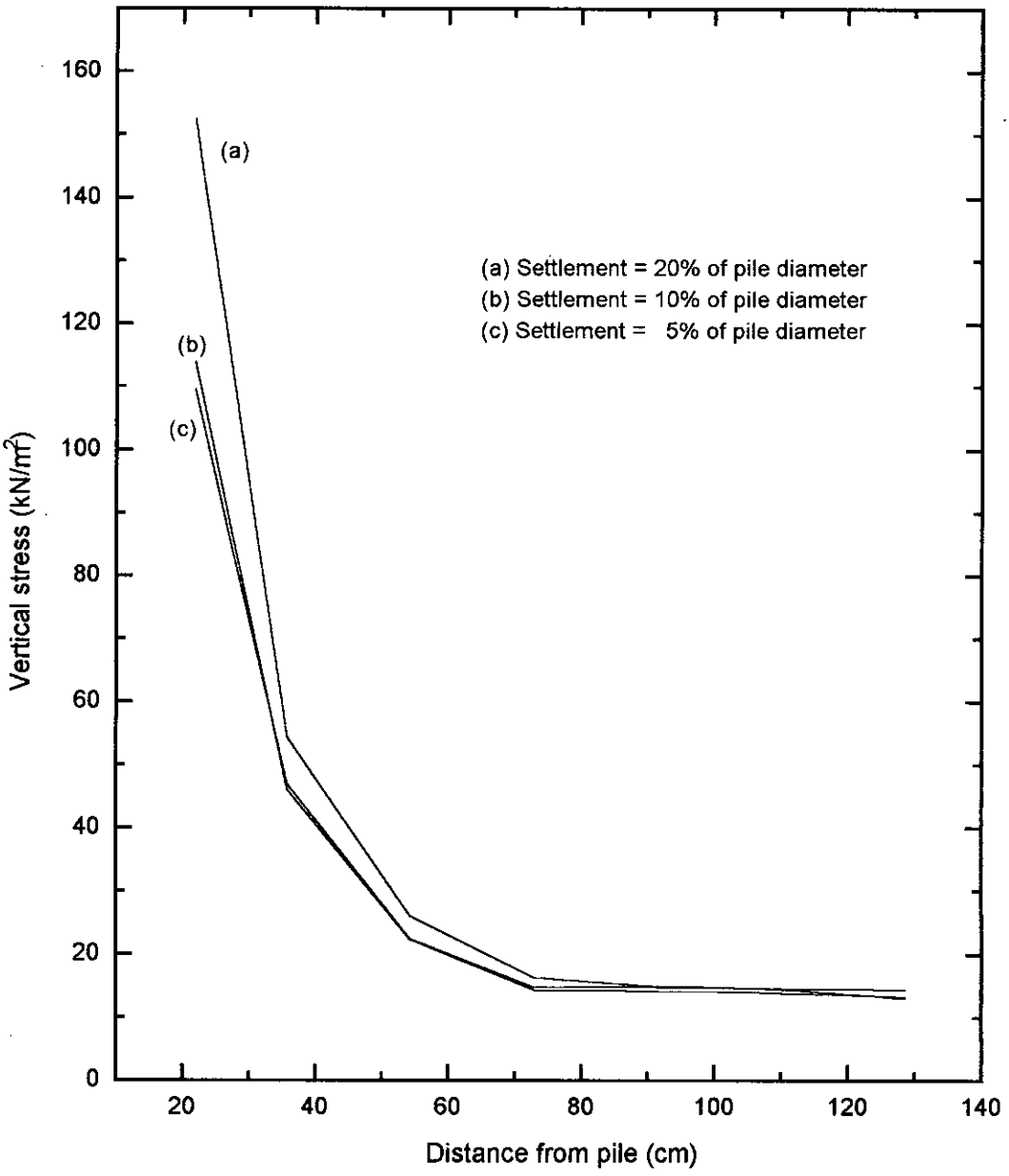

Figure B5.5 Vertical stress along outer soil of pile with distance from pile

(D = 203 mm, L/D = 5)

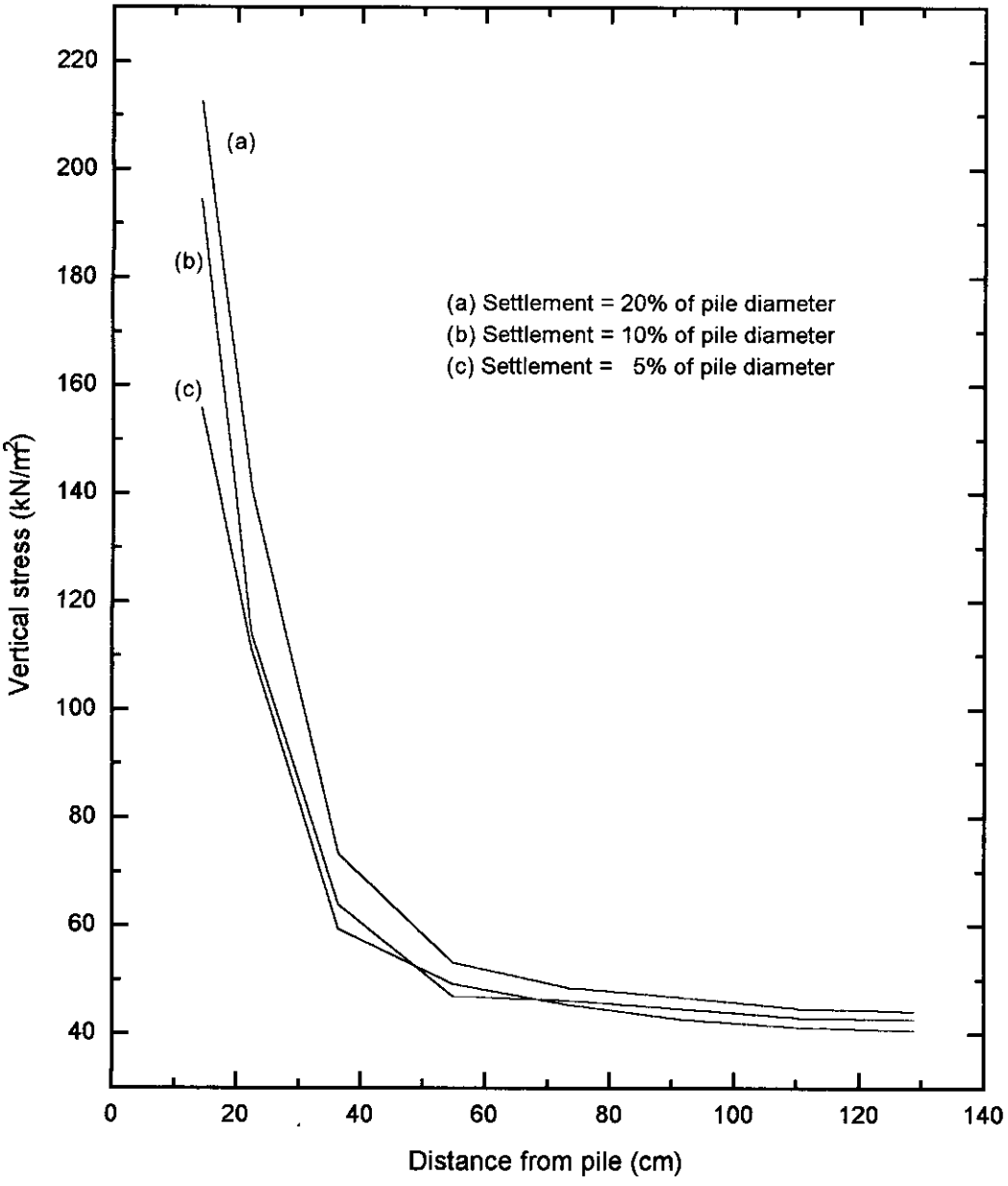

Figure B5.6 Vertical stress along outer soil of pile with distance from pile

(D = 203 mm, L/D = 10)

APPENDIX C

FINITE ELEMENT MESHES

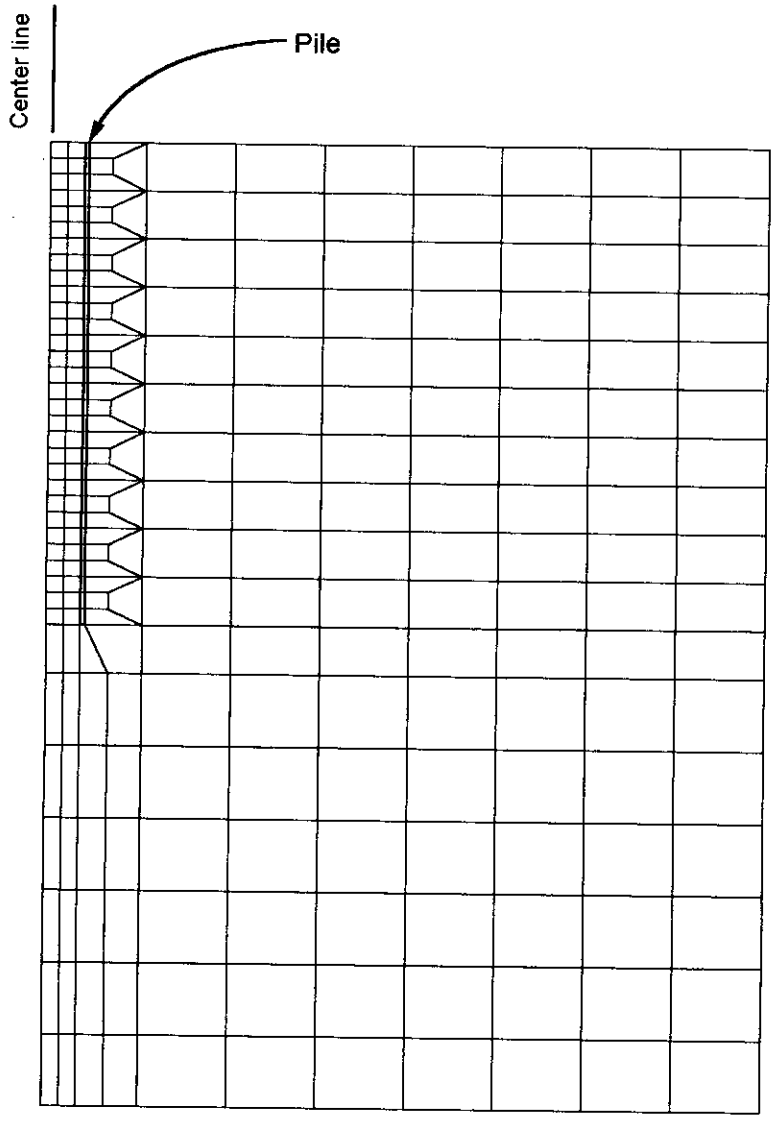

Figure C1 Finite element mesh (Diameter = 152 mm, Depth = 76.2 cm)

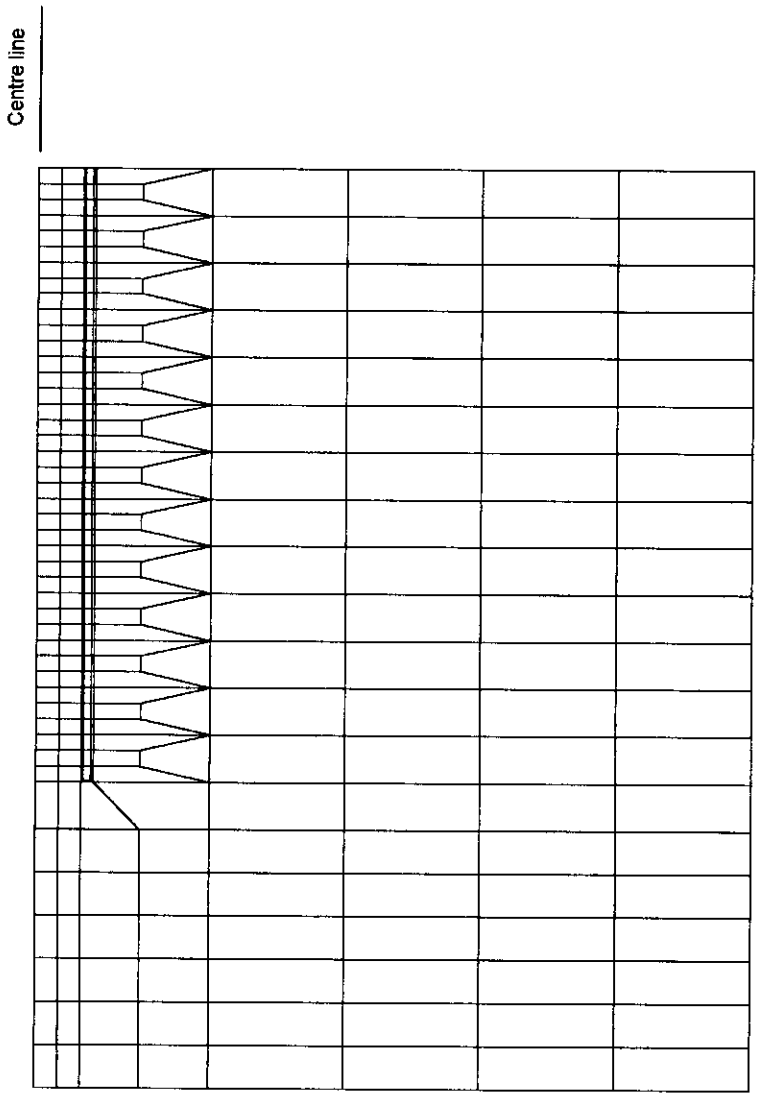

Figure C2 Finite element mesh (Diameter = 152 mm, Depth = 152.4 cm)

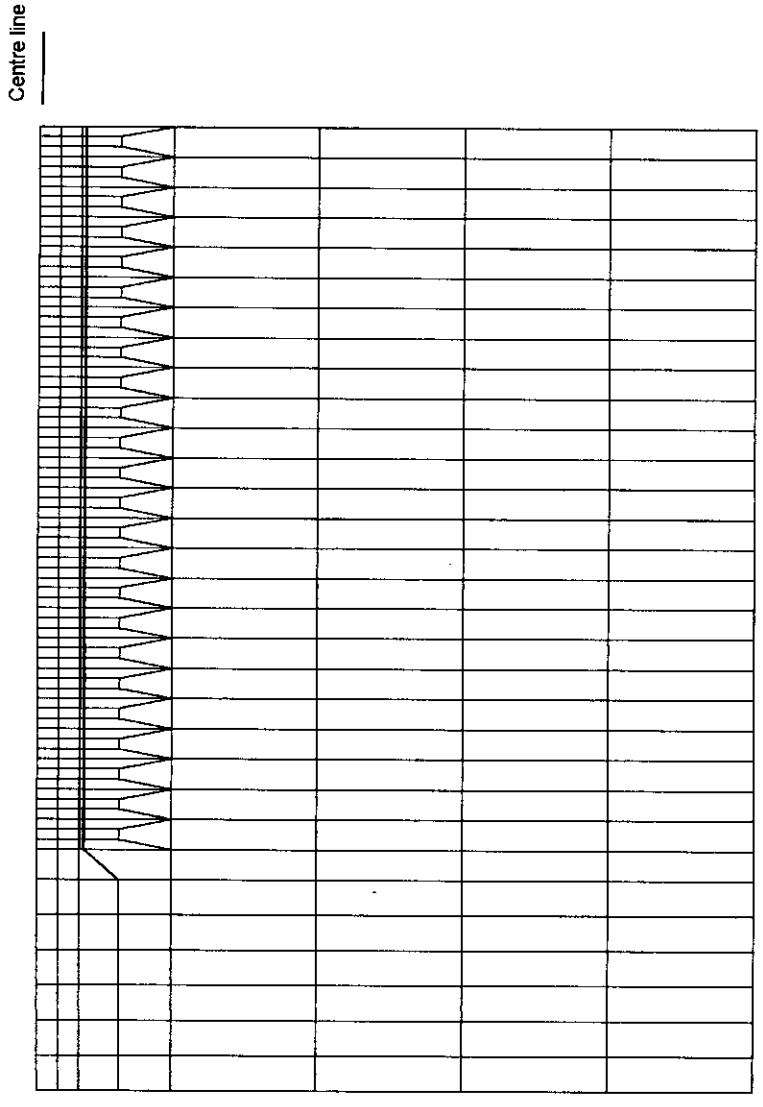

Figure C3 Finite element mesh (Diameter = 152 mm, Depth = 228.6 cm)

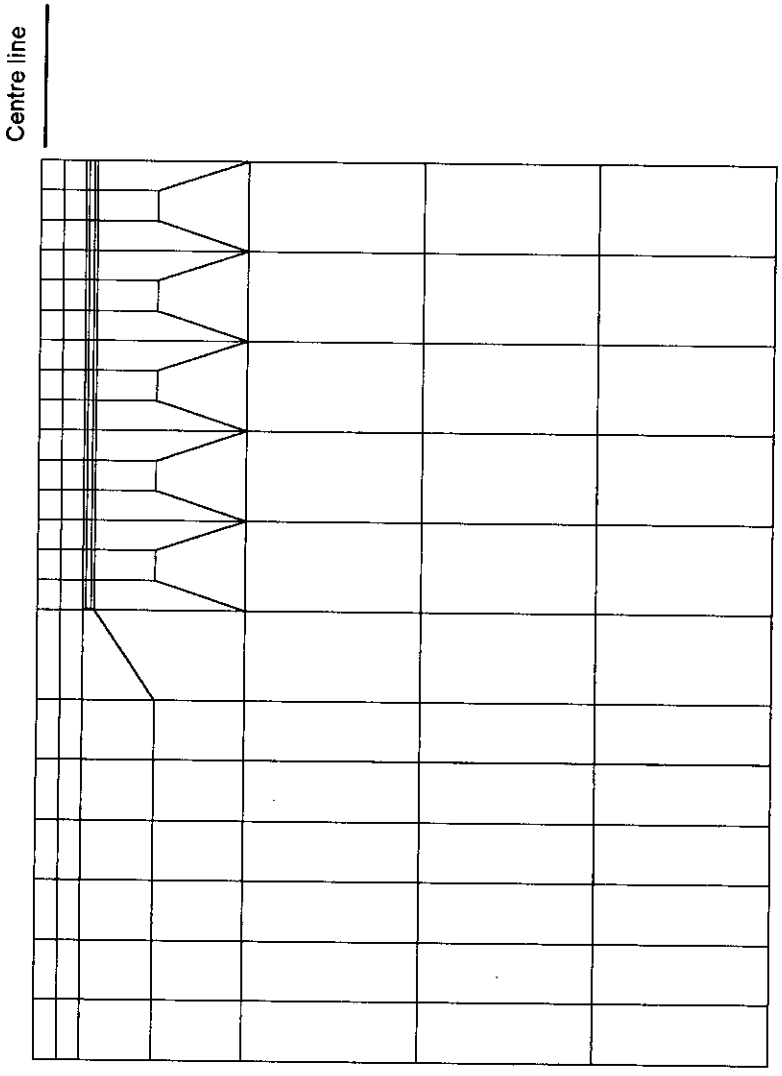

Figure C4 Finite element mesh (Diameter = 102 mm, Depth = 50.8 cm)

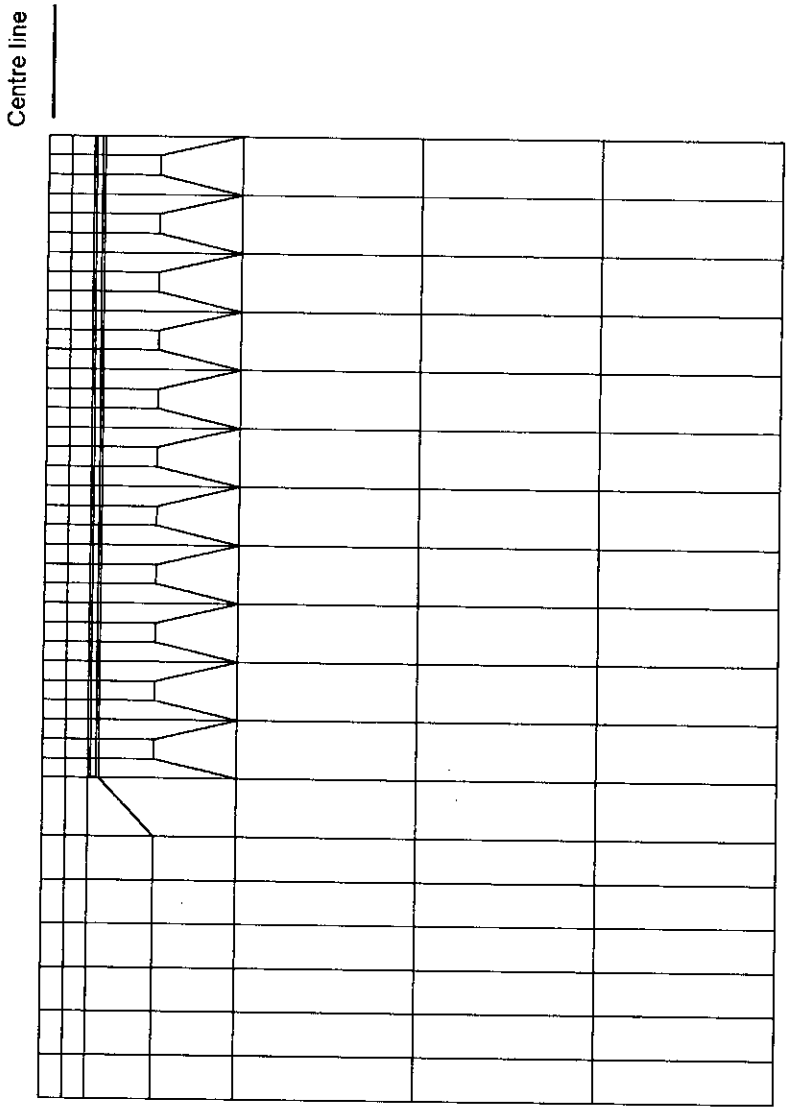

Figure C5 Finite element mesh (Diameter = 102 mm, Depth = 101.6 cm)

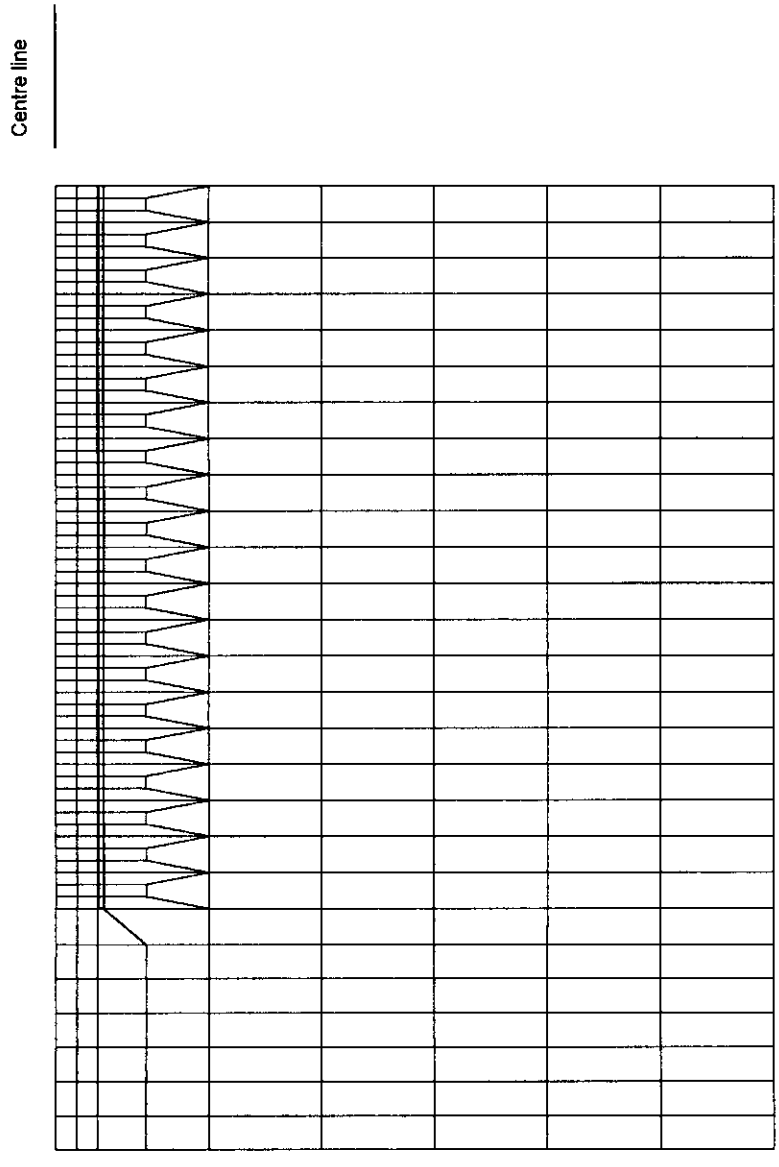

Figure C6 Finite element mesh (Diameter = 102 mm, Depth = 152.4 cm)

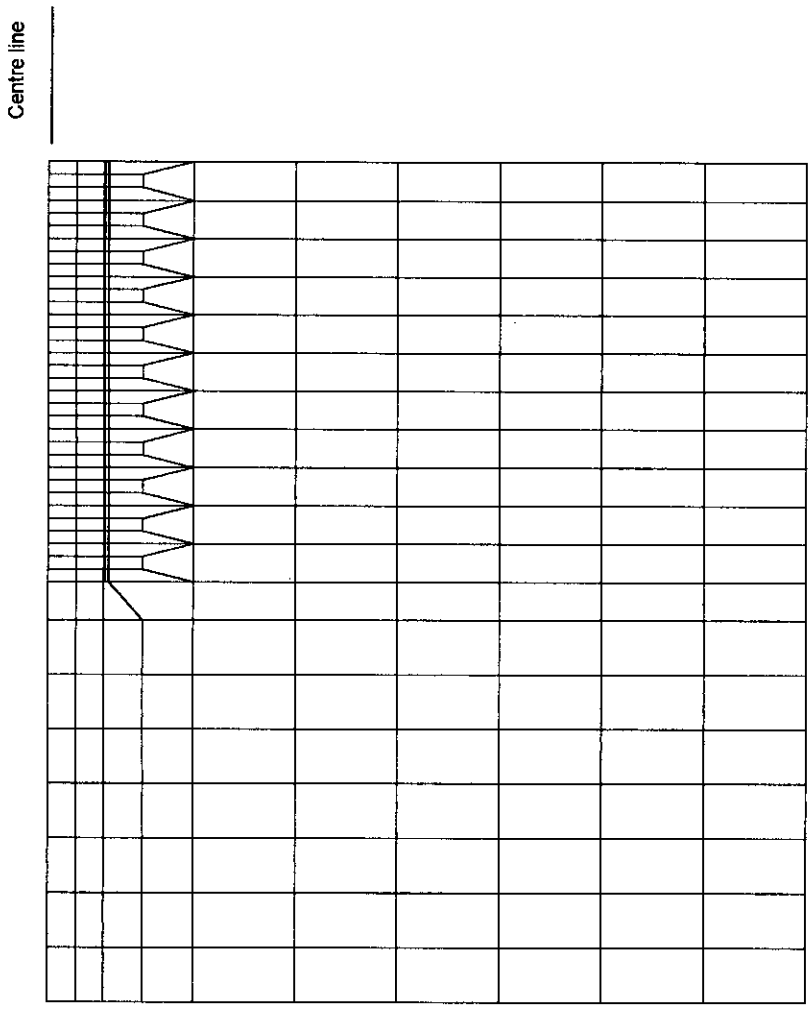

Figure C7 Finite element mesh (Diameter = 203 mm, Depth = 101.6 cm)

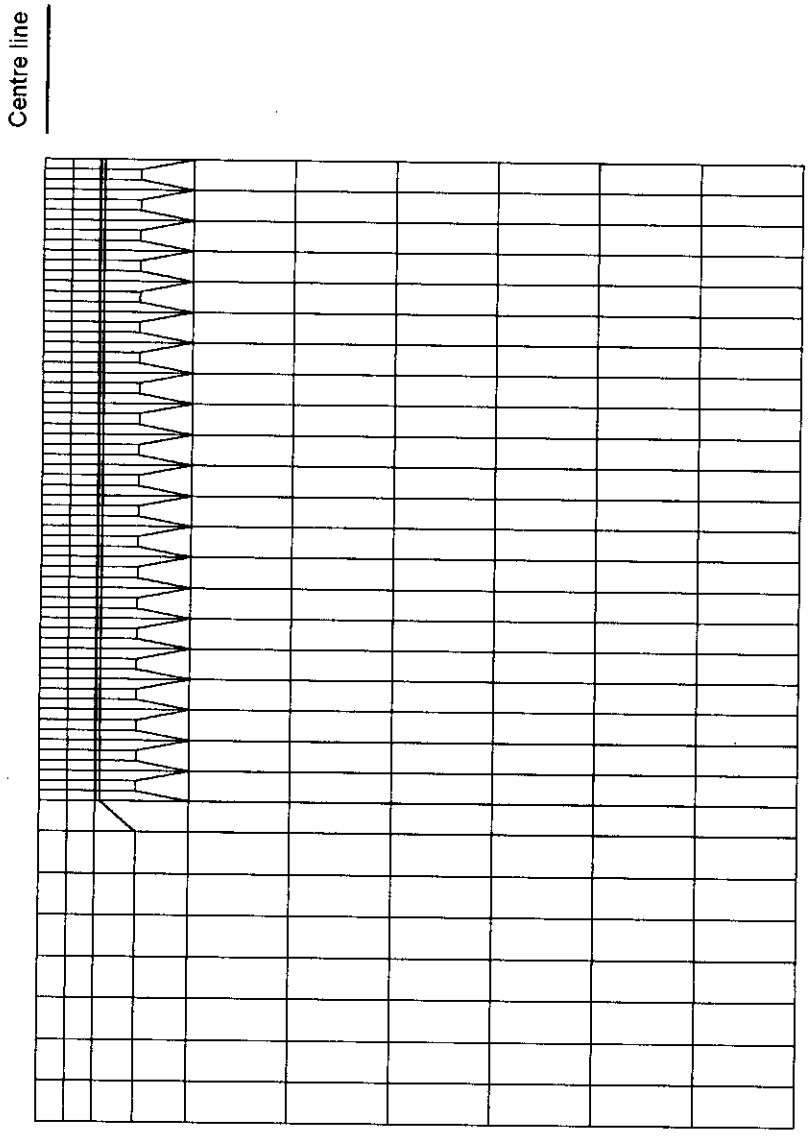

Figure C8 Finite element mesh (Diameter = 203 mm, Depth = 203.2 cm)

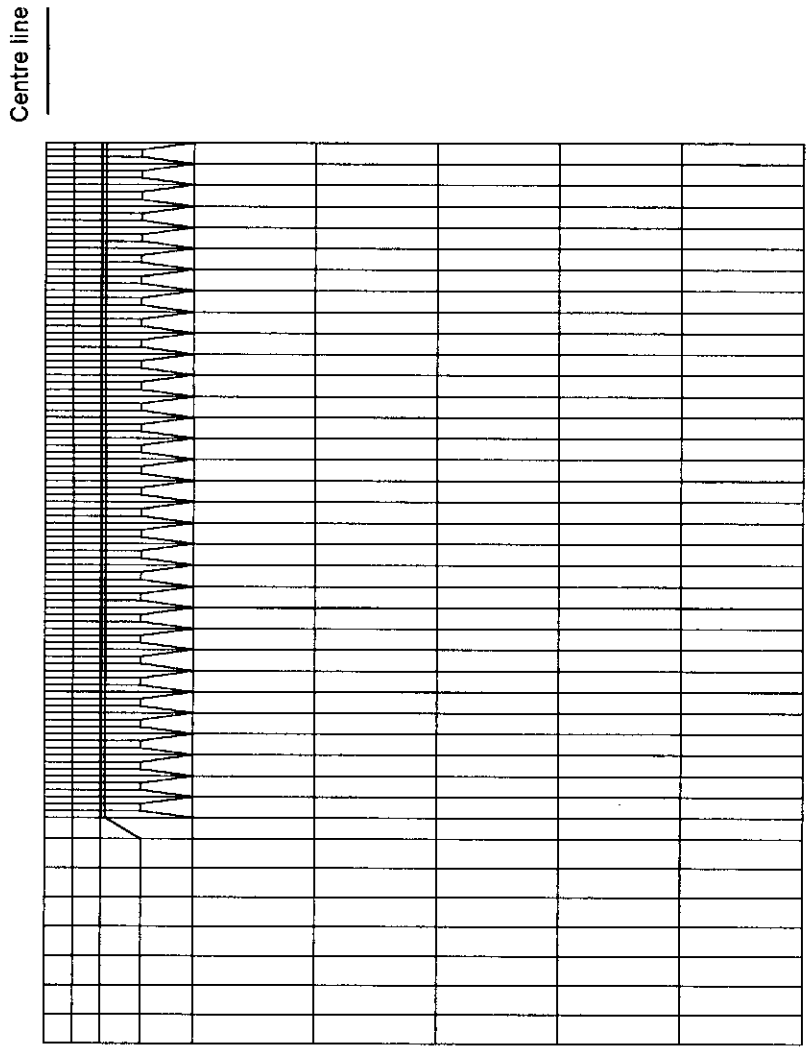

Figure C9 Finite element mesh (Diameter = 203 mm, Depth = 304.8 cm)

APPENDIX D

DATA GENERATION PROGRAMME

DATA GENERATION PROGRAMME

D1. MAIN PROGRAMME: PMESH

```
C     PROGRAM TO GENERATE THE CO-ORDINATE OF THE NODES
      DIMENSION X(10000),Y(10000),NREF(10000)
      COMMON ELNOD(10000,4),NETYP(10000),MZONE(10000)
      INTEGER ELNOD,NETYP,MZONE
      CHARACTER OP*1
      OPEN(3,FILE='CGP.DAT',STATUS='UNKNOWN')
      OPEN(4,FILE='CMP.DAT',STATUS='UNKNOWN')
      OPEN(5,FILE='FMESH.DAT',STATUS='UNKNOWN')
      PRINT*,'PILE RADIUS=?, OUTER EXTEND=?, DEPTH BELOW PILE=?'
      READ*,PR,XEX,HB
      PRINT*,'PILE LENGTH=?,PILE THICKNESS=?,INTERFACE THICK  CALCULATED'
      READ*,PL,TP
      PRINT*,'INTERNAL SOIL FULL OR NOT? Y/N'
      READ(*,81)OP
 81   FORMAT(A1)
      PRINT*,'COMMENT:  ??????'
      PRINT*,'VERTICAL DIVISION INDICATE PLUG DEPTH AS 3*PILE THICKNESS'
      PRINT*,'FOR INNER SOIL,HORIZONTAL DIV=?, VERTICAL DIV=?'
      READ*,INHD,INVD
C     TI=0.1*3*TP
      XI=PR/FLOAT(INHD)
      NP=NINT(PL/(3*5*TP))*3
      PRINT*,'NUMBER OF PILE DIVISION=', NP
      AL=PL/FLOAT(NP)
      TI=0.05*AL
      IF(OP.EQ.'Y')INVD=NP
      INVRDV=INVD+1
      INHRDV=INHD+1
C     INNER SOIL CO-ORDINATES
      II=0
      DO 22 I=1,INHRDV
      DO 22 J=1,INVRDV
      II=II+1
      X(II)=(I-1)*XI
      Y(II)=HB+(J-1)*AL
C     WRITE(5,50)X(II),Y(II)
C     WRITE(3,23)II,X(II),Y(II)
 22   CONTINUE
C
C     PILE ELEMENT CO-ORDINATES INCLUDING INTERFACE
      XT=PR+TI
      DO 14 I=1,2
      NP1=NP+1
      DO 14 J=1,NP1
      II=II+1
      X(II)=XT+(I-1)*TP
      Y(II)=HB+(J-1)*AL
```

```
      IF(J.EQ.1)Y(II)=HB+0.1*(TP+2*TI)
C     WRITE(5,50)X(II),Y(II)
C     WRITE(3,23)II,X(II),Y(II)
14    CONTINUE
      DO 15 J=1,NP1
      II=II+1
      X(II)=XT+TP+TI
      Y(II)=HB+(J-1)*AL

C     WRITE(5,50)X(II),Y(II)
C     WRITE(3,23)II,X(II),Y(II)
15    CONTINUE
C
C     CO-ORDINATE OF THE COMPLEX ZONE
      NC=NP/3*2
      XC=X(II)
      NCC=NC/2
C     DECIDE FOR SMALL ELEMENT, LENTH=2 OR 3*AL AND CORRECT NS
      NS=2
      DO 16 J=1,NCC
      II=II+1
      X(II)=XC+NS*AL
      YC=(3*J-2)*AL
      Y(II)=HB+YC
C     WRITE(5,50)X(II),Y(II)
C     WRITE(3,23)II,X(II),Y(II)
      II=II+1
      X(II)=XC+NS*AL
      Y(II)=HB+YC+AL
C     WRITE(5,50)X(II),Y(II)
C     WRITE(3,23)II,X(II),Y(II)
16    CONTINUE
C
C     CO-ORDINATE OF THE EXTERNAL SOIL MASS
C     DECIDE FOR LARGE ELEMENT, LENGTH=5 OR 6*AL AND CORRECT NL
      NL=5
      XC=X(II)+(NL-NS)*AL
17    PRINT*,'DIVISION OF THE EXTERNAL PORTION OF COMPLEX ZONE=?'
      READ*,NEX
      XE=(XEX-TI-NL*AL)/FLOAT(NEX)
      IF(XE.GT.(9*AL))GOTO 17
      NE1=NEX+1
      NC2=NCC+1
      DO 18 I=1,NE1
      DO 18 J=1,NC2
      II=II+1
      X(II)=XC+(I-1)*XE
      Y(II)=HB+(J-1)*3*AL
C     WRITE(5,50)X(II),Y(II)
C     WRITE(3,23)II,X(II),Y(II)
18    CONTINUE
      NLAST=II
```

```
      PRINT*,'NLAST=',NLAST
C
C     CO-ORDINATE OF THE SOIL MASS BELOW THE PILE
C     DECIDE DEPTH OF THE BELOW COMPLEX ZONE 3 OR 4*AL AND CORRECT NBE
      NBE=3
      HB1=HB-NBE*AL
19    PRINT*,'VERTICAL DIVISION OF DEPTH BELOW REF=?'
      READ*,NBD
      YC=HB1/FLOAT(NBD)
      IF(YC.GT.(3*XI))GOTO 19
      NTR=INHRDV+2+NEX
      NBD1=NBD+1
      XR2=0
      DO 20 I=1,NTR
      DO 21 J=1,NBD1
      II=II+1
      IF(I.LE.(INHD))XCH=XI
      IF(I.EQ.(INHD+1))XCH=2*TI+TP+NS*AL
      IF(I.EQ.(INHD+2))XCH=(NL-NS)*AL
      IF(I.GT.(INHD+2))XCH=XE
      X(II)=XR2
      Y(II)=HB1-(J-1)*YC
C     WRITE(5,50)X(II),Y(II)
C     WRITE(3,23)II,X(II),Y(II)
21    CONTINUE
      XR2=XR2+XCH
20    CONTINUE
      NVTX=II
C
C     TO FIND THE NODE OF THE REFERENCE LINE
      J=1
      DO 28 I=1,II
      IF(Y(I).NE.HB)GOTO 28
      NREF(J)=I
      J=J+1
28    CONTINUE
      CALL CONN1(INVD,INHD,NP,NEL,NEX)
      CALL CONN2(NEL,NBD,NLAST,INHD,NEX,NREF)
      WRITE(3,54)NVTX,NEL
54    FORMAT(/I5,I5,1X,'4',1X,'4',1X,'2',1X,'4')
      WRITE(3,53)
53    FORMAT(2(/))
      DO 60 I=1,NEL
      WRITE(5,51)(ELNOD(I,K),K=1,4)
51    FORMAT(4(1X,I5))
60    CONTINUE
      DO 55 I=1,NVTX
      WRITE(5,50)X(I),Y(I)
      WRITE(3,23)I,X(I),Y(I)
55    CONTINUE
      DO 56 I=1,NEL
      WRITE(3,26)I,NETYP(I),MZONE(I),(ELNOD(I,K),K=1,4)
```

```
26  FORMAT(I5,1X,I4,1X,I3,1X,4(1X,I5))
56  CONTINUE
    PRINT*,'THICKNESS OF THE INTERFACE ELEMENT=',TI
50  FORMAT(F6.2,1X,F6.2)
23  FORMAT(I5,F7.2,1X,F7.2)
    STOP
    END
```

D2. SUBROUTINE CONN2

```
$DEBUG
      SUBROUTINE CONN2(NEL,NBD,NLAST,INHD,NEXD,NREF)
      COMMON ELNOD(10000,4),NETYP(10000),MZONE(10000)
     DIMENSION NREF(10000)
C
      INTEGER ELNOD
C
C     CONNECTIVITY OF THE BOTTOM COMPLEX ZONE
     IVAR=1
     IFX=1
     V1=0
     V2=0
     V3=0
C      WRITE(3,27)
C 27   FORMAT(///'CONNECTIVITY FOR THE SOIL ZONE BELOW THE PILE'//)
     NTERM=INHD+2+NEXD
     DO 20 I=1,NTERM
     NEL=NEL+1
     NETYP(NEL)=4
     MZONE(NEL)=6
      ELNOD(NEL,1)=NREF(I)
      ELNOD(NEL,2)=NLAST+(I-1)*(NBD+1)+1
      ELNOD(NEL,3)=NLAST+I*(NBD+1)+1
      ELNOD(NEL,4)=NREF(I+1)
     IF(I.EQ.1)THEN
     WRITE(4,40)NEL,ELNOD(NEL,1),ELNOD(NEL,2),IVAR,IFX,V1,V3,V2
     ENDIF
     IF(I.EQ.NTERM)THEN
     WRITE(4,40)NEL,ELNOD(NEL,3),ELNOD(NEL,4),IVAR,IFX,V1,V3,V2
     ENDIF
 40   FORMAT(1X,I5,1X,2(I5,1X),2(I2),3(F3.1))
C      WRITE(5,51)(ELNOD(NEL,J),J=1,4)
C 51   FORMAT(4(I4))
C      WRITE(3,26)NEL,NETYP(NEL),MZONE(NEL),(ELNOD(NEL,J),J=1,4)
C 26   FORMAT(I3,I4,I3,4(I4))
 20   CONTINUE
C  CONNECTIVITY FOR THE SOIL ZONE BELOW THE BOTTOM COMPLEX ZONE
     NT=NTERM
     DO 25 I=1,NT
     ISTART=NLAST+(I-1)*(NBD+1)
     DO 25 J=1,NBD
     NEL=NEL+1
     NETYP(NEL)=4
     MZONE(NEL)=6
     ELNOD(NEL,1)=ISTART+J
     ELNOD(NEL,2)=ELNOD(NEL,1)+1
     ELNOD(NEL,3)=ELNOD(NEL,2)+NBD+1
     ELNOD(NEL,4)=ELNOD(NEL,3)-1
     IF(I.EQ.1)THEN
     WRITE(4,40)NEL,ELNOD(NEL,1),ELNOD(NEL,2),IVAR,IFX,V1,V3,V2
```

```
      ENDIF
      IF(I.EQ.NT)THEN
      IVAR=1
      WRITE(4,40)NEL,ELNOD(NEL,3),ELNOD(NEL,4),IVAR,IFX,V1,V3,V2
      ENDIF
      IF(J.EQ.NBD)THEN
      IVAR=2
      WRITE(4,40)NEL,ELNOD(NEL,2),ELNOD(NEL,3),IVAR,IFX,V1,V3,V2
      ENDIF
C     WRITE(5,51)(ELNOD(NEL,K),K=1,4)
C     WRITE(3,26)NEL,NETYP(NEL),MZONE(NEL),(ELNOD(NEL,K),K=1,4)
25    CONTINUE
      RETURN
      END
```

D3. SUBROUTINE CONN1

```
$DEBUG
      SUBROUTINE CONN1(INVD,INHD,NP,NEL,NEXD)
      COMMON ELNOD(10000,4),NETYP(10000),MZONE(10000)
C     CONNECTIVITY FOR THE INNER SOIL MASS
C
      INTEGER ELNOD,NETYP,MZONE
      IVAR=1
      IFX=1
      V1=0
      V2=0
      V3=0
      WRITE(4,41)
 41   FORMAT(8(/))
C     WRITE(3,31)
C 31  FORMAT(///'CONNECTIVITY OF THE UPPER SOIL ZONE'/'NE  NTYP  CON'//)
      NEL=0
      INVRDV=INVD+1
      INHRDV=INHD+1
      DO 10 I=1,INHRDV
      ISTART=(I-1)*(INVD+1)
      DO 10 J=1,INVD
      NEL=NEL+1
      ELNOD(NEL,1)=ISTART+J
      ELNOD(NEL,2)=ISTART+(INVD+1)+J
      ELNOD(NEL,3)=ELNOD(NEL,2)+1
      ELNOD(NEL,4)=ELNOD(NEL,1)+1
      IF(I.LT.INHRDV)THEN
       NETYP(NEL)=4
       MZONE(NEL)=1
      ELSE
       ELNOD(NEL,2)=ISTART+J
       ELNOD(NEL,3)=ISTART+(INVD+1)+J
       ELNOD(NEL,4)=ELNOD(NEL,3)+1
       ELNOD(NEL,1)=ELNOD(NEL,2)+1
       NETYP(NEL)=13
       MZONE(NEL)=2
      ENDIF
      IF(I.EQ.1)THEN
      WRITE(4,40)NEL,ELNOD(NEL,1),ELNOD(NEL,4),IVAR,IFX,V1,V3,V2
 40   FORMAT(1X,I5,1X,2(I5,1X),2(I2),3(F3.1))
      ENDIF
C     WRITE(5,51)(ELNOD(NEL,K),K=1,4)
C     WRITE(3,26)NEL,NETYP(NEL),MZONE(NEL),(ELNOD(NEL,K),K=1,4)
 10   CONTINUE
      NEL=NEL+1
      ELNOD(NEL,1)=INHD*INVRDV+1
      ELNOD(NEL,2)=ELNOD(NEL,1)+INVD+2*(NP+1)+1
      ELNOD(NEL,3)=ELNOD(NEL,2)-NP-1
      ELNOD(NEL,4)=ELNOD(NEL,3)-NP-1
```

```
      NETYP(NEL)=13
      MZONE(NEL)=2
C
C  CONNECTIVITY FOR THE PILE ZONE
      DO 11 I=1,2
      ISTART=INHRDV*INVRDV+(I-1)*(NP+1)
      DO 11 J=1,NP,1
      NEL=NEL+1
      ELNOD(NEL,1)=ISTART+J
      ELNOD(NEL,2)=ISTART+NP+1+J
      ELNOD(NEL,3)=ELNOD(NEL,2)+1
      ELNOD(NEL,4)=ELNOD(NEL,1)+1
      IF(I.EQ.1)THEN
       NETYP(NEL)=4
       MZONE(NEL)=3
      ELSE
       ELNOD(NEL,2)=ISTART+J
       ELNOD(NEL,3)=ISTART+NP+1+J
       ELNOD(NEL,4)=ELNOD(NEL,3)+1
       ELNOD(NEL,1)=ELNOD(NEL,2)+1
       NETYP(NEL)=13
       MZONE(NEL)=4
      ENDIF
C      WRITE(5,51)(ELNOD(NEL,K),K=1,4)
C      WRITE(3,26)NEL,NETYP(NEL),MZONE(NEL),(ELNOD(NEL,K),K=1,4)
 11   CONTINUE
C
C  CONNECTIVITY FOR THE COMPLEX ZONES
      IONE=INHRDV*INVRDV+2*(NP+1)-2
      IFIVE=(IONE+2)+(NP+1)-1
      ISEVEN=(IFIVE+1)+(NP/3)*2
      NC=NP/3
      DO 12 I=1,NC
      IONE=IONE+3
      IFIVE=IFIVE+2
      ISEVEN=ISEVEN+1
 12   CALL UNIT(IONE,IFIVE,ISEVEN,NEL)
C  CONNECTIVITY OF THE OUTER ZONE
      NC=NP/3
      DO 13 I=1,NEXD
      ISTART=INHRDV*INVRDV+(NP+1)*3+NC*2+(I-1)*(NC+1)
      DO 13 J=1,NC
      NEL=NEL+1
      ELNOD(NEL,1)=ISTART+J
      ELNOD(NEL,2)=ISTART+NC+1+J
      ELNOD(NEL,3)=ELNOD(NEL,2)+1
      ELNOD(NEL,4)=ELNOD(NEL,1)+1
      NETYP(NEL)=4
      MZONE(NEL)=5
      IF(I.EQ.NEXD)THEN
      WRITE(4,40)NEL,ELNOD(NEL,2),ELNOD(NEL,3),IVAR,IFX,V1,V3,V2
      ENDIF
```

```
C     WRITE(5,51)(ELNOD(NEL,K),K=1,4)
C 51  FORMAT(4(I4))
C     WRITE(3,26)NEL,NETYP(NEL),MZONE(NEL),(ELNOD(NEL,K),K=1,4)
C 26  FORMAT(I3,I4,I3,4(I4))
 13   CONTINUE
      RETURN
      END
```

D4 SUBROUTINE UNIT

```
      SUBROUTINE UNIT(IONE,IFIVE,ISEVEN,NEL)
      COMMON ELNOD(10000,4),NETYP(10000),MZONE(10000)
      INTEGER ELNOD,NETYP,MZONE
      NEL=NEL+1
      ELNOD(NEL,1)=IONE
      ELNOD(NEL,2)=ISEVEN
      ELNOD(NEL,3)=IFIVE
      ELNOD(NEL,4)=IONE+1
      NETYP(NEL)=4
      MZONE(NEL)=5
C     WRITE(5,51)(ELNOD(NEL,J),J=1,4)
C 51  FORMAT(4(I4))
C     WRITE(3,26)NEL,NETYP(NEL),MZONE(NEL),(ELNOD(NEL,K),K=1,4)
C 26  FORMAT(I3,I4,I3,4(I4))
      NEL=NEL+1
      ELNOD(NEL,1)=IONE+1
      ELNOD(NEL,2)=IFIVE
      ELNOD(NEL,3)=IFIVE+1
      ELNOD(NEL,4)=IONE+2
      NETYP(NEL)=4
      MZONE(NEL)=5
C     WRITE(5,51)(ELNOD(NEL,J),J=1,4)
C     WRITE(3,26)NEL,NETYP(NEL),MZONE(NEL),(ELNOD(NEL,K),K=1,4)
      NEL=NEL+1
      ELNOD(NEL,1)=IFIVE
      ELNOD(NEL,2)=ISEVEN
      ELNOD(NEL,3)=ISEVEN+1
      ELNOD(NEL,4)=IFIVE+1
      NETYP(NEL)=4
      MZONE(NEL)=5
C     WRITE(5,51)(ELNOD(NEL,J),J=1,4)
C     WRITE(3,26)NEL,NETYP(NEL),MZONE(NEL),(ELNOD(NEL,K),K=1,4)
      NEL=NEL+1
      ELNOD(NEL,1)=IONE+2
      ELNOD(NEL,2)=IFIVE+1
      ELNOD(NEL,3)=ISEVEN+1
      ELNOD(NEL,4)=IONE+3
      NETYP(NEL)=4
      MZONE(NEL)=5
C     WRITE(5,51)(ELNOD(NEL,J),J=1,4)
C     WRITE(3,26)NEL,NETYP(NEL),MZONE(NEL),(ELNOD(NEL,K),K=1,4)
      RETURN
      END
```

APPENDIX E

FEATURES OF THE PROGRAMME USED

FEATURES OF THE PROGRAMME USED

E.1 Introduction

The finite element method was introduced during the 1950s as a computer based technique for the stress analysis of continuous structures. During the 1960s the method was extended to non-structural problems. The finite element method has grown to be the most popular technique for predicting the behaviour of deformable bodies in different branches of engineering. Its popularity is mostly due to the fact that it is available to engineers as general-purpose computer programme.

A finite element programme CRISP (Britto & Gunn) was used in the study of pipe pile problem. CRISP was developed over a number of years by research workers in the Cambridge University Engineering Department Soil Mechanics Group, starting in 1975. Since 1977 A.M.Britto and M.J. Gunn have been responsible for the publication of documentation of the programme. The programme used was modified in 1990 by them.

The CRISP (CRItical State Programme) is an approximately 8000 line FORTRAN computer programme. The programme uses the finite element technique and allows prediction to be made of ground deformations using critical state theories. It is possible to predict the development of deformations with time due to consolidation by using this program.

Salient features of CRISP along with some relevant new features (Bari, 1996) are discussed in the following sections.

E.2 General Features

The critical state program, CRISP can tackle any size of problem depending on the amount of memory and processing power of the computer concerned. It contains facilities to analyse several soil-structure interaction problem provided realistic soil parameters are available. A brief summary of facilities provided by CRISP are as below:

a) *Types of analysis*:

Undrained, drained or fully coupled consolidation analysis of two dimensional plain strain or axisymmetric (with axisymmetric loading) or three dimensional bodies.

b) *Soil models*:

Isotropic and anisotropy elasticity, inhomogeneous elasticity (properties varying with depth, critical state soil models (Cam-Clay and Modified Cam-clay), elastic perfectly plastic models (with yield criterion by von Mises, Tresca, Drucker Prager, Mohr-Coloumb), the Schofield soil model.

c) *Element types*:

In CRISP, elements incorporated are: 3-nodal bar element, linear and cubic strain triangle, linear and cubic strain quadrilateral, linear strain brick element, 3-nodded beam element and 6-nodded interface element. The program has been designed so that new element types can be added with relatively little effort. In numbering the vertex nodes and the elements in the mesh, gaps in the numbering are allowed for; this permits the user to alter some part of the mesh without having to re-number of the mesh completely. Additional nodes along element sides and any inner nodes are assigned by the program.

d) *Non-linear techniques*:

Incremental (tangent stiffness) approach is used in non-linear analysis. Options are available for updating nodal co-ordinates with progress of analysis and for integration in time, $\theta = 1$ (consolidation analysis).

e) *Boundary conditions:*

Element sides can be given prescribed incremental values of displacements or excess pore pressures. Loading applied as nodal loads or pressure loading on element sides. Automatic calculation of loads simulating excavation, or construction when elements are removed or added.

f) *Miscellaneous:*

Stop-restart facility allows analysis to be continued from a previous run. Non-linear finite element analyses tends to be a time-consuming business for both the computer and the program user. Getting the size of the load increments right, usually involves re-running the program several times and examining the computer output. So that the user does not have to continually rerun the analysis from the start each time, a stop restart facility is provided. The stop restart facility also makes possible the production of graphical displays of the result.

CRISP solves the linear simultaneous stiffness equations using the frontal solution method to minimise operations on zero terms and to use minimum computer memory for the stiffness matrix. The program is based on the model program by Irons (1970), modified for variable numbers of degrees of freedom at nodal points.

E.3 Solution Technique

In most geotechnical analysis, non-linearity arises from material behaviour. The cause of non-linear response can be identified as being either geometric non-linearity or material nonlinearity. Geometric nonlinearity arises when large deformations of the structure take place. In that case equilibrium equations based on undeformed geometry are no longer sufficiently accurate. Material non-linearity rises when the stress-strain relation for the material is non-linear. In general, non-linearity of a system may be due to geometric non-linearity, material non-linearity or both together. According to Carter (Carter et al. 1977), the linear assumptions of small strains and small displacements is usually satisfactory in the solution of geotechnical problems, and so the non-linearity mainly due to material behaviour. In CRISP, the small displacement, small strain approach is used in analyses. The program contain the option of co-ordinate updating for the case of large displacement.

There are number of techniques for analysing non-linear problems using finite element. CRISP uses the incremental or tangent stiffness approach. The user divides the total load acting into a number of small increments and the program applies each of these incremental loads in turn. During each increment the

stiffness properties appropriate for the current stress levels are used in the calculations. In contrast to this approach elasto-plastic behaviour can be simulated by using larger size of increments and by performing iterations within each increment until convergence to the non-linear load-displacement curve is obtained.

The analysis can be divided into the following steps:

i) Calculation of incremental loads
ii) Application of the boundary conditions
iii) Assembly of the stiffness matrix
iv) Solution of the equations
v) Calculation of strains and stresses
vi) Output of results

E.3.1 Incremental blocks

When a non-linear or consolidation analysis is performed using CRISP, it is necessary to divide either the loading or the time span of the analyses into numbers of increments. CRISP calculates the incremental displacements for each increment using a tangent stiffness approach, i.e. the current stiffness properties are based on the stress at the start of each increment.

Total number of increments that are necessary will vary from problem to problem. While it is desirable to use as many increments as possible to obtain accurate results, the escalating computer costs that this entails will inevitably mean that some compromise is to be made between accuracy and cost. The recommended way of reviewing the results to determine whether enough increments have been used in an analysis is to examine the value of yield ratio (YR) at each integration point. The parameter yield ratio is defined as the ratio of the yield locus size at the end of the current increment to the size at the beginning of the current increment. The ratio is printed for each integration point. Value of about 1.02 (0.98, if softening) are generally regarded as leading to sufficiently accurate calculations. If values greater than 1.05 (less than 0.95, if softening) are seen, then the size of the load increments should be reduced.

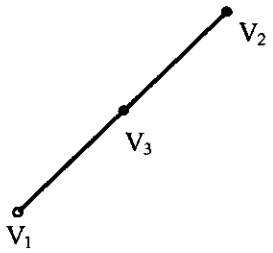

(a) 3 noded bar element

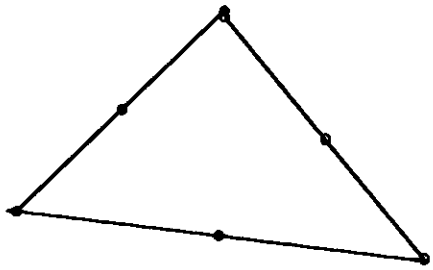

(b) 6 noded linear strain triangle

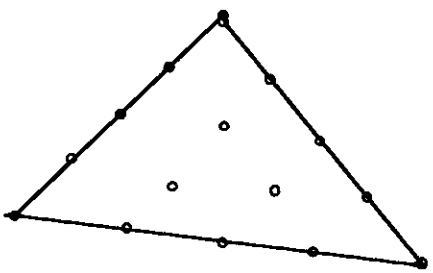

(c) 15 noded cubic strain triangle

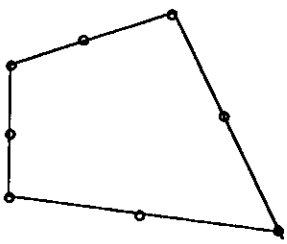

(d) Quadrilateral element

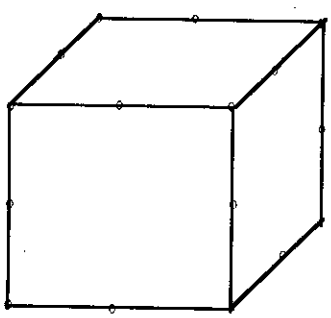

(e) 20 - noded linear strain brick element

(f) 6 - noded interface element

Figure E.1 Different finite elements used in CRISP

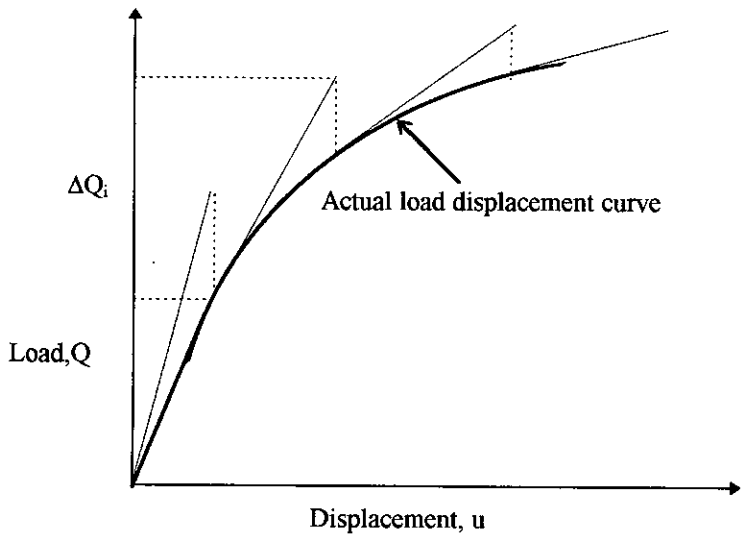

Figure E.2 Incremental and Iterative Technique

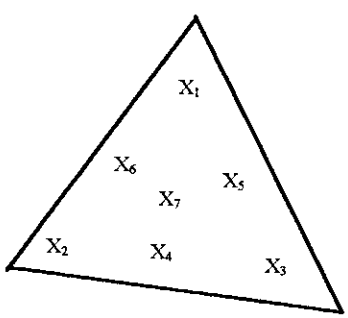

(a) Linear strain triangle

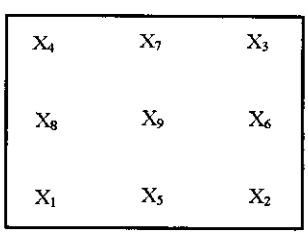

(b) 8 - noded quadrilateral

Figure E.3 Intregration Points

The analyses is sub-divided into one or more incremental blocks. Each increment block consists of one or more increments. The use of the increment block is adopted for two reasons: (a) removal of elements and additions of elements can be carried out over a number of increments and (b) with repeated application of loading increments can be grouped together as an increment block thereby reducing the amount of data input. Element stiffnesses are always added or removed in the first increment of a block, but the associated loads are distributed over all the increments in the block. Clearly this procedure introduces an extra degree of approximation in modelling, but it has been found to be satisfactory in practice.

E.3.2 Incremental stress-strain relations

In an elasto-plastic analysis the stiffness matrix of a finite element will be dependent on the stress state within the element. In general the stress state will vary across an element and the stiffness terms are calculated by integrating expressions dependent on these varying stress over the volume of each element. CRISP integrates these expressions numerically by sampling the stresses at particular points within the element and then using standard numerical integration rules for triangular areas. Options are available on whether the nodal co-ordinates are updated after each increment of the analysis. Internal loads and internal stresses may be assumed to be in equilibrium in relation to the original geometry of the finite element mesh based on small displacement assumption.

In order to perform non-linear finite element analysis using elasto-plastic models of soil behaviour, it is necessary to compute the modulus matrix D_{ep} relating an increment of strain to an increment of stress. The incremental strains are calculated as

$$\Delta\varepsilon = B\,\Delta q \qquad \text{E.1}$$

where $\Delta\varepsilon$, B and q are strain, strain-displacement matrix and nodal displacements respectively.

The cumulative strains are incremented by the incremental strains. The incremental stresses are then calculated from the incremental strains.

$$\Delta\sigma_i' = D_{ep}\Delta\varepsilon$$

$$\sigma_i' = \sigma_{i-1}' + \Delta\sigma_i' \qquad \text{E.2 (a,b)}$$

Starting from the yield function $f(\sigma, h) = 0$, and the plastic potential $g(\sigma, h) = 0$ there is a piece of standard manipulation to obtain a formula for D_{ep} (Zienkiewicz, 1977):

$$D_{ep} = \left[1 - \frac{D_E a\, a^T}{a^T D_E a - C^T H a}\right] D_E \qquad \text{E.3}$$

Where $a = \frac{\partial g}{\partial \sigma} = \frac{\partial f}{\partial \sigma}$, $C = \frac{\partial f}{\partial h}$ and H is a matrix relating changes in hardening parameters to changes in the incremental plastic strain $dh = H\, d\varepsilon^p$. Shape functions are used to calculate the co-ordinates of the integration points form the nodal co-ordinates.

$$x(\xi,\eta) = \sum_{i=1}^{N} N_i(\xi,\eta) x_i$$

$$y(\xi,\eta) = \sum_{i=1}^{N} N_i(\xi,\eta) y_i \qquad \text{E.4}$$

Depending upon the constitutive relationship being used, D matrix is calculated in different routine.

$$K = \sum_{i=1}^{n} B_i^T D_i B_i |J| W_i \qquad \text{E.5}$$

where i is the integration point.

The D matrix is independent of the stress level and therefore is a constant for a given element.

E.3.3 Solution of equations

CRISP uses the well known frontal method (Irons, 1970) to solve the assembled equations. In this method the global stiffness matrix is never fully assembled. The frontal solver in the program uses a one-dimensional array and is for the solving of symmetric stiffness matrices only. Therefore only problems of material behaviour which obey the associated flow rule can be analysed.

The frontal method begins as soon as the first element stiffness matrix has been assembled into the frontal region. The frontal region is made up of a one-dimensional array partitioned into four different regions. In this particular version it is as shown below:

Active front stiffness region	Active front loads region	Array for ill-conditioning check	Buffer
1	2	3	4

The element stiffness matrix is assembled into the appropriate locations in region 1. The elimination phase begins for all equations which are fully assembled. For these equations the corresponding variable is checked to see whether it is prescribed. The corresponding load term is also assembled into its assigned location in region 2. The coefficient of the complete equation are transferred to the buffer, one by one; at each stage the relevant column of terms is modified. The next element is then assembled and the whole procedure is repeated.

The frontal solution step is divided into the following three parts:

i) adding element stiffness matrix into front
ii) dealing with prescribed displacements and applied loads
iii) forward elimination and backward substitution

The solver can handle variable d.o.f of nodes and is independent of the type of element being used. A minimum amount of core is necessary to solve the

equations. This is calculated as the core required to keep all the stiffness terms, load terms and terms for ill-conditioning check when the front-width is at its maximum. The program is not capable of solving the equations if this minimum core is not provided.

E.4 Incorporation of Interface Element

Behaviour at junctions or interfaces between structure and soil elements involve relative slippage or separation of structure from soil. This may occur because of exceeding the limiting interface friction and inward movement of the structure. In order to obtain a better simulation of soil-structure interaction, special interface elements have to be used while using finite element method as the numerical tool.

Attempts have been made by a number of investigators to develop interface elements. Zienkiewicz, et al. (1970) suggested the use of continuous isoparametric elements with a simple non-linear material property for shear and normal stresses, assuming uniform strain in the thickness direction. In certain cases, ill conditioning of the stiffness matrix takes place in this case. Goodman, Taylor and Brekke (1968) developed interface element of zero thickness to account for relative movements between rock joints. Katona, et al. (1976) and Katona (1981) introduced a simple friction-contact interface element from the principle of virtual work modified by appropriate constraint conditions. Various deformation modes at the interface are incorporated in this formulation. Desai et al. (1984) proposed a thin-layer element, for using in structure-soil interaction and rock joints. Various deformation modes such as stick, slip, debonding and rebonding can be handled with this element. It is capable of providing improved definition of normal and shear behaviour; hence, it can be computationally more reliable than the zero thickness element. The formulation of this element is essentially the same as other solid elements. As such it is easier to program and implement. Inclusion of a finite thickness for the interface is realistic since there is very often a thin layer of soil which participates in the interaction behaviour. The thin layer element can easily be introduced in an interface having a curved configuration. The thin-layer element has been used in the present research and hence discussed here.

E.4.1 Interface behaviour

The physical behaviour of a structure-soil interface may involve relative movements that are both normal and tangential to the interface surface. The thin layer interface element is derived to account for various modes of deformations such as :

a) Stick or no-slip;
b) Slip or sliding;
c) Separation or debonding; and
d) Rebonding.

Figure E.4 shows various modes of deformation for a two-dimensional idealisation. An interface element is in stick or no-slip mode when there is no relative movement between the adjoining bodies, Fig. E.4(a). Slip or sliding occurs when relative movements take place in such a manner that the contact between the mating bodies is maintained, Fig. E.4(b). Separation or debonding mode occurs when gaps open up between two bodies that were in contact previously, Fig. E.4(c). An interface element in separation mode can return to stick mode in subsequent loading, which is referred to as rebonding, Fig. E.4(d).

In the concept of thin layer interface element (Desai et al. 1984) a basic assumption made is that the behaviour near the interface in a soil-structure interaction problem involves a finite thin zone. The behaviour of this thin zone can be significantly different from the behaviour of the surrounding structural and geological materials. This condition is simulated approximately by adopting appropriate constitutive laws for the element. Thus the thin layered interface element can be treated essentially like a solid isoparametric element, but with different constitutive properties.

The thin-layer interface element can be formulated by assuming it to be linear elastic, non-linear elastic or elastic-plastic. The stiffness matrix of the interface element, $[K]_i$ is written as

$$[K]_i = \int_v [B]^T [C]_i [B] dv \qquad \text{E.6}$$

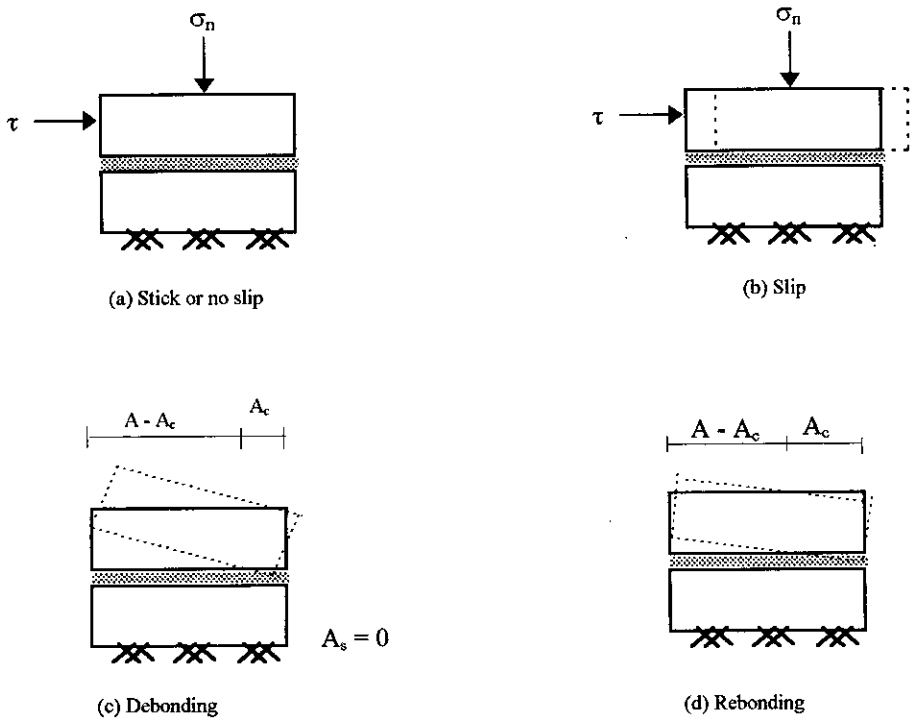

A = Total surface area
A_c = Contact area
A_s = Area of slip

Figure E.4 Schematic diagrams of modes of deformation at interface

where [B] = transformation matrix, v = volume and $[C]_i$ is the constitutive matrix. Then the element equations are written as

$$[K]_i\{q\} = \{Q\} \qquad \text{E.7}$$

where {q} = vector of nodal displacements and {Q} = vector of nodal forces.

For two dimensional plane-strain idealisation, the matrix $[C]_i$ and its inverse form $[D]_i$ are given as

$$[C]_i = \begin{bmatrix} C_1 & C_2 & 0 \\ C_2 & C_1 & 0 \\ 0 & 0 & G_i \end{bmatrix} \qquad \text{E.8}$$

where,

$$C_1 = \frac{E(1-\nu)}{(1+\nu)(1-2\nu)}$$

$$C_2 = \frac{E\nu}{(1+\nu)(1-2\nu)}$$

G_i = the shear modulus which is determined from laboratory tests.

and $$[D]_i = \begin{bmatrix} \frac{1-\nu^2}{E} & \frac{-\nu(1+\nu)}{E} & 0 \\ \frac{-\nu(1+\nu)}{E} & \frac{1-\nu^2}{E} & 0 \\ 0 & 0 & \frac{1}{G_i} \end{bmatrix} \qquad \text{E.9}$$

For non-linear elastic behaviour E, ν and G can be defined as variable moduli based on triaxial and direct shear tests.

In general, the stiffness properties of the interface elements are quite different from the properties of the adjacent continuum elements. It is assumed that the normal behaviour of the interface element is the same as regular soil elements; however the shear behaviour is quite different (Desai, et al. 1984).

E.4.2 Simulation of deformation modes

Various deformation modes that an interface can experience are incorporated in the thin layered element. It is assumed that before the application of load the interface elements are in stick or no-slip mode. Mohr-Coulomb criteria is used in order to identify the various modes of deformation. For a given increment of load, the normal stress, σ_n, and the total shear stress, τ, on the plane of interface elements are calculated. The modes of deformation are then checked and if the element is found to be in separation or slip mode, appropriate redistribution of stresses is performed. Details of the adopted procedure are given in the following steps.

i) The normal stress, σ_n, and shear stress, τ, due to the loading in a particular increment is calculated for the interface plane. Then, the sign of the normal stress, σ_n is checked. If it is found to be positive, the element can be either in stick mode or in slip mode (positive sign of σ_n indicates compressive stress while the negative sign indicates tensile stress). If σ_n is found to be negative, the element is considered to be in separation mode.

ii) For positive value of σ_n, the stick or slip mode is determined using the limiting shear stress of the interface place. The limiting shear stress, τ_L in the shear plane is calculated based on Mohr-Coulomb criteria as

$$\tau_L = C_a + \sigma_n \tan\phi_a \qquad \text{E.10}$$

where, C_a is the adhesion and ϕ_a is the angle of friction between structure and soil.

iii) If $|\tau_L| \geq |\tau|$ then, element is in non-slip or stick mode. In this case, there will be no re-distribution of stresses and no change in the stiffness parameters E and G_i.

iv) If $|\tau_L| < |\tau|$, the element is in slip mode. Now, the shear stress, τ, would be made equal to the limiting shear stress, τ_L. Thus the unbalanced load due to the excess shear stress $(\tau - \tau_L)$ would be applied at the nodes of the interface elements as self-equilibrating. Thus the stress is redistributed to the surrounding medium of interface element. The equivalent nodal loads due to stresses in an element is calculated by using.

$$\{F\} = \int [B]^T \{\sigma\} dv \qquad \text{E.11}$$

v) If σ_n is found to be negative, the element is considered to be in separation mode. In this case the unbalance equivalent nodal loads, corresponding to the stresses are calculated using Eq. (E.11), and is applied at the nodes of interface elements as self-equilibrating load in the next increment of load. The E and G_i values at this stage are actually zero. In order to avoid numerical difficulties, a very low value of E and G_i are assigned for the next step of analysis.

vi) To check the possibility of re-bonding, the sign of normal stress for each individual loading increment is checked. If it is found to be positive, the total normal stress which was negative previously is made to be equal to zero. As a result, it is no longer negative and falls into the category of stick or slip mode. Then the element would undergo the same steps as experienced by a normal interface element with positive normal stress.

The quality of simulation of the interface behaviour depends on a number of factors such as physical and geometrical properties of the surrounding media, non-linear material behaviour and the thickness of the thin-layer element. If the thickness is too large in comparison with the average contact dimension of the surrounding elements, the thin layer element will behave essentially as a solid element. If it is too small, computational difficulties may arise. Desai, et al. (1984) have proposed that for satisfactory simulation of the interface behaviour, the ratio of thickness to average contact dimension should lie between 0.01 and 0.1.

E.5 Input and Output of The Program

The input data which the user must provide the program can be divided into the following categories:

i) information describing the finite element mesh, i.e the co-ordinates of nodal points associated with each finite element.

ii) material properties associated with each finite element

iii) boundary conditions for the analysis

The CRISP program has two input files to be prepared by the user for any problem. First one is the geometry input file describing the geometry of the problem, includes nodal co-ordinates and doment connectivity. The second are is the main data input file incorporates all other data described in the subsequent sections.

E.5.1 Geometry part of program:

The geometry part of the input data consists of the types of elements being used in the mesh, the co-ordinates of all vertex nodes and the list of elements and the nodes associated with each.

Element and node numbering

Numbers assigned to each element and each vertex node in the finite element mesh must be unique (integer) and in the following ranges:

$1 \leq$ node number ≤ 750

$1 \leq$ element number $\leq N_{max}$ as specified by user

It is not necessary for either the node numbers or the element numbers to form a complete set of constitutive integers, i.e. there may be `gaps' in the numbering scheme adopted.

The geometry part of the program assigns numbers in the range 751 upwards to nodes on element sides and in element interiors. Co-ordinates of these nodes are calculated by linear interpolation from the co-ordinates of nodes at either end of the element sides. The elements are considered in the sequence they appeared in the input data. Each side of the element is considered in turn in the anti-clockwise order. The number of displacement nodes (side nodes) along the sides depends on the order of the element. The lower order elements presented here are the linear strain element, which have one node at the midpoint of the side.

Co-ordinate system

The program recommend to adopt a co-ordinate systems with the y - axis pointing upwards and x axis pointing to the right. If the x-axis points to the left then the program will calculate element areas and stiffness as negative quantities for element nodes numbers are listed in an anti-clockwise sense.

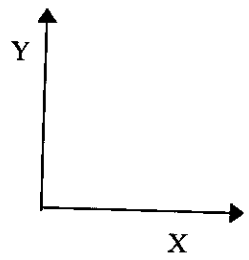

Figure E.5 Co-ordinate System

When the axisymmetric analysis option is selected it is assumed that the y axis is the axis of symmetry and the x axis is in the radial direction.

Material zone number

In considering the mesh, one has to identify different zones of material behaviour. Each zone is identified by a number, and all elements which are within that zone are given the same number. Zone number must be within the range of 1 to 10. Gaps in the number of zones are not allowed.

Nodal connectivity

The next input data are the node numbers which are associated with each element. The link between nodes and elements is referred to as element nodal connectivity. The number can begin at any node, but then should follow an anti-clockwise ordering. Specifying the nodes in clockwise order results in a negative value for the area of the element and will cause the program to stop at a later stage.

In case of interface element the nodes along the longer dimension should be input first, when defining connectivity.

E.5.2 Main part of the program

After specifying the geometry of mesh and its element configuration, parameters have to be set for this part of the program. The data generated from the run of geometry program is used during different runs of the main program. In the present study, axisymmetric analysis have been performed. Options have been selected not to update the co-ordinates after each increment but apply out of balance loads from one increment as correcting load in the next increment.

E.5.2.1 Material Properties

The program reads the material properties for the different material zones specified in the mesh. Material property types incorporated in the program are: (1) elastic, isotropic or anisotropy , (2) Elastic linear variation ith depth, (3) Modified cam-clay (MCC), (4) Cam-clay (CC), (5) Elastic perfectly plastic, and (6) The Schofield soil model (SCHO). Elastic isotropic property is used to define pile material characteristics and elastic perfectly plastic property is used to define the soil behaviour in the current analyses. For elastic isotropic material parameters to be defined are modulus of elasticity, Poisson's ratio, modulus of rigidity and unit weight of material. Stress-strain test is performed to determine these parameters (Fig. E.6).

For elastic perfectly plastic material model it is necessary to define yield criteria as von Mises, Tresea, Drucker-Prager, Mohr-Coulomb etc. Mohr-Coulomb criteria is used in the present research. Parameter necessary to define elastic-perfectly plastic model are Young's Modulus at any depth, Poisson's ratio, cohesion, angle of internal friction, rate of increase of Young's modulus and shear strength at ith depth if necessary and bulk unit weight of the soil. For model pile it is reasonable to use same Young's modulus and shear strength at any depth.

Special parameters are necessary to define interface element. These are: thickness or height of the interface element, t_i or b_i, modulus in the normal direction, K_n, shear modulus G_s , cohesion C_a, angle of wall friction δ etc. The C_a and δ values of interface element should be the C and φ value respectively for pile and soil interface; not for soil itself. Usually δ value is slightly lower than φ value in case of steel pile. For sand-pile interface C_a

can be assumed to be zero. The value of δ is assumed to be 2/3 φ in the current research.

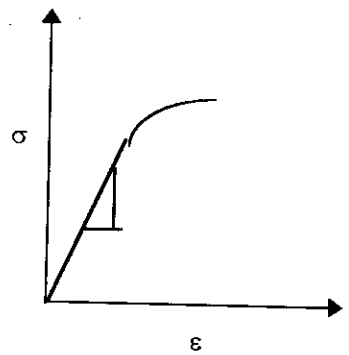

Figure E.6 Stress - Strain relation

The modulus in the normal direction of the interface elements (K_n) and the shear modulus of interface element (G_s) can be calculated form E and ν as follows:

$$K_n = \frac{E(1-\nu)}{(1+\nu)(1-2\nu)}$$

$$G_s = \frac{E}{2(1+\nu)} \qquad \text{E.12}$$

According to the assumption of the thin layered interface element (Desai et al. 1981) the normal behaviour of the interface elements is the same as regular soil elements, however, the shear behaviour is quite different (Desai, 1984). Thus value of E for interface element can be used as that of surrounding soil to calculate k_n. The value of G_s for interface can be obtained form shear test conduced between two dissimilar materials. In this research shear stiffness, G_s of the element is set to a very low value assuming a very high value of ν as recommended by Jayatheran (1996).

The residual shear modulus after the interface element has reached its limiting shear value G_{res} should have a very low value as it is almost equal to zero in reality. So in this study G_{res} has been assigned to be equal to 7 kN/m^2 arbitrarily to avoid the numerical problems.

E.5.2.2 Insitu stresses:

In an elasto-plastic analysis the stiffness matrix of a finite element will be dependent on the state of stress within the element. For this, insitu stress state is necessary in elasto-plastic finite element analysis.

In general the stress state will vary across an element, and the stiffness terms are calculated by integrating expressions dependent on these varying stresses over the volume of each element. CRISP integrates these expressions numerically 'sampling' the stresses at particular points within the element and then using standard numerical integration rules for triangular areas.

The insitu stresses that are to be assigned are σ_v' , σ_h' , U_o , and p_c' for the entire region of the mesh. The parameter p_c', isotropic preconsolidation pressure, is only needed for Cam-clay models. The calculation of the vertical effective stress is straightforward as:

$$\sigma_v' = \sigma_v - U \qquad \text{E.13}$$

where, vertical totals stress, $\sigma_v = \gamma_b h$

U = pore water pressure, can be easily calculated from the position of water table

γ_b = bulk density

h = depth

The calculation of the horizontal effective stress is not so straightforward because the co-efficient of earth pressure at rest depends on the stress history of the soil. In elastic analysis and some elastic perfectly plastic analysis it is quite common to set, $K_o = \frac{\nu'}{1-\nu'}$

Jaky (1944) gave a good approximation for K_o as:

$$K_o = 1\text{-}\sin\varphi \qquad \text{E.14}$$

Jaky's relation is used to calculate horizontal effective stress in the current analysis.

In situ stresses can be specified in every integration point for each element and it could also be specified for certain horizontal layers when insitu stresses for each element is interpolated from the given sets of reference points representing layers. The latter is used in the current study.

E.5.2.3 Boundary condition

The zero displacement boundary conditions has to be specified along the boundary that is restrained. In specifying these conditions it is necessary to specify the parts of boundary which are loaded. This specified loading or boundary condition is expected to be in equilibrium with the insitu stresses.

E.5.3 Output from the programs

Output consists of the incremental applied load, the out-of-balance load, element stresses, strains, nodal displacements and the total applied load at the nodes. The output are printed depending upon the output option. Depending upon these options stresses and strains are printed at element centroid or at all integration points or are not printed at all. Similarly displacements are printed at vertex nodes or all nodes or not printed at all.